Charles University

Faculty of Science

Study programme: Inorganic Chemistry

RNDr. Lucia Pazderová

Complexes of macrocyclic ligands with phosphonate and phosphinate pendant arms for molecular imaging

Komplexy makrocyklických ligandů s fosfonátovými a fosfinátovými pendantními rameny pro molekulární zobrazování

Doctoral thesis

Supervisor: Doc. RNDr. Vojtech Kubíček, Ph.D.

Prague, 2021

Prohlášení

Tímto prohlašuji, že jsem tuto závěrečnou práci vypracovala samostatně a že jsem uvedla všechny použité literární zdroje. Tato práce a ani její část nebyla použita k získání žádného jiného nebo stejného akademického titulu.

Declaration

Hereby I declare that this Thesis is my original work and that I have properly cited all the information resources. This work or its any part has not been submitted for any other or for the same academic degree.

In Prague, July 2021 Lucia Pazderová

Table of Contents

1 Abstract

In an effort to increase the thermodynamic stability and the kinetic inertness of the complexes, the five new azamacrobicyclic ligands derived from TACN, cyclen, and cyclam have been prepared. The ligands were decorated with phosphinate or phosphonate pendant arms to maintain fast complexation. Since the ascending importance of targeted diagnostic and therapy, the bone-targeted non-bridged cyclam derivative with phosphinate-bis(phosphonate) pendant arm (H_5**TE1P^{BP}**) has also been synthesized. The ligands were studied with respect to their application. The bridged TACN (H_2**bpbtacn**) and cyclen (H_4**bpbcen**) ligands show high macrocyclic basicity (logK_1 = 12.25 and 12.70, respectively). The thermodynamic stability of H_2**bpbtacn** with Cu(II) ion is more than ten orders of magnitude lower than that of the NOTA ligand. The stability constants of H_4**bpbcen** with Cu(II) and Zn(II) ions are comparable to those given for the DOTA. The stability of Ln(III)-**bpbcen** complexes is 7–10 orders of magnitude lower compared to DOTA complexes. For both ligands, the lower thermodynamic stability of the complexes is attributed to the high rigidity of the ligand structure. The bridged cyclam derivatives with phosphonate (H_4**TE2P**), bis(phosphinate) (H_4**TE2bpin**), or phosphinate (H_2**TE2P^{H}**) pendants are characterized by high stability of Cu(II) complexes (log$K$ = 23.97, 20.21 and 21.28, respectively) and high kinetic inertness ($t_{1/2}$ = 120 h, 11 h and 111 h, respectively; 1 M $HClO_4$, 90 °C). The formation kinetics of H_4**TE2P** and H_4**TE2bpin** derivative is very fast and the Cu(II) complexes are quantitatively formed in 2 s at pH ~6 and millimolar concentration. The non-bridged ligand H_5**TE1P^{BP}** is characterized by high macrocycle basicity (logK_1 < 13) and high selectivity for Cu(II) over Zn(II) and Ni(II) ions. The formation of the copper complex is very fast with a quantitative formation of the complex within 1 s (pH ~6, 0.05 mM). The complex is highly inert to acid-assisted decomplexation ($t_{1/2}$ = 1.4 min; 1 M $HClO_4$, 90 °C). Radiolabeling of H_5**TE1P^{BP}** is fast and effective with a specific activity ~30 Bq/μmol (pH 5.5, 25 °C) and the Cu(II) complex shows high affinity to hydroxyapatite in vitro and to bones in vivo. PET experiments in healthy mice and also in direct comparison with [^{18}F]fluoride in a rat femur defect model demonstrate the excellent suitability of H_5**TE1P^{BP}** as copper izotope carrier for imaging active bone compartments.

2 Abstrakt

Ve snaze zvýšit termodynamickou stabilitu a kinetickou inertnost komplexů bylo připraveno pět nových azamakrobicyklických ligandů odvozených od TACN, cyklenu a cyklamu. Pro zachování rychlé komplexace byla na ligandy navázána fosfinátová nebo fosfonátová pendantní ramena. Vzhledem ke vzrůstajícímu významu cílené diagnostiky a terapie byl syntetizován také nepřemostěný cyklamový derivát s fosfináto-bis(fosfonátovým) ramenem (H_5**TE1P^{BP}**) určený pro navázání na kostní tkáň. Ligandy byly studovány s ohledem na jejich aplikaci. Přemostěné ligandy odvozené od TACN (H_2**bpbtacn**) a cyklenu (H_4**bpbcen**) vykazují vysokou bazicitu makrocyklu (logK_1 = 12,25 a 12,70). Termodynamická stabilita komplexu H_2**bpbtacn** s Cu(II) iontem je o více než deset řádů nižší než u ligandu NOTA. Konstanty stability komplexů H_4**bpbcen** s ionty Cu(II) a Zn(II) jsou srovnatelné s konstantami uvedenými pro DOTA. Stabilita jeho komplexů s ionty Ln(III) je o 7–10 řádů nižší ve srovnání s komplexy DOTA. U obou ligandů je nižší termodynamická stabilita komplexů přičítána vysoké rigidnosti ligandu. Přemostěné cyklamové deriváty s fosfonátými (H_4**TE2P**), bis(fosfinátovými) (H_4**TE2bpin**) nebo fosfinátovými (H_2**TE2P^{H}**) rameny se vyznačují vysokou stabilitou komplexů Cu(II) (log$K$ = 23,97, 20,21 a 21,28) a vysokou kinetickou inertností ($t_{1/2}$ = 120 h, 11 h a 111 h; 1 M $HClO_4$, 90 °C). Kinetika tvorby komplexů H_4**TE2P** a H_4**TE2bpin** je velmi rychlá a měďnaté komplexy se kvantitativně vytvoří za 2 s při pH ~ 6 a milimolární koncentraci. Nepřemostěný ligand H_5**TE1P^{BP}** se vyznačuje vysokou bazicitou makrocyklu (logK_1 < 13) a vysokou selektivitou pro ionty Cu(II) oproti iontům Zn(II) a Ni(II). Tvorba měďnatého komplexu je velmi rychlá, komplex je kvantitativně vytvořen během 1 s při pH ~ 6 (0,05 mM). Komplex je vysoce inertní vůči kysele katalyzované dekomplexaci ($t_{1/2}$ = 1,4 min; 1 M $HClO_4$, 90 °C). Radioaktivní značení H_5**TE1P^{BP}** je rychlé a účinné se specifickou aktivitou ~ 30 Bq/μmol (pH = 5,5; 25 °C). Komplex vykazuje vysokou afinitu k hydroxoapatitu in vitro i ke kostem in vivo. PET experimenty na zdravých myších a také srovnávací experimenty s [^{18}F]fluoridem na modelu defektu stehenní kosti krysy ukazují vhodnost H_5**TE1P^{BP}** jako nosiče radioaktivních izotopů mědi pro zobrazování aktivních kostních kompartmentů.

3 Theoretical background

3.1 Molecular imaging

The early diagnostics of diseases has the highest importance in medicine. Identifying a health problem at the early stage can save the lives. Until today, the numerous diseases have not been fully understood and treatments have not been sufficiently and equally effective at each stage of illnesses. Despite of quick development of drug research, it will never reach the expected results without Molecular Imaging Techniques (MI). It is impossible to preserve the equivalent drug efficiency in each stage of the disease. Thus, the sooner the drug is applied, the better patient prognosis is obtained.

Molecular Imaging is focused on noninvasive visualisation, characterization and measurement of biological processes on molecular and cellular level. It is also known as an important preclinical and clinical research tool, which is joined to the process of drug development. These techniques visualize the pathophysiologic processes in real-time and provide information about specific molecular alterations underlying disease status. They create sectional images, which can be reconstructed into two-dimensional (2D) or three-dimensional (3D) images. Molecular Imaging can diagnose disease and evaluate response on therapy long before changes can be seen at the anatomical level. The most essential and utilized Molecular Imaging techniques include Magnetic Resonance Imaging (MRI), and radionuclide imaging via Positron Emission Tomography (PET) and Single-Photon Emission Computed Tomography (SPECT). Every mentioned method has certain advantages and limitations (see below). The choice of method depends on which techniques can provide the most complementary information to answer a specific pre-clinical or clinical question.[1,2,3,4]

3.1.1 Magnetic Resonance Imaging

The MRI has become one of the most utilized imaging techniques due to its outstanding soft-tissue contrast and high spatial resolution. It also allows for physiological and biochemical imaging.[5] This method does not make use of ionizing radiation. Imaging leans on the strong uniformly polarizing magnetic field, smaller magnetic field gradient and high-frequency magnetic field. Signal

production is based on resonance and relaxation features of nuclei (e.i., ^{1}H, ^{31}P) in the magnetic field. Via the spatial coding, the signal can be transformed onto the image.[6] The discrepancy of the signal intensity between every pixel and voxel is defined as a contrast. The drawback of the Magnetic Resonance Imaging is relatively weak sensitivity. This can result in deficient contrast of acquired images which makes the practical application harder.[7] The numerous contrast agents (CA) have been developed for the improvement of contrast and enhancement of diagnostic accuracy. Introduction of these chemical substances to tissues, which need to be displayed, can highlight the differentiation of normal and pathological tissues. The principal idea is the ability of CA to accelerate relaxation of the surrounding water protons. This is known as contrast-enhanced imaging. The contrast agents are produced as highly stable complexes, which can be applied to the patient in relatively high doses. The application of macrocyclic chemistry is considered for the key clinical success in medicine. The contrast agents are divided into two groups, namely positive (T_1) and negative (T_2) CA. Currently, gadolinium(III) paramagnetic chelates are commonly used as T_1 CA, while superparamagnetic materials such as ferric oxide nanoparticles (NP) act as T_2 CA. Many different compounds affect the NMR signal in various ways. Some of them enable selective targeting of certain pathologies and/or tissues.

In practice, the most common compounds for contrast enhancement are based on gadolinium(III) ion. Such contrast agents are paramagnetic and they shorten the longitudinal relaxation time T_1. Except for gadolinium-based CA, there are also other paramagnetic substances which are not so developed (e.g., manganese-based contrast agents).[6,8]

For Gd(III)-containing complexes, the efficacy can be measured with respect to the longitudinal relaxivity of the hydrogen nuclei. This relaxation parameter quantifies the extent to which the complex catalyzes shortening of the T_1 relaxation time of protons in water molecules. Coordination interactions are important in transferring the effect from the paramagnetic ion to the solvent. This contribution of the internal coordination sphere is generally the main contribution and is being studied in the preparation of new, more effective contrast agents. The rotational correlation time (τ_c) of the complex is also a key parameter affecting relaxivity. It can vary with increasing size and loss of molecule flexibility. It can also be

influenced by the presence of other particles in the solution, such as proteins or salts.[9,10] The gadolinium complexes dominate in the research works dealing with macrocyclic contrast agents and clinical applications of the Magnetic Resonance Imaging. The Gd(III) ion has two key features that make it an ideal option. Thanks to its seven unpaired electrons, it is highly paramagnetic and also has relatively slow electron relaxation due to its symmetrical S-state. The chelating agents are designed to leave one or two coordination sites available for binding water molecules to the encapsulated metal ion.[9,11] Adapting to the aforementioned requirements involves a change in the chelate structure. In addition to improving relaxation, modulation of pharmacokinetics and biodistribution can be accomplished through ligand modulation. However, the design of new chelating ligands must take into account the requirement of high thermodynamic stability to avoid exposure of the patient to the toxicity of the contrast agent.[7]

3.1.2 Nuclear medicine imaging

Over the past fifty years, nuclear imaging has developed from a predominantly experimental technique to a critical part of modern clinical practice. Nuclear medicine imaging is a method of imaging based on the detection of radiation from various parts of the body after administration of a radioactive tracer to a patient. The biologically interesting molecular species, labelled with a radioactive tracer, is distributed through the human body. They are concentrated in cells and provided studying normal physiology and identifying pathologies. Positron Emission Tomography and Single Photon Emission Computed Tomography have proven invaluable for oncology, cardiology and neurology and provide functional imaging data that complements MRI and Computed Tomography (CT) data. The radiopharmaceuticals used in nuclear medicine are mostly injected into a vein. The heart of any radiopharmaceutical is, of course, its positron- (PET) or gamma-emitting (SPECT) radionuclide. This must be produced, purified and incorporated to diagnostic radiopharmacum. The amount of radiation a patient receives during a typical nuclear medicine scan is usually very low. The crucial requirement in nuclear medicine is the high stability of radioactive agent to avoid nonspecific radioisotope deposition in tissues. Thus, high thermodynamic stability and kinetic inertness of complexes with radionuclides allow their safe usage. In order to form stable complexes, a strict relationship must

exist between the element (ionic radius, electronic configuration) and the ligand(s) (size of the molecule, number and nature of the coordinating groups in the molecule).[12,13,14]

3.1.2.1 Positron Emission Tomography

Positron Emission Tomography imaging is based on the detection of radiation emitted after the matter to energy conversion. This phenomenon appears when the negatively charged electron and positively charged positron get into contact.[14] The positron emitted from the radiotracer is annihilated by electron, producing two collinear photons, according to the equation: $e^+ + e^- \rightarrow \gamma + \gamma$. The efficiency of the PET system is conforming to its sensitivity or the lowest detectable concentration of the selected radiotracer. It is defined by spatial resolution and efficient detection of annihilation photons. The spatial resolution is fundamentally limited via the acollinearity of annihilation photons, the width of the detection elements in the detection ring, the change in depth of interaction in detection elements and the sensitivity of the detector ring for the detection of 511 keV photons.[15] Nowadays, several radionuclides are studied for theranostic usage (diagnosis and therapy), which plays an important role in medicine.[14]

The PET method, compared to its single photon analogue SPECT, shows higher resolution (2–4 mm^3 versus 6–8 mm^3 for SPECT) and higher sensitivity (up to ~10^{-12} M compared to ~10^{-6} M for SPECT). The resolution and sensitivity of PET are related to the intrinsic properties of the β^+ emission, with the resolution depending on the initial distance travelled by the β^+ photon before annihilation. This distance is a function of the decay energy. For this reason, low energy β^+ emissions are desirable because they provide a better resolution. The high sensitivity of PET is the result of the interplay of the detection of two γ-photons. Despite the undeniable advantages of PET imaging, the SPECT method is more clinically used. Perhaps only because it is a more established technique.[16,17,18]

Limitations of PET is a relatively low spatial resolution and requirement of cyclotron on-site for short-lived agents. On the other hand, it is highly sensitive and quantitative with the possibility of temporal monitoring.

The combination of PET with Computed Tomography (CT) is widely used in oncology, cardiology and for characterization of neurological disorders at an early stage.[19]

Unfortunately, there exist only a few radionuclides, which have an acceptable half-life with reasonable positron emission abundance.[14] The most common PET isotope is ^{18}F. However, its utilization is a matter of organic chemistry. In addition to this isotope, several metal nuclides are available. The most important metallic β^+ emitters are copper radionuclides (^{61}Cu, ^{62}Cu, ^{64}Cu), ^{68}Ga and ^{89}Zr. The half-life of the ^{61}Cu isotope is 3.3 hours. The decay occurs through β^+ emission (100%). ^{62}Cu decays almost exclusively through positron emission (100% β^+; $t_{1/2}$ = 9.27 min). Its short half-life makes it suitable for the dynamic study of organ function. The relatively short half-life of its parent nuclide ^{62}Zn (9.17 h) does not allow the operation of ^{62}Zn/^{62}Cu generator longer than for 3 days, which is a limitation that could avoid its widespread use for wider diagnostic applications. The half-life of ^{64}Cu isotope is 12.7 hours. It is sufficient time for synthesis of many radiopharmaceuticals. It is also long enough time for in vivo tracking of smaller and larger molecular carriers with slower clearance. The ^{64}Cu isotope has versatile utilization, thanks to its decay scheme. The decay of this nuclide combines electron capture (41%), β^- emission (19%) and β^+ emission (40%), which also leads to emission of Auger electrons with therapeutic potential.[20,21,22] The ^{64}Cu isotope is relatively readily available commercially. It can be produced in biomedical cyclotrons using proton radiation from an enriched ^{64}Ni isotope through ^{64}Ni(p,n)^{64}Cu decay.[19,21,23,24] The coordination scheme of an aqueous copper solution is limited to three oxidation states (I–III), but only oxidation number II is significant for radiomedicine.[23] The Cu(II) ion is classified as a borderline hard cation and therefore has a high affinity for borderline donor atoms such as nitrogen. Coordination numbers of copper are in the range of 4–6.[16,21,23,24] The copper forms complexes that have square-planar, square pyramidal, trigonal-bipyramidal, or octahedral geometry. Ability to create a stable complexes and a long half-life makes the isotope ^{64}Cu very perspective nuclide.[14,23,25]

The isotope ^{68}Ga has a half-life of 67.7 minutes. The decay is through β^+ emission (89%) and electron capture (11%). ^{68}Ga is an attractive PET nuclide because it is produced in commercially available ^{68}Ge/^{68}Ga generators and the

decay is mainly through β^+ emission.[14,18] Actually, ^{68}Ga isotope offers many advantages for imaging: rich positron emission, short half-life, without the need for a cyclotron on site.[20] In aqueous solution, the oxidation state of galium is 3+. It can exist in the free hydrated form only at acidic pH. *In vivo*, the ^{68}Ga(III) ion creates a very stable complex with transferrin. The mimicking of Fe(III) metabolic pathway makes difficulties in the development of suitable gallium chemistry. The Ga(III) ion can be classified as a hard cation preferring hard donor atoms such as oxygen and nitrogen. The most common gallium coordination number is 6.[14,16,24]

In many cases, a large amount of administrated drug is delivered also to normal tissues. This may cause several side-effects. The basic approach to overcoming these obstacles is the development of optimized and targeted delivery systems. Conjugation of drugs or contrast agents with receptor-binding molecules selectively increases their adherence or uptake by target cells. For purpose of target-selective therapeutic and/or diagnostic applications various molecules are used including antibodies and their fragments, peptides, nucleic acid small molecules, or others.[26,27,28,29] The labelling with peptides can be achieved through 1,4,7,10-tetraazacyclododecane-1,4,7,10-tetraacetic acid (DOTA).[20] The leading compound of ^{68}Ga-radiopharmaceuticals is [^{68}Ga]Ga-DOTA-TOC (Figure 1). This substance has a high affinity for somatostatin receptors and is clinically used for imaging neuroendocrine tumours.[14]

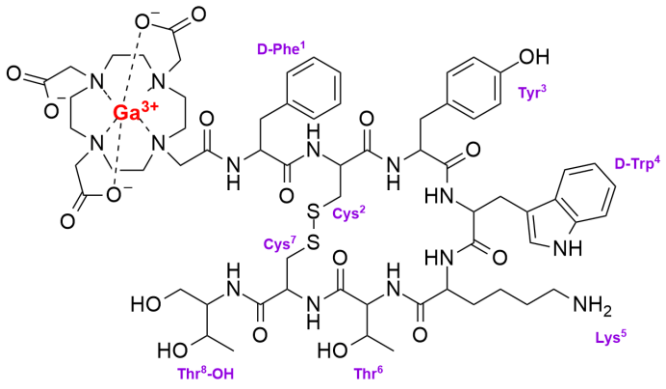

Figure 1: Structure of [68Ga]Ga-DOTA-TOC.

The half-life of zirconium-89 is 78.4 h. Such a long half-life allows PET imaging even a few days after administration. The decay proceeds via positron emission (23%) and electron capture (77%) to the stable isotope ^{89}Y. Due to the easy availability of the target material in natural form, the ^{89}Y(p,n)^{89}Zr nuclear reaction is considered the most suitable for the production of ^{89}Zr in medical cyclotrons. Zirconium(IV) cation is, as well as Ga(III) ion, a very hard acidic metal ion and is prone to hydrolysis and hydroxide formation under less acidic conditions. Zr(IV) ion is resistant to redox reactions under biological conditions. It is considered a hard Lewis acid with coordination number 8. Although many radiolabeled ^{89}Zr-complexes have been developed for various applications in nuclear medicine, the radioimmunoscintigraphy (Immuno PET) is regarded to be the most important application of this isotope. The relatively slow pharmacokinetics of monoclonal antibodies ($t_{1/2}$ = 3–4 days) is complemented by the long half-life of zirconium-89. The siderophoric ligand deferoxamine (DFO) is the most important chelator of Zr(IV) (Figure 2). It is a hexadentate ligand containing three hydroxamate groups for chelating metal and a primary amine tail for conjugation to a biomolecule. Two coordination sites remain available for coordination with, for example, water molecules. Due to the numerous advantages, the ^{89}Zr-based Immuno-PET is developing at a dynamic speed.[14,30,31,32,33]

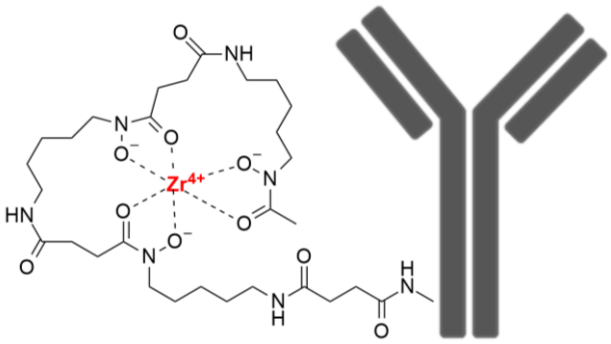

Figure 2: Schematic overview of ^{89}Zr-labeled antibody using DFO as chelator.

3.1.2.2 Single-Photon Emission Computed Tomography

The SPECT method is able to detect γ-photons of different energies emitted by radionuclides which are injected into the bloodstream. Following the expansion of PET, it seemed that SPECT would be replaced by this more powerful technique because SPECT has lower spatial resolution and is less quantitative than PET. In fact, it still plays an important role in diagnostic nuclear medicine.[34,35] The main reason is its wide availability, existence of many probes and lower financial cost. By far the most used radionuclide in SPECT is the ^{99m}Tc isotope. The number of clinical examinations using this isotope exceeds the number of PET agents.[34,36] ^{99m}Tc isotope has single-energy gamma emmision decay and 6.0 hours half-life.[37] The physical characteristics of radionuclide ($E\gamma$ = 140.5 keV) occur minimal radiation burden to the patient and are almost ideal for SPECT imaging. Metastable technetium-99 decays into a very weak β^- emitter ^{99}Tc, which does not interfere or reduce image quality.[13] ^{99m}Tc is prepared in ^{99}Mo/^{99m}Tc generators, which provide technetium in its highest oxidation state +7.[38] Technetium has a wide range of oxidation states but, for applications in nuclear medicine, the most common states are +1, +3 and +5. Nowadays, this radionuclide is the driving force of medical imaging and is used in 70–80% of all radiodiagnostic scans. Typical donor groups in technetium complexes are amines, amides, thiols, phosphines and isonitriles. The coordination numbers of technetium range from 4 to 9.[39]

Chemistry of technetium is remarkable due to this element is able to form characteristic inorganic functional moieties.[34]

The complexes of technetium(I) are characterized by high stability, inertness and tend to prefer an octahedral coordination geometry. Undoubtedly, the best-known ^{99m}Tc(I) radiotracer is ^{99m}Tc(I)-hexakis(2-methoxy-2-methylpropyl)nitrile, also known as [^{99m}Tc]Tc-MIBI or [^{99m}Tc]Tc-sestamibi (Figure 3). The main clinical aplication of [^{99m}Tc] Tc-MIBI is the myocardial imaging.[13,40]

^{99m}Tc(III) ion has a d^4 electron configuration and forms a hexa or heptacoordinated complexes with wide range of ligands. The most widely known tracers are [^{99m}Tc]Tc-teboroxime and [^{99m}Tc]Tc-Q12 (Figure 3) and both are

myocardial perfusion imaging agents. Teboroxim is the boronic acid adduct of technetium dioximes (BATO) family of compounds and the Q12, also known as [^{99m}Tc] Tc-furifosmin, is a hexacoordinated compound with two trans monodentate trialkylphosphine ligands and one tetradentate N_2O_2-based Schiff base ligand.[13,41]

The compounds of ^{99m}Tc(V) represent the biggest part of radiotracers based on technetium. The complexes have a d^2 electron configuration and generally prefer a pentacoordinated square pyramidal or a hexacoordinated octahedral geometry. The majority ^{99m}Tc(V) compounds can be divided on two groups. The first group constituted substances containing [^{99m}Tc] $[Tc(V)=O]^{3+}$ bonds and the second one involving [^{99m}Tc] $[Tc(V)=N]^{2+}$ bonds.[42]

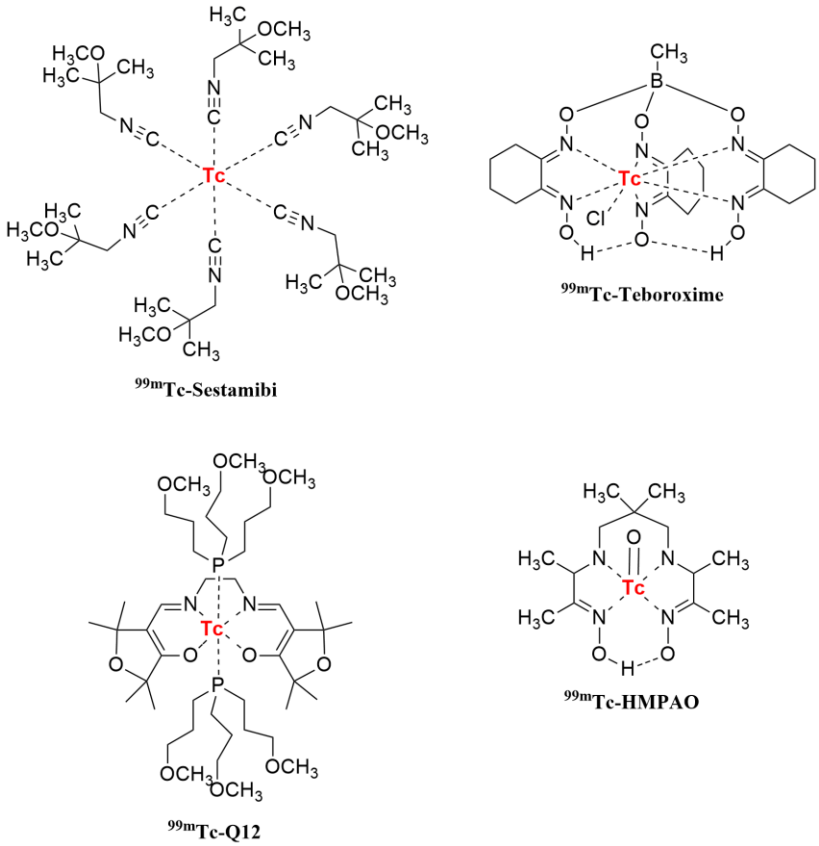

Figure 3: [^{99m}Tc]Tc-MIBI, [^{99m}Tc]Tc-Teboroxime, [^{99m}Tc]Tc-Q12, [^{99m}Tc]Tc-HMPAO (omitting charges for simplicity).

The [^{99m}Tc]Tc-hexamethylpropyleneamine oxime ([^{99m}Tc]Tc-HMPAO; Figure 3) is an example of the first group of compounds. It represents

a second-generation complex with primary application in brain imaging. However, the potential of this radiopharmacum lies in the ability to label leukocytes. Thus, it is used as a whole-cell labelling reagent for intra-abdominal infections and inflammatory bowel disease.[13,43,44,45]

After the ^{99m}Tc isotope, ^{111}In is the most popular metal radionuclide for SPECT. The half-life of ^{111}In is 2.8 days. The decay takes place by means of electron capture (100%) with emissions of γ radiation. ^{111}In is commercially produced in a cyclotron by proton bombardment of a cadmium target (^{111}Cd(p,n)^{111}In or ^{112}Cd(p,2n)^{111}In reaction). The In(III) ion is a relatively hard cation, making it preferable for chelators with hard donor atoms. Indium can reach coordination numbers 7 and 8. One of the main applications is labelling of red cells, platelets and leukocytes. In order to pass cell membranes and label intracellular proteins, the nuclide has to create complexes with lipophilic chelators. One of those lipophilic chelators used for this purpose is the 8-hydroxyquinoline (oxine) and forms the hexacoordinated [^{111}In]In(oxinate)$_3$ (Figure 4).[39,46,47,48,49]

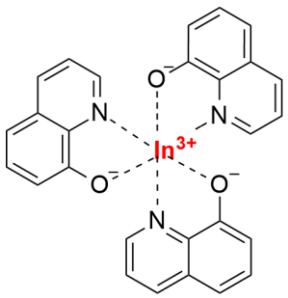

Figure 4: [^{111}In]In(oxinate)$_3$

3.2 Chelating agents

Metal isotopes cannot be administered to the patient in free form but must be bound to a suitable carrier. However, there are only a few chelating systems that are commonly used. Each chelating group should show a high reactivity towards the metal, which should lead to a stable coordination arrangement.[34,50,51,52,53] In medical applications, great emphasis is put on high thermodynamic stability and kinetic inertness of the compounds. The optimal ligand should bind the target metal ion with high specificity, yield and complexation rate. The kinetic inertness of the resulting complex has a higher priority over the thermodynamic stability because it prevents transchelation and transmetalation after injection of the complex into the body.[54,55]

The most commonly used chelators in MRI and radioactive contrast agents can be divided into acyclic and macrocyclic. In general, complexes with acyclic chelates (e.g. EDTA or DTPA) are less kinetically inert than complexes with macrocyclic ligands, although thermodynamic stability is comparable.[56] Despite the unique coordination chemistry of each metal, there is a group of chelating ligands used in a wide variety of radioactive isotopes. The azacrown derivatives TACN (1,4,7-triazacyclononane), cyclene (1,4,7,10-tetraazacyclododecane) and cyclam (1,4,8,11-tetraazacyclotetradecane) are the most studied (Figure 5).

The affinity of tetraazamacrocycles for specific ion depends on the size of cycle, the flexibility of the backbone and the character and number of coordinating atoms. Various macrocyclic polyamine derivatives have been prepared. They show increased affinity and stability of the complex towards certain metallic cations (transition metals or lanthanoids). The azamacrocyclic complexes have found use in a wide range of application depending on the type of chelated ion. However, most applications involve medical imaging agents.[57,58,59,60,61] The coordination and solution chemistry of metal ions must be well known in order to prepare a suitable chelating ligand. Stability is a key issue for all complexes in a biological system because the metal ion must remain bound and in some cases, the complex must be eliminated unchanged. It is of the utmost importance that the chelating ligand corresponds to the particular radioactive isotope. The total charge of the complex must also be taken into account, as it may affect the biodistribution

of the radiopharmaceutical. Macrocyclic chelates form highly stable complexes and provide the opportunity to tune the coordination environment through functionalization.[39,62] It is well known that thermodynamic and kinetic stability of complexes increase in the order of monodentate ligand < linear or branched chelating ligand < macrocyclic ligand < macrobicyclic ligand or cryptate (applies to the same donor atoms). This sequence can be simply explained as follows: with the same complementarity, the stability of the complex increases with the topological complexity of the ligand, which is evident from the chelating effect, the macrocyclic effect and the cryptate effect.[63,64]

Numerous highly pre-organized molecules, such as azamacrobicycles, have also been synthesized. The majority is based on cyclen and cyclam.[65] It seems that kinetic inertness of bridged macrocyclic complexes, especially in aqueous solution, is truly outstanding. The acid assisted decomplexation became the appropriate indicator of inertness.[54,66,67] Nowadays, the synthesis of bridged polyazamacrocycles is of high interest. They are characterized by unusual basicity (proton-spongies character),[68,69,70,71,72,73] redox behaviour[74,75] and coordination chemistry.[64,76,77,78,79] Based on the size, macrocyclic ligands can be divided into two groups. Smaller cycles allow the coordination of only one metal ion, while larger bicyclic derivatives allow the coordination of two metal ions in individual macrocyclic cavities. However, these are generally not very suitable for molecular imaging, as the presence of two coordination centres usually complicates metal coordination and system stability.[39,62]

The systematic study of macrobicyclic compounds with different chain length and various donor atoms and substituents on nitrogen atoms allowed to individualize the remarkable rigidity thanks to topological features of cage-like ligands. The preorganization affects basicity of nitrogen atoms and, thus, these molecules show higher basicity than analogous acyclic or monocyclic compounds. The higher basicity was explained as a consequence of the dense hydrogen network formed by the acidic proton inside the macrobicyclic cavity.[80,81,82,83,84,85,86,87]

Despite the considerable scientists effort and the wide range of cyclen and cyclam tetraazamacrocyclic derivatives, such as their tetracarboxymethylated derivatives DOTA (1,4,7,10-tetraazacyclododecane-1,4,7,10-tetraacetic acid;

Figure 5) and TETA (1,4,8,11-tetraazacyclotetradecane-1,4,8,11-tetraacetic acid; Figure 5), there is emphasized need for more inert chelators to increase stability of their complexes *in vivo*. With this in mind, new ligand systems have been developed including those based on bridging of two adjacent nitrogen atoms (side-bridged; sb) and two non-adjacent nitrogen atoms (cross-bridged; cb) tetraazamacrocycles.[54,88] The connecting of adjacent nitrogens in macrocycle provides an appropriate method for reducing the propensity of a macrocycle to bind to transition metal ions in a *cis*-(folded) conformation rather than a *trans*-(planar) conformation. The connection of non-adjacent nitrogen atoms creates the cross-bridged derivatives which may adopt conformations where every nitrogen lone pair is pointing inside the cavity. Furthermore, the short bridging chain causes the relative rigidity of the ligand and the pointing of nitrogen lone pairs in a *cis*-folded geometry encourages distorted coordination modes as tetrahedral, distorted trigonal bipyramidal, pseudo-octahedral or also distorted square pyramidal.[89,90,91,92,93] The short bridge rigidizes macrocycle and gives the ligand topological features of classical cryptands. The numerous studies have shown that the complexes of the first-row transition metals with ethylene cross-bridged tetraazamacrocycles are among the most kinetically stable complexes. Nonetheless, their tetradentate disposition ensures additional coordination sites which are labile and allow a reactivity and/or binding ability. Ethylene and propylene cross-bridged ligands have become the most widely used group of macrobicycles.[73,75,94]

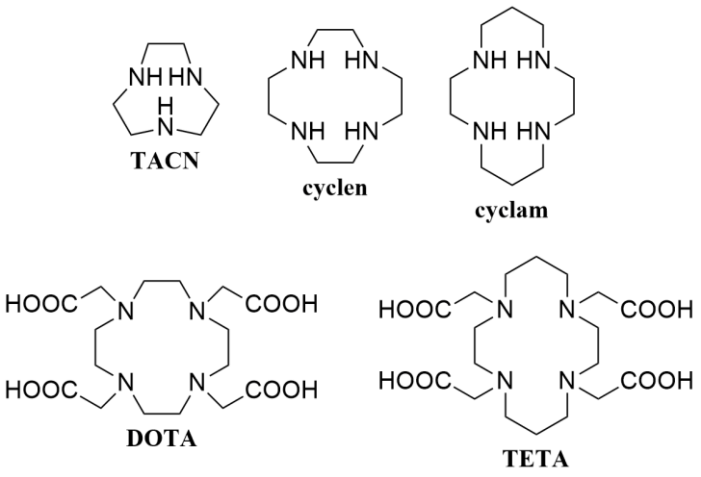

Figure 5: Non-bridged ligands discussed in the text.

Forty years ago, Wainwright reported the first case of bridging by simple *cis*-alkylation of a macrocycle. The ethylene bridged cyclam was prepared using cyclam and 1,2-dibromoethane (sb-cyclam; Figure 7).[89] Two years later, Ramasubbu and Wainwright prepared a similar compound based on cyclen (sb-cyclen; Figure 7).[90,95] The preparation of side-bridged derivatives was also discussed in works of Hancock and coworkers, who prepared various ethylene-bridged macrocyclic tetraamines to promote *trans*-coordination of the transition metal cations.[76,92,96,97] The first cross-bridged structure was designed and synthesized by Weisman and coworkers in 1990. The approach based on bisaminal chemistry brought the *N*-methylated cross-bridge cyclam derivative. Preparation of bisaminal lies in the reaction of cyclam with glyoxal in acetonitrile. The exhaustive methylation of bisaminal leads to dimethylated bisaminal diiodide which is transformed into the product by reductive ring cleavage (Scheme 1). The high regioselectivity of bis quaternization lies in the conformation of bisaminal (Figure 6). The molecule has a convex and concave face. Only the two nitrogen lone pairs on the convex face are sterically available for alkylation.[54,91,93,98,99]

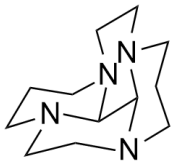

Figure 6: Conformation of bisaminal.

The similar cyclen derivative was prepared by Bencini and coworkers.[84] The high rigidity of derivatives caused by ethylene bridge gave their copper complexes outstanding kinetic inertness.[63,64,100] The bridged derivative of functionalized cyclam was first introduced in 2000 by Wong and coworkers (cb-TE2A; Figure 7).[92] Its cyclen counterpart cb-DO2A (Figure 7) was synthesized a few years later. In complexation studies with copper, it showed much lower kinetic stability than cb-TE2A.[56] Since then, various ethylene-bridged derivatives have been designed and prepared by numerous research groups.[55,67,101,102,103,104,105]

Another interesting and studied type of bridge is the propylene bridge. In 1995, Springborg and coworkers published propylene cross-bridged tetraazamacrocyclic compound, pcb-cyclen (Figure 7). The particular attention was paid to preparation and study of complexes of this ligand with Cu(II) ion with additional ligands (Br^-, I^-, OH^-, H_2O and NH_3) bound in the vacant coordination site.[106,107] In 2011, Odendaal and coworkers reported a new propylene-bridged DOTA derivative (Figure 7). The copper complex of pcb-DO2A showed higher in vitro stability than copper complex of cb-TE2A.[108,109] The cyclam-based derivatives were also studied. Pandya and coworkers introduced various types of azamacrocyclic chelators which were able to form stable Cu(II) complexes, including pcb-TE2A (Figure 7). The usage of the bridge for conjugation with biomolecules was also interesting. This research group also prepared a ligand derived from pcb-TE2A with attached NCS functional group to the propylene bridge for conjugation to appropriate biomolecule (pcb-TE2A-Bn-NCS; Figure 7). The Cu(II)-pcb-TE2A was found to show much higher kinetic stability than Cu(II)-cb-TE2A in acid-assisted decomplexation studies. The quantitative radiolabeling of pcb-TE2A with ^{64}Cu was achieved under milder conditions compared to cb-TE2A. Moreover, the Cu(II)-pcb-TE2A showed high resistance to reduction-mediated demetallization.[109,110,111] Compared to their structural analogues (cb-TE2A and TE2A-Bn-NCS), the propylene bridged derivatives of TE2A showed potential as promising bifunctional chelators for ^{64}Cu.[52]

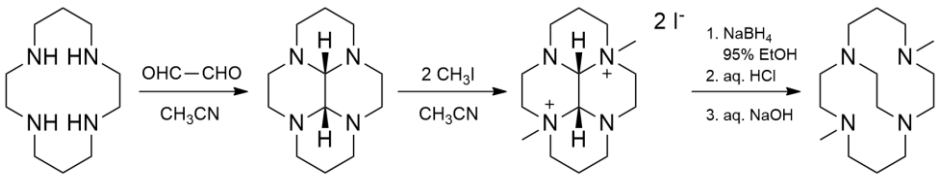

Scheme 1: Preparation of *N*-methylated cross-bridge cyclam derivative.

The derivatives with more than three members of the bridged were also prepared. For example, in addition to the ethylene cross-bridge, Bencini and coworkers published cyclen derivatives with tetra-, penta- and hepta-methylene

bridges.[71,112,113] Denat and coworkers designed and synthesized two small aza-cryptands derived from cyclam. The first derivative contains -CH_2-Ph-CH_2- cross-bridge and the second one has -CH_2-Py-CH_2- unit (Figure 8).[65] Dapporto and coworkers prepared the cross-bridged cyclen derivatives with a bridge containing a -C_2H_4**X**C_2H_4- unit, where X represents -N(CH_3)-, -N(Bz)-, -NH- or -CH_2NHCH_2- (Figure 8). In their work, they paid attention to the influence of nitrogen atoms protonation on cage-like topology.[80]

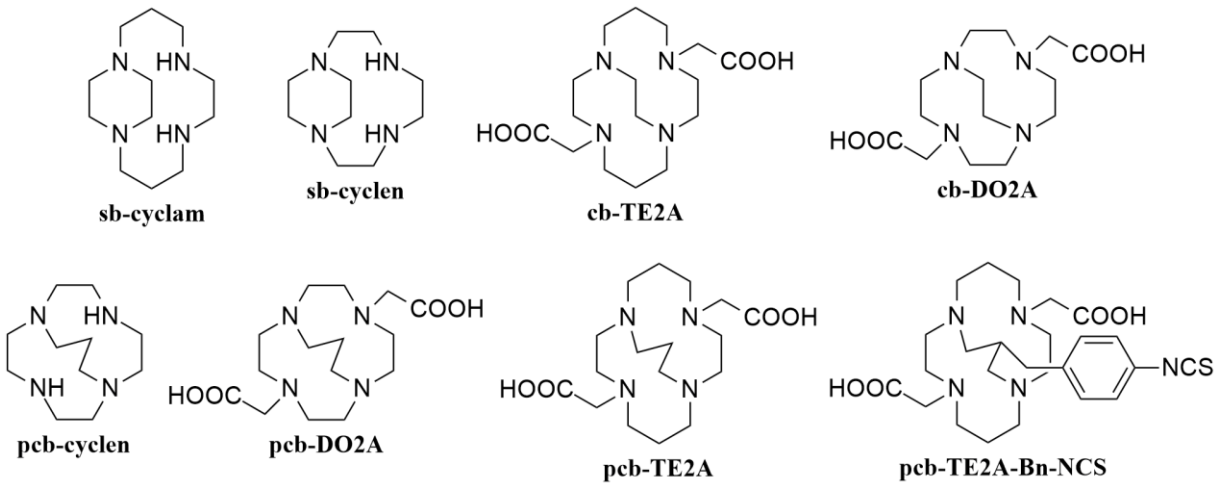

Figure 7: Ethylene and propylene bridged ligands discussed in the text.

The ligand backbone based on hexaammine macrobicyclic cage is used in sarcophagines (Sar) ligand family. The encapsulating character of sarcophagines results in impressively stable complexes. The mentioned ligands are capable of quantitative binding of copper(II) ions with a high complexation rate. The complexation runs under soft conditions at remarkably low concentrations, at room temperature and in the pH range 4–9. Due to these properties, sarcophagine ligands are especially suitable for radiopharmaceutical applications in PET.[54,104,105,114,115,116] The well-known example of the sarcophagine ligand is Diamsar (1,8-Diamino-3,6,10,13,16,19-hexaazabicyclo(6,6,6)eicosane; Figure 8).[117]

Nowadays, scientists are focused mainly on the preparation of ethylene-bridged derivatives which complexes are sufficiently stable for use in medical applications. The commonly used strategy for metal drug design is termed

a *bifunctional approach*. The pharmaceuticals consist of a chelating group for metal and a pharmacophore which are connected by a suitable chemical linker to form a conjugated complex. The pharmacophore should be selected exactly according to the intended biological target from a multitude of endogenous and exogenous biomolecules (antibodies, proteins, peptides and other biologically relevant small molecules), or drug libraries.[54,118,119] Attention is also paid to the *N*-functionalization of azamacrocycles. The pendant arms are used for structure and feature modification. There are several pendants used for these purposes. The most common are, for example, acetate, pyridine, amide, phenolate, picolinate pendant arms. Furthermore, ligands based on phosphonic and phosphinic acids form a significant group of chelators. This work also deals with phosphorous armed derivatives. Therefore, the content of the following chapter is focused on this type of compounds.

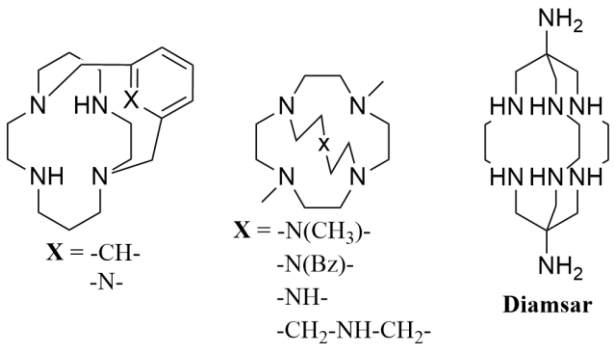

Figure 8: Ligands with the multi-membered bridge.

3.3 Pendant arms

The azamacrocycles themselves have not the best properties for usage in MRI or radiomedicine. Their complexes are struggling with several obstacles. The first one is the positive charge of the resulting complex since the azamacrocyclic skeleton has no charge. The charged complexes are not suitable for most biomedical applications. Working with a relatively high concentration of the contrast medium causes a problem with the ionic strength of the solution, for example in MRI. Another problem is the generally slow complexation of the metal ion. The complexation of macrocyclic compounds does not occur sequentially as it knows for the linear ligands. Coordinated bonds arise simultaneously. An example is a cyclen complex in which all four bonds are formed at the same time. For acceleration of complexation, they need assistance for metal ion transfer to the macrocyclic cavity. Also, the stability of azamacrocycles is not sufficient for safe usage. To overcome the mentioned problems and to create potentially applicable substances, pendant arms are attached to the macrocycles.[120] The suitable selection of pendants also enables ligand selectivity for the particular metal ion. A multitude of synthetic methods for preparing the macrocycles as well as for ligand functionalization by incorporating pendant arms exist. Some of the most used pendants were mentioned in the previous chapter. A lot of attention has been paid to the preparation of acetate functionalized azamacrocyclic chelators, such as derivatives of DOTA, TETA (Figure 5) and NOTA (1,4,7-triazacyclononane-1,4,7-triacetic acid; Figure 9), based on cyclen, cyclam and TACN, respectively.[57,118,119,121] Acetate-functionalized substances also include bridged derivatives. However, they have an even slower rate of complex formation compared to non-bridged derivatives. An example is bifunctional chelator cb-TE2A whose binding to radio-copper is slow, and, it requires relatively harsh labelling conditions (heating to 95 °C for approximately 1.5 hours). This circumstance may constrain its bioconjugation with more fragile target groups.

To solve the slow kinetics of the formation, Ferdani and coworkers developed the second generation of cross-bridged derivatives comprising phosphonate pendant arms. Specifically, it is a cb-cyclam with two phosphonate pendants (cb-TE2P; Figure 9) and cb-cyclam with one acetate arm and one phosphonate arm (cb-TE1A1P; Figure 9).[55] Boswell and coworkers came with a

new ethylene side-bridged cyclam analogue featuring one pendant acetate arm and one pendant methylene phosphonate arm (sb-TE1A1P; Figure 9).[122] The above provides insight into the importance of another widely used pendant arms. These pendants are derivatives of phosphoric acid in which either one hydroxyl group is replaced by an organic substituent (phosphonic acids; Figure 10) or two hydroxyl groups are substituted by organic substituents or hydrogen and an organic substituent (phosphinic acids; Figure 10). The other classification of these substances is according to the distance of the phosphonate group from the macrocycle nitrogen. The methylene group is the most common spacer between phospho(i)nates and the nitrogen atom of the ring. Compounds with this spacer are called α-phospho(i)nates. Thus, attached pendant arm represents an important coordination component of the ligand. A group called distal phospho(i)nates includes compounds with longer spacer than methylene. On the contrary, such pendants do not participate in coordination. Alternatively, they remain only weakly coordinated.

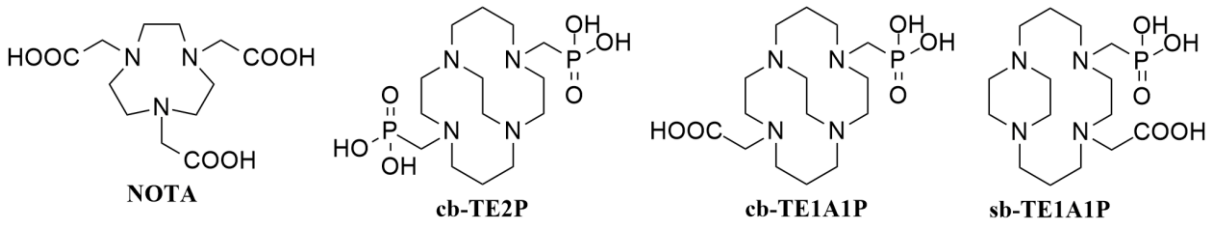

Figure 9: NOTA ligand and ethylene bridged ligands with phosphonate/acetate pendant arms.

The phospho(i)nate derivatives undergo dissociation at a lower pH than carboxylates and modify the basicity of the ring amine groups. It has been reported that cyclen and cyclam derivatives with these pendants have accelerated metal binding kinetics compared to their carboxylate analogues while retaining the high thermodynamic stability of their complexes.[120,123,124,125,126,127] They also show excellent coordination selectivity. The protonation of phospho(i)nates oxygen atom is difficult to achieve. As a result, the metal complexes are sufficiently stable on proton-catalyzed dissociation pathways, which is essential for *in vivo* applications. Phospho(i)nates also increase the hydrophilicity of the

complexes, which alters the pharmacokinetics.[128,129,130,131,132,133,134] Several tetraazamacrocyclic chelators with phosphorus pendants have already been studied.[127,134,135,136,137,138,139,140,141] The following pages are devoted to features and applications of the phospho(i)nate derivatives.

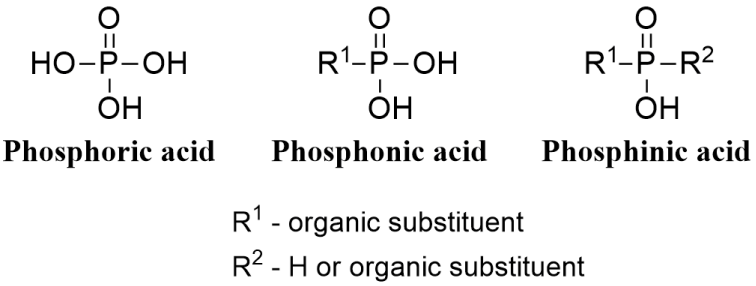

Figure 10: Structure of organophosphorus acids.

3.3.1 Phosphonates

Bone metastases are a class of cancer metastases that result from the invasion of a tumour into the bone. They are a common syndrome of many advanced cancers. Solid matter that forms inside the bone is associated with severe pain, spinal cord compression, and pathological fractures. As many as 50% of patients prescribed anti-resorptive drugs for the treatment of bone metastases develop new bone metastases, skeletal complications and disease progression. This fact emphasizes the need for new therapies.[142,143,144,145,146,147] The characteristic feature of phosphonates is increased absorption on hydroxyapatite (HAP), which is a major inorganic component of bone tissue. Thus, compounds containing a phosphonate group are efficiently adsorbed on the bone surface and are used for bone targeting. The coordination of the metal ion in the macrocyclic cavity leads the phosphonate groups of these ligands to a relative position that is effective for binding to the bone surface. Biodistribution experiments have shown that at least three phosphonate and two bis(phosphonate) groups are required for efficient bone binding. The complexes with bis(phosphonate) pendant arms are very crucial for targeting purposes. Since the bis(phosphonate) group is not coordinated to the central metal ion, it remains active in targeting bone. Conventional treatments, including systemic administration of bisphosphonate drugs, aim to

reduce pain and improve the patient's quality of life. In addition to the therapy of osteolytic bone tumours, bis(phosphonates) can act as anti-resorptive agents in several types of bone diseases, such as osteoporosis, Paget's disease and rheumatoid arthritis.[143,148,149,150,151,152,153,154] Therefore, special attention will be paid to these compounds (see below). The complexes of phosphonates with radionuclides are widely used as radiodiagnostics (^{99m}Tc, ^{186}Re), radiotherapeutics (^{90}Y, ^{153}Sm, ^{166}Ho) and for the palliative treatment of bone metastases (^{153}Sm, ^{186}Re).[126,149,152,153,154,155,156]

Many polyphosphonate complexes have been studied and used as bone targeting agents. In 1984, Kabachnik and coworkers introduced methylphosphonic group to cyclen and TACN and synthetized 1,4,7,10-tetraazacyclododecane-1,4,7,10-tetrakis(methylphosphonic) acid (DOTP; Figure 11)[157] and 1,4,7-triazacyclononane-1,4,7-tris(methylphosphonic) acid (NOTP; Figure 11),[158] respectively. Three years later, the same research group prepared methylphosphonate derivative of TETA specifically 1,4,7,11-tetraazacyclotetradecane-1,4,7,11-tetrakis(methylphosphonic) acid (TETP; Figure 11).[159] The most common ligand is DOTP. The ligand forms stable complexes with many metal ions and has therefore been used as a carrier for a wide variety of radionuclides.[153,160,161,162,163]

A series of DOTA analogues containing two (DO2P^{1,7}; Figure 11), three (DO3P; Figure 11) or four (DOTP) methylphosphonic pendants were radiolabeled with ^{64}Cu in high radiochemical yields. All showed significant bone uptake which makes them potential PET bone imaging agents, as well as bone palliation and therapy agents.[120,126,164,165,166] Of the three complexes, ^{64}Cu-DO2P^{1,7} showed the most optimal clearance through blood and liver. ^{64}Cu-DO3P and ^{64}Cu-DOTP showed higher liver uptake and longer retention of liver activity. The reason is presumably the large negative charge of the complexes under physiological conditions. Due to their structural similarity to DOTA analogue, DOTP and its monoesters have been extensively studied for their potential applications as MRI contrast agents and clinical uses as NMR shift and relaxation reagents.[120,126,164,165,166,167,168,169,170]

The ligands were also studied for application in MRI imaging. The DO2P^{1,4} ligand (Figure 11) with Mn(II) ion showed low relaxivity. There is probably not

enough space for directly coordinated water in its coordinating sphere. Thus, the relaxation is caused only by the contributions of the second and/or outer sphere. Studies on Ln(III) complexes have led to the conclusion that the Gd(III) complex exists in equilibrium of mono- and bis-hydrated species in an aqueous solution. The complex showed a higher relaxivity than the Gd(III) complex of DO3A ligand with two coordinated water molecules. Presumably due to the presence of strong hydration of the second sphere induced by phosphonate groups. Compared to its 1,7-analogue, the Gd(III) complex of DO2P^{1,4} is ~1 order of magnitude more stable. The reason could be a disubstituted ethylenediamine-like structural motif that allows more efficient wrapping of metal ions. Measurement of ^{17}O NMR shift of the water signal showed that the aforementioned DO2P^{1,7} ligand with dysprosium formes the complex with two water molecules coordinated in the inner sphere. The water proton relaxivity data for Gd(III) and Eu(III) complexes provided information about the formation of diprotonated *out-of-cage* complexes at pH below 6.5. The phosphonate groups of DO2P in these complexes are only involved in the bond with the lanthanide cation.[165,171]

The cyclam derivatives with methylenephosphonic arms were also investigated. Specific attention was paid to Cu(II) binding due to the increased selectivity of the cyclam ring system for small metal ions.[125,164,172] The TE1P ligand (Figure 11) forms a very stable Cu(II) complex (logβ(CuL) = 27.34) with high selectivity for copper. The stability of the zinc complex is more than 6 orders of magnitude lower (logβ(ZnL) = 21.03).[124] The cyclam derivatives with methylenephosphonic pendants in trans position (1,8) and the substituent R = H, Me, CH_2Ph in positions 4 and 11 shown high basicity as a consequence of the intramolecular hydrogen bonds. It suggests the high thermodynamic stability of their metal complexes. The ligand with substituent R = H (TE2P^{1,8}; Figure 11) has a high selectivity for copper ions with fast complexation kinetics at pH close to physiological and a high kinetic inertness. High hydrophilicity is also significant due to the presence of phosphonate groups.[125,172] The cyclam ligand with methylphosphonic acid in position 1 and 4 was also studied (TE2P^{1,4}; Figure 11). Its complexing properties towards selected metal ions were detected. As well as TE2P^{1,8} ligand, TE2P^{1,4} has a high selectivity for Cu(II) ions (logβ(CuL) = 27.21).

The stability of the zinc and nickel complexes is notably lower with values of the stability constant 20.16 and 21.92, respectively.[173]

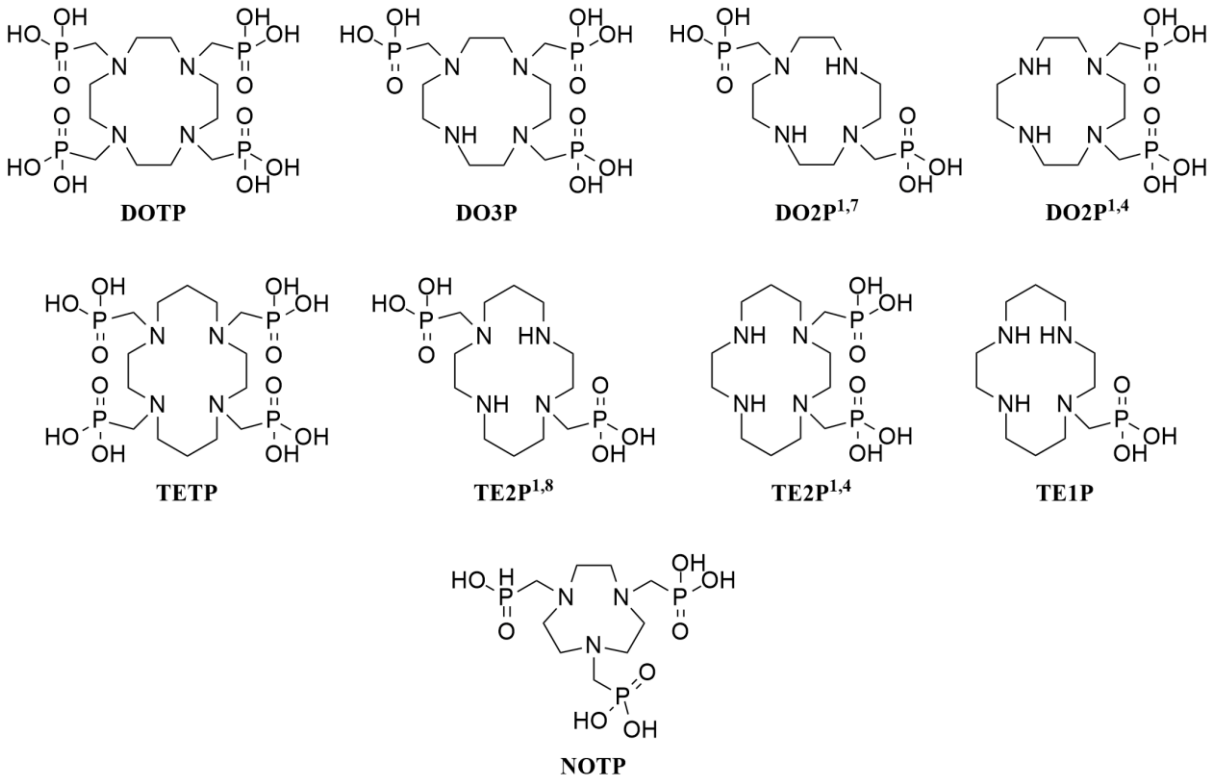

Figure 11: α-phosphonate ligands discussed in the text.

In 1988, Medveď and coworkers have started with the preparation of distal phosphonates.[174] Concretely, they synthesized the TACN derivative in which ring nitrogen atoms are separated from the phosphonate group by ethylene moiety (NOTP^{et}; Figure 12). In comparison with methylene spacer, the presence of a longer chain led to change in the dissociation mechanisms of the compound. Authors investigated the complexation character of the ligand with a wide range of divalent and trivalent ions. The comparison of efficiency and selectivity of complex formation between NOTP and NOTP^{et} showed that the latter has high selectivity to Cu(II) and is generally a more selective agent towards the studied cations. Contrary, the complex formation with NOTP^{et} is much less efficient. This is presumably due to the lower stability of six-membered chelate rings of compound NOTP^{et} compared to the five-membered rings formed by the pendant

groups of NOTP. Polikarpov and coworkers studied analogous cyclen derivative DOTP^{et} (Figure 12) and compared the properties of complexing agents with methylene (NOTP, DOTP and TETP) and ethylene (NOTP^{et} and DOTP^{et}) spacer. The characteristic feature of DOTP^{et} ligand is the formation of an extremely stable complex with Cu(II) ion. In addition, the stability constant of the copper complex is up to 12 orders of magnitude higher than the stability constants of the Co(II) and Ni(II) complexes. It turns out that the ethylene ones are weaker acids but they outperform their analogues in the selectivity of complexation. In the complex formation efficiency, all studied ligands are comparable.[175]

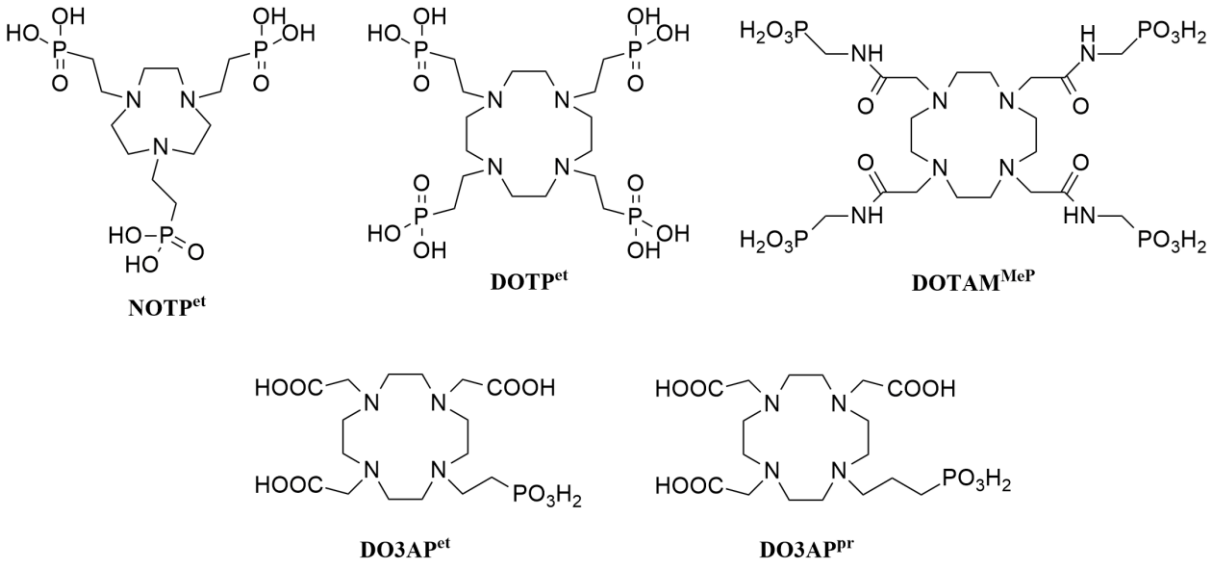

Figure 12: Distal phosphonate ligands discussed in the text.

The use of distal phosphonates as MRI contrast agents was investigated. Zhang and coworkers studied a pH-sensitive tetraamide-based ligand with extended non-coordinating phosphonate side chains (DOTAM^{MeP}; Figure 12).[176] Its Gd(III) complex showed a unique sensitivity of water relaxivity, indicating its suitability for use in MRI experiments to monitor pH changes. Lanthanide complexes of DO3A-alkylphosphonate ligands were also studied with the same intention. Specifically, these are ethyl- and propylphosphonates (DO3AP^{et}, DO3AP^{pr}; Figure 12).[177,178] Relaxometric experiments were performed on Gd(III) complexes. It was found that changing the pH of the medium from pH 7 to pH 4

increased the longitudinal relaxation of the GdDO3A-ethylphosphonate and GdDO3A-propylphosphonate complexes by 50% and 60%, respectively. Luminescence studies on europium(III) complexes supported the findings. This change is explained by the decrease in the number of coordinated water molecules from two to one.

Bis(phosphonates)

Vitha and coworkers prepared the DOTA analogue with phosphinato-bis(phosphonate) pendant arm ($DO3AP^{BP}$; Figure 13). The study with HAP model shown that the relaxivity of Gd(III)-$DO3AP^{BP}$ complex is high. The geminal bis(phosphonic acid) moiety is a highly effective bone-seeking group and remains free for anchoring to osseous tissue. Thus, this compound has potential as a positive MRI contrast agent for bone and other calcified tissues.[153,179] The research of Meckel and coworkers was aimed at evaluating the pharmacokinetics and behaviour of the three bis(phosphonate)-functionalized ligands derived from DOTA ($DOTAM^{BP}$, BPAPD and $DO3AP^{BP}$; Figure 13). High bone uptake values were observed for all studied bisphosphonates. It was also found that the ^{68}Ga-labelled compounds showed rapid clearance from the blood and renal system. ^{68}Ga complexes were also characterized by low binding to soft tissue, leading to a high bone to blood ratio.[142] Bergmann and coworkers recorded very positive results in the field of potential treatment of bone metastases. They synthesized dimeric bis(phosphonate) structures based on DOTA and DO2A ($DOTA(M^{BP})_2$ and $DO2A(P^{BP})_2$; Figure 13). The prepared macrocycles were labelled with ^{177}Lu β-emitter. The complexes showed high bone uptake along with very low soft tissue accumulation.[143] Holub and coworkers studied two NOTA-like ligands with geminal bis(phosphonic acid) attached through acetamide ($NOTAM^{BP}$; Figure 13) or methylenephosphinate ($NO2AP^{BP}$; Figure 13) spacers. Compounds were designed for the complexation of ^{68}Ga. $NO2AP^{BP}$ ligand showed a significantly faster complexation in chemical and radiolabeling studies. This comparison demonstrates the positive effect of phosphinates on the complexation rate. Unfortunately, both ligands suffer from slower complex formation compared to NOTA. The reason is a strong *out-of-cage* binding of bis(phosphonate) group. The efficient binding of ^{68}Ga complexes to HAP was confirmed by *in vitro* sorption

studies. The complexes showed selective and high bone uptake in healthy rats by biodistribution studies *ex vivo* and by PET imaging *in vivo*.[148]

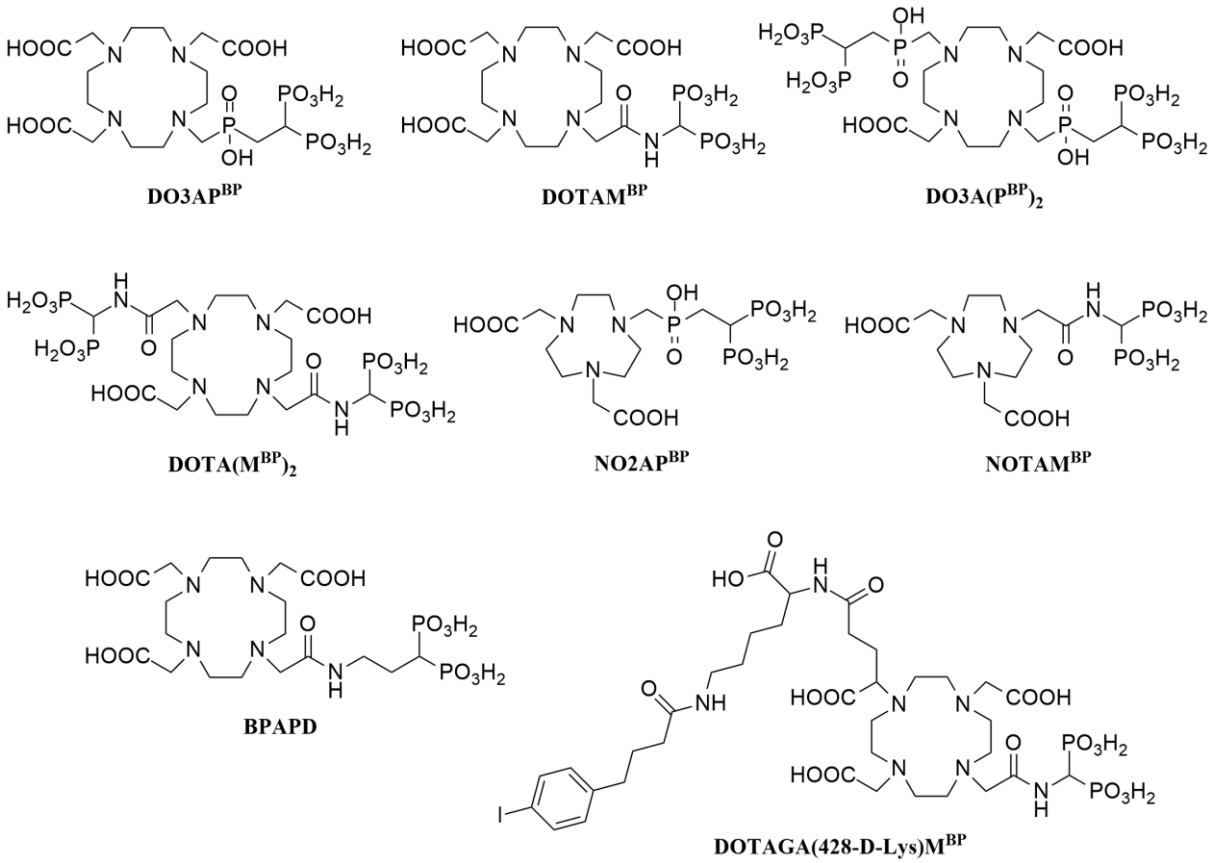

Figure 13: Bis(phosphonate) ligands discussed in the text.

Blood clearance of bis(phosphonates) in the blood is usually rapid. As a rule, only 30%–40% of the administered dose is retained in the skeleton. Most of the activity is flushed out of the body through the urinary system. Longer blood circulation may increase the accumulation of bis(phosphonate) compounds in bone metastases. Because albumin is the most abundant protein in human plasma, in order to expose the body to a sufficient concentration of a therapeutic agent for a sufficiently long time, pharmaceuticals with albumin-binding peptides have been developed. This strategy has also been used for macrocyclic derivatives bearing bis(phosphonates). Meckel and coworkers modified the DOTAM^{BP} with human albumin binding entity (DOTAGA(**428**-D-Lys)M^{BP}; Figure 13) and studied the pharmacokinetics both ligands labelled with ^{68}Ga(III). It was found that the

^{68}Ga-DOTAGA(**428**-D-Lys)M^{BP} shows significantly longer blood circulating time than ^{68}Ga-DOTAM^{BP} and delayed body clearance. Moreover, the ratio between the high-metabolic joints and the ordinary bone was also better for the modified ligand compared to the non-modified parent compound.[144,145,146,147,180,181,182]

Recently, our research group found that the introduction of a strongly complexing pendant, such as bis(phosphonate) group, leads to a reduction in the rate of in-cage complex formation due to excessive stabilization of the *out-of-cage* intermediate.[183,184,185] Therefore, it is necessary to keep in mind the possible limitations associated with the above-mentioned in the design of new effective bone targeting agents.

3.3.2 Phosphinates

Phosphinates are a very interesting group for the design of new ligands. One of their most important advantages is the structural variations of phosphorus substituents. The functionalization can be obtained via changing of R group in $NCH_2P(R)O_2H$ arm.[141,186,187,188,189,190] The pentavalency of phosphorus enables attachment of alkyl or aryl substituent which may lead to easier linkage to biomolecules, the control of ligand and complex lipophilicity or improvement of the ion selectivity of macrocyclic compounds. Each phosphinate group may bear two carbon atoms. Thus, it is one of the few negatively charged groups which can be incorporated in the middle of the chain.[191,192,193] This exceptional property brings several advantages. It is possible to form ligands in which the macrocycle already has a compensated positive charge of the complex. It is also possible to form ligands with macrobicyclic structure. Another benefit is a significant increase in the complexation degree. It has been found that the introduction of a bis(phosphinate) pendant into the macrocyclic ring significantly affects complexation. Nevertheless, this group has not yet gained adequate attention. The evidence is a low number of publications and complexation studies on mentioned theme.[194,195,196]

The disadvantage of phosphinates compared to carboxylate or phosphonate analogues is the formation of complexes with lower stability. Lazar and coworkers prepared methylene(ethyl)phosphinate derivative based on cyclen (DOTEP;

Figure 14). The phosphinate pendants are protonated only below pH 4. In comparison with DOTA, ligand forms less stable complexes with Cu(II), Zn(II), Cd(II) and Ln(III) ions. The main reason is the lower basicity of nitrogen and oxygen donor atoms. The similarity was found in the formation rate of lanthanide complexes. The DOTEP ligand, as well as DOTA, has a relatively slow rate of complexation in the pH range 6–7. On the contrary, the kinetic stability of $Ln(DOTEP)^-$ complexes is high. In strong acid, they release free Ln(III) ions rather slowly.[141]

Three investigated TRAP ligands (triazacyclononane phosphinic acids; Figure 14) were also compared with the DOTA derivative as one of common Ga(III) ion chelators. The 1,4,7-triazacyclononane derivatives bearing methylphosphinic (TRAP-H), methyl(phenyl)phosphinic (TRAP-Ph), or methyl(hydroxymethyl)phosphinic acid (TRAP-OH) pendant arms exhibited high thermodynamic selectivity for galium(III) ions. The complexes were kinetically inert in both acidic and alkaline solutions. Moreover, compared to DOTA derivatives, these new ligands show fast complexation (minutes) of Ga(III) over a wide pH range. Therefore, they may be an attractive alternative for the development of ^{68}Ga radiopharmaceuticals.[140] High thermodynamic stability and kinetic inertness also characterize the galium(III) complex of trisubstituted triazacyclononane with methyl(2-carboxyethyl)phosphinic acid pendant arms (TRAP-Pr; Figure 14). With a stability constant value of 26.24 and a high inertness to decomplexation, the Ga(III)-TRAP-Pr is suitable for positron emission tomography. Besides, labelling of the ligand with ^{68}Ga is possible at ambient temperature and over a wide pH range.[197]

The work of Pulukkody and coworkers has shown the versatility of macrocyclic azaphosphinic acids as complexing agents for *in vivo* applications. Through the selective functionalization of one ring nitrogen atom or by changing of *P*-substituent nature, they synthesized 18 novel cyclen compounds. Their anionic, neutral and cationic yttrium and gadolinium complexes differed in lipophilicity and dissociation kinetics. Ligands DO3MePM and DOTMeP^{Ph} displayed the best properties (Figure 14). The bifunctional complexing agent DO3MePM showed short synthesis, efficient ^{90}Y labelling and easy protein

conjugation. The Gd(III)-DOTMeP^{Ph} complex, in turn, is an interesting agent for MRI imaging. It is relatively stable *in vivo* with easy synthesis and purification.[189]

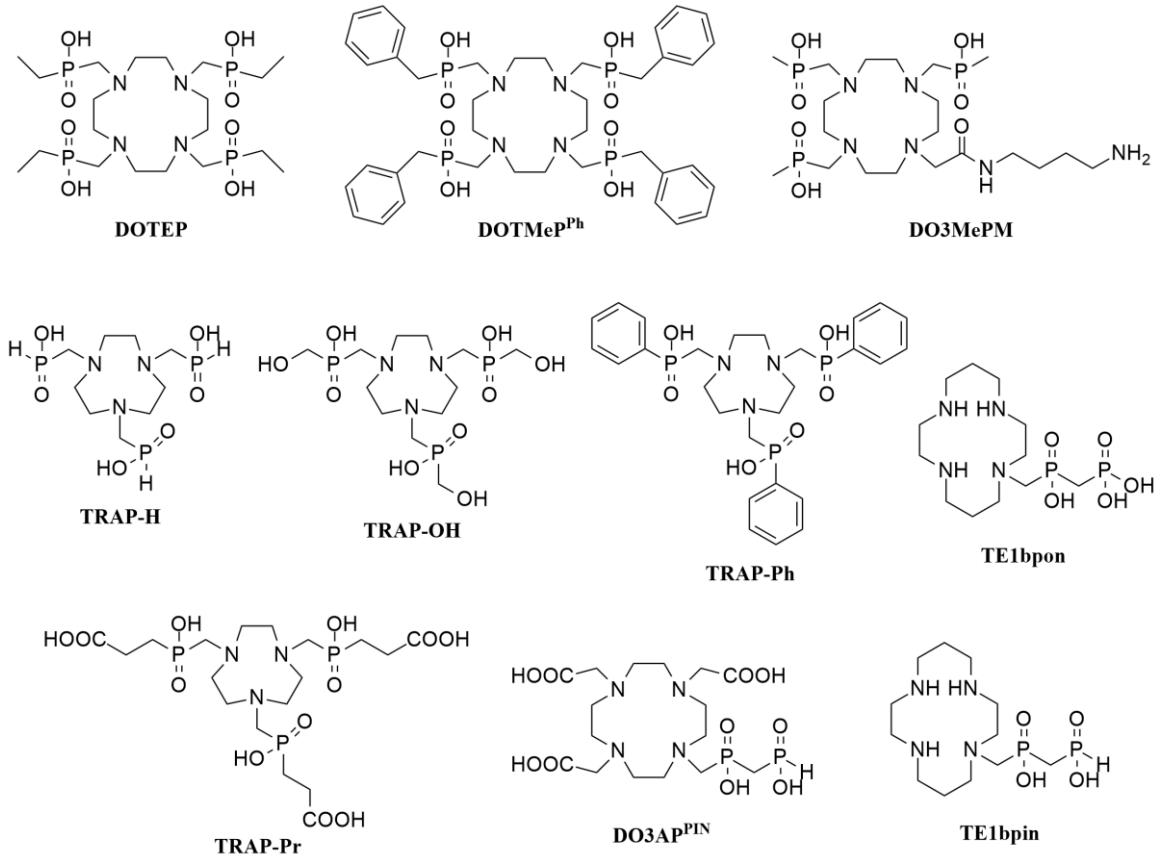

Figure 14: α-phosphinate ligands discussed in the text.

Cyclam derivatives bearing geminal bis(phosphinic) (TE1bpin; Figure 14) or phosphinato-phosphonic (TE1bpon; Figure 14) pendant arms have been synthesized and studied as potential copper(II) chelators for nuclear medicine applications. The ligands showed a unique combination of excellent properties. They were characterized by good selectivity for copper ions. The complexes had high thermodynamic stability and kinetic inertness. Radiolabeling with ^{64}Cu was fast and effective even at room temperature. Moreover, the specific activities of the complexes were much higher than the activities of the NOTA and DOTA complexes prepared under the same conditions.[196] The excellent properties provided by the bis(phosphinate) group were also demonstrated on the DOTA analogue bearing this pendant arm (DO3AP^{PIN}; Figure 14). An improved yield of

^{177}Lu(III) radiolabel was found for this ligand, which forms stable intermediates under acidic conditions.[183]

Another group of derivatives are distal phosphinates. Examples are nonadentate ligands based on triazacyclononane containing pyridyl-2-phosphinate groups. These are chelators suitable for the complexation of Ln(III) ions for use in luminescent applications. Phosphorus substituents have a common configuration in the complex and more effectively protect the excited Ln(III) ion from intermolecular quenching processes. Europium(III) complexes were investigated in cell imaging applications and selected terbium(III) complexes were studied as potential oxygen sensors. Emissive lanthanide(III) complexes are used as tags in biological assays or as intracellular optical probes.[198,199,200] Substances prepared by Walton and coworkers containing phenylphosphinate or methylphosphinate form an isostructural series of solid state complexes (TACN-pyridine-R-phosphinate; Figure 15).[201,202] The Ln(III) ion is effectively protected from the solvent environment, which results in a very low relaxivity of the gadolinium complexes in the aqueous environment. This also leads to suppression of the deactivation of the emissive lanthanide excited state by the vibrational energy transfer to the solvent oscillators. Thus, the total quantum emission yields are very high for terbium(III), samarium(III) and dysprosium(III) complexes in the aqueous environment and the lifetime in the excited state is long and does not change significantly in D_2O. Furthermore, a series of high-emission europium(III) complexes were prepared. In designing these systems, highly efficient shielding of the Eu(III) ion using triazacyclononane-based nonadentate ligands was combined with strongly absorbing *p*-substituted aryl-alkynyl groups (Figure 15). The complexes enter mammalian cells by macropinocytosis and selectively stain mitochondria. This allows the observation of Eu(III) emission *in cellulo* by time-limited spectral imaging. It is possible to use them in microscopic imaging.[199]

Many similar structures have been prepared and studied with *p*-methoxy, *p*-oxyacetate, *p*-gluconamide, and many other substituents. Complexes of such substances readily enter mammalian cells, preferentially staining mitochondria and subsequently migrating to lysosomes. Because it is easy to attach substituents to ring nitrogen or *p*-aryl sites, the development of additional organelle-specific or

responsive emission probes operating at low concentrations due to their high inherent optical brightness can be expected.[200,203,204]

The specific examples given above show the benefits of the usage of phosphinates. With their versatility, they make a significant contribution to the design of new, more efficient imaging agents for a wide range of medical applications. Our group has been very intensively involved in the preparation of phosphorus derivatives for decades. Therefore, many of them are mentioned in the submitted text.

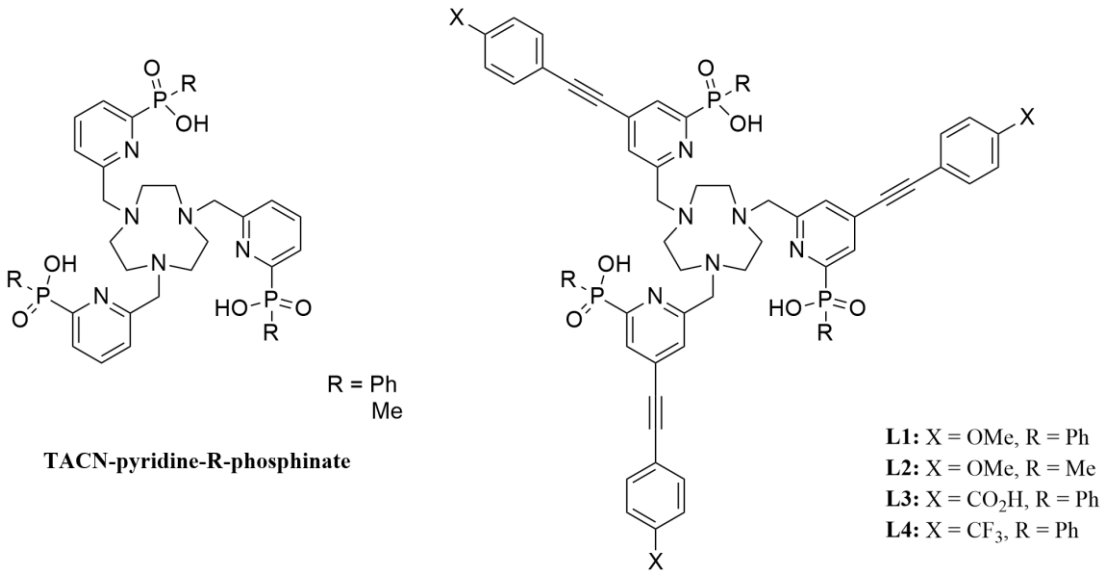

Figure 15: Distal phosphinate ligands discussed in the text.

4 Bis(phosphinate)-bridged ligands

Until now, only a few scientific works have dealt with the introduction of a phosphorus moiety into the macrocyclic chain.[191,192,193] Excellent features of bis(phosphinic acid), which our group verified in recent studies,[183,196] inspired us to use this group in the preparation of macrobicyclic ligands. The TACN and the cyclen core have been chosen as default monocycles. The designed compounds bring the first insight into the properties of such modified ligands and their complexes with selected metal ions. The following chapters will be devoted to the synthetic strategy of ligands and the structure of their complexes. Their thermodynamic properties will be also discussed. All details on this topic are presented in the papers reprinted in Appendices 1[205] and 2[206].

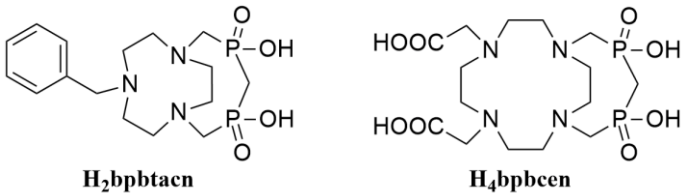

Figure 16: The macrobicyclic derivatives of TACN and cyclen.

4.1 Results and Discussion

4.1.1 Synthesis and structure

The synthetic strategy was based on the two-step reaction of the Mannich-type and the subsequent alkylation in the case of the cyclen derivative (Schemes 2 and 3). Each synthetic step is characterized by a high yield. In the first step, the selected azamacrocycle (cyclen or 1-benzyl-1,4,7-triazacyclononane) was treated with methylene-bis(phosphinic acid) and paraformaldehyde under acidic conditions in aq. HCl. The sub-stoichiometric amount of paraformaldehyde ensured monosubstitution. The excess of azamacrocycle and methylene-bis(phosphinic acid) was removed by purification on a strong cation-exchange resin. The second step included the reaction of compound **1a** or **1b** from the first step and paraformaldehyde under acidic condition. The reaction

was performed under high dilution to prevent polymerization. The TACN product (H_2**bpbtacn**; Figure 16) was obtained after purification on a strong cation-exchange resin (Scheme 2). The cyclen precursor (compound **2b**) was purified by strong cation-exchange and flash chromatography. The two secondary amino groups of compound **2b** were modified with chloroacetic acid which was added to the reaction in two portions. The alkylation ran under alkali conditions in presence of LiOH. The cyclen product (H_4**bpbcen**; Figure 16) was obtained after purification of the mixture on a strong cation-exchange resin (Scheme 3).

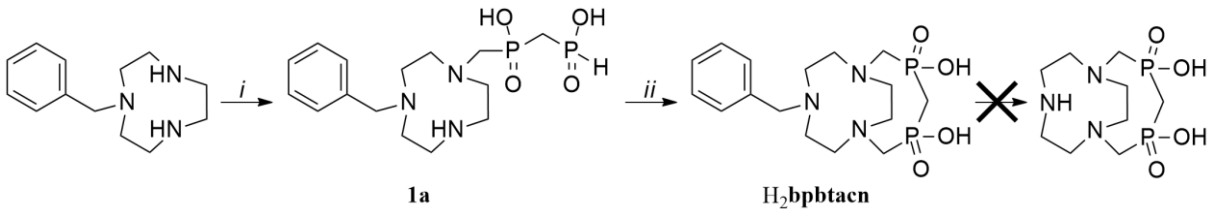

Scheme 2: Synthesis of H_2**bpbtacn**. (*i*) $CH_2(PO_2H_2)_2$, $(CH_2O)_n$, 6 M aq. HCl, 60 °C, 3 d (83%); (*ii*) $(CH_2O)_n$, conc. aq. HCl:AcOH (1:1), high-dilution, 80 °C, 4 d (86%).

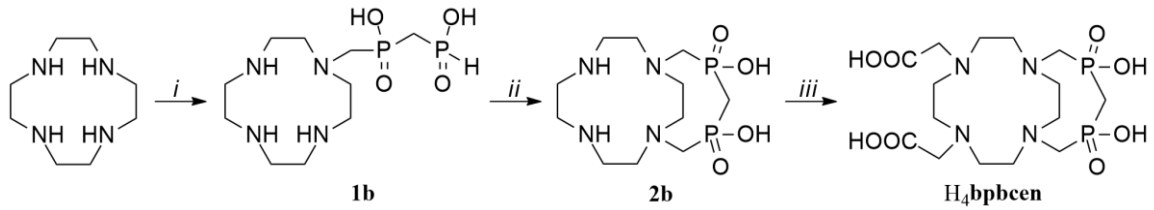

Scheme 3: Synthesis of H_4**bpbcen**. (*i*) $CH_2(PO_2H_2)_2$, $(CH_2O)_n$, 6 M aq. HCl, 40 °C, 2 d (75%); (*ii*) $(CH_2O)_n$, 6 M aq. HCl, high-dilution, 90 °C, 24 h (61%); (iii) $ClCH_2COOH$, water, pH ~12 (LiOH), 60 °C, 3 d (87%).

The original idea was to remove protecting benzyl group from H_2**bpbtacn** after connection of the bis(phosphinic) side bridge to TACN ring. Such a macrobicycle would have an available secondary amine for further functionalization. Unfortunately, deprotection was unsuccessful despite a number of attempts. No reaction was observed when debenzylation methods run under ambient conditions (Pd/C with hydrogen or transfer hydrogenation by formate and hypophosphite). Increasing the temperature or pressure of the hydrogen, in turn,

led to the decomposition of the macrobicyclic structure. The decomposition occurred even after treatment with Cbz-chloride. Due to the unsuccessful deprotection, the benzylated ligand H_2**bpbtacn** was further investigated.

The copper and nickel complexes of H_2**bpbtacn** and copper complex of H_4**bpbcen** were prepared and their crystal structures were obtained. Because of a very similar structural motif found in H_2**bpbtacn** complexes, the attention will be paid only to solid-state Cu(II) complex.

Complexes of H_2**bpbtacn** and H_4**bpbcen** with Cu(II) ion are quite different. The copper complex [{Cu(**bpbtacn**)}$_2$]·5H_2O formes structural motif consisting of centrosymmetric dimeric species. The central metal ion is hexacoordinated with distorted octahedral geometry. The equatorial plane comprises of two nitrogen atoms from macrocycle (N1 and N4) and two oxygen atoms from bis(phosphinic) side bridge (O11$^{\#}$ and O21$^{\#}$) originating from the centrosymmetry-related neighbouring unit (Figure 17). Coordinated bis(phosphonate) thus formes a six-membered chelate ring. The axial positions are very distant due to significant Jahn-Teller distortion and are occupied with nitrogen atom N7 and oxygen atom O11 of the same ligand unit. Geometric parameters of Cu(II) coordination sphere are outlined in Table 1.

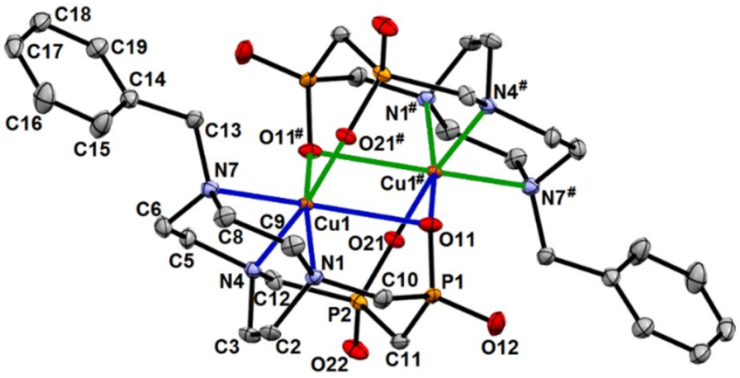

Figure 17: Molecular structure of the dimeric complex unit {[Cu(**bpbtacn**)]}$_2$ found in the crystal structure of [{Cu(**bpbtacn**)}$_2$]·5H_2O. Hydrogen atoms are not displayed for sake of clarity. Selected centrosymmetry-related atoms are labelled by "#". Coordination bonds of each ligand molecule are highlighted in blue or green, respectively.

The crystal structure of the Li_2[Cu(**bpbcen**)]·$4H_2O$ is formed by two centrosymmetrically related [Cu(**bpbcen**)]$^{2-}$ units connected through tetrahedral coordination to one of Li(I) counter-ion. The connection is via two oxygen atoms of bis(phosphonic) bridge (O11 and O21), one oxygen atom of the acetate pendant (O31) and one oxygen atom of bis(phosphinate) (O22$^{\#}$) from centrosymmetry-related unit. The central metal ion is pentacoordinated and possesses a geometry of distorted square-pyramid. All four nitrogen atoms of macrocycles are coordinated. The N_4-basal plane is almost perfectly symmetric. The fifth position is occupied with an oxygen atom (O11) of the side bridge bis(phosphinate) moiety. Because of the short chelate ring, the apical oxygen is unsymmetrically placed. The oxygen atom (O31) of one acetate pendant arm is rotated towards the copper ion (Figure 18). However, the Cu···O31 distance is too long (3.28 Å) to be a semicoordinative interaction (Table 1).

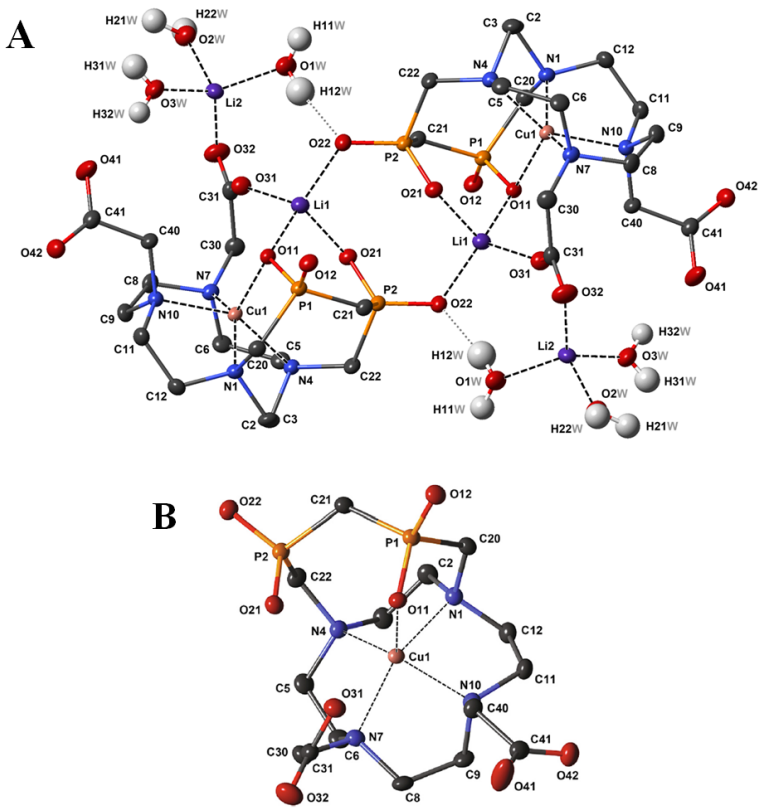

Figure 18: (A) Dimeric structure {Li[Li(H_2O)$_3$][Cu(**bpbcen**)]}$_2$ found in the crystal structure of Li_2[Cu(**bpbcen**)]·$4H_2O$. The carbon-bound hydrogen atoms and one water molecule of crystallization are not displayed for sake of clarity. (B) Molecular structure of [Cu(**bpbcen**)]$^{2-}$ species found in the crystal structure of Li_2[Cu(**bpbcen**)]·$4H_2O$. The hydrogen atoms are not displayed for sake of clarity.

Table 1: Geometric parameters of Cu(II) coordination sphere found in the crystal structures of $[\{Cu(bpbtacn)\}_2]\cdot 5H_2O$ and $Li_2[Cu(bpbcen)]\cdot 4H_2O$.

$[\{Cu(\mathbf{bpbtacn})\}_2]\cdot 5H_2O$		$Li_2[Cu(\mathbf{bpbcen})]\cdot 4H_2O$	
Distances (Å)			
Cu1–N1	2.049(1)	Cu1–N1	2.068(2)
Cu1–N4	2.044(1)	Cu1–N4	2.120(2)
Cu1···N7	2.330(1)	Cu1–N7	2.072(2)
Cu1–O11$^{\#}$	1.935(1)	Cu1–N10	2.073(2)
Cu1–O21$^{\#}$	1.966(1)	Cu1–O11	2.194(2)
Cu1···O11	2.641(1)		
Angles (°)			
N1–Cu1–N4	84.16(5)	N1–Cu1–N4	84.07(7)
N1–Cu1···N7	80.26(5)	N1–Cu1–N7	148.31(7)
N1–Cu1–O11$^{\#}$	164.72(5)	N1–Cu1–N10	85.36(7)
N1–Cu1–O21$^{\#}$	96.70(5)	N1–Cu1–O11	87.56(6)
N1–Cu1···O11	84.73(4)	N4–Cu1–N7	87.32(7)
N4–Cu1···N7	83.88(5)	N4–Cu1–N10	148.50(7)
N4–Cu1–O11$^{\#}$	88.76(5)	N4–Cu1–O11	116.52(6)
N4–Cu1–O21$^{\#}$	172.54(5)	N7–Cu1–N10	86.29(7)
N4–Cu1···O11	109.29(4)	N7–Cu1–O11	123.33(7)
N7···Cu1–O11$^{\#}$	112.48(5)	N10–Cu1–O11	92.53(6)
N7···Cu1–O21$^{\#}$	88.95(4)		
N7···Cu1···O11	158.94(4)		
O11$^{\#}$–Cu1–O21$^{\#}$	92.08(4)		
O11$^{\#}$–Cu1···O11	84.87(4)		
O21$^{\#}$–Cu1···O11	78.17(4)		

Symmetry code #: $-x+1, -y+1, -z+1$.

The similarity of the ligands lies in rigidity of the macrobicyclic structure, which does not allow simultaneous coordination of the azamacrocycle amine groups and both phosphinate anions of the pendant to the same metal ion. The bidentate attachment is possible, but either to the central atom of the second molecule (H_2**bpbtacn**) or to the counter-ion (H_4**bpbcen**). In addition, the fact that the bis(phosphinate) is monocoordinated does not allow to obtain the same

geometry for all three nitrogen atoms in H_2**bpbtacn**. Thus, one of the macrocycle chelate rings has to be twisted in the opposite direction to other ones. This phenomenon is very uncommon in complexes of TACN derivatives and suggests the considerable steric strain in the coordinated ligand.

4.1.2 Equilibrium studies

Protonation constants of the ligands and stability constants of their complexes with selected metal ion have been determined by potentiometric titrations. For the H_2**bpbtacn** ligand, the three protonation constants were found. The first two determined constants are connected with macrocycle protonation ($\log K_1$ = 12.25 and $\log K_2$ = 5.74). The first protonation occurs in the strong alkaline region. The value is quite high, which may be concerned with the strong intramolecular hydrogen bond found in the solid-state structure of the ligand dilithium(I) salt (Appendix 1). This is also related to the observation of our research group that the introduction of a geminal bis(phosphinate) pendant does not decrease the basicity of the ring amines as in the case of a simple phosphinate group.[120,196] This observation is also applied for H_4**bpbcen** ligand with five determined protonation constants. The first two protonations lie within the range typical for ring amine protonations of substituted cyclen derivatives ($\log K_1$ = 12.70 and $\log K_2$ = 9.15). The distribution diagrams showed that the monoprotonated species [H**bpbtacn**]$^-$ and the diprotonated species [H_2**bpbcen**]$^{2-}$ are dominant in the neutral region. The bis(phospinate) group of both ligands is protonated only in strongly acidic solution (pH < 2.5; Table 2A).

For H_2**bpbtacn** ligand, only stability constants for copper complexes could be determined. The monoprotonated species [Cu(H**bpbtacn**)]$^+$ is formed at the strongly acidic pH (~1). It is presumably enabled by coordination of bis(phosphonate) group due to its high acidity. This assumption is also supported by UV-Vis measurements. The formation of a protonated complex was followed by increasing the intensity of d-d transition band in the pH range 1–4. The position of the absorption band remains unchanged, which indicates coordination of oxygen donor atoms only (Figure 19). The fully deprotonated complex [Cu(**bpbtacn**)] is formed at pH > 4. The UV-Vis spectrum shows the blue shift of the absorption band maximum due to the coordination of ring nitrogen atoms on Cu(II) ion.

Unfortunately, the value of the stability constant for the stated complex is low and is more than ten orders of magnitude lower than that of $[Cu(NOTA)]^-$ (Table 2B).[207] This is attributed not only to the lower basicity of the macrocycle but also to the high rigidity of the ligand structure. It is also responsible for the sterically unfavourable TACN ring conformation described above. During the potentiometry, no changes of titration curves were observed for complexes of Zn(II) and Ni(II) ions at pH < 4. At this pH range, only a negligible amount of complex was formed, which suggests even lower stability of the zinc and nickel complexes compared to the copper complex. This observation also coincides with the Irving-Williams series for the order of complex stabilities. The insoluble metal complexes were formed and precipitated in the measuring cell at pH > 4.

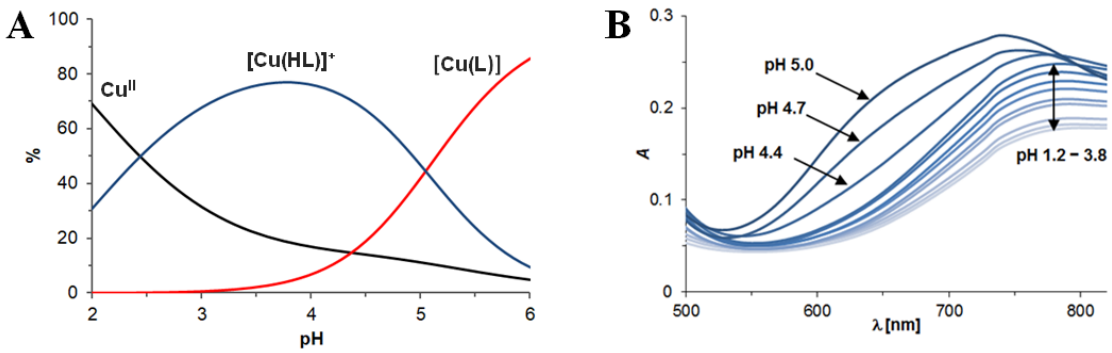

Figure 19: Distribution diagram (A) and the UV-Vis spectra (B) of Cu(II)-H_2**bpbtacn** system.

The thermodynamic properties of the second studied ligand H_4**bpbcen** were examined with divalent metal ions (Cu^{II}, Zn^{II}) but also with selected trivalent lanthanide ions (La^{III}, Gd^{III}, Lu^{III}). Copper and zinc systems are mutually similar. In comparison to Cu(II)-H_2**bpbtacn** system, their distribution diagrams additionally contain the diprotonated species. Complexation of metal ions, as for H_2**bpbtacn**, begins in the strongly acidic region to form a neutral [M(H_2**bpbcen**)] species. The chemical model of the Cu(II)-H_4**bpbcen** system was confirmed via the UV-Vis measurements at various pH. The result showed perfect conformity of d-d transition band intensity at 650 nm with a distribution diagram (Figure 20). The monoprotonated $[M(H\mathbf{bpbcen})]^-$ species reaches the maximum abundance at pH ~3.5. At this pH, the fully deprotonated species $[M(\mathbf{bpbcen})]^{2-}$ starts to form.

As well as for Cu(II)-H_2**bpbtacn**, the [M(**bpbcen**)]$^{2-}$ are dominant species in the neutral region. The values of the stability constants of mono- and diprotonated species correspond to the values of protonation constants logK_3 and logK_4 of the free ligand. The mentioned indicates coordination of all nitrogen donor atoms which is supported by UV-Vis absorption spectres of the [Cu(H_2**bpbcen**)] species. The values of stability constants for [Cu(**bpbcen**)]$^{2-}$ and [Zn(**bpbcen**)]$^{2-}$ complexes, unlike for the [Cu(**bpbtacn**)], are quite high. They are in accordance with the Irving-Williams series and are higher than stability constants for analogous ligands with phosphorous pendant arms.[171] This may be associated to high macrocycle basicity of the H_4**bpbcen** ligand.

For the Ln(III)-H_4**bpbcen** systems, the similarity of stability constants and distribution diagrams is obvious. The distribution diagram consists of only two species, namely [M(H_2**bpbcen**)]$^{+}$ and [M(**bpbcen**)]$^{-}$. The absence of the monoprotonated species is very common for Ln(III)-DOTA-like systems. It points to transfer of the *out-of-cage* complex to the *in-cage* complex via simultaneously removing of two protons bound on the ring nitrogen atoms at pH > 6. Thus, the diprotonated complex is coordinated only through donor atoms of pendants and the complexation starts at pH 1–2. Dominant species in the neutral region is the negative fully deprotonated [M(**bpbcen**)]$^{-}$ complex. The thermodynamic stability of the Ln(III) complexes is very low. In comparison to Ln(III)-DOTA complexes, the values of stability constants are 7–10 orders of magnitude lower.[208,209] This is also reflected in the formation of Ln(III) hydroxides already in a weakly alkaline environment. Presumably, even behind these values are the steric requirements of bis(phosphinate) group. The pendant arms in the Ln(III)-H_4**bpbcen** complexes cannot have a synchronous orientation and one phosphinate group must be turned in the opposite direction. Thus, the simultaneous coordination of both phosphinate moieties is not allowed. All determined stability constants are displayed in Table 2B.

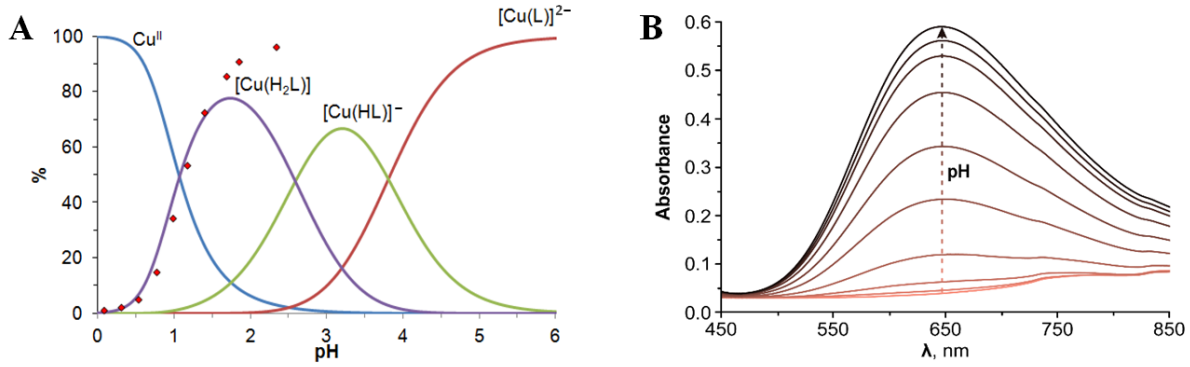

Figure 20: Distribution diagram (A) and the UV-Vis spectra (B) of Cu(II)-H$_4$**bpbcen** system. The absorption of Cu(II) complex at 648 nm is shown as red dots.

Table 2: (A) Stepwise protonation constants of the ligands. Overall protonation constants log*β* of the ligands are given in italics. (B) Stability constants logK_{ML} of the complexes.

	H$_2$**bpbtacn**	H$_4$**bpbcen**
A		
logK_1	12.25	12.70
	12.25±0.01	*12.70±0.01*
logK_2	3.65	9.15
	15.90±0.02	*21.85±0.01*
logK_3	1.44	4.39
	17.35±0.02	*26.24±0.01*
logK_4	–	2.26
		28.50±0.01
logK_5	–	1.08
		29.58±0.02
B		
Cu(II)	11.18	22.97
Zn(II)	–	19.59
La(III)	–	14.89
Gd(III)	–	14.90
Lu(III)	–	15.60

4.2 Conclusions

The combination of macrocyclic ring with a geminal bis(phosphinate) side bridge arise the new class of macrobicyclic ligands. The preparation of the TACN-based derivative was a two-step procedure including the Mannich-type reactions. The ligand containing the cyclen core was synthesized by the combination of two-step Mannich-type reactions and alkylation. Both ligands were obtained in high yield. Potentiometric studies revealed low thermodynamic stability of the H_2**bpbtacn** complex with Cu(II) ion which is attributed to the high rigidity of the ligand structure. The high rigidity is also responsible for monodentate coordination of the bis(phosphinate) group and the sterically unfavourable conformation of the TACN ring. On the other hand, the stability of the Cu(II) and Zn(II) complexes of H_4**bpbcen** is similar to related DOTA-like derivatives which is presumably associated with the higher basicity of the macrocycle. Unfortunately, despite the same number and type of donor atoms, the H_4**bpbcen** is not appropriate for the coordination of lanthanide ions. This is also related to the geometry of the macrobicyclic ligand as in the case of the H_2**bpbtacn**. Given the properties of the H_2**bpbtacn** and H_4**bpbcen** derivatives, it is obvious that the other members of this class of chelators must have an optimized structure. Then new possibilities for their application in coordination chemistry will open up.

5 Cyclam derivatives for complexation of copper radioisotopes

Copper is a promising therapeutic element and its radioisotopes are attracting increasing attention. Cyclam and its derivatives are the ligands of the first choice for copper ions due to the high thermodynamic selectivity for Cu(II) and the high kinetic inertness of their complexes.[125,196] We also focused on the design, synthesis and study of cyclam chelators. Specifically, these are three bridged ligands with phosphonate (H_4**cb-TE2P**), bis(phosphinate) (H_4**cb-TE2bpin**) or phosphinate (H_2**cb-TE2P^{H}**) pendants and a non-bridged derivative with phosphinate-bis(phosphonate) (H_5**TE1P^{BP}**) pendant arm (Figure 21). The structure of the bridged derivatives was chosen in an effort to increase the stability of the complexes and simultaneously accelerate the complex formation depending on the type of the used pendant arm. The ligand with bis(phosphonate) pendant, in turn, was designed for bone targeting and also to study the effect of a strongly coordinating pendant arm on the complexation rate.

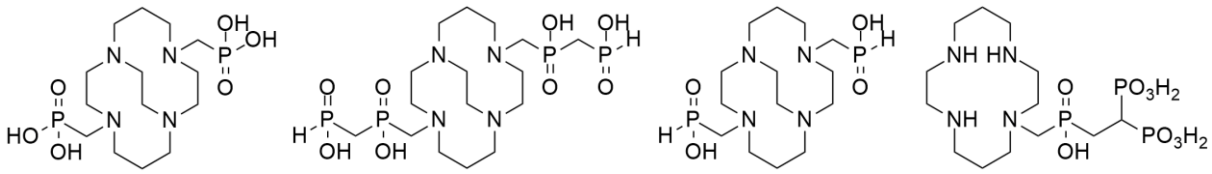

Figure 21: The cyclam derivatives with phosphorus pendant arms.

The submitted chapter mainly deals with thermodynamic properties of the ligands and their Cu(II) complexes, as well as the formation and dissociation kinetics of these complexes. Moreover, the sorption on HAP, labelling and biodistribution studies are reported for the non-bridged derivative. Less attention is paid to the synthesis and structure of presented compounds. All detailed information on the studied ligands is given in Appendices 3[103] and 4.

5.1 Results and Discussion

5.1.1 Synthesis and structure

The synthetic strategy of the presented ligands is based on phospha-Mannich reaction. Cb-derivatives were prepared via reaction of cb-cyclam with paraformaldehyde and the corresponding phosphorus precursor, specifically, phosphorous acid, methylene-bis(phosphinic acid) and hypophosphorous acid for H_4**TE2P**, H_4**TE2bpin** and H_2**TE2P^{H}**, respectively (Scheme 4). The products were obtained by purification on strong cation exchange resin and in a high yield for phosphonate and phosphinate derivatives (~80%). The reaction for bis(phosphinate) derivative does not proceed quantitatively, thus, the H_4**TE2bpin** was isolated in a moderate yield (48%). The H_5**TE1P^{BP}** ligand was prepared by reaction of triprotected cyclam with bis(phosphonate)-phosphinate reagent. After deprotection and purification on strong cation exchange resin, the H_5**TE1P^{BP}** was obtained in zwitter-ionic form in 74% yield (Scheme 5).

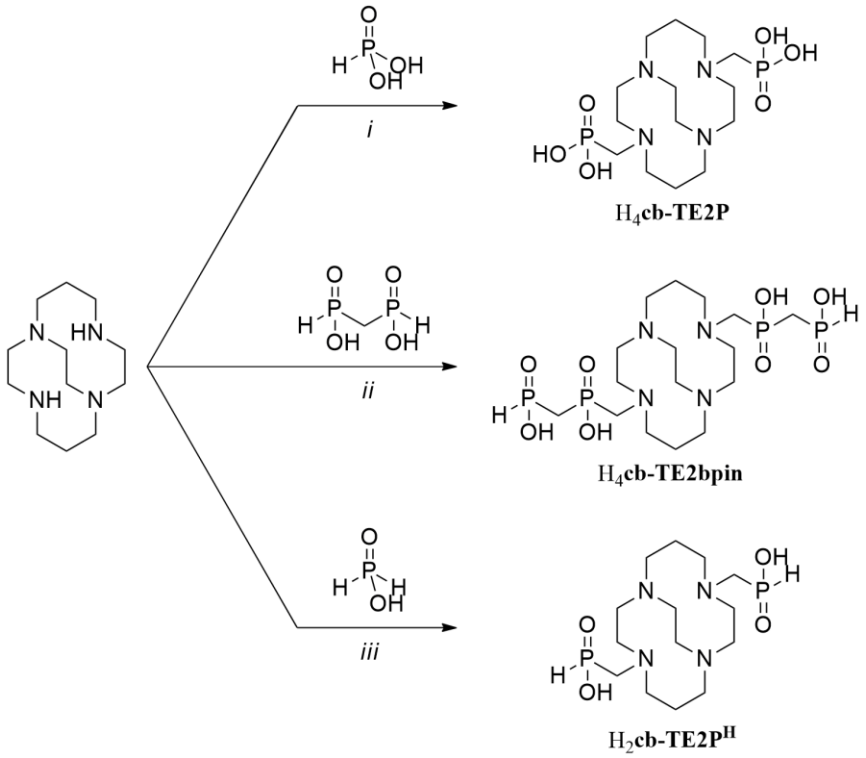

Scheme 4: Synthesis of cb-cyclam derivatives. (*i*) $(CH_2O)_n$, 12 M aq. HCl, 35 °C, 7 d (82%); (*ii*) $(CH_2O)_n$, 6 M aq. HCl, 60 °C, 2 d (48%); (iii) $(CH_2O)_n$, 50% aq. H_3PO_2, 60 °C, 3 h (78%).

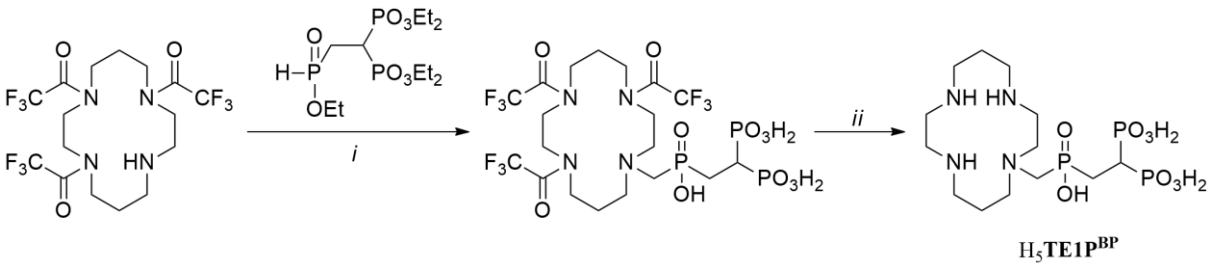

Scheme 5: Synthesis of H_5**TE1P**^{BP} ligand. (*i*) $(CH_2O)_n$, dry pyridine, pyridine hydrobromide, Ar atmosphere, 40 °C, 18 h (79%); (*ii*) 6 M aq. HCl, reflux, 18 h (74%).

The solid-state structures of H_2**TE2P**^{H} and H_5**TE1P**^{BP} ligand were determined. The H_2**TE2P**^{H} ligand crystallized in the pentahydrate form. Nitrogen atoms bearing the methylphosphinate groups are protonated and together with all nitrogen atoms of the macrocycle and one oxygen atom of each methylphosphinate group participated in the intramolecular hydrogen bond system. The intermolecular hydrogen bond system is formed by remaining phosphinate oxygen atoms and water molecules of crystallization. The geometry, bond lengths, and structure of hydrogen bonds are similar to those reported previously for the crystal structure of H_2**TE2P**$^{1,8}\cdot HCl\cdot 4H_2O$.[123] Compared to the described structure, the H_5**TE1P**^{BP} ligand does not contain such a rich network of intramolecular hydrogen bonds. One phosphonate group is disordered in two positions. This leads to two structures differing in the hydrogen bond system which is not observed in H_2**TE2P**$^{H}\cdot 5H_2O$. In one structure of the H_5**TE1P**^{BP}, the disordered phosphonate group forms an intramolecular hydrogen bond with the phosphinate oxygen atom, while in the other structure it forms an intramolecular hydrogen bond to another phosphonate group. Both structures have two hydrogen atoms attached to the secondary amines of the macrocycle and one of the protonated nitrogen atoms forms a short intramolecular hydrogen bond to the oxygen atom of the phosphinate group. Each phosphonate group is monoprotonated (Appendices 3 and 4).

After prolonged exposure of the copper phosphinate complex aqueous solutions to air, the coordinated ligand was oxidized and the [Cu(H_2**TE2P**)$\cdot 2H_2O$] complex crystallized from the system. In this complex, the central copper atom is hexacoordinated in the distorted octahedral coordination sphere, and two oxygen atoms from the phosphonate groups are located in the *cis* positions due to ligand

preorganization. All details as well as geometrical parameters of the crystal structure are given in Appendix 3.

5.1.2 Equilibrium studies

Protonation and stability constants of studied ligands and their complexes were determined by potentiometric titrations. The UV-Vis or NMR titrations were used when the measurements were performed in a strongly acidic or strongly alkaline environment, respectively. The high value of the first protonation constant was found for all studied ligands. The values were even so high for cross-bridged cyclam derivatives that they could not be determined even by NMR titrations. Therefore, after comparison with other analogous ligands, this value was fixed in the calculations at 15. Although the cb-cyclam itself is characterized by high basicity and behaves as a proton sponge,[68] such high values were surprising for the H_4**cb-TE2bpin** and H_2**cb-TE2P^{H}** ligands. The reason is that, unlike the phosphonate group, the phosphinate group generally reduces the basicity of the ring nitrogen atoms.[120] The effect of the pendant arm was obvious at the second protonation constant of cb-derivatives. Consistent with the above, this value is quite high for H_4**cb-TE2P** (11.22) but significantly lower for the phosphinate derivatives H_4**cb-TE2bpin** (6.89) and H_2**cb-TE2P^{H}** (6.35). For the non-bridged derivative, the second protonation constant was also determined by NMR titrations. Because the values of the highly basic constants are close to each other, it was not possible to distinguish them completely. Compared to related cyclam ligands with phosphorus pendants,[124,125,196] the values of the protonation constants of the H_5**TE1P^{BP}** ligand are higher (Appendix 4). The protonation constants logK_3 and logK_4 presumably describe the protonations of the bis(phosphonate) group and are comparable to the protonation constants of the M(II)-**TE1P^{BP}** complexes. In these complexes, the metal ion is bound in the macrocyclic cavity and the bis(phosphinate) group remains free (Table 3A).

The stability constants of the Cu(II) complexes are relatively high for all studied bridged ligands. The highest value was found for the phosphonate derivative (23.97), due to its high basicity of amines.

Despite the high basicity of the macrocycles of bridged derivatives, stability constants of their complexes are lower than those of the related non-bridged phosphorus derivatives H_2**TE1bpin** (25.83; Figure 14)[196], H_3**TE1bpon** (27.66; Figure 14)[196] or pentacoordinated and hexacoordinated isomers of H_4**TE2P**^{1,8} (25.40 and 26.50, respectively; Figure 11)[125]. The H_5**TE1P**^{BP} ligand also forms the more stable copper complex (29.16; Table 3 and Appendix 4). The explanation is the high rigidity of the cb-cyclam core, which does not allow the coordination of all four nitrogen atoms of the macrocycle in the equatorial plane of the square pyramidal or bipyramidal coordination sphere.

Table 3: (A) Stepwise protonation constants of the ligands. Overall protonation constants logβ of the ligands are given in italics. (B) Stability constants of the complexes.

	H_4**cb-TE2P**	H_4**cb-TE2bpin**	H_2**cb-TE2P**^{H}	H_5**TE1P**^{BP}
A				
logK_1	~15	~15	~15	
				2 × 13.38
logK_2	11.22	6.89	6.35	*26.76±0.04*
	26.22±0.01	*21.89±0.01*	*21.35±0.01*	
logK_3	7.34	2.60	–	11.83
	33.56±0.01	*24.49±0.01*		*38.59±0.01*
logK_4	4.63	1.35	–	7.32
	38.19±0.01	*25.84±0.01*		*45.91±0.01*
logK_5	–	–	–	3.29
				49.20±0.02
logK_6	–	–	–	2.07
				51.27±0.02
B				
Cu(II)	23.97	20.21	21.28	29.16
Zn(II)	–	–	–	20.74
Ni(II)	–	–	–	25.92

The distribution diagrams of cb-derivatives are quite different from each other. The Cu(II)-H_4**cb-TE2P** system includes diprotonated, monoprotonated and

fully deprotonated species, while the [Cu(H**cb-TE2P**)]$^{-}$ is the dominant species in the neutral region. Protonation occurs at the uncoordinated oxygen atom of the phosphonate of each phosphonate group. The distribution diagram of the bis(phosphinate) derivative contains monoprotonated and fully deprotonated species and the [Cu(**cb-TE2bpin**)]$^{2-}$ is dominant at pH above 4. The H_2**cb-TE2P^{H}** ligand does not form protonated species and the [Cu(**cb-TE2P^{H}**)] is dominant over the entire studied pH range (Figure 22).

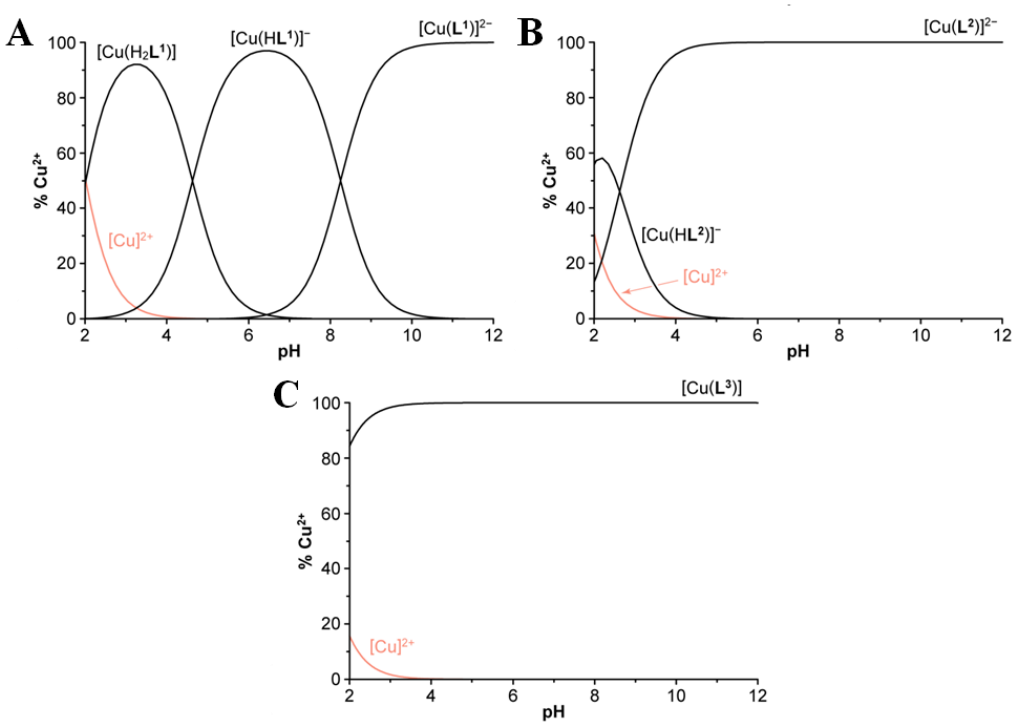

Figure 22: Distribution diagrams of (A) Cu(II)-H_4**cb-TE2P**, (B) Cu(II)-H_4**cb-TE2bpin** and (C) Cu(II)-H_2**cb-TE2P^{H}** systems ($c_M = c_L = 4$ mM, 25 °C, $I = 0.1$ M NMe_4Cl).

More extensive thermodynamic studies have been performed for the H_5**TE1P^{BP}** derivative. Stability constants, as well as protonation constants with Cu(II), Ni(II) and Zn(II) ions, were determined. UV-Vis titration was used for the evaluation of the Cu(II)-H_5**TE1P^{BP}** system since the complex is fully formed at a very low pH (1.6). The preformed complexes were utilized to determine protonation constants by potentiometric titrations. As mentioned above, the stability of the copper complex is high and the phosphinate-bis(phosphonate)

ligand is also characterized by a high selectivity for Cu(II) over Zn(II) and Ni(II) ions (Table 3B). From values of stability constants, it can be concluded that the metal ions are bound in the cavity of the macrocycle. The determined protonation constants, in turn, indicate that the bis(phosphonate) group is not coordinated to the bound metal ions (Table 4). A comparison of the distribution diagram of Cu(II)-H_5**TE1P^{BP}** system (Figure 23A) with the distribution diagrams of the above cross-bridged derivatives shows that the former shows a higher abundance of different protonated species. In addition to the mono and diprotonated species found in the Cu(II)-H_4**cb-TE2P** system, the triprotonated neutral [Cu(H_3**TE2P^{BP}**)] species are present in the strongly acidic region. Diprotonated [Cu(H_2**TE2P^{BP}**)]$^-$ and monoprotonated [Cu(H**TE2P^{BP}**)]$^{2-}$ species are present in the neutral region, in contrast to the H_4**cb-TE2bpin** and H_2**cb-TE2P^{H}** copper complexes, which are fully deprotonated in this pH range. On the contrary, the formation of a deprotonated complex of H_5**TE1P^{BP}** derivative begins up to pH 10. Regarding comparison with related non-bridged ligands, the value of the H_3**TE1bpon** ligand stability constant is closest to the value of the H_5**TE1P^{BP}** ligand. However, a comparison of their distribution diagrams shows only minimal system similarity.[196]

Transmetallation can be excluded due to the favourable thermodynamic and kinetic properties of the Cu(II)-**TE1P^{BP}** complex. Therefore, ternary complexes with Cu(II), Zn(II), Ca(II) and Mg(II) ions were also studied, as the bis(phosphonate) group interacts with metal ions present in solution. Diverse chemical models were found with species in ratios 1:1, 1:2 and 2:1 of Cu(II)-**TE1P^{BP}** complex to M(II). The values of the stability constants indicate the highest stability for ternary complexes in which one bis(phosphonate) group is attached to one metal ion. Contrariwise, species in which two bis(phosphonate) molecules bind to one metal ion or one bis(phosphonate) molecule coordinates two metal ions show significantly lower thermodynamic stability (Appendix 4). The distribution diagram of the {Cu(II)-H_5**TE1P^{BP}**}-Ca(II) ternary system is characterized by a significant excess of ternary species already at a ratio of 1:1 and the dominant species in the neutral region is monoprotonated neutral species [Ca{Cu(H**TE1P^{BP}**)}] (Figure 23B).

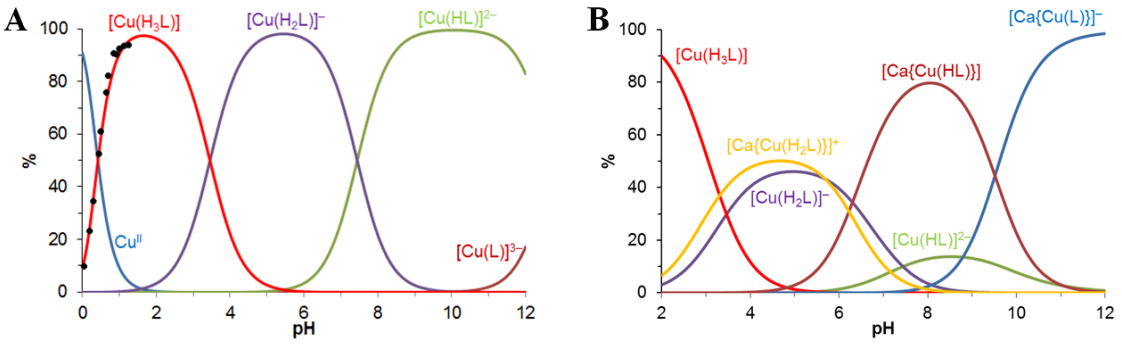

Figure 23: Distribution diagrams of (A) Cu(II)-H_5**TE1P^{BP}** system (absorbance at 580 nm is shown as black dots) and (B) {Cu(II)-H_5**TE1P^{BP}**}-Ca(II) ternary system ($c_{Cu} = c_L = c_{Ca} = 4$ mM, only 1:1 complexes were included for simplicity reason).

Table 4: Protonation constants logK_n of *in-cage* complexes of H_5**TE1P^{BP}** (I = 0.1M NMe_4Cl, 25 °C).

	Cu(II)	Zn(II)	Ni(II)
logK_1	12.69	12.29	11.76
logK_2	7.44	7.48	6.86
logK_3	3.46	4.35	–

5.1.3 Formation kinetics

The rate of copper complex formation with cyclam ligands was studied by UV-Vis measurements. The obtained data were treated by a series of equations, which are stated in Appendices 3 and 4 with a detailed explanation. Copper complexes of H_4**cb-TE2P**, H_4**cb-TE2bpin** and H_5**TE1P^{BP}** were formed quickly, thus, the stopped-flow technique was used. Generally accepted complexation mechanism of macrocycles with pendant arms proceeds in two steps. The first equilibrium step involves the formation of the *out-of-cage* complex in which the metal ion is bound only through the pendant arms, while the macrocyclic cavity is blocked by protons bound to the amines. In the rate-determining step, the amines are deprotonated and the metal ion is bound in a macrocyclic cavity to form an *in-cage* complex. For the bridged ligands, the measurement was performed with an excess of metal ion, while the H_5**TE1P^{BP}** was measured with an excess of both metal and ligand. The obtained rate constants $^f k_{obs}$ were plotted as a function of Cu(II)/ligand concentration at different pH values (Figures 24 and 26).

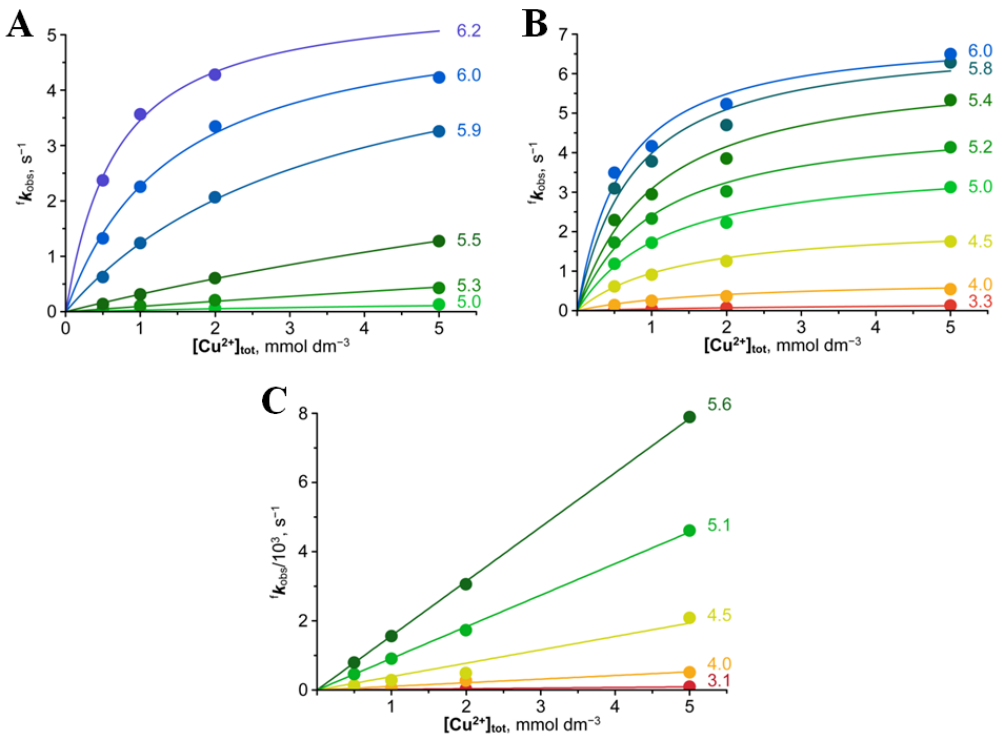

Figure 24: Formation of Cu(II) complexes: $^{f}k_{obs}$ of (A) H$_4$**cb-TE2P**, (B) H$_4$**cb-TE2bpin** and (C) H$_2$**cb-TE2P^{H}** as function of copper(II) concentration (c_L = 0.1 mM, 25 °C) at various pH values (given in the figures). Only selected curves are displayed. Solid lines represent the best fits according to Equation 2 or 6 (Appendix 3).

The ligands H$_4$**cb-TE2P** (at pH > 5.5) and H$_4$**cb-TE2bpin** (at the entire measured pH range) show saturation curves indicating the formation of a stable reaction intermediate corresponding to the *out-of-cage* complex (Figure 24). The rate of *in-cage* complexation is proportional to the concentration of the *out-of-cage* intermediate. Thus, *out-of-cage* species are formed quantitatively with a large excess of metal ions. A more detailed analysis of the Cu(II)-H$_4$**cb-TE2P** system was precluded due to the saturation shape of the curve only in a narrow pH range. Nevertheless, there is a significant change in the values of the conditional stability constant (K*) with pH (Figure 25). This change can be attributed to the dissociation of the proton from the monoprotonated phosphonate group because increasing the negative charge also increases the stability of the *out-of-cage* complex. The conditional stability constant values of the Cu(II)-H$_4$**cb-TE2bpin** system, in turn, were calculated individually for each pH value (Figure 25). It was found that their change with pH is not significant as the coordinated bis(phosphinate) groups do

not undergo any protonation/deprotonation in the studied pH range. Thus, since the change of log*K** values is less than the one logarithmic unit, it is most likely associated with deprotonation of the macrocycle. The complex shows the highest *K** values among the studied bridged complexes due to the bidentate coordination of each bis(phosphinate) moiety.

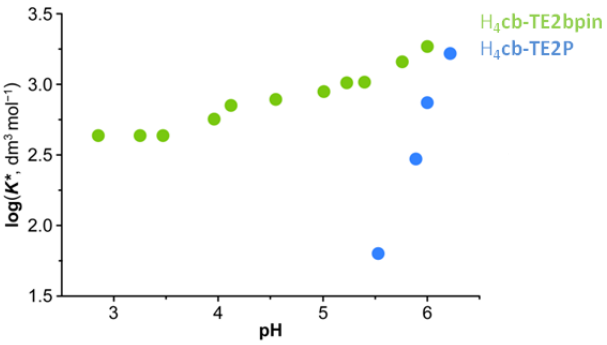

Figure 25: Comparison of the *out-of-cage* complex conditional stability constants *K** (**B**) as a function of pH for Cu(II)-H$_4$**cb-TE2P** (blue) and Cu(II)-H$_4$**cb-TE2bpin** (green) at 25 °C.

The ligands H$_4$**cb-TE2P** (at pH < 5.5) and H$_2$**cb-TE2P^{H}** (at the entire measured pH range) show a linear shape of the $^{f}k_{obs}$ as a function of Cu(II) concentration (Figure 24). This indicates low stability of *out-of-cage* intermediates and thus low *K** values. The reason is the weak monodentate coordination of the phosphine group and therefore the conditional stability constants could not be determined. Based on the obtained data and their analysis, a reaction Scheme 6 was suggested for these systems.

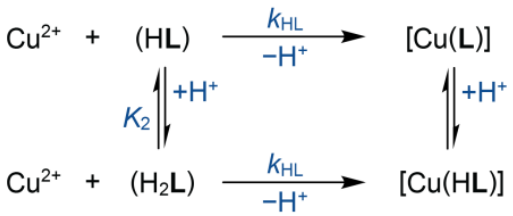

Scheme 6: Formal reaction scheme for the formation of the *in-cage* Cu(II) complexes. Charges of ligand and complex species are omitted.

The formation kinetics of the non-bridged H_5**TE1P^{BP}** derivative was studied for metal and ligand excess. The bis(phosphonate) pendant arm is a strongly complexing group, and for bis(phosphonate) ligands, the formation of different types of *out-of-cage* complexes ("oc") is possible depending on the excess of metal and ligand.[184,185] In addition to the $[M(L)]^{oc}$ *out-of-cage* complex, which is quantitatively formed in the entire studied pH range, the formation of dinuclear complexes $[M_2(L)]^{oc}$ and complexes with two coordinated ligands $[M(L)_2]^{oc}$ is also possible. The rate constants ($^{f}k_{obs}$) determined with an excess of metal ion significantly differ from the rate constants determined with an excess of ligand. This finding confirms the presence of *out-of-cage* species with different stoichiometry (Figure 26). Also for this ligand, the rate constants for each pH were determined and subsequently plotted. In both cases (metal ion excess and ligand excess), the curves have a saturation shape in the whole studied pH range similar to the H_4**cb-TE2bpin** ligand. The change of the conditional stability constants with pH for $[M_2(L)]^{oc}$ and $[M(L)_2]^{oc}$ is negligible and their values show that the coordination of the second ligand molecule is stronger than the coordination of the second metal ion.

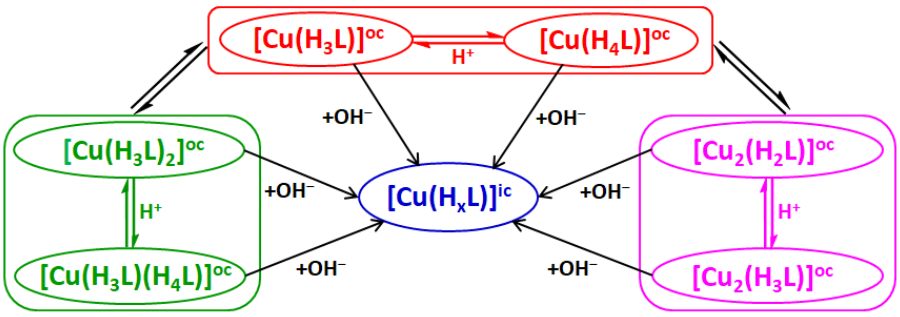

Scheme 7: Expected pathways of the *out-of-cage* ("oc") into the *in-cage* ("ic") complex transformations in the Cu(II)-H_5**TE1P^{BP}** system.

Since the rate-determining step is the deprotonation of the macrocycle and the transfer of the metal ion into the cavity, the rate constants usually show considerable changes with pH. This phenomenon was observed for formation rates constants for the transformation of the corresponding *out-of-cage* complexes ($^{f}k_{ML}$,

$^{f}k_{ML2}$ and $^{f}k_{M2L}$) which were plotted as a function of pH (Appendix 4). The nonlinear shape of their curves suggests that each *out-of-cage* complex is present in two different protonated forms. Then the overall mechanism can be described by Scheme 7.

Thus, the analyzed data show that the least reactive intermediate in the studied Cu(II)-H_5**TE1P^{BP}** system is $[M(L)]^{oc}$. Its conversion to the *in-cage* complex is ~4-times slower than the conversion of the $[M(L)_2]^{oc}$ intermediate. The explanation is the assumption that the second ligand molecule in the $[M(L)_2]^{oc}$ intermediate helps to deprotonate the macrocycle. In the case of the $[M_2(L)]^{oc}$ intermediate, the conversion is up to 3 orders of magnitude faster compared to $[M(L)]^{oc}$ intermediate. This is presumably due to the weaker binding of the second metal ion in the intermediate which allows its easier transfer from the bis(phosphonate) group to the macrocyclic cavity.

Table 5: Comparison of calculated 99% complexation times of H_4**cb-TE2P**, H_4**cb-TE2bpin**, H_2**cb-TE2P^{H}** and H_5**TE1P^{BP}** and their related ligands (10-times Cu(II) ion excess, 25 °C).

	pH 4	pH 6
H_4**cb-TE2P**	4.7 h	1.6 s
H_4**cb-TE2Pbpin**	14 s	0.2 s
H_4**cb-TE2P^{H}**	14.7 h	14.5 min
H_5**TE1P^{BP}**	24 s	0.1 s
H_2**TE1bpin**[a] [196]	8.4 s	0.1 s
H_4**TE2P^{1,8}** [125]	64.5 s	0.2 s

[a] Formation of the first *in-cage* Cu(II) complex.

The complexity of the Cu(II)-H_5**TE1P^{BP}** system makes it difficult to compare with other ligands. The only direct comparison is possible in terms of the time required for 99% complexation of the studied cyclam derivatives (Table 5). The slowest complexation of Cu(II) ions was found for the bridged phosphinate ligand which is in the range of hours at pH 4 and the range of minutes at pH 6. The rate of complex formation for the H_4**cb-TE2P** derivative is also slow at pH 4

(4.7 h). However, the rate of complexation increases rapidly with increasing pH, and at pH 6, the copper cation is coordinated within a few seconds. The best results achieved H_4**cb-TE2Pbpin** and H_5**TE1P^{BP}** ligands. Their rates of complex formation are already in the range of seconds at pH 4 and the quantitative formation occurs within 1 s at pH 6. These ligands are also the most similar to the formation rates of the non-bridged ligands H_2**TE1bpin** and H_4**TE2P**[1,8] and this similarity is evident throughout the whole studied pH range (Appendices 3 and 4).

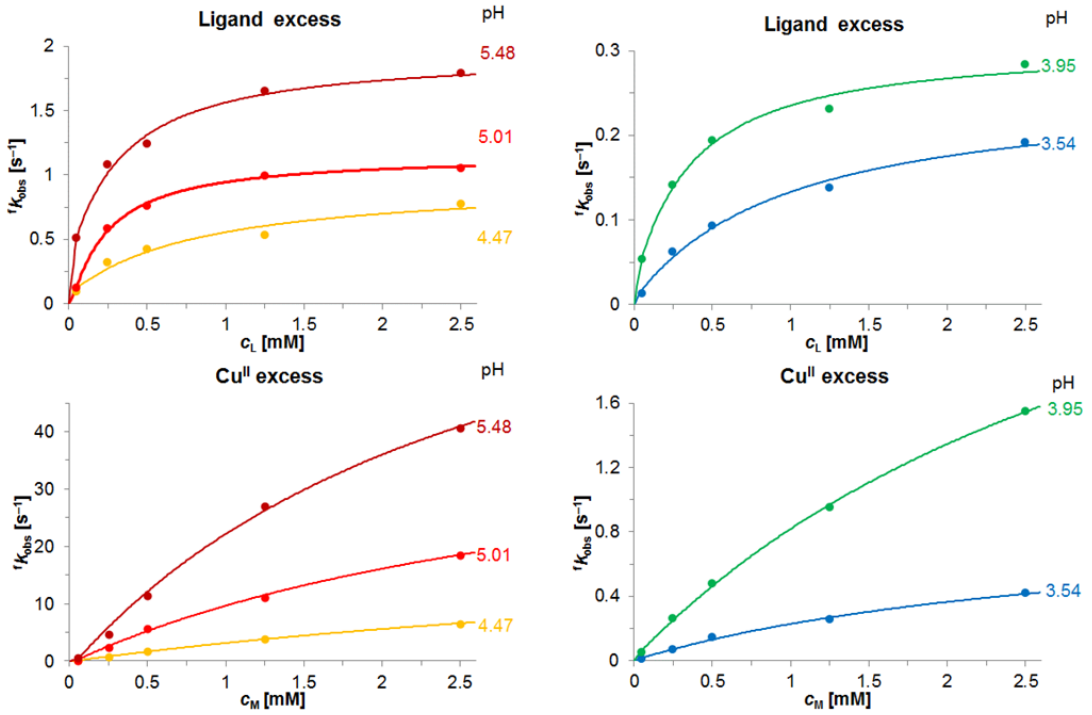

Figure 26: Observed formation rate constants (I = 0.1 M KCl, 25 °C) as function of ligand concentration (left, c_M = 0.05 mM) or Cu(II) concentration (right, c_L = 0.05 mM). The lines represent the best fits according to Equations 1, S1 and S2 (Appendix 4).

5.1.4 Dissociation kinetics

The dissociation kinetics of copper complexes were studied by UV-Vis spectroscopy using acid-assisted dissociation experiments. The equations used for experimental data fitting are given in Appendices 3 and 4. All studied complexes are characterized by high kinetic inertness. The dissociation profiles of bridged derivatives differ from each other. For the Cu(II)-H_4**TE2P** system, the curve has a

saturation character indicating protonation in the studied pH range. Mono and diprotonated species are thermodynamically stable and therefore this protonation is most likely associated with the formation of triprotonated species. In the Cu(II)-H_4**TE2bpin**, the dissociation scheme is similar because the terminal phosphinate group in bis(phosphinate) can be protonated without compromising the stability of the coordination cage. Thus, the observed protonation also corresponds to the formation of a triprotonated complex, which is the dominant species in the dissociation pathway. The dissociation profile of this system has a linear shape indicating a very low value of the third protonation constant of the complex. In the case of the phosphinate Cu(II)-H_2**TE2P^{H}** complex, the dissociation profile has a parabolic shape. Two protonations are required to form a reactive species and logaritm of the corresponding protonation constants reach negative values. Because the deprotonated complex is thermodynamically stable, the kinetically active species should be diprotonated. As well as for the Cu(II)-H_4**cb-TE2P** system, the non-bridged copper complex Cu(II)-H_5**TE1P^{BP}** has a saturation shape of dissociation profile. This indicates the presence of the complex in two forms differing in the protonation state. Since the $[Cu(H_3$**TE1P^{BP}**$)]^+$ species is thermodynamically stable, the protonation corresponds to the formation of $[Cu(H_4$**TE1P^{BP}**$)]^{2+}$ species. Data treating showed that $[Cu(H_4$**TE1P^{BP}**$)]^{2+}$ is the only kinetically active species. Graphs of the dissociation rate constant ($^{d}k_{obs}$) as a function of acid concentration are shown in Appendices 3 and 4.

The complexes are compared based on dissociation half-lifes ($t_{1/2}$) due to different dissociation mechanisms (Table 6). Under conditions of 1 M $HClO_4$ and 90 °C, the copper complexes of the bridged ligands H_4**cb-TE2P** and H_2**cb-TE2P^{H}** show extreme kinetic inertness with half-lifes of 120 h and 111 h, respectively. However, for phosphinate, the dissociation half-life shortens sharply with increasing acid concentration. This is described by a different protonation scheme of the complex. The half-life of the bis(phosphinate) complex (10.7 h) is one order of magnitude shorter than the half-life of Cu(II)-H_4**cb-TE2P** and is similar to the half-life of the hexacoordinated copper complex of H_4**TE2P^{1,8}** ligand (13.4 h).[125] This, in turn, is explained by the strong chelating ability of the bis(phosphinate) group even in a very acidic environment. The half-life of the

phosphinate-bis(phosphonate) complex is the shortest between the studied ligands and is at the range of minutes. Since the bridged ligands are more kinetically inert,[66,67] this result is not surprising for the non-bridged derivative. The half-life of 1.4 minutes corresponds to the half-lives reported for the related pentacoordinated Cu(II)-H$_4$**TE2P**^{1,8} complex (49 s)[125] or Cu(II)-H$_2$**TE1bpin** complex (40 s).[196] The result suggests only a negligible role of the bis(phosphonate) group in the dissociation process. Despite the significant difference in inertness, this ligand is also suitable for *in vivo* usage.

Table 6: Dissociation half-lifes of the discussed Cu(II) complexes (90 °C; [a,b] recalculated from original data).

	$t_{1/2}$
H$_4$**cb-TE2P**	120 h
H$_4$**cb-TE2Pbpin**	10.7 h
H$_4$**cb-TE2P**^{H}	111 h
H$_5$**TE1P**^{BP}	1.4 min
H$_2$**TE1bpin**[a] [196]	40 s
H$_4$**TE2P**^{1,8}[a] [125]	49 s
H$_4$**TE2P**^{1,8}[b] [125]	13.4 h

[a] Pentacoordinated isomer.
[b] Hexacoordinated *trans* isomer.

5.1.5 Radiochemical labelling experiments

The radiolabeling of H$_5$**TE1P**^{BP} was fast and effective with specific activity around 30 Bq/µmol at pH 5.5 and ambient temperature. The results of sorption efficiency are comparable to results of experiments performed with non-radioactive copper on hydroxyapatite at physiological pH (Appendix 4). The small animal PET of mice points to bone-selective accumulation of radiotracer (Figure 27). The plateau is reached after 30–60 minutes and the high target-to-background ratio is preserved for at least 24 hours. [^{64}Cu]Cu(II)-H$_5$**TE1P**^{BP} showed rapid blood clearance and elimination via the renal pathway within 30 minutes. Importantly, the mice showed no apparent accumulation of [^{64}Cu]Cu(II)-H$_5$**TE1P**^{BP} in liver which indicates the high chelator

stability *in vivo*. The observed results indicate that [^{64}Cu]Cu(II)-H$_5$**TE1P^{BP}** preferentially accumulates in skeletal regions with elevated metabolic turnover similarly as it has been reported for other radiolabeled bisphosphonates.[210,211]

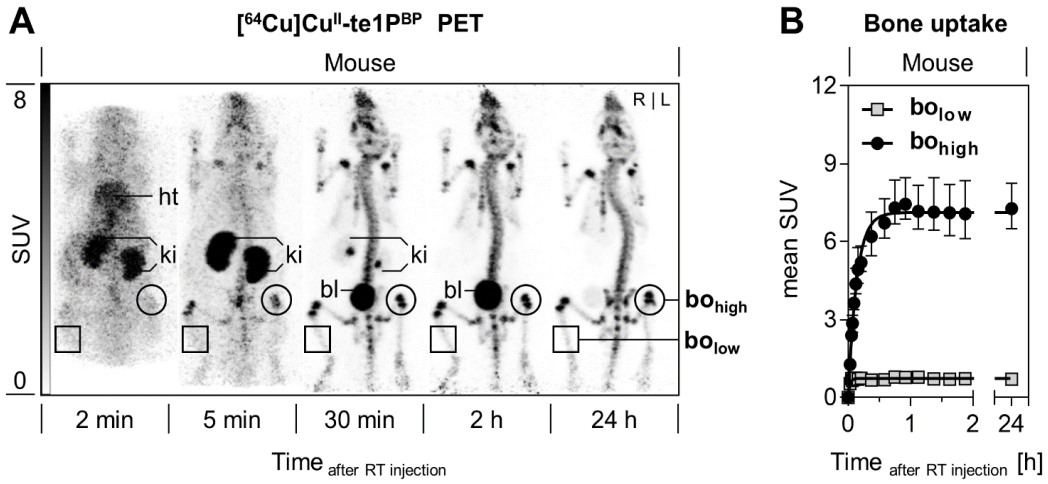

Figure 27: Dynamic PET imaging of [^{64}Cu]Cu(II)-H$_5$**TE1P^{BP}** in mice: the tracer shows rapid renal excretion and efficient skeletal uptake (A), plateaus between 30 and 60 min after injection and remains stable for 24 h (B). Description: (bo$_{high}$) skeletal regions with the highest bone uptake; (bo$_{low}$) skeletal regions with the lowest bone uptake; (ht) heart; (ki) kidney; (bl) bladder; (SUV) standardized uptake value; (RT) radiotracer; (L) left; (R) right.

The small animal PET of rats showed the similar uptake pattern as was observed for mice (Figure 28). Skeletal region selectivity of [^{64}Cu]Cu(II)-**TE1P^{BP}** in rats is consistent with [^{18}F]fluoride, which is thought to preferentially bind to bone mineral deposited by osteoblasts.[212,213] Thus, the selectivity of [^{64}Cu]Cu(II)-**TE1P^{BP}** for skeletal regions of increased bone remodeling may underlie similar physiological mechanisms. Furthermore, [^{64}Cu]Cu(II)-H$_5$**TE1P^{BP}** showed higher uptake in critical bone defect regions of the right femur compared to the healthy reference regions in the left femur, which support its usefulness as a potential PET radiotracer for evaluation of bone healing in preclinical and clinical settings.

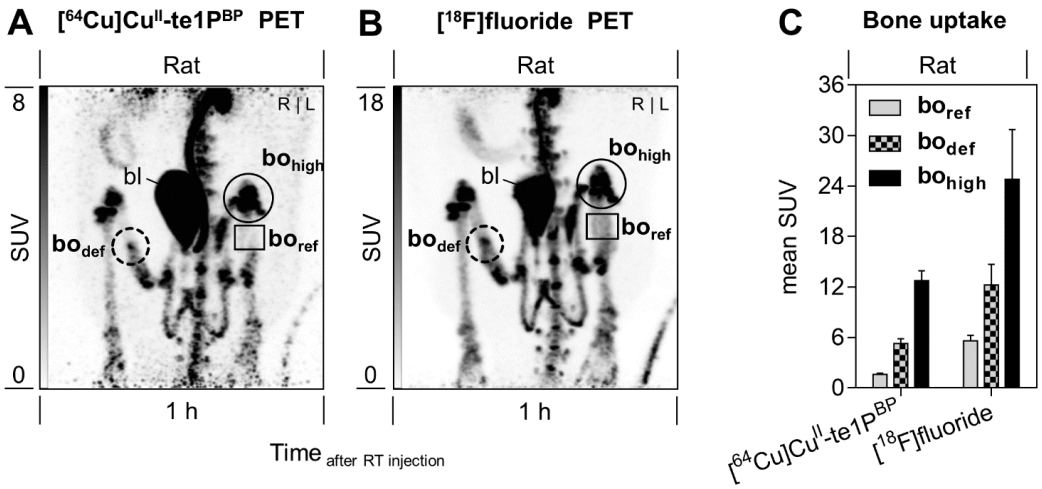

Figure 28: Comparison between [^{64}Cu]Cu(II)-H$_5$**TE1P^{BP}** (**A**) and [^{18}F]fluoride (**B**) in the same rats; static PET imaging of a critical bone defect in rats 1 h after injection (**A**, **B**) and bone uptake (**C**); description: (bo_{def}) critical bone defect in the right femur; (bo_{ref}) healthy bone reference region in the left femur; (bo_{high}) skeletal regions with the highest bone uptake; (bl) bladder; (SUV) standardized uptake value; (RT) radiotracer; (L) left; (R) right.

5.2 Conclusions

The presented cross-bridged cyclam derivatives with phosphonate, bis(phosphine) and phosphine pendants and the non-bridged cyclam derivative with phosphinate-bis(phosphonate) pendant arm have been designed, synthesized and studied as potential carriers of copper radioisotopes in nuclear medicine. All ligands are characterized by high macrocycle basicity. The thermodynamic stability of copper complexes is high and sufficient for biomedical applications. However, the bridged ligands show lower stability of Cu(II) complexes compared to the non-bridged phosphinate-bis(phosphonate) derivative. The non-bridged ligand is also characterized by significant selectivity for Cu(II) over Ni(II) and Zn(II) ions. The kinetic inertness of the complexes is very high and the dissociation half-lives of the bridged complexes are in the range of hours at 1 M $HClO_4$ and 90 °C. Complex formation is fast. The H_4**TE2bpin** and H_5**TE1P^{BP}** complexes form almost immediately in a millimolar scale at pH ~6. The worst result was achieved for the H_2**TE2P^{H}** derivative. Its rate of complexation is in the range of minutes at the same pH. This is due to the significantly lower stability of the *out-of-cage* complex and/or the less efficient proton transfer from the ligand cavity. The bis(phosphonate) group of the non-bridged ligand is not coordinated to the Cu(II) ion bound in the macrocycle, therefore its properties are unchanged and it can bind to other metal ions in solution. This is important for complex speciation in body fluids and final biodistribution. The bis(phosphonate) group is also capable of efficient absorption on HAP as well as bone tissue. Thus, the excellent properties of H_4**TE2P**, H_4**TE2bpin** and H_5**TE1P^{BP}** ligands indicate a high potential for possible use in radiomedicine.

6 Declaration of contribution

Hereby, the author of this doctoral thesis declares that her contribution to the work was as follows:

Part I (Bis(phosphinate)-bridged ligands): synthesis, purification and characterization of the ligands, preparation and crystallization of the complexes and measurement of the thermodynamic properties by potentiometry and UV-Vis spectroscopy.

Part II (Cyclam derivatives for complexation of copper radioisotopes): measurement of the formation and dissociation kinetics by UV-Vis and NMR spectroscopy, sorption studies on hydroxyapatite and participation in the measurement of thermodynamic properties by potentiometry.

The author also actively participated in the evaluation of kinetic, thermodynamic and sorption results and the preparation of all the publications.

7 Acknowledgements

The greatest thanks belong to my supervisor Doc. Vojtěch Kubíček. I appreciate his mental support, excellent ideas and the time he devoted to me. At the same time, I want to express my gratitude to Prof. Petr Hermann for helpful advice, Dr. Ivana Císařová for solving and Doc. Honza Kotek for refining the X-ray structures, RNDr. Jana Havlíčková for help with potentiometric titrations, Dr. Marcel Ehn for help with preparative HPLC and flash chromatography, Mgr. Ondřej Zemek for measuring the mass spectra and Mgr. Filip Koucký for performing the NMR titration. I also thank Prof. Přemysl Lubal from Masaryk University for allowing me to measure the stopped-flow spectroscopy. Last but not least, I am thankful to Prof. Petr Štěpnička for opportunity to work at the Department of Inorganic Chemistry at Charles University.

This work was supported by the Grant Agency of the Czech Republic (19-17380S) and Masaryk University (MUNI/A/1424/2019). The study was conducted within the framework of COST Action CA18202 (NECTAR) the Inter-COST project MSMT (LTC 20044).

8 References

[1] Application of Plasma to Humans (Blood Coagulation and Regenerative Medicine). (2019). *Plasma Medical Science*, 319-384. https://doi.org/10.1016/B978-0-12-815004-7.00006-8

[2] Molecular Imaging. (2014). *Nuclear Medicine*, 16-23. https://doi.org/10.1016/B978-0-323-08299-0.00002-X

[3] Kim, D. (2017). Principles and Methods of Molecular Imaging in Stroke. *Primer On Cerebrovascular Diseases*, 332-338. https://doi.org/10.1016/B978-0-12-803058-5.00070-9

[4] Wang, Z., Chang, T., & Slauter, R. (2017). Use of Imaging for Preclinical Evaluation. *A Comprehensive Guide To Toxicology In Nonclinical Drug Development*, 921-938. https://doi.org/10.1016/B978-0-12-803620-4.00035-9

[5] Brosnan, R. (2018). Utilization of Magnetic Resonance Imaging and Magnetic Resonance Angiography for Cardiac Thrombus. *Cardiovascular Thrombus*, 115-121. https://doi.org/10.1016/b978-0-12-812615-8.00008-9

[6] Bangerter, N., Morrell, G., & Grech-Sollars, M. (2020). Magnetic resonance imaging. *Bioengineering Innovative Solutions For Cancer*, 163-194. https://doi.org/10.1016/B978-0-12-813886-1.00008-5

[7] Zheng, X., Li, L., Sun, L., & Yan, C. (2016). Lanthanide Nanoparticles. *Including Actinides*, 301-335. https://doi.org/10.1016/bs.hpcre.2016.05.001

[8] Jay, W. (1989). Advances in Magnetic Resonance Imaging. *American Journal Of Ophthalmology*, *108*(5), 592-596. https://doi.org/10.1016/0002-9394(89)90440-6

[9] Mewis, R., & Archibald, S. (2010). Biomedical applications of macrocyclic ligand complexes. *Coordination Chemistry Reviews*, *254*(15-16), 1686-1712. https://doi.org/10.1016/j.ccr.2010.02.025

[10] Hagberg, G., Mamedov, I., Power, A., Beyerlein, M., Merkle, H., & Kiselev, V. et al. (2014). Diffusion properties of conventional and calcium-sensitive MRI contrast agents in the rat cerebral cortex. *Contrast Media & Molecular Imaging*, *9*(1), 71-82. https://doi.org/10.1002/cmmi.1535

[11] Hermann, P., Kotek, J., Kubíček, V., & Lukeš, I. (2008). Gadolinium(iii) complexes as MRI contrast agents: ligand design and properties of the complexes. *Dalton Transactions*, (23), 3027-3047. https://doi.org/10.1039/B719704G

[12] Parker, D. (2015). Radioisotope tracer techniques. *Industrial Tomography*, 223-234. https://doi.org/10.1016/b978-1-78242-118-4.00008-3

[13] MacPherson, D., Fung, K., Cook, B., Francesconi, L., & Zeglis, B. (2019). A brief overview of metal complexes as nuclear imaging agents. *Dalton Transactions*, *48*(39), 14547-14565. https://doi.org/10.1039/C9DT03039E

[14] Salvadori, P., Filidei, E., & Giorgetti, A. (2019). Positron-Emitting Radiopharmaceuticals. *Nuclear Medicine Textbook*, 57-98. https://doi.org/10.1007/978-3-319-95564-3_3

[15] Cates, J., Gu, Y., & Levin, C. (2015). Direct conversion semiconductor detectors in positron emission tomography. *Modern Physics Letters A*, *30*(14), 1530011. https://doi.org/10.1142/S0217732315300116

[16] Ramogida, C., & Orvig, C. (2013). Tumour targeting with radiometals for diagnosis and therapy. *Chemical Communications*, *49*(42), 4720-4739. https://doi.org/10.1039/C3CC41554F

[17] Holub, J., Meckel, M., Kubíček, V., Rösch, F., & Hermann, P. (2014). Gallium(III) complexes of NOTA-bis (phosphonate) conjugates as PET radiotracers for bone imaging. *Contrast Media & Molecular Imaging*, *10*(2), 122-134. HTTPS://DOI.ORG/10.1002/cmmi.1606

[18] Pniok, M., Kubíček, V., Havlíčková, J., Kotek, J., Sabatie-Gogová, A., & Plutnar, J. et al. (2014). Thermodynamic and Kinetic Study of Scandium(III) Complexes of DTPA and DOTA: A Step Toward Scandium Radiopharmaceuticals. *Chemistry - A European Journal*, *20*(26), 7944-7955. https://doi.org/10.1002/chem.201402041
[19] Preshlock, S., Tredwell, M., & Gouverneur, V. (2016). 18F-Labeling of Arenes and Heteroarenes for Applications in Positron Emission Tomography. *Chemical Reviews*, *116*(2), 719-766. https://doi.org/10.1021/acs.chemrev.5b00493
[20] Calabria, F., & Schillaci, O. (2020). *Radiopharmaceuticals* (2nd ed.). Springer International Publishing. https://doi.org/10.1007/978-3-030-27779-6
[21] Boschi, A., Martini, P., Janevik-Ivanovska, E., & Duatti, A. (2018). The emerging role of copper-64 radiopharmaceuticals as cancer theranostics. *Drug Discovery Today*, *23*(8), 1489-1501. https://doi.org/10.1016/j.drudis.2018.04.002
[22] Anderson, C., & Ferdani, R. (2009). Copper-64 Radiopharmaceuticals for PET Imaging of Cancer: Advances in Preclinical and Clinical Research. *Cancer Biotherapy And Radiopharmaceuticals*, *24*(4), 379-393. https://doi.org/10.1089/cbr.2009.0674
[23] Zeglis, B., Houghton, J., Evans, M., Viola-Villegas, N., & Lewis, J. (2014). Underscoring the Influence of Inorganic Chemistry on Nuclear Imaging with Radiometals. *Inorganic Chemistry*, *53*(4), 1880-1899. https://doi.org/10.1021/ic401607z
[24] Wadas, T., Wong, E., Weisman, G., & Anderson, C. (2010). Coordinating Radiometals of Copper, Gallium, Indium, Yttrium, and Zirconium for PET and SPECT Imaging of Disease. *Chemical Reviews*, *110*(5), 2858-2902. https://doi.org/10.1021/cr900325h
[25] Banerjee, S., Pullambhatla, M., Foss, C., Nimmagadda, S., Ferdani, R., & Anderson, C. et al. (2014). 64Cu-Labeled Inhibitors of Prostate-Specific Membrane Antigen for PET Imaging of Prostate Cancer. *Journal Of Medicinal Chemistry*, *57*(6), 2657-2669. https://doi.org/10.1021/jm401921j
[26] Accardo, A., Tesauro, D., & Morelli, G. (2013). Peptide-based targeting strategies for simultaneous imaging and therapy with nanovectors. *Polymer Journal*, *45*(5), 481-493. https://doi.org/10.1038/pj.2012.215
[27] Byrne, J., Betancourt, T., & Brannon-Peppas, L. (2008). Active targeting schemes for nanoparticle systems in cancer therapeutics. *Advanced Drug Delivery Reviews*, *60*(15), 1615-1626. https://doi.org/10.1016/j.addr.2008.08.005
[28] Janib, S., Moses, A., & MacKay, J. (2010). Imaging and drug delivery using theranostic nanoparticles. *Advanced Drug Delivery Reviews*, *62*(11), 1052-1063. https://doi.org/10.1016/j.addr.2010.08.004
[29] Wu, H., & Chang, D. (2010). Peptide-Mediated Liposomal Drug Delivery System Targeting Tumor Blood Vessels in Anticancer Therapy. *Journal Of Oncology*, *2010*, 1-8. https://doi.org/10.1155/2010/723798
[30] Price, E., & Orvig, C. (2014). The Chemistry of Inorganic Nuclides (86Y,68Ga,64Cu,89Zr,124I). *The Chemistry Of Molecular Imaging*, 105-135. https://doi.org/10.1002/9781118854754.ch5
[31] Zhang, Y., Hong, H., & Cai, W. (2011). PET Tracers Based on Zirconium-89. *Current Radiopharmaceuticalse*, *4*(2), 131-139. https://doi.org/10.2174/1874471011104020131
[32] Van de Watering, F., Rijpkema, M., Perk, L., Brinkmann, U., Oyen, W., & Boerman, O. (2014). Zirconium-89 Labeled Antibodies: A New Tool for Molecular Imaging in Cancer Patients. *Biomed Research International*, *2014*, 1-13. https://doi.org/10.1155/2014/203601
[33] Jalilian, A., & Osso, J. (2017). Production, applications and status of zirconium-89 immunoPET agents. *Journal Of Radioanalytical And Nuclear Chemistry*, *314*(1), 7-21. doi:10.1007/s10967-017-5358-z

[34] Duatti, A. (2021). Review on 99mTc radiopharmaceuticals with emphasis on new advancements. *Nuclear Medicine And Biology*, *92*, 202-216. https://doi.org/10.1016/j.nucmedbio.2020.05.005
[35] Klein, R., Celiker-Guler, E., Rotstein, B., & deKemp, R. (2020). PET and SPECT Tracers for Myocardial Perfusion Imaging. *Seminars In Nuclear Medicine*, *50*(3), 208-218. https://doi.org/10.1053/j.semnuclmed.2020.02.016
[36] Rahmim, A., & Zaidi, H. (2008). PET versus SPECT: strengths, limitations and challenges. *Nuclear Medicine Communications*, *29*(3), 193-207. https://doi.org/10.1097/MNM.0b013e3282f3a515
[37] Imstepf, S., Pierroz, V., Raposinho, P., Bauwens, M., Felber, M., & Fox, T. et al. (2015). Nuclear Targeting with an Auger Electron Emitter Potentiates the Action of a Widely Used Antineoplastic Drug. *Bioconjugate Chemistry*, *26*(12), 2397-2407. https://doi.org/10.1021/acs.bioconjchem.5b00466
[38] Sampson, C. (1994). *Textbook of radiopharmacy* (pp. 29-49). Amsterdam: OPA.
[39] Carroll, V., Demoin, D., Hoffman, T., & Jurisson, S. (2012). Inorganic chemistry in nuclear imaging and radiotherapy: current and future directions. *Radiochimica Acta*, *100*(8-9), 653-667. https://doi.org/10.1524/ract.2012.1964
[40] Piwnica-Worms, D., Kronauge, J., & Chiu, M. (1990). Uptake and retention of hexakis (2-methoxyisobutyl isonitrile) technetium(I) in cultured chick myocardial cells. Mitochondrial and plasma membrane potential dependence. *Circulation*, *82*(5), 1826-1838. https://doi.org/10.1161/01.cir.82.5.1826
[41] Zheng, Y., Ji, S., Tomaselli, E., Ernest, C., Freiji, T., & Liu, S. (2014). Effect of co-ligands on chemical and biological properties of 99mTc(III) complexes [99mTc(L)(CDO)(CDOH)2BMe] (L=Cl, F, SCN and N3; CDOH2=cyclohexanedione dioxime). *Nuclear Medicine And Biology*, *41*(10), 813-824. https://doi.org/10.1016/j.nucmedbio.2014.07.009
[42] Volkert, W., Hoffman, T., Seger, R., Troutner, D., & Holmes, R. (1984). 99mTc-propylene amine oxime (99mTc-PnAO); a potential brain radiopharmaceutical. *European Journal Of Nuclear Medicine*, *9*(11), 511-516. https://doi.org/10.1007/BF00263256
[43] Nowotnik, D., Canning, L., Cumming, S., Harrison, R., Higley, B., & Nechvatal , G. et al. (1985). Development of a 99Tcm-labelled radiopharmaceutical for cerebral blood flow imaging. *Nuclear Medicine Communications*, *6*(9), 499-506. https://doi.org/10.1097/00006231-198509000-00002
[44] Sharp, P., Smith, F., Gemmell, H., Lyall, D., Evans, N., & Gvozdanovic, D. et al. (1986). Technetium-99m HM-PAO stereoisomers as potential agents for imaging regional cerebral blood flow: human volunteer studies. *Journal Of Nuclear Medicine*, *27*(2), 171-177.
[45] Roddie, M., Peters, A., Danpure, H., Osman, S., Henderson, B., & Lavender, J. et al. (1988). Inflammation: imaging with Tc-99m HMPAO-labeled leukocytes. *Radiology*, *166*(3), 767-772. https://doi.org/10.1148/radiology.166.3.3340775
[46] Davey, R. J., & AuBuchon, J. P. (2007). Post-Transfusion Red Blood Cell and Platelet Survival and Kinetics: Basic Principles and Practical Aspects. Blood Banking and Transfusion Medicine, 455-466.
[47] Snyder, E., Moroff, G., Simon, T., & Heaton, A. (1986). Recommended methods for conducting radiolabeled platelet survival studies. *Transfusion*, *26*(1), 37-42. https://doi.org/10.1046/j.1537-2995.1986.26186124029.x
[48] AuBuchon, J., & Brightman, A. (1989). Use of indium-111 as a red cell label. *Transfusion*, *29*(2), 143-147. https://doi.org/10.1046/j.1537-2995.1989.29289146833.x
[49] Loken, M., Clay, M., Carpenter, R., Boudreau, R., & McCullough, J. (1985). Clinical Use of lndium-111 Labeled Blood Products. *Clinical Nuclear Medicine*, *10*(12), 902-911. https://doi.org/10.1097/00003072-198512000-00024

[50] Zeglis, B., & Lewis, J. (2011). A practical guide to the construction of radiometallated bioconjugates for positron emission tomography. *Dalton Transactions*, *40*(23), 6168-6195. https://doi.org/10.1039/C0DT01595D
[51] Liu, S. (2008). Bifunctional coupling agents for radiolabeling of biomolecules and target-specific delivery of metallic radionuclides. *Advanced Drug Delivery Reviews*, *60*(12), 1347-1370. https://doi.org/10.1016/j.addr.2008.04.006
[52] Sarkar, S., Bhatt, N., Ha, Y., Huynh, P., Soni, N., & Lee, W. et al. (2018). High in Vivo Stability of 64Cu-Labeled Cross-Bridged Chelators Is a Crucial Factor in Improved Tumor Imaging of RGD Peptide Conjugates. *Journal Of Medicinal Chemistry*, *61*(1), 385-395. https://doi.org/10.1021/acs.jmedchem.7b01671
[53] Theobald, A., & Sampson, C. (2011). *Sampson's textbook of radiopharmacy* (pp. 101–124). Pharmaceutical Press.
[54] Anderson, C. J., Wadas, T. J., Wong, E. H., & Weisman, G. R. (2008). Cross-bridged macrocyclic chelators for stable complexation of copper radionuclides for PET imaging. *The quarterly journal of nuclear medicine and molecular imaging : official publication of the Italian Association of Nuclear Medicine (AIMN) [and] the International Association of Radiopharmacology (IAR), [and] Section of the Society of...*, *52*(2), 185–192.
[55] Ferdani, R., Stigers, D., Fiamengo, A., Wei, L., Li, B., & Golen, J. et al. (2012). Synthesis, Cu(ii) complexation,64Cu-labeling and biological evaluation of cross-bridged cyclam chelators with phosphonate pendant arms. *Dalton Trans.*, *41*(7), 1938-1950. https://doi.org/10.1039/c1dt11743b
[56] Boswell, C., Sun, X., Niu, W., Weisman, G., Wong, E., Rheingold, A., & Anderson, C. (2004). Comparative in Vivo Stability of Copper-64-Labeled Cross-Bridged and Conventional Tetraazamacrocyclic Complexes. *Journal Of Medicinal Chemistry*, *47*(6), 1465-1474. https://doi.org/10.1021/jm030383m
[57] Abdulwahaab, B., Burke, B., Domarkas, J., Silversides, J., Prior, T., & Archibald, S. (2016). Mono- and Bis-Alkylation of Glyoxal-Bridged Tetraazamacrocycles Using Mechanochemistry. *The Journal Of Organic Chemistry*, *81*(3), 890-898. https://doi.org/10.1021/acs.joc.5b02464
[58] Mewis, R., & Archibald, S. (2010). Biomedical applications of macrocyclic ligand complexes. *Coordination Chemistry Reviews*, *254*(15-16), 1686-1712. https://doi.org/10.1016/j.ccr.2010.02.025
[59] Price, E., & Orvig, C. (2014). Matching chelators to radiometals for radiopharmaceuticals. *Chem. Soc. Rev.*, *43*(1), 260-290. https://doi.org/10.1039/c3cs60304k
[60] Caravan, P. (2009). Protein-Targeted Gadolinium-Based Magnetic Resonance Imaging (MRI) Contrast Agents: Design and Mechanism of Action. *Accounts Of Chemical Research*, *42*(7), 851-862. https://doi.org/10.1021/ar800220p
[61] Caravan, P., Ellison, J., McMurry, T., & Lauffer, R. (1999). Gadolinium(III) Chelates as MRI Contrast Agents: Structure, Dynamics, and Applications. *Chemical Reviews*, *99*(9), 2293-2352. https://doi.org/10.1021/cr980440x
[62] Ramogida, C., & Orvig, C. (2013). Tumour targeting with radiometals for diagnosis and therapy. *Chemical Communications*, *49*(42), 4720-4739. https://doi.org/10.1039/C3CC41554F
[63] Hubin, T., McCormick, J., Collinson, S., Buchalova, M., Perkins, C., & Alcock, N. et al. (2000). New Iron(II) and Manganese(II) Complexes of Two Ultra-Rigid, Cross-Bridged Tetraazamacrocycles for Catalysis and Biomimicry. *Journal Of The American Chemical Society*, *122*(11), 2512-2522. https://doi.org/10.1021/ja990366f
[64] Busch, D. (1993). The complete coordination chemistry - one practioner's perspective. *Chemical Reviews*, *93*(3), 847-860. https://doi.org/10.1021/cr00019a001

[65] Denat, F., Lacour, S., Brandès, S., & Guilard, R. (1997). A two-step synthesis of new macrobicyclic aza-ligands starting from “trans”dioxocyclam as diprotected macrocycle. *Tetrahedron Letters*, *38*(25), 4417-4420. https://doi.org/10.1016/s0040-4039(97)00944-1
[66] Woodin, K., Heroux, K., Boswell, C., Wong, E., Weisman, G., & Niu, W. et al. (2005). Kinetic Inertness and Electrochemical Behavior of Copper(II) Tetraazamacrocyclic Complexes: Possible Implications for in Vivo Stability. *European Journal Of Inorganic Chemistry*, *2005*(23), 4829-4833. https://doi.org/10.1002/ejic.200500579
[67] Heroux, K., Woodin, K., Tranchemontagne, D., Widger, P., Southwick, E., & Wong, E. et al. (2007). The long and short of it: the influence of N-carboxyethyl versusN-carboxymethyl pendant arms on in vitro and in vivo behavior of copper complexes of cross-bridged tetraamine macrocycles. *Dalton Transactions*, (21), 2150-2162. https://doi.org/10.1039/b702938a
[68] Alder, R. (1989). Strain effects on amine basicities. *Chemical Reviews*, *89*(5), 1215-1223. https://doi.org/10.1021/cr00095a015
[69] Hancock, R., & Martell, A. (1989). Ligand design for selective complexation of metal ions in aqueous solution. *Chemical Reviews*, *89*(8), 1875-1914. https://doi.org/10.1021/cr00098a011
[70] Ciampolini, M., Nardi, N., Valtancoli, B., & Micheloni, M. (1992). Small aza cages as “fast proton sponges” and strong lithium binders. *Coordination Chemistry Reviews*, *120*, 223-236. https://doi.org/10.1016/0010-8545(92)80053-T
[71] Bencini, A., Bianchi, A., Bazzicalupi, C., Ciampolini, M., Dapporto, P., & Fusi, V. et al. (1993). Synthesis and characterization of an aza-cage behaving as a ‘proton sponge’. Crystal structures of its mono- and tri-protonated species. *J. Chem. Soc., Perkin Trans. 2*, (1), 115-120. https://doi.org/10.1039/P29930000115
[72] Ingham, A., Rodopoulos, M., Coulter, K., Rodopoulos, T., Subramanian, S., & McAuley, A. (2002). Synthesis, characterization and reactivity of some macrobicyclic and macrotricyclic hetero-clathrochelate complexes. *Coordination Chemistry Reviews*, *233-234*, 255-271. https://doi.org/10.1016/S0010-8545(02)00031-0
[73] Springborg, J. (2003). Adamanzanes—bi- and tricyclic tetraamines and their coordination compoundsElectronic supplementary information (ESI) available: tables of variations in Nax–M–Nax angles as a function of cavity size and the radius of the central ion. Dalton Transactions, (9), 1653-1665. https://doi.org/10.1039/B300510K
[74] Alder, R. (1990). Intrabrigehead chemistry. *Tetrahedron*, *46*(3), 683-713. https://doi.org/10.1016/S0040-4020(01)81354-5
[75] Hubin, T. (2003). Synthesis and coordination chemistry of topologically constrained azamacrocycles. *Coordination Chemistry Reviews*, *241*(1-2), 27-46. https://doi.org/10.1016/S0010-8545(02)00307-7
[76] Hancock, R., Pattrick, G., Wade, P., & Hosken, G. (1993). Structurally reinforced macrocyclic ligands. *Pure And Applied Chemistry*, *65*(3), 473-476. https://doi.org/10.1351/pac199365030473
[77] Dietrich, B., Viout, P., & Lehn, J. (1993). *Macrocyclic chemistry*. VCH.
[78] Hubin, T., Alcock, N., Morton, M., & Busch, D. (2003). Synthesis, structure, and stability in acid of copper(II) and zinc(II) complexes of cross-bridged tetraazamacrocycles. *Inorganica Chimica Acta*, *348*, 33-40. https://doi.org/10.1016/S0020-1693(03)00036-7
[79] Hubin, T., McCormick, J., Collinson, S., Alcock, N., Clase, H., & Busch, D. (2003). Synthesis and X-ray crystal structures of iron(II) and manganese(II) complexes of unsubstituted and benzyl substituted cross-bridged tetraazamacrocycles. *Inorganica Chimica Acta*, *346*, 76-86. https://doi.org/10.1016/S0020-1693(02)01427-5

[80] Dapporto, P., Paoli, P., Bazzicalupi, C., Bencini, A., Nardi, N., Valtancoli, B., & Fusi, V. (1996). Conformational investigation of some macrobicyclic compounds and of their monoprotonated cations through a comparison between X-ray crystal structures and molecular dynamics simulations. *Supramolecular Chemistry*, *7*(3), 195-200. https://doi.org/10.1080/10610279608027516
[81] Bencini, A., Bianchi, A., Chimichi, S., Ciampolini, M., Dapporto, P., & Garcia-Espana, E. et al. (1991). Lithium binder in aqueous solution. Synthesis and characterization of the new cage 4,10,15-trimethyl-1,4,7,10,15-pentaazabicyclo[5.5.5]heptadecane (L). Protonation and lithium complex formation. Crystal structures of [HL][BPh4] and [LiL][BPh4]. *Inorganic Chemistry*, *30*(19), 3687-3691. https://doi.org/10.1021/ic00019a024
[82] Bencini, A., Bianchi, A., Ciampolini, M., Dapporto, P., Micheloni, M., & Nardi, N. et al. (1992). Synthesis and characterization of the aza-cage 4-benzyl-10,15-dimethyl-1,4,7,10,15-pentaazabicyclo[5.5.5]heptadecane (L). Its proton transfer properties and lithium complex. The crystal structure of the monoprotonated salt [HL][BPh4]. *Journal Of The Chemical Society, Perkin Transactions 2*, (2), 181-184. https://doi.org/10.1039/P29920000181
[83] Bencini, A., Bianchi, A., Borselli, A., Chimichi, S., Ciampolini, M., & Dapporto, P. et al. (1990). Selective lithium encapsulation in aqueous solution by the new cage 4,10-dimethyl-1,4,7,10,15-pentaazabicyclo[5.5.5]heptadecane (L). Synthesis, characterization, and structural aspects. Crystal structures of [LiL](ClO4) and [CuL]Br2.cntdot.3H2O. *Inorganic Chemistry*, *29*(18), 3282-3286. https://doi.org/10.1021/ic00343a005
[84] Bencini, A., Bianchi, A., Bazzicalupi, C., Ciampolini, M., Fusi, V., & Micheloni, M. et al. (1994). Proton inclusion properties of a new azamacrocycle. Synthesis, characterization and crystal structure of [H3L][Cl]3·2H2O (L = 4,10-dimethyl-1,4,7,10-tetraazabicyclo [5.5.2] tetradecane). *Supramolecular Chemistry*, *3*(2), 141-146. https://doi.org/10.1080/10610279408029852
[85] Smith, P., Dye, J., Cheney, J., & Lehn, J. (1981). Proton cryptates. Kinetics and thermodynamics of protonation of the [1.1.1] macrobicyclic cryptand. *Journal Of The American Chemical Society*, *103*(20), 6044-6048. https://doi.org/10.1021/ja00410a009
[86] Ciampolini, M., Mangani, S., Micheloni, M., Orioli, P., Vizza, F., & Zanobini, F. (1986). Crystal Structure of the Hydrobromic Salt of 12,17-Dimethyl-1,5,9,12,17-penta-azabicyclo[7,5,5]nonadecane, a Satured Azacryptand Behaving as "protonic sponge". *Gazzetta Chimica Italiana*, *116*, 189-192.
[87] Koutsantonis, G., Lee, J., Lengkeek, N., Nealon, G., Skelton, B., & White, A. (2009). Synthesis and characterisation of trinuclear metal complexes derived from carboxymethyl-substituted sarcophagine macrobicyclic cage amines. *Journal Of Inclusion Phenomena And Macrocyclic Chemistry*, *66*(1-2), 61-66. https://doi.org/10.1007/s10847-009-9634-6
[88] Ma, M., Cooper, M., Paul, R., Shaw, K., Karas, J., & Scanlon, D. et al. (2011). Macrobicyclic Cage Amine Ligands for Copper Radiopharmaceuticals: A Single Bivalent Cage Amine Containing Two Lys3-bombesin Targeting Peptides. *Inorganic Chemistry*, *50*(14), 6701-6710. https://doi.org/10.1021/ic200681s
[89] Wainwright, K. P. (1980). Bridging alkylation of saturated polyaza macrocycles: a means for imparting structural rigidity. *Inorganic Chemistry*, *19*(5), 1396-1398. https://doi.org/10.1021/ic50207a062
[90] Ramasubbu, A., & Wainwright, K. (1982). Structurally reinforced cyclen: a rigidly trans-co-ordinating twelve-membered macrocycle. *Journal Of The Chemical Society, Chemical Communications*, (5), 277-278. https://doi.org/10.1039/c39820000277
[91] Weisman, G., Rogers, M., Wong, E., Jasinski, J., & Paight, E. (1990). Cross-bridged cyclam. Protonation and lithium cation (Li+) complexation in a diamond-lattice cleft. *Journal Of The American Chemical Society*, *112*(23), 8604-8605. https://doi.org/10.1021/ja00179a067

[92] Wong, E., Weisman, G., Hill, D., Reed, D., Rogers, M., & Condon, J. et al. (2000). Synthesis and Characterization of Cross-Bridged Cyclams and Pendant-Armed Derivatives and Structural Studies of Their Copper(II) Complexes. *Journal Of The American Chemical Society*, *122*(43), 10561-10572. https://doi.org/10.1021/ja001295j
[93] Bernier, N., Allali, M., Tripier, R., Conan, F., Patinec, V., & Develay, S. et al. (2006). New side-bridged bismacrocycles and cross-bridged macrotricycles. Syntheses and Cu(ii) complexation study. *New Journal Of Chemistry*, *30*(3), 435-441. https://doi.org/10.1039/B515150C
[94] Shircliff, A., Burke, B., Davilla, D., Burgess, G., Okorocha, F., & Shrestha, A. et al. (2020). An ethylene cross-bridged pentaazamacrocycle and its Cu2+ complex: constrained ligand topology and excellent kinetic stability. *Chemical Communications*, *56*(54), 7519-7522. https://doi.org/10.1039/d0cc00919a
[95] Kowallick, R., Neuburger, M., Zehnder, M., & Kaden, T. (1997). Metal Complexes with Macrocyclic Ligands. PartXLV Axial coordination tendency in reinforced tetraazamacrocyclic complexes. *Helvetica Chimica Acta*, *80*(3), 948-959. https://doi.org/10.1002/hlca.19970800326
[96] Hancock, R., Dobson, S., Evers, A., Wade, P., Ngwenya, M., Boeyens, J., & Wainwright, K. (1988). More rigid macrocyclic ligands that show metal ion size-based selectivity. Crystallographic, molecular mechanics, and formation constant study of the complexes of bridged cyclen. *Journal Of The American Chemical Society*, *110*(9), 2788-2794. https://doi.org/10.1021/ja00217a016
[97] Cooper, S. (1992). *Crown compounds* (p. 167). VCH.
[98] Weisman, G., Wong, E., Hill, D., Rogers, M., Reed, D., & Calabrese, J. (1996). Synthesis and transition-metal complexes of new cross-bridged tetraamine ligands. *Chemical Communications*, (8), 947-948. https://doi.org/10.1039/CC9960000947
[99] Weisman, G., Ho, S., & Johnson, V. (1980). Tetracyclic tetraamines by glyoxal-macrocyclic tetraamine condensation. *Tetrahedron Letters*, *21*(4), 335-338. https://doi.org/10.1016/s0040-4039(01)85466-6
[100] Hubin, T., McCormick, J., Collinson, S., Busch, D., & Alcock, N. (1998). Ultra rigid cross-bridged tetraazamacrocycles as ligands—the challenge and the solution. Chemical Communications, (16), 1675-1676. https://doi.org/10.1039/A802060D
[101] Boswell, C., Regino, C., Baidoo, K., Wong, K., Bumb, A., & Xu, H. et al. (2008). Synthesis of a Cross-Bridged Cyclam Derivative for Peptide Conjugation and 64Cu Radiolabeling. *Bioconjugate Chemistry*, *19*(7), 1476-1484. https://doi.org/10.1021/bc800039e
[102] Rodríguez-Rodríguez, A., Regueiro-Figueroa, M., Esteban-Gómez, D., Tripier, R., Tircsó, G., & Kálmán, F. et al. (2016). Complexation of Ln3+ Ions with Cyclam Dipicolinates: A Small Bridge that Makes Huge Differences in Structure, Equilibrium, and Kinetic Properties. *Inorganic Chemistry*, *55*(5), 2227-2239. https://doi.org/10.1021/acs.inorgchem.5b02627
[103] Pazderová, L., David, T., Hlinová, V., Plutnar, J., Kotek, J., & Lubal, P. et al. (2020). Cross-Bridged Cyclam with Phosphonate and Phosphinate Pendant Arms: Chelators for Copper Radioisotopes with Fast Complexation. *Inorganic Chemistry*, *59*(12), 8432-8443. https://doi.org/10.1021/acs.inorgchem.0c00856
[104] Liu, W., Hao, G., Long, M., Anthony, T., Hsieh, J., & Sun, X. (2009). Imparting Multivalency to a Bifunctional Chelator: A Scaffold Design for Targeted PET Imaging Probes. *Angewandte Chemie International Edition*, *48*(40), 7346-7349. https://doi.org/10.1002/anie.200903556
[105] Lewis, E., Boyle, R., & Archibald, S. (2004). Ultrastable complexes for in vivo use: a bifunctional chelator incorporating a cross-bridged macrocycle. *Chemical Communications*, (19), 2212-2213. https://doi.org/10.1039/B406906D

[106] Springborg, J., Kofod, P., Olsen, C., Toftlund, H., & Søtofte, I. (1995). Synthesis and Crystal Structure of a Small Bicyclic Tetraaza Proton Sponge, 1,4,7,10-Tetraazabicyclo[5.5.3]pentadecane Dibromide Perchlorate. *Acta Chemica Scandinavica*, *49*, 547-554. https://doi.org/10.3891/acta.chem.scand.49-0547
[107] Springborg, J., & Søtofte, I. (1997). Synthetic, Thermodynamic and Crystallographic Studies of Pentacoordinated Copper(II) Complexes with [$2^4.3^1$]Adamanzane, 1,4,7,10-Tetraazabicyclo[5.5.3]pentadecane, and Bromide, Iodide, Hydroxide, Water or Ammonia. *Acta Chemica Scandinavica*, *51*, 357-366. https://doi.org/10.3891/acta.chem.scand.51-0357
[108] Odendaal, A., Fiamengo, A., Ferdani, R., Wadas, T., Hill, D., & Peng, Y. et al. (2011). Isomeric Trimethylene and Ethylene Pendant-armed Cross-bridged Tetraazamacrocycles and in Vitro/in Vivo Comparisions of their Copper(II) Complexes. *Inorganic Chemistry*, *50*(7), 3078-3086. https://doi.org/10.1021/ic200014w
[109] Pandya, D., Dale, A., Kim, J., Lee, H., Ha, Y., An, G., & Yoo, J. (2012). New Macrobicyclic Chelator for the Development of Ultrastable64Cu-Radiolabeled Bioconjugate. *Bioconjugate Chemistry*, *23*(3), 330-335. https://doi.org/10.1021/bc200539t
[110] Pandya, D., Bhatt, N., An, G., Ha, Y., Soni, N., & Lee, H. et al. (2014). Propylene Cross-Bridged Macrocyclic Bifunctional Chelator: A New Design for Facile Bioconjugation and Robust 64Cu Complex Stability. *Journal Of Medicinal Chemistry*, *57*(17), 7234-7243. https://doi.org/10.1021/jm500348z
[111] Bhatt, N., Soni, N., Ha, Y., Lee, W., Pandya, D., & Sarkar, S. et al. (2015). Phosphonate Pendant Armed Propylene Cross-Bridged Cyclam: Synthesis and Evaluation as a Chelator for Cu-64. *ACS Medicinal Chemistry Letters*, *6*(11), 1162-1166. https://doi.org/10.1021/acsmedchemlett.5b00362
[112] Bencini, A., Bianchi, A., Borselli, A., Ciampolini, M., Micheloni, M., & Paoli, P. et al. (1990). Structural aspects of the protonation of small cages. Preparation of the new aza-cage 12,17-dimethyl-1,9,12,17-tetra-azabicyclo[7.5.5]nonadecane (L). Thermodynamic studies on solution equilibria. Crystal structures of [H2L][CoCl4] and [H2L1][CoCl4] salts. *J. Chem. Soc., Perkin Trans. 2*, (1), 209-214. https://doi.org/10.1039/P29900000209
[113] Bencini, A., Bianchi, A., Bazzicalupi, C., Ciampolini, M., Dapporto, P., & Fusi, V. et al. (1993). Synthesis and characterization of an aza-cage, basicity behaviour and crystal structure of its diprotonated species. *Journal Of The Chemical Society, Perkin Transactions 2*, (4), 715-720. https://doi.org/10.1039/P29930000715
[114] Sargeson, A. (1996). The potential for the cage complexes in biology. *Coordination Chemistry Reviews*, *151*, 89-114. https://doi.org/10.1016/s0010-8545(96)90197-6
[115] McArdle, H., Gross, S., Creaser, I., Sargeson, A., & Danks, D. (1989). Effect of chelators on copper metabolism and copper pools in mouse hepatocytes. *American Journal Of Physiology-Gastrointestinal And Liver Physiology*, *256*(4), G667-G672. https://doi.org/10.1152/ajpgi.1989.256.4.G667
[116] Di Bartolo, N., Sargeson, A., Donlevy, T., & Smith, S. (2001). Synthesis of a new cage ligand, SarAr, and its complexation with selected transition metal ions for potential use in radioimaging†. *Journal Of The Chemical Society, Dalton Transactions*, (15), 2303-2309. https://doi.org/10.1039/B103242A
[117] Engelhardt, L., Grøndahl, L., Harrowfield, J., Ralph, S., Sargeson, A., & Skelton, B. et al. (2011). Copper(II) environments in some macrobicycle complexes at room and low temperatures: some novel binuclear chloro-bridged systems. *Journal Of Inclusion Phenomena And Macrocyclic Chemistry*, *71*(3-4), 353-362. http://dx.doi.org/10.1007/s10847-011-9952-3
[118] Smith, R., Huskens, D., Daelemans, D., Mewis, R., Garcia, C., & Cain, A. et al. (2012). CXCR4 chemokine receptor antagonists: nickel(ii) complexes of configurationally restricted macrocycles. *Dalton Transactions*, *41*(37), 11369-11377. https://doi.org/10.1039/C2DT31137B

[119] Khan, A., Silversides, J., Madden, L., Greenman, J., & Archibald, S. (2007). Fluorescent CXCR4 chemokine receptor antagonists: metal activated binding. *Chem. Commun.*, (4), 416-418. https://doi.org/10.1039/B614557D
[120] Lukeš, I., Kotek, J., Vojtíšek, P., & Hermann, P. (2001). Complexes of tetraazacycles bearing methylphosphinic/phosphonic acid pendant arms with copper(II), zinc(II) and lanthanides(III). A comparison with their acetic acid analogues. *Coordination Chemistry Reviews*, *216-217*, 287-312. https://doi.org/10.1016/S0010-8545(01)00336-8
[121] Yapp, D., Ferreira, C., Gill, R., Boros, E., Wong, M., & Mandel, D. et al. (2013). Imaging Tumor Vasculature Noninvasively with Positron Emission Tomography and RGD Peptides Labeled with Copper 64 Using the Bifunctonal Chelates DOTA, Oxo-DO3A. and PCTA. *Molecular Imaging*, *12*(4), 263-272. https://doi.org/10.2310/7290.2012.00044
[122] Boswell, C., Regino, C., Baidoo, K., Wong, K., Milenic, D., & Kelley, J. et al. (2009). A novel side-bridged hybrid phosphonate/acetate pendant cyclam: Synthesis, characterization, and 64Cu small animal PET imaging. *Bioorganic & Medicinal Chemistry*, *17*(2), 548-552. https://doi.org/10.1016/j.bmc.2008.11.073
[123] Stigers, D., Ferdani, R., Weisman, G., Wong, E., Anderson, C., & Golen, J. et al. (2010). A new phosphonate pendant-armed cross-bridged tetraaminechelator accelerates copper(ii) binding for radiopharmaceutical applications. *Dalton Trans.*, *39*(7), 1699-1701. https://doi.org/10.1039/b920871b
[124] Füzerová, S., Kotek, J., Císařová, I., Hermann, P., Binnemans, K., & Lukeš, I. (2005). Cyclam (1,4,8,11-tetraazacyclotetradecane) with one methylphosphonate pendant arm: a new ligand for selective copper(ii) binding. *Dalton Transactions*, (17), 2908-2915. https://doi.org/10.1039/B507062G
[125] Kotek, J., Lubal, P., Hermann, P., Císařová, I., Lukeš, I., & Godula, T. et al. (2003). High Thermodynamic Stability and Extraordinary Kinetic Inertness of Copper(II) Complexes with 1,4,8,11-Tetraazacyclotetradecane-1,8-bis(methylphosphonic acid): Example of a Rare Isomerism between Kinetically Inert Penta- and Hexacoordinated Copper(II) Complexes. *Chemistry - A European Journal*, *9*(1), 233-248. https://doi.org/10.1002/chem.200390017
[126] Sun, X., Wuest, M., Kovacs, Z., Sherry, D., Motekaitis, R., & Wang, Z. et al. (2003). In vivo behavior of copper-64-labeled methanephosphonate tetraaza macrocyclic ligands. *JBIC Journal Of Biological Inorganic Chemistry*, *8*(1), 217-225. https://doi.org/10.1007/s00775-002-0408-5
[127] Svobodová, I., Havlíčková, J., Plutnar, J., Lubal, P., Kotek, J., & Hermann, P. (2009). Metal Complexes of 4,11-Dimethyl-1,4,8,11-tetraazacyclotetradecane-1,8-bis(methylphosphonic acid) - Thermodynamic and Formation/Decomplexation Kinetic Studies. *European Journal Of Inorganic Chemistry*, *2009*(24), 3577-3592. https://doi.org/10.1002/ejic.200900358
[128] Bianchini, C., Giambastiani, G., Laschi, F., Mariani, P., Vacca, A., Vizza, F., & Zanello, P. (2003). Synthesis, characterization and coordination chemistry of the new tetraazamacrocycle 4,10-dimethyl-1,4,7,10-tetraazacyclododecane-1,7-bis(methanephosphonic acid monoethyl ester) dipotassium salt. *Organic & Biomolecular Chemistry*, *1*(5), 879-886. https://doi.org/10.1039/b210655h
[129] Bel'skii, F., Polikarpov, Y., & Kabachnik, M. (1992). Cyclopendant ligands. *Russian Chemical Reviews*, *61*(2), 221-242. http://dx.doi.org/10.1070/RC1992v061n02ABEH000942
[130] Cole, E., Copley, R., Howard, J., Parker, D., Ferguson, G., & Gallagher, J. et al. (1994). 1,4,7-Triazacyclononane-1,4,7-triyltrimethylenetris-(phenylphosphinate) enforces octahedral geometry: crystal and solution structures of its metal complexes and comparative biodistribution studies of radiolabelled indium and gallium complexes. *Journal Of The Chemical Society, Dalton Transactions*, (11), 1619-1629. https://doi.org/10.1039/DT9940001619

[131] Atwood, J., MacNicol, D., Davies, J., Vogtle, F., Lehn, J., & Reinhoudt, D. (1996). *Comprehensive Supramolecular Chemistry*. Pergamon.
[132] Harrison, A., Walker, C., Pereira, K., Parker, D., Royle, L., Pulukkody, K., & Norman, T. (1993). Hepato-biliary and renal excretion in mice of charged and neutral gadolinium complexes of cyclic tetra-aza-phosphinic and carboxylic acids. *Magnetic Resonance Imaging*, *11*(6), 761-770. https://doi.org/10.1016/0730-725X(93)90194-I
[133] Norman, T., Parker, D., Royle, L., Harrison, A., Antoniw, P., & King, D. (1995). Improved tumour targeting with recombinant antibody–macrocycle conjugates. *J. Chem. Soc., Chem. Commun.*, (18), 1877-1878. https://doi.org/10.1039/C39950001877
[134] Dean Sherry, A. (1997). MR imaging and spectroscopy applications of lanthanide complexes with macrocyclic phosphonate and phosphonate ester ligands. *Journal Of Alloys And Compounds*, *249*(1-2), 153-157. https://doi.org/10.1016/s0925-8388(96)02518-2
[135] Geraldes, C., Marques, M., Castro, B., & Pereira, E. (2000). Study of Copper(II) Polyazamacrocyclic Complexes by Electronic Absorption Spectrophotometry and EPR Spectroscopy. *European Journal Of Inorganic Chemistry*, *2000*(3), 559-565. https://doi.org/10.1002/(SICI)1099-0682(200003)2000:3<559::AID-EJIC559>3.0.CO;2-J
[136] Lubal, P., Kývala, M., Hermann, P., Holubová, J., Rohovec, J., Havel, J., & Lukeš, I. (2001). Thermodynamic and kinetic study of copper(II) complexes with N-methylene(phenylphosphinic acid) derivatives of cyclen and cyclam. *Polyhedron*, *20*(1-2), 47-55. https://doi.org/10.1016/S0277-5387(00)00586-6
[137] Giambastiani, G., Oberhauser, W., Bianchini, C., Laschi, F., Sorace, L., & Brueggeller, P. et al. (2005). Synthesis and Characterisation of a Novel Copper(II) Azamacrocycle-Phosphonate 3D Polymeric Network. *European Journal Of Inorganic Chemistry*, *2005*(11), 2027-2031. https://doi.org/10.1002/ejic.200500118
[138] Svobodová, I., Lubal, P., Plutnar, J., Havlíčková, J., Kotek, J., Hermann, P., & Lukeš, I. (2006). Thermodynamic, kinetic and solid-state study of divalent metal complexes of 1,4,8,11-tetraazacyclotetradecane (cyclam) bearing two trans (1,8-)methylphosphonic acid pendant arms. *Dalton Trans.*, (43), 5184-5197. https://doi.org/10.1039/B603251F
[139] Rudovský, J., Kotek, J., Hermann, P., Lukeš, I., Mainero, V., & Aime, S. (2005). Synthesis of a bifunctional monophosphinic acid DOTA analogue ligand and its lanthanide(iii) complexes. A gadolinium(iii) complex endowed with an optimal water exchange rate for MRI applications. *Org. Biomol. Chem.*, *3*(1), 112-117. https://doi.org/10.1039/B410103K
[140] Šimeček, J., Schulz, M., Notni, J., Plutnar, J., Kubíček, V., Havlíčková, J., & Hermann, P. (2011). Complexation of Metal Ions with TRAP (1,4,7-Triazacyclononane Phosphinic Acid) Ligands and 1,4,7-Triazacyclononane-1,4,7-triacetic Acid: Phosphinate-Containing Ligands as Unique Chelators for Trivalent Gallium. *Inorganic Chemistry*, *51*(1), 577-590. https://doi.org/10.1021/ic202103v
[141] Lazar, I., Sherry, A., Ramasamy, R., Brucher, E., & Kiraly, R. (1991). Synthesis and complexation properties of a new macrocyclic polyaza polyphosphinate ligand, DOTEP (1,4,7,10-tetraazacyclododecane-1,4,7,10-tetrakis(methyleneethylphosphinate)). *Inorganic Chemistry*, *30*(26), 5016-5019. https://doi.org/10.1021/ic00026a030
[142] Meckel, M., Fellner, M., Thieme, N., Bergmann, R., Kubicek, V., & Rösch, F. (2013). In vivo comparison of DOTA based 68Ga-labelled bisphosphonates for bone imaging in non-tumour models. *Nuclear Medicine And Biology*, *40*(6), 823-830. https://doi.org/10.1016/j.nucmedbio.2013.04.012
[143] Bergmann, R., Meckel, M., Kubíček, V., Pietzsch, J., Steinbach, J., Hermann, P., & Rösch, F. (2016). 177Lu-labelled macrocyclic bisphosphonates for targeting bone metastasis in cancer treatment. *EJNMMI Research*, *6*(1). https://doi.org/10.1186/s13550-016-0161-3
[144] Weilbaecher, K., Guise, T., & McCauley, L. (2011). Cancer to bone: a fatal attraction. *Nature Reviews Cancer*, *11*(6), 411-425. https://doi.org/10.1038/nrc3055

[145] Rubini, G., Nicoletti, A., Rubini, D., & Asabella, A. (2014). Radiometabolic Treatment of Bone-Metastasizing Cancer: From 186Rhenium to 223Radium. *Cancer Biotherapy And Radiopharmaceuticals*, *29*(1), 1-11. https://doi.org/10.1089/cbr.2013.1549
[146] Paes, F., & Serafini, A. (2010). Systemic Metabolic Radiopharmaceutical Therapy in the Treatment of Metastatic Bone Pain. *Seminars In Nuclear Medicine*, *40*(2), 89-104. https://doi.org/10.1053/j.semnuclmed.2009.10.003
[147] Meckel, M., Kubíček, V., Hermann, P., Miederer, M., & Rösch, F. (2016). A DOTA based bisphosphonate with an albumin binding moiety for delayed body clearance for bone targeting. *Nuclear Medicine And Biology*, *43*(11), 670-678. https://doi.org/10.1016/j.nucmedbio.2016.07.009
[148] Holub, J., Meckel, M., Kubíček, V., Rösch, F., & Hermann, P. (2014). Gallium(III) complexes of NOTA-bis (phosphonate) conjugates as PET radiotracers for bone imaging. *Contrast Media & Molecular Imaging*, *10*(2), 122-134. https://doi.org/10.1002/cmmi.1606
[149] Zhang, S., Gangal, G., & Uludağ, H. (2007). 'Magic bullets' for bone diseases: progress in rational design of bone-seeking medicinal agents. *Chem. Soc. Rev.*, *36*(3), 507-531. https://doi.org/10.1039/b512310k
[150] Kubíček, V., & Lukeš, I. (2010). Bone-seeking probes for optical and magnetic resonance imaging. *Future Medicinal Chemistry*, *2*(3), 521-531. https://doi.org/10.4155/fmc.09.162
[151] Palma, E., Correia, J., Campello, M., & Santos, I. (2011). Bisphosphonates as radionuclide carriers for imaging or systemic therapy. *Molecular Biosystems*, *7*(11), 2950-2966. https://doi.org/10.1039/c1mb05242j
[152] Fleisch, H. (2000). *Bisphosphonates in Bone Disease* (4th ed.). Academic Press.
[153] Vitha, T., Kubíček, V., Kotek, J., Hermann, P., Vander Elst, L., & Muller, R. et al. (2009). Gd(iii) complex of a monophosphinate-bis(phosphonate) DOTA analogue with a high relaxivity; Lanthanide(iii) complexes for imaging and radiotherapy of calcified tissues. *Dalton Transactions*, (17), 3204-3214. https://doi.org/10.1039/b820705d
[154] Shea, J., & Miller, S. (2005). Skeletal function and structure: Implications for tissue-targeted therapeutics. *Advanced Drug Delivery Reviews*, *57*(7), 945-957. https://doi.org/10.1016/j.addr.2004.12.017
[155] Wang, D., Miller, S., Kopecková, P., & Kopecek, J. (2005). Bone-targeting macromolecular therapeutics. *Advanced Drug Delivery Reviews*, *57*(7), 1049-1076. https://doi.org/10.1016/j.addr.2004.12.011
[156] Ogawa, K., & Washiyama, K. (2012). Bone Target Radiotracers for Palliative Therapy of Bone Metastases. *Current Medicinal Chemistry*, *19*(20), 3290-3300. https://doi.org/10.2174/092986712801215865
[157] Kabachnik, I., Medved', T., Bel'skii, F., & Pisareva, S. (1984). Synthesis and acid-base and complex-forming properties of 1,4,7,10-tetrakis(dihydroxyphosphorylmethyl)-1,4,7,10-tetraazacyclododecane. *Bulletin Of The Academy Of Sciences Of The USSR Division Of Chemical Science*, *33*(4), 777-782. https://doi.org/10.1007/BF00947832
[158] Kabachnik, M., Medved', T., Polikarpov, Y., Shcherbakov, B., Bel'skii, F., Matrosov, E., & Pasechnik, M. (1984). Synthesis and study of a new complexone-N,N′,N″-tris-(dihydroxyphosphorylmethyl)-1,4,7-triazacyclononane. *Bulletin Of The Academy Of Sciences Of The USSR Division Of Chemical Science*, *33*(4), 769-777. https://doi.org/10.1007/BF00947831
[159] Pisareva, S., Bel'skii, F., Medved', T., & Kabachnik, M. (1987). Synthesis and complexing properties of 1,5,8,12-tetrakis(dihydroxyphqsphorylmethyl)-1,5,8,12-tetraazacyclotetradecane, a cyclopendant phosphororganic complexon. *Bulletin Of The Academy Of Sciences Of The USSR Division Of Chemical Science*, *36*(2), 372-376. https://doi.org/10.1007/BF00959385

[160] Datta, A., Panwar, P., Chuttani, K., & Mishra, A. K. (2009). Synthesis of [sup.99m]Tc-DOTMP and its preclinical evaluation as a multidentate imaging agent for skeletal metastases. *Cancer Biotherapy & Radiopharmaceuticals*, *24*(1), 123-128. https://doi.org/10.1089/cbr.2008.0536
[161] Kubíček, V., Rudovský, J., Kotek, J., Hermann, P., Vander Elst, L., & Muller, R. et al. (2005). A Bisphosphonate Monoamide Analogue of DOTA: A Potential Agent for Bone Targeting. *Journal Of The American Chemical Society*, *127*(47), 16477-16485. https://doi.org/10.1021/ja054905u
[162] Vitha, T., Kubíček, V., Hermann, P., Elst, L., Muller, R., & Kolar, Z. et al. (2008). Lanthanide(III) Complexes of Bis(phosphonate) Monoamide Analogues of DOTA: Bone-Seeking Agents for Imaging and Therapy. *Journal Of Medicinal Chemistry*, *51*(3), 677-683. https://doi.org/10.1021/jm7012776
[163] Ogawa, K., Kawashima, H., Shiba, K., Washiyama, K., Yoshimoto, M., & Kiyono, Y. et al. (2009). Development of [90Y]DOTA-conjugated bisphosphonate for treatment of painful bone metastases. *Nuclear Medicine And Biology*, *36*(2), 129-135. https://doi.org/10.1016/j.nucmedbio.2008.11.007
[164] Boswell, C., Regino, C., Baidoo, K., Wong, K., Milenic, D., & Kelley, J. et al. (2009). A novel side-bridged hybrid phosphonate/acetate pendant cyclam: Synthesis, characterization, and 64Cu small animal PET imaging. *Bioorganic & Medicinal Chemistry*, *17*(2), 548-552. https://doi.org/10.1016/j.bmc.2008.11.073
[165] Burai, L., Ren, J., Kovacs, Z., Brücher, E., & Sherry, A. (1998). Synthesis, Potentiometry, and NMR Studies of Two New 1,7-Disubstituted Tetraazacyclododecanes and Their Complexes Formed with Lanthanide, Alkaline Earth Metal, Mn2+, and Zn2+Ions⊥. *Inorganic Chemistry*, *37*(1), 69-75. https://doi.org/10.1021/ic970599c
[166] Kotek, J., Hermann, P., Císařová, I., Rohovec, J., & Lukeš, I. (2001). The cis/trans-isomerism on cobalt(III) complexes with 1,4,8,11-tetraazacyclotetradecane-1,8-bis(methylphosphonic acid). *Inorganica Chimica Acta*, *317*(1-2), 324-330. https://doi.org/10.1016/S0020-1693(01)00348-6
[167] Fleisch, H., Russell, R., Bisaz, S., Mühlbauer, R., & Williams, D. (1970). The Inhibitory Effect of Phosphonates on the Formation of Calcium Phosphate Crystals in vitro and on Aortic and Kidney Calcification in vivo. *European Journal Of Clinical Investigation*, *1*(1), 12-18. https://doi.org/10.1111/j.1365-2362.1970.tb00591.x
[168] Russell, R., Mühlbauer, R., Bisaz, S., Williams, D., & Fleisch, H. (1970). The influence of pyrophosphate, condensed phosphates, phosphonates and other phosphate compounds on the dissolution of hydroxyapatitein vitro and on bone resorption induced by parathyroid hormone in tissue culture and in thyroparathyroidectomised rats. *Calcified Tissue Research*, *6*(1), 183-196. https://doi.org/10.1007/BF02196199
[169] Zieba, A., Sethuraman, G., Perez, F., Nancollas, G., & Cameron, D. (1996). Influence of Organic Phosphonates on Hydroxyapatite Crystal Growth Kinetics. *Langmuir*, *12*(11), 2853-2858. https://doi.org/10.1021/la950842p
[170] Amjad, Z. (1987). The influence of polyphosphates, phosphonates, and poly(carboxylic acids) on the crystal growth of hydroxyapatite. *Langmuir*, *3*(6), 1063-1069. https://doi.org/10.1021/la00078a032
[171] Bárta, J., Hermann, P., & Kotek, J. (2019). Coordination Behavior of 1,4-Disubstituted Cyclen Endowed with Phosphonate, Phosphonate Monoethylester, and H-Phosphinate Pendant Arms. *Molecules*, *24*(18), 3324. https://doi.org/10.3390/molecules24183324

[172] Kotek, J., Vojtíšek, P., Císařová, I., Hermann, P., Jurečka, P., Rohovec, J., & Lukeš, I. (2000). Bis(methylphosphonic Acid) Derivatives of 1,4,8,11-Tetraazacyclotetradecane (Cyclam). Synthesis, Crystal and Molecular Structures, and Solution Properties. *Collection Of Czechoslovak Chemical Communications*, *65*(8), 1289-1316. https://doi.org/10.1135/cccc20001289
[173] Havlíčková, J., Medová, H., Vitha, T., Kotek, J., Císařová, I., & Hermann, P. (2008). Coordination properties of cyclam (1,4,8,11-tetraazacyclotetradecane) endowed with two methylphosphonic acid pendant arms in the 1,4-positions. *Dalton Transactions*, (39), 5378-5386. https://doi.org/10.1039/b803235a
[174] Medved', T., Kabachnik, M., Goryunova, I., Shcherbakov, B., Bel'skii, F., Petrovskii, P., & Polikarpov, Y. (1988). A new cyclopendant organophosphorus complexone –1,4,7-tris(β-dihydroxyphosphorylethyl)-1,4,7-triazacyclononane. *Bulletin Of The Academy Of Sciences Of The USSR Division Of Chemical Science*, *37*(9), 1890-1895. https://doi.org/10.1007/bf00962508
[175] Polikarpov, Y., Bel'skii, F., Pisareva, S., & Kabachnik, M. (1989). New cyclopendant organophosphorus complexing agent-1,4,7,10-tetrakis (?-dihydroxyphosphorylethyl)-1,4,7,10-tetraazacyclododecane. *Bulletin Of The Academy Of Sciences Of The USSR Division Of Chemical Science*, *38*(9), 1945-1949. https://doi.org/10.1007/bf00957797
[176] Zhang, S., Wu, K., & Sherry, A. (1999). A Novel pH-Sensitive MRI Contrast Agent. *Angewandte Chemie International Edition*, *38*(21), 3192-3194. https://doi.org/10.1002/(sici)1521-3773(19991102)38:21<3192::aid-anie3192>3.0.co;2-#
[177] Mamedov, I., Mishra, A., Angelovski, G., Mayer, H., Pålsson, L., Parker, D., & Logothetis, N. (2007). Synthesis and characterization of lanthanide complexes of DO3A-alkylphosphonates. *Dalton Transactions*, (45), 5260-5267. https://doi.org/10.1039/b711351j
[178] Mamedov, I., Táborský, P., Lubal, P., Laurent, S., Vander Elst, L., & Mayer, H. et al. (2009). Relaxometric, Thermodynamic and Kinetic Studies of Lanthanide(III) Complexes of DO3A-Based Propylphosphonates. *European Journal Of Inorganic Chemistry*, *2009*(22), 3298-3306. https://doi.org/10.1002/ejic.200900149
[179] Kubíček, V., Vitha, T., Kotek, J., Hermann, P., Vander Elst, L., & Muller, R. et al. (2010). Towards MRI contrast agents responsive to Ca(II) and Mg(II) ions: metal-induced oligomerization of dota-bisphosphonate conjugates. *Contrast Media & Molecular Imaging*, *5*(5), 294-296. https://doi.org/10.1002/cmmi.386
[180] Nguyen, A., Reyes, A., Zhang, M., McDonald, P., Wong, W., Damico, L., & Dennis, M. (2006). The pharmacokinetics of an albumin-binding Fab (AB.Fab) can be modulated as a function of affinity for albumin. *Protein Engineering Design And Selection*, *19*(7), 291-297. https://doi.org/10.1093/protein/gzl011
[181] Dennis, M., Zhang, M., Meng, Y., Kadkhodayan, M., Kirchhofer, D., Combs, D., & Damico, L. (2002). Albumin Binding as a General Strategy for Improving the Pharmacokinetics of Proteins. *Journal Of Biological Chemistry*, *277*(38), 35035-35043. https://doi.org/10.1074/jbc.M205854200
[182] Andersen, J., Dee Qian, J., & Sandlie, I. (2006). The conserved histidine 166 residue of the human neonatal Fc receptor heavy chain is critical for the pH-dependent binding to albumin. *European Journal Of Immunology*, *36*(11), 3044-3051. https://doi.org/10.1002/eji.200636556
[183] Procházková, S., Kubíček, V., Kotek, J., Vágner, A., Notni, J., & Hermann, P. (2018). Lanthanide(iii) complexes of monophosphinate/monophosphonate DOTA-analogues: effects of the substituents on the formation rate and radiolabelling yield. *Dalton Transactions*, *47*(37), 13006-13015. https://doi.org/10.1039/c8dt02608d
[184] Procházková, S., Hraníček, J., Kubíček, V., & Hermann, P. (2016). Formation kinetics of europium(III) complexes of DOTA and its bis(phosphonate) bearing analogs. *Polyhedron*, *111*, 143-149. https://doi.org/10.1016/j.poly.2016.03.039

[185] Procházková, S., Kubíček, V., Böhmová, Z., Holá, K., Kotek, J., & Hermann, P. (2017). DOTA analogues with a phosphinate-iminodiacetate pendant arm: modification of the complex formation rate with a strongly chelating pendant. *Dalton Transactions*, *46*(31), 10484-10497. https://doi.org/10.1039/C7DT01797A
[186] David, T., Křečková, P., Kotek, J., Kubíček, V., & Lukeš, I. (2012). 1-hydroxy-1,1-bis(H-phosphinates): Synthesis, stability, and sorption properties. *Heteroatom Chemistry*, *23*(2), 195-201. https://doi.org/10.1002/hc.21003
[187] Bazakas, K., & Lukeš, I. (1995). Synthesis and complexing properties of polyazamacrocycles with pendant N-methylenephosphinic acid. *Journal Of The Chemical Society, Dalton Transactions*, (7), 1133-1137. https://doi.org/10.1039/dt9950001133
[188] Broan, C., Jankowski, K., Kataky, R., & Parker, D. (1990). Synthesis and complex stability of parent and C-functionalised derivatives of 1,4,7-triazacyclononane-1,4,7-tris[methylene(methylphosphinic acid)]: an effective new complexing agent. *Journal Of The Chemical Society, Chemical Communications*, (23), 1738-1739. https://doi.org/10.1039/C39900001738
[189] Pulukkody, K., Norman, T., Parker, D., Royle, L., & Broan, C. (1993). Synthesis of charged and uncharged complexes of gadolinium and yttrium with cyclic polyazaphosphinic acid ligands for in vivo applications. *Journal Of The Chemical Society, Perkin Transactions 2*, (4), 605-620. https://doi.org/10.1039/P29930000605
[190] Cole, E., Parker, D., Ferguson, G., Gallagher, J., & Kaitner, B. (1991). Synthesis and structure of chiral metal complexes of polyazacycloalkane ligands incorporating phosphinic acid donors. *Journal Of The Chemical Society, Chemical Communications*, (20), 1473-1475. https://doi.org/10.1039/C39910001473
[191] Weekes, D., Jaraquemada-Peláez, M., Kostelnik, T., Patrick, B., & Orvig, C. (2017). Di- and Trivalent Metal-Ion Solution Studies with the Phosphinate-Containing Heterocycle DEDA-(PO). *Inorganic Chemistry*, *56*(17), 10155-10161. https://doi.org/10.1021/acs.inorgchem.7b01117
[192] Lee, Y., Kim, S., Jung, D., & Hanh, J. (2015). Synthesis and Acid Catalytic Activity of 1,5,3,7-Diazadiphosphocine-1,5-dicarboxylic Acids. *Asian Journal Of Chemistry*, *27*(4), 1481-1483. https://doi.org/10.14233/ajchem.2015.18518
[193] Aime, S., Cavallotti, C., Gianolio, E., Giovenzana, G., Palmisano, G., & Sisti, M. (2002). One-step synthesis of a new eight-membered cyclic ligand from glycine, formaldehyde and hypophosphorous acid. *Tetrahedron Letters*, *43*(46), 8387-8389. https://doi.org/10.1016/S0040-4039(02)01950-0
[194] David, T., Procházková, S., Kotek, J., Kubíček, V., Hermann, P., & Lukeš, I. (2014). Aminoalkyl-1,1-bis(phosphinic acids): Stability, Acid-Base, and Coordination Properties. *European Journal Of Inorganic Chemistry*, *2014*(26), 4357-4368. https://doi.org/10.1002/ejic.201402420
[195] David, T., Procházková, S., Havlíčková, J., Kotek, J., Kubíček, V., Hermann, P., & Lukeš, I. (2013). Methylene-bis[(aminomethyl)phosphinic acids]: synthesis, acid–base and coordination properties. *Dalton Trans.*, *42*(7), 2414-2422. https://doi.org/10.1039/C2DT32045B
[196] David, T., Kubíček, V., Gutten, O., Lubal, P., Kotek, J., & Pietzsch, H. et al. (2015). Cyclam Derivatives with a Bis(phosphinate) or a Phosphinato–Phosphonate Pendant Arm: Ligands for Fast and Efficient Copper(II) Complexation for Nuclear Medical Applications. *Inorganic Chemistry*, *54*(24), 11751-11766. https://doi.org/10.1021/acs.inorgchem.5b01791
[197] Notni, J., Hermann, P., Havlíčková, J., Kotek, J., Kubíček, V., & Plutnar, J. et al. (2010). A Triazacyclononane-Based Bifunctional Phosphinate Ligand for the Preparation of Multimeric 68Ga Tracers for Positron Emission Tomography. *Chemistry - A European Journal*, *16*(24), 7174-7185. https://doi.org/10.1002/chem.200903281

[198] Soulié, M., Latzko, F., Bourrier, E., Placide, V., Butler, S., & Pal, R. et al. (2014). Comparative Analysis of Conjugated Alkynyl Chromophore-Triazacyclononane Ligands for Sensitized Emission of Europium and Terbium. *Chemistry - A European Journal*, *20*(28), 8636-8646. https://doi.org/10.1002/chem.201402415
[199] Walton, J., Bourdolle, A., Butler, S., Soulie, M., Delbianco, M., & McMahon, B. et al. (2013). Very bright europium complexes that stain cellular mitochondria. *Chemical Communications*, *49*(16), 1600-1602. https://doi.org/10.1039/c2cc35247h
[200] Butler, S., Lamarque, L., Pal, R., & Parker, D. (2014). EuroTracker dyes: highly emissive europium complexes as alternative organelle stains for live cell imaging. *Chemical Science*, *5*(5), 1750-1756. https://doi.org/10.1039/c3sc53056f
[201] Walton, J., Bari, L., Parker, D., Pescitelli, G., Puschmann, H., & Yufit, D. (2011). Structure, resolution and chiroptical analysis of stable lanthanide complexes of a pyridylphenylphosphinate triazacyclononane ligand. *Chemical Communications*, *47*(45), 12289-12291. https://doi.org/10.1039/c1cc14904k
[202] Walton, J., Carr, R., Evans, N., Funk, A., Kenwright, A., & Parker, D. et al. (2012). Isostructural Series of Nine-Coordinate Chiral Lanthanide Complexes Based on Triazacyclononane. *Inorganic Chemistry*, *51*(15), 8042-8056. https://doi.org/10.1021/ic300147p
[203] Butler, S., McMahon, B., Pal, R., Parker, D., & Walton, J. (2013). Bright Mono-aqua Europium Complexes Based on Triazacyclononane That Bind Anions Reversibly and Permeate Cells Efficiently. *Chemistry - A European Journal*, *19*(29), 9511-9517. https://doi.org/10.1002/chem.201301273
[204] McMahon, B., Pal, R., & Parker, D. (2013). A bright and responsive europium probe for determination of pH change within the endoplasmic reticulum of living cells. *Chemical Communications*, *49*(47), 5363-5365. https://doi.org/10.1039/c3cc42308e
[205] Pazderová, L., Kubíček, V., Kotek, J., & Hermann, P. (2021). 1,4,7-Triazacyclononane (tacn) with N,N ′-bridging methylene-bis(phosphinic acid) group and its complexes. *Zeitschrift Für Anorganische Und Allgemeine Chemie*, *647*(12), 1261-1268. https://doi.org/10.1002/zaac.202100107
[206] Pazderová, L., David, T., Kotek, J., Kubíček, V., & Hermann, P. (2021). Complexes of cyclen side-bridged with a methylene-bis(phosphinate) group. *Polyhedron*, *196*, 114994. https://doi.org/10.1016/j.poly.2020.114994
[207] Kubíček, V., Böhmová, Z., Ševčíková, R., Vaněk, J., Lubal, P., & Poláková, Z. et al. (2018). NOTA Complexes with Copper(II) and Divalent Metal Ions: Kinetic and Thermodynamic Studies. *Inorganic Chemistry*, *57*(6), 3061-3072. https://doi.org/10.1021/acs.inorgchem.7b02929
[208] (a) Martell, A., & Smith, R. Vols. 1–6. *Critical stability constants* (pp. 1974-1989). Plenum Press. (b) NIST Standard Reference Database 46 (Critically Selected Stability Constants of Metal Complexes), Version 7.0, 2003. (c) Baes, C., & Mesmer, R. (1976). *The hydrolysis of cations*. Wiley.
[209] Anderegg, G., Arnaud-Neu, F., Delgado, R., Felcman, J., & Popov, K. (2005). Critical evaluation of stability constants of metal complexes of complexones for biomedical and environmental applications* (IUPAC Technical Report). *Pure And Applied Chemistry*, *77*(8), 1445-1495. https://doi.org/10.1351/pac200577081445
[210] Zhong, Z., Peck, A., Li, S., VanOss, J., Snider, J., & Droscha, C. et al. (2015). 99mTC-Methylene diphosphonate uptake at injury site correlates with osteoblast differentiation and mineralization during bone healing in mice. *Bone Research*, *3*(1). https://doi.org/10.1038/boneres.2015.13

[211] Ventura, M., Franssen, G., Oosterwijk, E., Boerman, O., Jansen, J., & Walboomers, X. (2014). SPECT vs. PET monitoring of bone defect healing and biomaterial performancein vivo. *Journal Of Tissue Engineering And Regenerative Medicine*, *10*(10), 843-854. https://doi.org/10.1002/term.1862
[212] Toegel, S., Hoffmann, O., Wadsak, W., Ettlinger, D., Mien, L., & Wiesner, K. et al. (2006). Uptake of bone-seekers is solely associated with mineralisation! A study with 99mTc-MDP, 153Sm-EDTMP and 18F-fluoride on osteoblasts. *European Journal Of Nuclear Medicine And Molecular Imaging*, *33*(4), 491-494. https://doi.org/10.1007/s00259-005-0026-x
[213] Mathavan, N., Koopman, J., Raina, D., Turkiewicz, A., Tägil, M., & Isaksson, H. (2019). 18F-fluoride as a prognostic indicator of bone regeneration. *Acta Biomaterialia*, *90*, 403-411. https://doi.org/10.1016/j.actbio.2019.04.008

9 List of appendices

1. Pazderová, L., Kubíček, V., Kotek, J., & Hermann, P. (2021). 1,4,7-Triazacyclononane (tacn) with N,N′-bridging methylene-bis(phosphinic acid) group and its complexes. *Zeitschrift Für Anorganische Und Allgemeine Chemie*, *647*(12), 1261-1268. https://doi.org/10.1002/zaac.202100107

2. Pazderová, L., David, T., Kotek, J., Kubíček, V., & Hermann, P. (2021). Complexes of cyclen side-bridged with a methylene-bis(phosphinate) group. *Polyhedron*, *196*, 114994. https://doi.org/10.1016/j.poly.2020.114994

3. Pazderová, L., David, T., Hlinová, V., Plutnar, J., Kotek, J., & Lubal, P. et al. (2020). Cross-Bridged Cyclam with Phosphonate and Phosphinate Pendant Arms: Chelators for Copper Radioisotopes with Fast Complexation. *Inorganic Chemistry*, *59*(12), 8432-8443. https://doi.org/10.1021/acs.inorgchem.0c00856

4. Pazderová, L., Benešová, M., Havlíčková, J., Vojtíčková, M., Kotek, J., Lubal, P., Ullrich, M., Walther, M., Schulze, S., Neuber, Ch., Rammelt, S., Pietzsch, H., Pietzsch, J., Kubíček, V., & Hermann, P. (2021). Cyclam with a phosphinate-bis(phosphonate) pendant arm: a bone-targeting carrier of copper radionuclides. *Journal of Medicinal Chemistry*, submitted for publication

Appendix 1

Pazderová, L., Kubíček, V., Kotek, J., & Hermann, P. (2021). 1,4,7-Triazacyclononane (tacn) with N,N′-bridging methylene-bis(phosphinic acid) group and its complexes. *Zeitschrift Für Anorganische Und Allgemeine Chemie*, *647*(12), 1261-1268. https://doi.org/10.1002/zaac.202100107

Journal of Inorganic and General Chemistry
ZAAC
Zeitschrift für anorganische und allgemeine Chemie

DOI: 10.1002/zaac.202100107

ARTICLE

1,4,7-Triazacyclononane (tacn) with *N,N′*-bridging methylene-bis(phosphinic acid) group and its complexes

Lucia Pazderová,[a] Vojtěch Kubíček,*[a] Jan Kotek,[a] and Petr Hermann[a]

A bicyclic ligand, 1,4,7-triazacyclononane 1,4-bridged with methylene-bis(phosphinate) and bearing benzyl substituent on the remaining amino group, was synthesized from *N*-benzyl-tacn and $CH_2(PO_2H_2)_2$ by two sequential Mannich-type reactions in a high yield. Basicity of the macrocycle is high ($pK_1 = 12.25$). Complexes with Cu^{II} and Ni^{II} ions show dimeric structures in the solid state. The structures exhibit distorted octahedral environment with two ring amino groups from one molecule and two oxygen atoms of chelating bis(phosphinate) anion from the other molecule in the equatorial plane, and with the apical positions occupied by the remaining macrocycle amino group and by one of the phosphinate oxygen atoms. The metal ions in the dimers are additionally bridged by one phosphinate group. Stability of the Cu^{II} complex is more than ten orders of magnitude lower than that of the $[Cu(nota)]^-$ complex due to a different number and different nature of the pendant arms, and inappropriate arrangement of donor atoms in the ligand bicyclic structure. Rigidity of the short P–C–P chain of the geminal methylene-bis(phosphinate) does not allow simultaneous coordination of both phosphinate groups and the ring amines to the same metal ion. The low solubility of Ni^{II} and Zn^{II} complexes disabled determination of their stability constants.

Introduction

Polyazamacrocyclic ligands are widely used as chelating agents for complexation of metal ions. These chelators are intensively used as metal ion carriers in medicine. The most important techniques utilizing complexes of polyazamacrocyclic ligands are magnetic resonance imaging (MRI),[1–3] and positron emission tomography (PET) or single-photon emission computerized tomography (SPECT) in nuclear medicine.[4–10] The 1,4,7-triazacyclononane (tacn, Chart 1) is one of the most utilized polyazamacrocycles.[11–14] Cavity of tacn derivatives with coordinating pendant arms (e.g. H_3nota, Chart 1) is suitable for octahedral complexation of small metal ions such as Cu^{II}, Ga^{III} or Fe^{III} and, thus, the complexes commonly show a high thermodynamic stability and they are often kinetically inert.[11,12] Recently, macrobicyclic ligands has attracted increasing interest due to improved thermodynamic and kinetic properties of their complexes.[15] Presence of another ring on the polyazamacrocyclic skeleton generally leads to an increased stability of the complexes due to a more pre-organized structure of the whole ligand. Various short hydrocarbon chains have been used to bridge opposite or adjacent nitrogen atoms of azamacrocycles. Typical examples are ethylene side-bridged (sb-cyclam), and ethylene (cb-cyclam) or propylene (pcb-cyclam) cross-bridged cyclams (Chart 1) and their derivatives modified on the remaining secondary amino groups. The general drawback of these bridged chelators is their slow complexation. To overcome this shortcoming, various coordinating pendant arms have been attached to the macrocyclic core. Our research group has worked with azamacrocycles bearing phosphonate/phosphinate pendant arms for a long time and we have shown that these phosphorus acid pendants often enhance complexation rate.[16–20] Recently, we have reported very promising results for azamacrocycles bearing methylene-bis(phosphinic acid) pendant arms.[21–25] These ligands show an excellent metal-binding kinetics. The high acidity of the bis(phosphinic acid) group results in an efficient metal ion binding already in acidic solutions and the phosphinate groups have also a good ability to form hydrogen bonds. Both properties accelerate complexation.

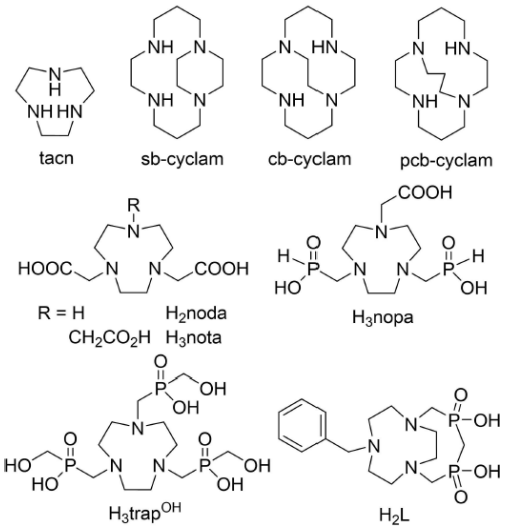

Chart 1. Ligands discused in this paper.

[a] *L. Pazderová, V. Kubíček, J. Kotek, P. Hermann*
Department of Inorganic Chemistry, Faculty of Science, Charles University, Hlavova 8, 128 40 Prague 2, Czech Republic
E-mail: kubicek@natur.cuni.cz

Supporting information for this article is available on the WWW under https://doi.org/10.1002/zaac.202100107

The phosphinate group also offers a unique capability for coordination chemistry as it is the only negatively charged group which allows its integration into a carbon chain. It opens a broad field for design of new ligands. Despite that, only a little attention has been devoted to ligands with phosphinate group integrated into a (macro)cycle.[26–28] Because of its good complexing ability mentioned above, we intended to test the methylene-bis(phosphinic acid) group as a bridging component in the bicyclic structure. Thus, macrobicyclic ligand comprising of tacn and the *N,N'*- bis(phosphinate) bridge (H_2L, Chart 1) was synthesized. The benzyl group was originally suggested as a protection of one macrocycle amine group. Removal of the group would lead to bis(phosphinate)-bridged tacn bearing one reactive secondary nitrogen atom. Such macrocyle could be further modified with a coordinating pendant arm or with a reactive (bifunctional) group which would allow attachment of the ligand/complex into functional constructs such as e.g. targeted complexes for molecular imaging applications. However, the deprotection was unsuccessful and, thus, the benzylated ligand H_2L was further investigated as this ligand anyway brings the first insight into properties of the bis(phosphinate)-bridged tacn core. Here, we report on synthesis of the ligand, determination of its protonation constant and its Cu^{II} complex thermodynamic stability, and on solid-state structures of its complexes with Cu^{II}, Ni^{II} and Li^{I} ions.

Results and Discussion

Ligand synthesis

The target ligand, H_2L, was prepared by a two-step reaction sequence utilizing two Mannich-type reactions in aqueous HCl (Scheme 1). In the first step, 1-benzyl-1,4,7-triazacyclononane (Bn-tacn) was modified with one bis(phosphinate) pendant arm by reaction with methylene-bis(*H*-phosphinic acid) and paraformaldehyde. Monosubstitution of both reactants was ensured by a sub-stoichiometric amount of paraformaldehyde. The excess of Bn-tacn and the bis(*H*-phosphinic acid) was removed by purification on a strong cation exchange resin. Compound **1** was obtained in the form of hydrochloride in 83% yield. In the second step, the remaining P–H bond and the secondary amine group of compound **1** mutually reacted using an excess of paraformaldehyde to yield H_2L. The intramolecular reaction was performed under high dilution to prevent polymerization. Ion-exchange chromatography and lyophlization gave H_2L hydrochloride as beige foam in 86% yield.

The benzyl group was originally supposed as a mono-*N*-protection of the azamacrocycle. However, deprotection was unsuccessful despite a number of attempts. No reaction was observed at ambient conditions (hydrogenation on Pd/C with hydrogen, or formate, or hypophosphite as hydrogen sources), whereas harsher conditions (a high temperature, a high hydrogen pressure) as well as other debenzylation methods (e.g. reaction with Cbz-chloride) led to decomposition of the macrobicyclic skeleton.

Crystal structures

Crystals of composition $Li_2(HL)(NO_3)\cdot 3H_2O$ were isolated from a solutions neutralized with LiOH during trials to prepare the Ga^{III} complex of H_2L. Ligand molecule is protonated on an amino group bearing the bis(phosphinate) bridge (Figure 1). Conformation of the triazacyclononane is stabilized by strong intramolecular hydrogen bonds between protonated and non-protonated azacycle amino groups (distances N1···N4/7 = 2.29/2.70 Å, respectively, Table S1). This arrangement explains rather high value of the first protonated constant of H_2L (see below). Both Li^{I} ions are tetrahedrally coordinated. The coordination sphere of one Li^{I} ion (Li1) consists from two oxygen atoms of the phosphinate pendant arms (from two different ligand molecules) and is closed by one of nitrate oxygen atoms and by a water molecule. Coordination sphere of the other Li^{I} ion (Li2) consists from three bis(phosphinate) oxygen atoms (from two different ligand molecules) and is closed by a water molecule; one of the bis(phosphinate) anion forms a six-membered chelate ring. Coordination of phosphinates from different ligand molecules to the same Li^{I} ion results in formation of 2D polymeric structure which is stabilized by a network of medium-to-strong intermolecular hydrogen bonds between water molecules and phosphinate oxygen atoms. Geometries of Li^{I} coordination spheres are outlined in Table S2.

Complexes of H_2L with Cu^{II} and Ni^{II} ions were obtained at slightly alkaline pH affording single crystals of compositions $[\{Cu(L)\}_2]\cdot 5H_2O$ and $[\{Ni(L)\}_2]\cdot 4H_2O$, respectively. In both compounds, a very similar structural motif consisting from centrosymmetric dimeric species $\{[M(L)]\}_2$ was observed. Thus, only molecular structure of the dimeric complex species $\{[Cu(L)]\}_2$ found in the crystal structure of $[\{Cu(L)\}_2]\cdot 5H_2O$ is shown in

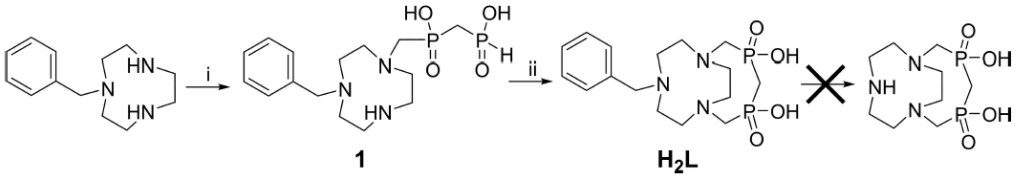

Scheme 1. Synthesis of H_2L. (*i*) $CH_2(PO_2H_2)_2$, $(CH_2O)_n$, 6 M aq. HCl, 60 °C, 3 d (83%); (*ii*) $(CH_2O)_n$, conc. aq. HCl:AcOH (1:1), high-dilution, 80 °C, 4 d (86%).

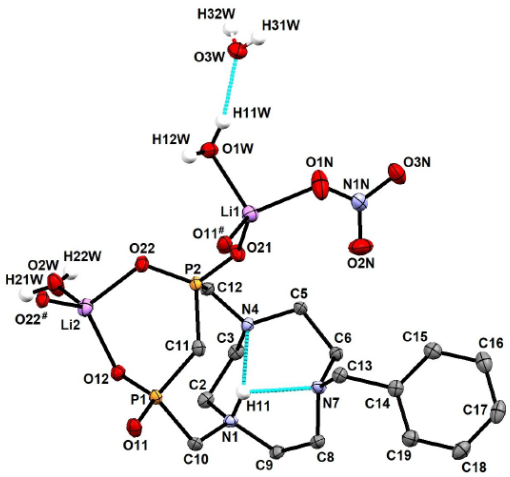

Figure 1. Structural motif found in the crystal structure of $Li_2(HL)(NO_3)\cdot 3H_2O$. Hydrogen bonds are shown as turquoise dashed lines. Carbon-bound hydrogen atoms are not displayed for the sake of clarity. Oxygen atoms O11# and O22# closing coordination spheres of Li^I ions belong to neighbouring ligand molecules.

Table 1. Geometries of Cu^{II} and Ni^{II} coordination spheres found in the crystal structures of $[\{Cu(L)\}_2]\cdot 5H_2O$ and $[\{Ni(L)\}_2]\cdot 4H_2O$.

$[\{Cu(L)\}_2]\cdot 5H_2O$		$[\{Ni(L)\}_2]\cdot 4H_2O$	
Distances (Å)			
Cu1–N1	2.049(1)	Ni1–N1	2.092(1)
Cu1–N4	2.044(1)	Ni1–N4	2.139(1)
Cu1···N7	2.330(1)	Ni1–N7	2.199(1)
Cu1–O11#	1.935(1)	Ni1–O11#	2.039(1)
Cu1–O21#	1.966(1)	Ni1–O21#	2.060(1)
Cu1···O11	2.641(1)	Ni1–O11	2.138(1)
Angles (°)			
N1–Cu1–N4	84.16(5)	N1–Ni1–N4	82.40(4)
N1–Cu1···N7	80.26(5)	N1–Ni1–N7	81.54(4)
N1–Cu1–O11#	164.72(5)	N1–Ni1–O11#	161.41(4)
N1–Cu1–O21#	96.70(5)	N1–Ni1–O21#	102.05(4)
N1–Cu1···O11	84.73(4)	N1–Ni1–O11	88.21(4)
N4–Cu1···N7	83.88(5)	N4–Ni1–N7	83.33(4)
N4–Cu1–O11#	88.76(5)	N4–Ni1–O11#	90.60(4)
N4–Cu1–O21#	172.54(5)	N4–Ni1–O21#	165.99(4)
N4–Cu1···O11	109.29(4)	N4–Ni1–O11	105.70(4)
N7···Cu1–O11#	112.48(5)	N7–Ni1–O11#	114.87(4)
N7···Cu1–O21#	88.95(4)	N7–Ni1–O21#	84.21(4)
N7···Cu1···O11	158.94(4)	N7–Ni1–O11	165.39(4)
O11#–Cu1–O21#	92.08(4)	O11#–Ni1–O21#	88.86(3)
O11#–Cu1···O11	84.87(4)	O11#–Ni1–O11	77.08(4)
O21#–Cu1···O11	78.17(4)	O21#–Ni1–O11	87.81(3)

Symmetry code #: $-x+1, -y+1, -z+1$.

Figure 2. Molecular structure of $\{[Ni(L)]\}_2$ and overlay of the Cu^{II} and Ni^{II} complexes are shown in Figures S1 and S2.

The coordination sphere around the central metal ions is a distorted octahedron with bond angles significantly deviating from theoretical 90 and 180° (Table 1). The equatorial plane of the metal ions is formed by nitrogen atoms N1 and N4 of the macrocycle and by oxygen atoms $O11^{\#}$ and $O21^{\#}$ of bis (phosphinate) group originating from the centrosymmetry-related neighboring unit and the bis(phosphinate) group forms a six-membered chelate ring. The axial positions of the octahedron are occupied by N7 and O11 atoms of the first ligand molecule (that coordinated by nitrogen atoms N1 and N4; the macrocycle is coordinated in facial fashion). In the Cu^{II} complex, the axial positions are very distant, *d*(Cu1–N7) and *d*(Cu1···O11) 2.33 and 2.64 Å, respectively, resulting in the pseudo-octahedral coordinating mode due to significant Jahn-Teller distortion.

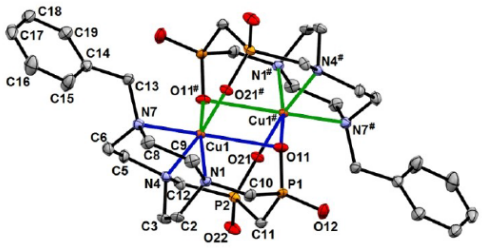

Figure 2. Molecular structure of the dimeric complex unit $\{[Cu(L)]\}_2$ found in the crystal structure of $[\{Cu(L)\}_2]\cdot 5H_2O$. Hydrogen atoms are not displayed for sake of clarity. Selected centrosymmetry-related atoms are labelled by "#". Coordination bonds of each ligand molecule are highlighted in blue or green, respectively.

In the Ni^{II} complex, corresponding axial distances are much shorter than those found in the Cu^{II} complex whereas they are still slightly longer than the equatorial ones (Table 1). The equatorial planes are distorted (mean deviations of the atoms forming the equatorial planes are 0.18 and 0.28 Å for the Cu^{II} and Ni^{II} complexes, respectively) with the central metal ions lying slightly out of theoretical equatorial planes (0.05 and 0.02 Å for the Cu^{II} and Ni^{II}, respectively). However, analysis of dihedral angles between triangles defined by donor atoms coordinated in the equatorial positions shows only negligible tetrahedral twist of the basal plane (Table S3).[29]

A detailed view on the geometry of the coordinated macrocycle in the $[\{Cu(L)\}_2]$ and $[\{Ni(L)\}_2]$ complexes show several important aspects. Geometry of the ligand does not allow bidentate coordination of bis(phosphinate) to the metal ion that is bound in the macrocyclic cavity of the same ligand molecule. On the contrary, the bis(phosphinate) group could be coordinated, in the bidentate chelating mode, to the metal ion bound by azacycle of the neighboring ligand molecule. The coordination bond lengths in this chelating units are similar to those of previously reported structures where bis(phosphinate) anion is coordinated as a O,O′-chelate in the Cu^{II} equatorial plane.[30]

Table 2. Protonation constants of the title ligand and related compounds (25 °C, $I = 0.1$ M $(NMe)_4Cl$). Overall protonation constants $\log\beta_{HnL}$ of the title ligand (with their standard deviation) are given in parentheses.

Constant	Ligand					
	H_2L	tacn[a]	H_3nota[b]	H_3nopa[c]	H_3trap^{OH}[d]	H_2no2a[e]
$\log K_1$	12.25 (12.25 ± 0.01)	10.42	13.17	12.06	11.47	11.82
$\log K_2$	3.65 (15.90 ± 0.02)	6.82	5.74	3.90	3.85	6.70
$\log K_3$	1.44 (17.35 ± 0.02)	–	3.22	1.95	1.30	2.87
$\log K_4$	–	–	1.96	–	–	1.6
$\log K_5$	–	–	0.78	–	–	–

[a] Ref. [41], $I = 0.1$ M KNO_3. [b] Refs. [35,37]. [c] Ref. [39]. [d] Ref. [18]. [e] Ref. [38], $I = 1.0$ M KCl.

The most surprising aspect is a geometry of the coordinated macrocycle. Presence of the monocoordinated bis(phosphinate) bridge does not allow possessing the same geometry on all three nitrogen atoms and one macrocycle chelate ring has to be twisted in the opposite direction to other ones, leading to overall macrocycle conformation λλ,δ/δδλ. (Table S4). Such conformation is very uncommon in complexes of tacn derivatives and it points to steric strain in the coordinated ligand. The strain also results in a low dihedral angle of the phosphinate-bridged ethylenediamine fragment of macrocycle (25 and 27° for Cu^{II} and Ni^{II} structures, respectively) when compared to torsion of other chelate rings (36–55°, see Table S4; in the related Cu^{II}/Ni^{II} complexes with H_3nota,[31–34] the torsion angles of all three ethylene groups are uniform and lie in range 44–52°, Table S5).

As the result, the M–N–C–C–N– chelate ring of the phosphinate-bridged macrocycle fragment is close to planarity with angles between N–M–N and C···M···C planes about 13° in both structures and with deviations of the atoms from the mean planes less than 0.16 Å. For other chelate rings, the values are much larger (24–29°, see Table S4) and they are similar to the values found in Cu^{II} and Ni^{II} complexes with H_3nota (24–26°, Table S5).[31–34]

Protonation and stability constants

Protonation constants of the ligand and stability constants of its Cu^{II} complexes were determined by potentiometry. Three protonation constants of the title ligand were found (Table 2). The first protonation occurs in alkaline region. The value of the corresponding constant ($\log K_1$ 12.25) coincides to the value found for H_3nota ($\log K_1$ 13.17).[35] The value is quite high and probably it is connected with the strong intramolecular hydrogen bond found in the solid-state structure of ligand dilithium (I) salt (see above). It is also in an agreement with the previous observations showing that bis(phosphinate) group does not significantly decrease the first protonation constant of macrocycles if compared with analogous acetate-containing ligands.[21–23,36] The second protonation constant of H_2L ($\log K_2$ 3.65) presumably describes binding of the second proton to the macrocycle. The constant is significantly lower than that of H_3nota ($\log K_2$ 5.74)[35,37] or H_2no2a ($\log K_2$ 6.70)[38] and it is in line with the values for phosphinic acid analogues of H_3nota.[18,19,39,40] The bis(phosphinate) group is protonated only in the strongly acidic solution ($\log K_3$ 1.44). The ligand distribution diagram is shown in Figure 3A; the monoprotonated $[HL]^-$ species is the dominant one in the neutral region, and the uncharged diprotonated species $[H_2L]$ is present only in the acidic region.

Stability constants were determined only for the Cu^{II}-H_2L system (Table 3) and distribution diagram of the system is shown in Figure 3B. Complexation starts with formation of monoprotonated species $[Cu(HL)]^+$ at pH ~ 1. Formation of the complex even in such low pH is probably enabled by binding of the bis(phosphinate) group due to its high acidity. Dissociation constant of the protonated complex, $\log K_a$ 5.05, indicates that the proton is localized on a ring nitrogen atom. The protonation

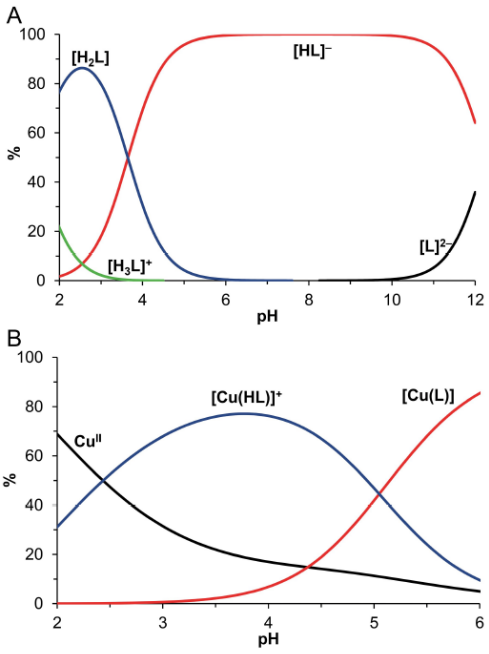

Figure 3. Distribution diagrams of H_2L (A) and Cu^{II}-H_2L system (B) ($c_M = c_L = 4$ mM, 25 °C, $I = 0.1$ M NMe_4Cl).

Table 3. Stability ($\log K_{CuL}$) and protonation ($\log K_n$) constants of Cu^{II} complexes with the title ligand, tacn and H_3nota (25 °C, $I = 0.1$ M $(NMe)_4Cl$). Overall protonation constants ($\log\beta_{HnLCu}$) of the title ligand (with their standard deviations) are given in parentheses.

Equilibrium	Ligand H_2L	tacn[a]	H_3nota[b]	H_3trap^{OH} [c]
$Cu + L \leftrightarrow [Cu(L)]$	11.18 (11.18 ± 0.03)	15.52	23.33	15.53
$[Cu(L)] + H \leftrightarrow [Cu(HL)]$	5.05 (16.23 ± 0.02)	–	2.65	–
$[Cu(HL)] + H \leftrightarrow [Cu(H_2L)]$	–	–	1.04	–

[a] Ref. [41], $I = 0.1$ M KNO_3. [b] Ref. [37]. [c] Ref. [18].

is connected with a weak coordination of one macrocycle nitrogen atom due to Jahn-Teller distortion of the Cu(II) coordination sphere (see above). Maximum abundance of the protonated complex is reached at pH ~ 4. The fully deprotonated complex [Cu(L)] is formed in the neutral region and it precipitates at pH ~ 6 (under conditions used in the titration experiments). The UV-VIS spectra of the Cu^{II} complex as function of pH are shown in Figure 4. Formation of the protonated complex in the pH region 1–4 leads to d-d transition band intensity increase, while its position remains constant. It indicates oxygen-only donor atom set in both, Cu^{II} aqua-ion and in $[Cu(HL)]^+$ complex, and, therefore, a bidentate chelating coordination of the bis(phosphinate) group might be expected. At pH > 4, formation of the non-protonated complex [Cu(L)] leads to the blue shift of the absorption band maxima due to the coordination of nitrogen atoms in the Cu^{II} equatorial plane. Value of the stability constant ($\log K_{CuL}$ 11.18, Table 3) points to a low stability of the [Cu(L)] complex. It is about four orders of magnitude lower than that of $[Cu(tacn)]^{2+}$ complex ($\log K_{CuL}$ 15.52)[41] and about twelve orders of magnitude lower than that of the $[Cu(nota)]^-$ complex ($\log K_{CuL}$ 23.33).[37]

Stability constants of the Zn^{II} and Ni^{II} complexes could not be determined. No changes of titration curves induced by presence of the metal ions were observed at pH < 4 and the insoluble metal complexes precipitate was formed at pH > 4. The negligible solubility of the complexes was also observed in polar organic solvents and their mixtures with water. The negligible abundance of metal complexes at pH < 4 indicates even lower stability of the complexes if compared with that of the Cu^{II} complex. It is expectable if order of the complex stabilities given by Irwing-Williams series is considered. In addition, a formation of protonated complex is expected to be observed only for the Cu^{II} complex analogously to data for complexes of H_3nota and its analogues due to Jahn-Teller distortion of these comlexes.[37]

The low stability of the H_2L complex cannot be attributed solely to the decreased macrocycle basicity as the Cu^{II} stability constant is several orders of magnitude lower than those reported for other phosphinate tacn derivatives (e.g. $\log K_{CuL} = 15.53$ for H_3trap^{OH}).[19] Stability is also negatively influenced by rigidity of the macrobicyclic structure as it is described above for the complexes in the solid state. The ligand rigidity does not allow simultaneous coordination of azamacrocycle amine groups and both phosphinate anions of the pendant to the same metal ion and it also induces sterically non-convenient conformation of the coordinated tacn ring. To reach a higher stability of the complexes, more flexible bridge might be used. The bridge could be prolonged both, between the two phosphinate groups or between the bis(phosphinate) group and macrocycle. However, synthesis of such structural motifs represents a challenge and it goes behind the frame of the presented work.

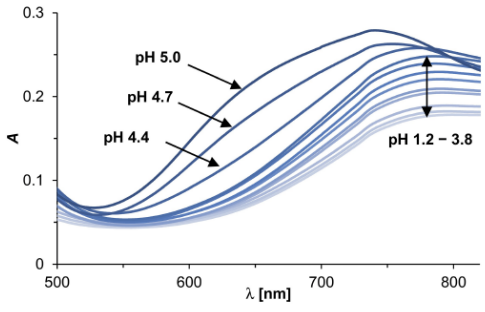

Figure 4. The UV-VIS spectra of the Cu^{II}-H_2L system ($c_M = c_L = 10$ mM, 25 °C).

Conclusion

The 1,4,7-triazacyclononane was modified with methylene-bis (phosphinic acid) group bridging two nitrogen atoms. The ligand was synthesized by two consequent Mannich-type reactions in a high yield. The ligand shows lower protonation constants than H_3nota due to presence of phosphinate pendants. The solid-state structures indicate that simultaneous coordination of all macrocycle nitrogen atoms and both phosphinate groups to one metal ion is impossible due to geometrical reasons. Stability of the Cu^{II} complex is more than ten orders of magnitude lower than that of $[Cu(nota)]^-$ due to rigidity of the macrobicyclic structure resulting in only monodentate coordination of bis(phosphinate) group and in the sterically disadvantageous conformation of chelates formed by the tacn ring. The presented results show that the studied ligand binds the first row transition metal ions, however, the

complexes show only limited stability due to rigidity and inappropriate geometry of the macrobicycle.

Experimental Section

General

All commercially available starting materials were used without further purification. Methylene-bis(phosphinic acid) was synthesized from commercial $CH_2(PCl_2)_2$ (Georganics, Slovakia) by careful hydrolysis.[42] 1-Benzyl-1,4,7-triazacyclononane was prepared according to the published procedure.[43,44] The ^1H (400 MHz), ^{13}C (100 MHz) and ^{31}P (161 MHz) NMR spectra were acquired at 25 °C on the Bruker 400 Avance spectrometer. NMR experiments at elevated temperature were performed on the Varian S300 – ^1H (300 MHz) and ^{31}P (121 MHz) NMR spectra. All NMR measurements were performed in D_2O. The methyl signal of *t*-BuOH was used as an internal standard (δ = 1.2 and 30.3 ppm for ^1H and ^{13}C NMR, respectively); ^{31}P NMR spectra were referenced to external 85% H_3PO_4 (δ = 0.0 ppm). All values of chemical shifts are given in ppm and coupling constants in Hz. The ESI-MS spectra were recorded on the Bruker Esquire 3000 spectrometer with an ion-trap detection in the negative or positive modes. Merck aluminum foils with silica gel 60 F254 were used for TLC.

Synthesis

Compound 1: The 1-benzyl-1,4,7-triazacyclononane (1.425 g; 6.50 mmol; 4 equiv.) and methylene-bis(phosphinic acid) (0.468 g; 3.25 mmol; 2 equiv.) were dissolved in aq. HCl (6 M; 30 ml). Paraformaldehyde (0.049 g; 1.63 mmol; 1 equiv.) was added in one portion and the flask was quickly stoppered. Reaction mixture was stirred at 60 °C for 3 days. The course of the reaction was monitored by ^{31}P NMR. After cooling to room temperature, the mixture was concentrated under vacuum and several times co-evaporated with water. The crude product was purified on a strong cation exchange resin (Dowex 50; ~150 ml; H^+-form; water→10% aq. pyridine). The pyridine fraction was concentrated under vacuum and pyridine was removed by co-distillation with water. Finally, the residue was dissolved in 1% aq. HCl and evaporated. The resulting oil was dissolved in water (200 ml). Lyophilization gave yellow-brown product (0.612 g, 83%). Elem. anal. (calcd. for $C_{15}H_{27}N_3O_4P_2 \cdot 0.25H_2O \cdot 2HCl$: C, 39.79; H, 6.57; N, 9.28). Found: C, 39.78; H, 6.53; N, 9.23. **NMR (D_2O/NaOD, pD ~13)**: ^1H δ 2.06 (P–CH_2–P, dd, 2H, $^2J_{HP}$ = 16 Hz, $^3J_{HH}$ = 2 Hz); 2.45–2.53 (*cycle*, m, 2H); 2.58–2.78 (*cycle*, m, 8H); 2.82 (cycle, t, 2H, $^3J_{HH}$ = 6 Hz); 2.89 (N–CH_2–P, d, 2H, $^2J_{HP}$ = 7 Hz); 3.73 (CH_2–Ph, s, 2H); 7.17 (*PH*, d, 1H, $^1J_{HP}$ = 530 Hz); 7.36–7.59 (*Ph*, m, 5H). $^{13}C\{^1H\}$ δ 35.6 (P–CH_2–P, t, $^1J_{CP}$ = 76 Hz); 45.6 (*cycle*, s); 45.8 (*cycle*, s); 50.0 (*cycle*, s); 52.1 (*cycle*, d); 53.6 (*cycle*, d, $^3J_{CP}$ = 4 Hz); 54.3 (*cycle*, d, $^3J_{CP}$ = 8 Hz); 58.8 (N–CH_2–P, d, $^1J_{CP}$ = 108 Hz); 61.0 (CH_2–Ph, s); 128.0 (^{14}CH, s); 129.0 (^{13}CH, ^{15}CH, s); 130.6 (^{12}CH, ^{16}CH, s); 139.2 (^{11}CH, s). ^{31}P δ 18.8 (*PH*, dt, 1P, $^1J_{PH}$ = 531 Hz, $^2J_{PH}$ = 18 Hz); 32.5 (*P*–CH_2–N, m, 1P). MS (negative mode): *m/z* 374.2 ($[M-H^+]^-$), 749.5 ($[M+M-H^+]^-$); (positive mode): *m/z* 376.3 ($[M+H^+]^+$), 751.5 ($[M+M+H^+]^+$), 773.5 ($[M+M+Na^+]^+$). R_f 0.2 (EtOH:conc. aq. ammonia 2:1).

H_2L: Compound 1 (0.288 g; 0.767 μmol; 1.0 equiv) was dissolved in conc. aq. HCl/AcOH mixture (1/1; 700 ml) and paraformaldehyde (1.153 g; 38.4 mmol; 50.0 equiv.) was added in one portion. The flask was closed and heated at 80 °C for 4 days. Progress of the reaction was monitored by TLC. The mixture was concentrated under vacuum and residual HCl was removed by repeated co-evaporation with water. The crude product was purified on a strong cation-exchange resin (Dowex 50; ~50 ml; H^+-form; water→10% aq. pyridine). The pyridine fraction containing product was evaporated. Finally, the residue was dissolved in 1% aq. HCl and evaporated. The resulting oil was dissolved in water (250 ml). Lyophilization gave product as a beige foam (0.231 g, 86%). Elem. anal. (calcd. for $C_{16}H_{27}N_3O_4P_2 \cdot H_2O \cdot 0.5HCl$: C, 45.37; H, 7.02; N, 9.92; P, 14.62; Cl, 4.18). Found: C, 45.22; H, 6.86; N, 9.91; P, 14.66; Cl, 4.52. **NMR (D_2O, pD ~1)**: ^1H δ 2.20–2.39 (H5, m, 1H); 2.51 (H5, m, 1H); 3.05–3.17 (H2 or H3, m, 4H); 3.23 (H1, m, 4H); 3.28–3.53 (H2 or H3 and H1, m, 8H); 3.07 (H6, s, 2H); 7.48–7.56 (H9 and H10, m, 3H); 7.57–7.64 (H8, m, 2H). $^{13}C\{^1H\}$ δ 34.2 (C5, t, $^1J_{CP}$ = 75 Hz); 49.9 (C3, s); 52.8 (C1, s); 53.1 (C2, d, $^3J_{CP}$ = 7 Hz); 56.2 (C4, d, $^1J_{CP}$ = 107 Hz); 61.3 (C6, s); 129.2 (C7, s); 130.0 (C9, s); 131.1 (C10, s); 132.4 (C8, s). $^{31}P\{^1H\}$ δ 31.7 (s). MS (negative mode): *m/z* 386 ($[M-H^+]^-$), 773 ($[M+M-H^+]^-$); (positive mode): *m/z* 388 ($[M+H+]^+$), 775 ($[M+M+H^+]^+$). R_f 0.4 (EtOH:conc. aq. ammonia 2:1). Numbering scheme of compound H_2L is shown in Scheme 2.

Potentiometric titrations

Potentiometry was performed according to the previously published procedures; to prepare stock solutions and chemicals and for further details on equipment, electrode system calibration, titration procedures and data treatment, see refs. 45,46. Throughout the paper, pH means $-\log[H^+]$. Protonation and stability constants were determined in 0.1 M $(NMe_4)Cl$ at 25.0 °C with pK_w = 13.81. Ligand was titrated in the pH range 1.8–12.1 with ~60 points per titration (c_L = 4 mM). Stability constants of the Cu^{II} complexes were determined by titration in the pH range 1.6–6.5 with ~30 points per titration and three parallel titrations ($c_L = c_M$ = 4 mM). The titration data were treated using the program OPIUM[47] selecting the chemical model with the best fit and performance.

UV-VIS measurements

UV-VIS spectra were recorded on spectrophotometer Specord 50 Plus (Analytik Jena AG). The temperature was 25 °C maintained by a Peltier block. Samples were prepared from stock solutions of ligand and metal ion and pH was adjusted with aqueous HCl and KOH solutions.

Preparation of single crystals

$Li_2(HL)(NO_3) \cdot 3H_2O$: H_2L (10 mg, 23.6 μmol) was dissolved in aq. solution of $Ga(NO_3)_3$ (476 μl, 0.04706 M, 22.4 μmol). The mixture was stirred and pH was increased to 8 by slow addition of diluted aq. LiOH solution. The mixture was stirred at 80 °C overnight. The precipitate was filtered off. Single crystals of $Li_2(HL)(NO_3) \cdot 3H_2O$ were obtained by diffusion of acetone vapor into the filtrate.

$[\{Cu(L)\}_2] \cdot 5H_2O$: H_2L (10 mg, 23.6 μmol) was dissolved in aq. solution of $CuCl_2$ (427 μl, 0.05246 M, 22.4 μmol) and pH was increased to 8 by slow addition of diluted aq. LiOH solution. The mixture was stirred overnight at 80 °C. The fine blue precipitate was

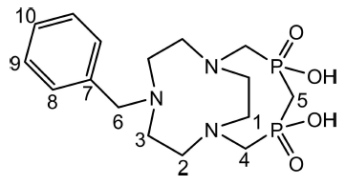

Scheme 2. Numbering scheme of compound H_2L.

filtered off. Single crystals of $[\{Cu(L)\}_2]\cdot 5H_2O$ were obtained by diffusion of acetone vapor into the filtrate.

$[\{Ni(L)\}_2]\cdot 4H_2O$: H_2L (10 mg, 23.6 μmol) was dissolved in aq. solution of $Ni(NO_3)_2$ (428 μl, 0.05229 M, 22.4 μmol). The pH was slowly increased to pH 8 by addition of diluted aq. LiOH solution. The fine green precipitate was formed at neutral pH. Single crystals of $[\{Ni(L)\}_2]\cdot 5H_2O$ were obtained by a thermal recrystallization upon heating the suspension at 80 °C overnight.

Crystal structure determination

The Bruker D8 VENTURE Kappa Duo PHOTON100 diffractometer with IμS micro-focus sealed tube was used for diffraction data collection using Mo-$K\alpha$ ($\lambda = 0.71073$ Å) radiation at 120 K ($Li_2(HL)(NO_3)\cdot 3H_2O$ and $[\{Cu(L)\}_2]\cdot 5H_2O$) or 150 K ($[\{Ni(L)\}_2]\cdot 4H_2O$), respectively (Cryostream Cooler, Oxford Cryosystem). Data were analysed using the SAINT (Bruker AXS Inc.) software package. Data were corrected for absorption effects using the multi-scan method (SADABS). All structures were solved by direct methods (SHELXT2014)[48] and refined using full-matrix least-squares techniques (SHELXL2014).[49] All non-hydrogen atoms were refined anisotropically, and all hydrogen atoms were found in the difference density map. In the case of $[Cu(L)]\cdot 2.5H_2O$, one of water molecules of crystallization was best refined with half-occupancy to obtain reasonable thermal factors. The hydrogen atoms bound to the carbon atoms were fixed in theoretical positions using $U_{eq}(H) = 1.2\ U_{eq}(C)$ to keep a number of parameters low, and only hydrogen atoms bound to heteroatoms (N, O) were fully refined. Selected experimental and refinement data of individual structures are outlined in Table S6. The data for the structures reported here were deposited at the Cambridge Crystallographic Data Centre under numbers CCDC-2056029–2056031.

Acknowledgements

Support from the Grant Agency of the Czech Republic (19-17380S) is acknowledged. This work was carried out in the framework of COST Action CA18202 (NECTAR). We thank Dr. I. Císařová (Charles University) for X-ray data collection.

Keywords: polyazamacrocycles · phosphinate complexes · bicyclic ligands · macrocyclic ligands · transition metals

[1] *Contrast Agents for MRI: Experimental Methods*; V. C. Pierre, M. J. Allen, Eds.; RSC: London, **2018**.
[2] a) P. Hermann, J. Kotek, V. Kubíček, I. Lukeš, *Dalton Trans.* **2008**, 3027; b) H. Li, T. J. Meade, *J. Am. Chem. Soc.* **2019**, *141*, 17025; c) T. J. Clough, L. Jiang, K.-L. Wong, N. J. Long, *Nature Commun.* **2019**, *10*, 1420; d) J. Wahsner, E. M. Gale, A. Rodríguez-Rodríguez, P. Caravan, *Chem. Rev.* **2019**, *119*, 957.
[3] A. Gupta, P. Caravan, W. S. Price, C. Platas-Iglesias, E. M. Gale, *Inorg. Chem.* **2020**, *59*, 6648.
[4] C. F. Ramogida, C. Orvig, *Chem. Commun.* **2013**, *49*, 4720.
[5] B. M. Zeglis, J. L. Houghton, M. J. Evans, N. Viola-Villegas, J. S. Lewis, *Inorg. Chem.* **2014**, *53*, 1880.
[6] T. W. Price, J. Greenman, G. J. Stasiuk, *Dalton Trans.* **2016**, *45*, 15702.
[7] L. E. McInnes, S. E. Rudd, P. S. Donnelly, *Coord. Chem. Rev.* **2017**, *352*, 499.
[8] A. J. Amoroso, I. A. Fallis, S. J. A. Pope, *Coord. Chem. Rev.* **2017**, *340*, 198.
[9] E. Boros, A. B. Packard, *Chem. Rev.* **2019**, *119*, 870.
[10] T. I. Kostelnik, C. Orvig, *Chem. Rev.* **2019**, *119*, 902.
[11] P. Chaudhuri, K. Wieghardt, *Prog. Inorg. Chem.* **1987**, 35, 329.
[12] T. Joshi, B. Graham, L. Spiccia, *Acc. Chem. Res.* **2015**, 48, 2366.
[13] T. Joshi, M. Kubeil, A. Nsubuga, G. Singh, G. Gasser, H. Stephan, *ChemPlusChem* **2018**, *83*, 554.
[14] E. Macedi, A. Bencini, C. Caltagirone, V. Lippolis, *Coord. Chem. Rev.* **2020**, *407*, 213151.
[15] a) K. S. Woodin, K. J. Heroux, C. A. Boswell, E. H. Wong, G. R. Weisman, W. Niu, S. A. Tomellini, C. J. Anderson, L. N. Zakharov, A. L. Rheingold, *Eur. J. Inorg. Chem.* **2005**, 4829; b) L. M. P. Lima, Z. Halime, R. Marion, N. Camus, R. Delgado, C. Platas-Iglesias, R. Tripier, *Inorg. Chem.* **2014**, *53*, 5269; c) A. Rodríguez-Rodríguez, M. Regueiro-Figueroa, D. Esteban-Gómez, R. Tripier, G. Tircsó, F. K. Kálmán, A. C. Bényei, I. Tóth, A. de Blas, T. Rodríguez-Blas, C. Platas-Iglesias, *Inorg. Chem.* **2016**, *55*, 2227.
[16] J. Kotek, P. Lubal, P. Hermann, I. Císařová, I. Lukeš, T. Godula, I. Svobodová, P. Táborský, J. Havel, *Chem. Eur. J.* **2003**, *9*, 233.
[17] M. Försterová, I. Svobodová, P. Lubal, P. Táborský, J. Kotek, P. Hermann, I. Lukeš, *Dalton Trans.* **2007**, 535.
[18] J. Notni, P. Hermann, J. Havlíčková, J. Kotek, V. Kubíček, J. Plutnar, N. Loktionova, P. J. Riss, F. Rösch, I. Lukeš, *Chem. Eur. J.* **2010**, *16*, 7174.
[19] J. Šimeček, M. Schulz, J. Notni, J. Plutnar, V. Kubíček, J. Havlíčková, P. Hermann, *Inorg. Chem.* **2012**, *51*, 577.
[20] R. Ševčík, J. Vaněk, R. Michalicová, P. Lubal, P. Hermann, I. C. Santos, I. Santos, M. P. C. Campello, *Dalton Trans.* **2016**, *45*, 12723.
[21] T. David, V. Kubíček, O. Gutten, P. Lubal, J. Kotek, H.-J. Pietzsch, L. Rulíšek, P. Hermann, *Inorg. Chem.* **2015**, *54*, 11751.
[22] S. Procházková, V. Kubíček, J. Kotek, A. Vagner, J. Notni, P. Hermann, *Dalton Trans.* **2018**, *47*, 13006.
[23] M. Paúrová, T. David, I. Císařová, P. Lubal, P. Hermann, J. Kotek, *New J. Chem.* **2018**, *42*, 11908.
[24] T. David, V. Hlinová, V. Kubíček, R. Bergmann, F. Striese, N. Berndt, D. Szöllősi, T. Kovács, D. Máthé, M. Bachmann, H.-J. Pietzsch, P. Hermann, *J. Med. Chem.* **2018**, *61*, 8774.
[25] L. Pazderová, T. David, V. Hlinová, J. Plutnar, J. Kotek, P. Lubal, V. Kubíček, P. Hermann, *Inorg. Chem.* **2020**, *59*, 8432.
[26] S. Aime, C. Cavallotti, E. Gianolio, G. B. Giovenzana, G. Palmisano, M. Sisti, *Tetrahedron Lett.* **2002**, *43*, 8387.
[27] Y. G. Lee, S. T. Kim, D. I. Jung, J. T. Hanh, *Asian J. Chem.* **2015**, *27*, 1481.
[28] D. M. Weekes, M. de Guadalupe Jaraquemada-Peláez, T. I. Kostelnik, B. O. Patrick, C. Orvig, *Inorg. Chem.* **2017**, *56*, 10155.
[29] E. L. Muetterties, L. J. Guggenberger, *J. Am. Chem. Soc.* **1974**, *96*, 1748.
[30] T. David, S. Procházková, J. Kotek, V. Kubíček, P. Hermann, I. Lukeš, *Eur. J. Inorg. Chem.* 2014, 4357.
[31] K. Wieghardt, U. Bossek, P. Chaudhuri, W. Herrmann, B. C. Menke, J. Weiss, *Inorg. Chem.* **1982**, *21*, 4308.
[32] S. Pant, M. T. V. Hearn, K. Saito, *Aust. J. Chem.* **2010**, *63*, 502.
[33] Q.-X. Li, Q. Li, R. Chen, X.-L. Yang, J.-Y. Zhou, H.-B. Xu, *Inorg. Chem. Commun.* **2010**, *13*, 1293.
[34] M. J. van der Merwe, J. C. A. Boeyens, R. D. Hancock, *Inorg. Chem.* **1985**, *24*, 1208–1213.
[35] B. Drahoš, V. Kubíček, C. S. Bonnet, P. Hermann, I. Lukeš, É. Tóth, *Dalton Trans.* **2011**, *40*, 1945.
[36] T. David, S. Procházková, J. Havlíčková, J. Kotek, V. Kubíček, P. Hermann, I. Lukeš, *Dalton Trans.* **2013**, *42*, 2414.
[37] V. Kubíček, Z. Böhmová, R. Ševčíková, J. Vaněk, P. Lubal, Z. Poláková, R. Michalicová, J. Kotek, P. Hermann, *Inorg. Chem.* **2018**, *57*, 3061.
[38] I. Lázár, R. Király, Z. Takács, *J. Coord. Chem.* **2000**, *51*, 293.

[39] G. Máté, J. Šimeček, M. Pniok, I. Kertész, J. Notni, H. Wester, L. Galuska, P. Hermann, *Molecules* **2015**, *20*, 13112.
[40] K. Bazakas, I. Lukeš, *J. Chem. Soc., Dalton Trans.* **1995**, 1133.
[41] R. Yang, L. J. Zompa, *Inorg. Chem.* **1976**, 15, 1499.
[42] C. King, D. M. Roundhill, F. R. Fronczek, *Inorg. Chem.* **1986**, *25*, 1290.
[43] A. J. Blake, I. A. Fallis, S. Parsons, S. A. Ross, M. Schröder, *J. Chem. Soc, Dalton Trans.* **1996**, 525.
[44] A. J. Blake, I. A. Fallis, R. O. Gould, S. Parsons, S. A. Ross, M. Schröder, *J. Chem. Soc, Dalton Trans.* **1996**, 4379.
[45] V. Kubíček, J. Havlíčková, J. Kotek, G. Tircsó, P. Hermann, É. Tóth, I. Lukeš, *Inorg. Chem.* **2010**, *49*, 10960.
[46] M. Försterová, I. Svobodová, P. Lubal, P. Táborský, J. Kotek, P. Hermann, I. Lukeš, *Dalton Trans.* **2007**, 535.
[47] a) M. Kývala, I. Lukeš, *International Conference Chemometrics '95*, Pardubice, Czech Republic, **1995**, p. 63; b) M. Kývala, P. Lubal, I. Lukeš, *IX. Spanish-Italian and Mediterranean Congress on Thermodynamics of Metal Complexes (SIMEC 98)*, Girona, Spain, **1998**. The full version of the OPIUM program is available (free of charge) on http://www.natur.cuni.cz/_kyvala/opium.html.
[48] a) G. M. Sheldrick, SHELXT2014/5. Program for Crystal Structure Solution from Diffraction Data, University of Göttingen, Göttingen, **2014**; b) G. M. Sheldrick, *Acta Crystallogr. Sect. A.* **2008**, *A64*, 112.
[49] a) C. B. Hübschle, G. M. Sheldrick, B. Dittrich, ShelXle: a Qt graphical user interface for SHELXL. University of Göttingen, Göttingen, **2014**; b) C. B. Hübschle, G. M. Sheldrick, B. Dittrich, *J. Appl. Cryst.* **2011**, *44*, 1281; c) G. M. Sheldrick, SHELXL-2014/7. Program for Crystal Structure Refinement from Diffraction Data, University of Göttingen, Göttingen, **2017**; d) G. M. Sheldrick, *Acta Crystallogr. Sect. C* **2015**, *C71*, 3.

Manuscript received: March 24, 2021
Accepted manuscript online: April 21, 2021

1,4,7-Triazacyclononane (tacn) with *N,N'*-bridging methylene-bis(phosphinic acid) group and its complexes

Lucia Pazderová, Vojtěch Kubíček,* Jan Kotek, Petr Hermann

Department of Inorganic Chemistry, Faculty of Science, Charles University, Hlavova 8, 128 40 Prague 2, Czech Republic. e-mail: kubicek@natur.cuni.cz

Table of content

Table S1. Parameters of intramolecular hydrogen bonds found in the crystal structure of $Li_2(HL)(NO_3)\cdot 3H_2O$

D–H	*d*(D–H), Å	*d*(H···A), Å	<DHA, °	*d*(D···A), Å	A
N1–H11	0.91(2)	1.92(2)	129(2)	2.585(1)	N4
N1–H11	0.91(2)	2.10(2)	122(1)	2.699(1)	N7

Table S2. Geometry of Li^I coordination spheres found in the crystal structure of $Li_2(HL)(NO_3)\cdot 3H_2O$

Distances, Å			
Li1–O21	1.879(2)	Li2–O12	1.951(2)
Li1–O11$^{\#1}$	1.959(2)	Li2–O22	1.989(2)
Li1–O1W	1.991(2)	Li2–O22$^{\#2}$	1.942(2)
Li1–O1N	2.004(2)	Li2–O2W	1.895(3)
Angles, °			
O21–Li1–O11$^{\#1}$	113.6(1)	O12–Li2–O22	103.4(1)
O21–Li1–O1W	113.8(1)	O12–Li2–O22$^{\#2}$	119.2(1)
O21–Li1–O1N	118.2(1)	O12–Li2–O2W	108.1(1)
O11$^{\#1}$–Li1–O1W	97.3(1)	O22–Li2–O22$^{\#2}$	95.8(1)
O11$^{\#1}$–Li1–O1N	111.5(1)	O22–Li2–O2W	114.6(1)
O1W–Li1–O1N	99.7(1)	O22$^{\#2}$–Li2–O2W	114.9(1)

Symmetry code: #1: $x, -y+1/2, z-1/2$; #2: $-x+2, -y+1, -z+1$.

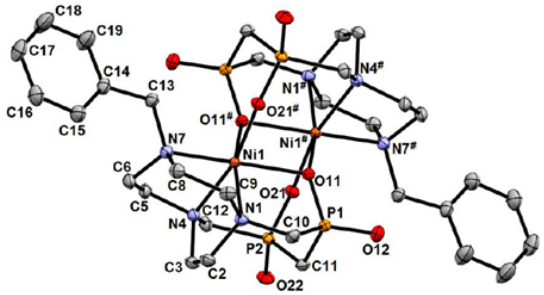

Figure S1. Molecular structure of the dimeric complex unit $[\{Ni(L)\}_2]$ found in the crystal structure of $[\{Ni(L)\}_2]\cdot 4H_2O$. Hydrogen atoms are not displayed for sake of clarity. Selected centrosymmetry-related atoms are labelled by "#".

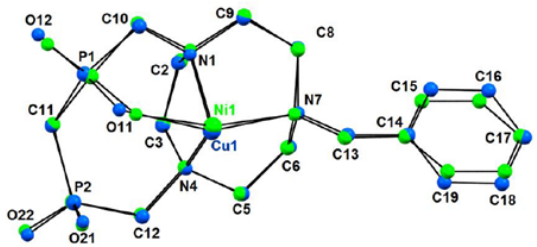

Figure S2. Overlay of the molecular structures of the [M(L)] fragment (the structurally independent part of the dimeric unit) found in the crystal structures of $[\{Cu(L)\}_2]\cdot 5H_2O$ (blue) and $[\{Ni(L)\}_2]\cdot 4H_2O$ (green). Hydrogen atoms are not displayed for the sake of clarity.

Table S3. Dihedral angles between triangles A and B defined in N_2O_2 equatorial plane found in Cu^{II} and Ni^{II} coordination spheres in the crystal structures of $[\{Cu(L)\}_2]\cdot 5H_2O$ and $[\{Ni(L)\}_2]\cdot 4H_2O$

Triangle A	Triangle B	$[\{Cu(L)\}_2]\cdot 5H_2O$	$[\{Ni(L)\}_2]\cdot 4H_2O$	Theory for T_d	Theory for D_{4h}
N1···N4···O11$^{\#}$	N1···N4···O21$^{\#}$	14.22(8)	20.14(6)	70.5	0
N4···O11$^{\#}$···O21$^{\#}$	N4···O11$^{\#}$···N1	15.22(9)	22.77(5)	70.5	0
O11$^{\#}$···O21$^{\#}$···N1	O11$^{\#}$···O21$^{\#}$···N4	13.93(8)	19.65(5)	70.5	0
O21$^{\#}$···N1···N4	O21$^{\#}$···N1···O11$^{\#}$	14.14(7)	21.02(5)	70.5	0
N1···O11$^{\#}$···N4	N1···O11$^{\#}$···O21$^{\#}$	159.73(7)	150.55(5)	70.5	180
N4···O21$^{\#}$···N1	N4···O21$^{\#}$···O11$^{\#}$	159.50(8)	149.99(5)	70.5	180

Symmetry code #: $-x+1, -y+1, -z+1$.

Table S4. Geometries of M–N–C–C–N– chelate rings found in the crystal structures of $[\{Cu(L)\}_2]\cdot 5H_2O$ and $[\{Ni(L)\}_2]\cdot 4H_2O$

Parameter		$[\{Cu(L)\}_2]\cdot 5H_2O$	$[\{Ni(L)\}_2]\cdot 4H_2O$
Dihedral angles of ethylene bridges in the M–N–C–C–N– chelate rings, °			
N1–C2–C3–N4		−24.6(2)	−26.8(2)
N4–C5–C6–N7		55.3(2)	55.1(1)
N7–C8–C9–N1		−35.5(2)	−36.2(1)
Angles inclined between planes defined by atoms forming the M–N–C–C–N– chelate rings, °			
Plane 1	Plane 2		
N1–M–N4	C2···M···C3	12.5(1)	13.5(1)
N4–M–N7	C5···M···C6	28.4(1)	27.9(1)
N7–M–N1	C8···M···C9	24.1(1)	25.0(1)
Planarity of the M–N–C–C–N– chelate rings (deviations of atoms from the average plane), Å			
M–N1–C2–C3–N4–		Cu1: 0.0265(6)	Ni1: 0.0403(5)
		N1: −0.0974(8)	N1: −0.1181(7)
		C2: 0.1410(10)	C2: 0.1592(8)
		C3: −0.1103(10)	C3: −0.1103(8)
		N4: 0.0401(8)	N4: 0.0290(7)
M–N4–C5–C6–N7–		Cu1: −0.1369(6)	Ni1: −0.1320(5)
		N4: 0.3152(9)	N4: 0.3050(7)
		C5: −0.3661(11)	C5: −0.3682(9)
		C6: 0.1517(11)	C6: 0.1601(9)
		N7: 0.0361(8)	N7: 0.0351(7)
M–N7–C8–C9–N1–		Cu1: 0.2348(6)	Ni1: 0.2596(5)
		N7: −0.1665(8)	N7: −0.1942(7)
		C8: 0.0015(10)	C8: 0.0081(8)
		C9: 0.3172(10)	C9: 0.3362(8)
		N1: −0.3870(9)	N1: −0.4097(7)

Table S5. Geometries of M–N–C–C–N– chelate rings found in the crystal structures of Cu^{II}–H_3nota nd Ni^{II}–H_3nota complexes[1–4]

CCDC No.	771135	771135	955138	1114280	1138346	1138347
(metal ion)	Cu1	Cu2	Cu	Cu	Ni	Cu(Cl)[a]
			isomer			
	ΛΛΛλλλ	ΛΛΛλλλ	ΔΔΔλλλ	ΛΛΛλλλ	ΛΛΛδδδ	ΔΔλλλ
			torsion angles, °			
N1–C2–C3–N4	−48.6	−50.3	−44.2	−47.1	46.3	−44,2
N4–C5–C6–N7	−48.5	−49.0	−49.1	−47.8	46.3	−51,2
N7–C8–C9–N1	−48.4	−49.1	−49.4	−44.8	46.3	−51.6
			angles between planes, °			
N1–M–N4 vs. C2···M···C3	24.1	25.5	23.4	24.2	25.4	24.0
N4–M–N7 vs. C5···M···C6	25.6	26.4	25.2	24.3	25.4	24.9
N7–M–N1 vs. C8···M···C9	25.4	24.6	24.2	24.1	25.4	24.6

[a]: one of acetate pendant arm of H_3nota is not coordinated and coordination sphere is closed by chloride ion

Table S6. Experimental crystallographic data for the reported crystal structures

Parameter	$Li_2(HL)(NO_3)\cdot 3H_2O$	$[\{Cu(L)\}_2]\cdot 5H_2O$	$[\{Ni(L)\}_2]\cdot 4H_2O$
Formula	$C_{16}H_{32}Li_2N_4O_{10}P_2$	$C_{16}H_{30}CuN_3O_{6.5}P_2$	$C_{16}H_{29}N_3NiO_6P_2$
M_r	516.27	493.91	480.07
Habit	plate	plate	prism
Colour	colourless	blue	blue-green
Crystal system	monoclinic	triclinic	triclinic
Space group	$P2_1/c$	$P\bar{1}$	$P\bar{1}$
a, Å	19.1832(5)	9.9755(5)	9.6345(7)
b, Å	10.0543(3)	9.9853(4)	10.1279(8)
c, Å	11.8801(3)	11.7991(6)	11.2754(9)
α, °	90	94.932(2)	69.487(2)
β, °	92.556(1)	113.323(2)	68.966(2)
γ, °	90	107.706(1)	87.525(2)
U, Å^3	2289.08(11)	999.10(8)	957.50(13)
Z	4	2	2
D_{calc}, g cm^{-3}	1.498	1.642	1.665
μ, mm^{-1}	0.250	1.296	1.221
Unique refl.	5249	4544	4394
Obsd. refl. ($I>2\sigma(I)$)	4934	4392	4328
$R(I>2\sigma(I))$	0.0290	0.0236	0.0201
R'(all)	0.0309	0.0246	0.0204
$wR(I>2\sigma(I))$	0.0752	0.0645	0.0516
wR'(all)	0.0766	0.0656	0.0518
CCDC number	2056030	2056029	2056031

References

[1] K. Wieghardt, U. Bossek, P. Chaudhuri, W. Herrmann, B. C. Menke, J. Weiss, *Inorg. Chem.* **1982**, *21*, 4308.

[2] S. Pant, M. T. V. Hearn, K. Saito, *Aust. J. Chem.* **2010**, *63*, 502.

[3] Q.-X. Li, Q. Li, R. Chen, X.-L. Yang, J.-Y. Zhou, H.-B. Xu, *Inorg. Chem. Commun.* **2010**, *13*, 1293.

[4] M. J. van der Merwe, J. C. A. Boeyens, R. D. Hancock, *Inorg. Chem.* **1985**, *24*, 1208–1213.

Appendix 2

Pazderová, L., David, T., Kotek, J., Kubíček, V., & Hermann, P. (2021). Complexes of cyclen side-bridged with a methylene-bis(phosphinate) group. *Polyhedron*, *196*, 114994. https://doi.org/10.1016/j.poly.2020.114994

Polyhedron 196 (2021) 114994

Contents lists available at ScienceDirect

Polyhedron

journal homepage: www.elsevier.com/locate/poly

Complexes of cyclen side-bridged with a methylene-bis(phosphinate) group

Lucia Pazderová, Tomáš David, Jan Kotek, Vojtěch Kubíček *, Petr Hermann

Department of Inorganic Chemistry, Faculty of Science, Charles University, Hlavova 8, 128 40 Prague 2, Czech Republic

ARTICLE INFO

Article history:
Received 1 November 2020
Accepted 19 December 2020
Available online 24 December 2020

Keywords:
Azacycles
Macrobicyclic ligands
Cyclen
Bis(phosphinate)
Stability constants

ABSTRACT

A macrobicyclic cyclen-based ligand containing a geminal bis(phosphinate) *N,N′*-bridge was synthesized via a Mannich-type reaction. The other two macrocycle amine groups were modified with two acetate pendants, yielding ligand H_4**L**. The cyclen-bis(phosphinate) intermediate, the ligand salt $Na_{0.5}(H_5$**L**$)(H_{3.5}$**L**$)Cl{\cdot}20H_2O$ and Cu^{II} complex $Li_2[Cu($**L**$)]{\cdot}4H_2O$ were characterized by single-crystal X-ray diffraction. The ligand protonation constants and the stability constants of H_4**L** complexes with Cu(II) and Zn(II) and lanthanide(III) ions were determined by potentiometry. The ligand protonation constants and the stability constants of H_4**L** complexes with Cu(II) and Zn(II) ions are similar to those of H_4dota. Conversely, the stabilities of its Ln(III) complexes are ~ 7–10 orders of magnitude lower than those of H_4dota complexes due to steric restrictions of the methylene-bis(phosphinate) side bridge. Therefore, these findings indicate that the ligand H_4**L** is suitable for the complexation of transition metal ions.

1. Introduction

Molecular imaging supports several modern diagnostic non-invasive methods, including Magnetic Resonance Imaging (MRI), Positron Emission Tomography (PET) and Single-Photon Emission Computed Tomography (SPECT). Images created by these methods are enhanced using contrast agents (MRI) or radiotracers (PET and SPECT), which are administered to patients. Many MRI contrast agents or radiotracers are based on transition metals or lanthanides [1–12]. The metal ions must be administered in the form of a highly stable complex to avoid metal ion (radio)toxicity and/or non-specific deposition in tissues. Therefore, any metal ion must be bound by a specific ligand to preserve the desired function of the imaging probe and to avoid any complex dissociation in vivo. The most common requirement is that the complex is eliminated from the body with no change.

To ensure in vivo stability, macrocyclic ligands are often utilized as metal ion carriers because their complexes are endowed with not only high thermodynamic stability but also kinetic inertness. The most common ligands used in molecular imaging are derivatives of macrocyclic polyamines, tacn, cyclen and cyclam (Chart 1). However, in some cases, the thermodynamic stability and kinetic inertness of their complexes and the selectivity to the metal ion are insufficient. Therefore, considerable research efforts has focused on developing new ligands that form complexes with higher selectivity, thermodynamic stability and kinetic inertness.

A successful strategy for improving the properties of these complexes has been the use of macrobicyclic skeletons [4,8,9,11,12]. The most common macrobicyclic ligands are cryptands, such as diamsar [13] (Chart 1), and *N,N′*-bridged tetraazamacrocycles, including cb-cyclen or cb-cyclam (Chart 1) [14–17]. Unfortunately, many of these macrobicyclic ligands show slow complexation rates, thereby significantly limiting the synthesis of radiopharmaceuticals.

Our research group has been investigating ligands with phospho(i)nate pendant arms towards improving complexation rates and overcoming the aforementioned limitations. The comparison of phospho(i)nate-bearing azamacrocycles with their carboxylate analogues has shown that the former provide faster metal-binding kinetics without adversely affecting the high thermodynamic stability of their complexes [18–23]. However, the phosphinate group is rather unique one among negatively charged coordinating groups as its phosphorus atom is attached to two carbon atoms. Thus, the phosphinate group can be located within a carbon chain and directly incorporated into the macrocyclic skeleton. Moreover, the phosphinate placement within the macrocycle may improve complex stability due to its negative charge. For example, if the phosphinate group is located inside the macrocycles, its negative charge will likely balance the positive charge of a metal ion without requiring additional negatively charged pendant arms, a highly desirable property for biomedical applications. Yet, only a few

* Corresponding author.
E-mail address: kubicek@natur.cuni.cz (V. Kubíček).

https://doi.org/10.1016/j.poly.2020.114994
0277-5387/

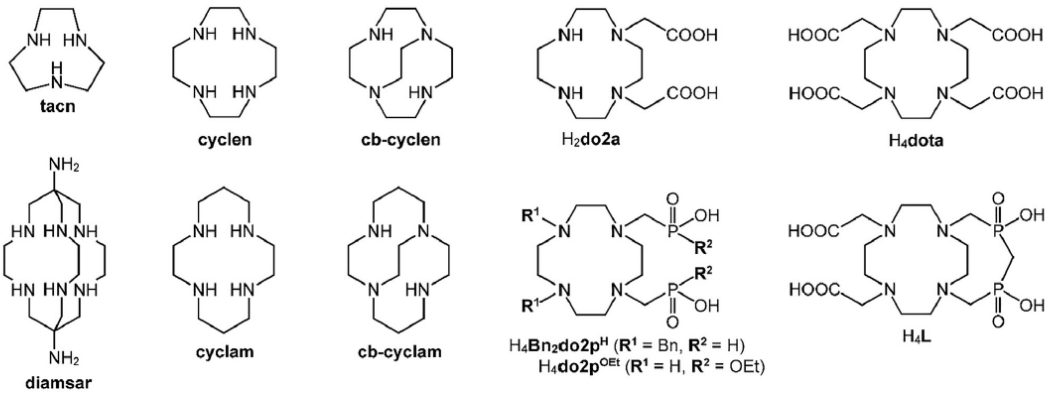

Chart 1. Ligands discussed in this paper.

studies have reported macrocyles with a phosphinate group inside the ring [24–26].

Recently, we have studied macrocyclic ligands with geminal bis (phosphinate) pendant arms and their complexes[18,27–29]. Our results indicated that the presence of the geminal bis(phosphinate) group significantly accelerates metal binding kinetics. Here, we propose a new macrobicyclic ligand combining cyclen and a bis (phosphinate) side-bridge (H_4**L**, Chart 1). Hence, this paper reports the synthesis of the ligand and the thermodynamic study of its complexes with trivalent lanthanide, Cu^{II} and Zn^{II} ions.

2. Results and discussion

2.1. Ligand synthesis

The title ligand, H_4**L**, was synthesized by a multi-step reaction sequence utilizing Mannich-type and alkylation reactions (Scheme 1). In the first step, cyclen was modified with one bis (phosphinate) pendant arm in a reaction with methylene-bis(phosphinic acid) and paraformaldehyde under acidic conditions. Monosubstitution was controlled by a sub-stoichiometric amount of paraformaldehyde. The excess of cyclen and bis(phosphinic) acid was removed on ion exchange resins. Compound **1** was obtained in 75% yield. In the second step, compound **1** was treated with an excess of paraformaldehyde to yield the macrobicycle **2**. The reaction was performed under highly diluted conditions to prevent polymerization. After ion-exchange and flash chromatography, compound **2** was isolated as a fine white powder in 61% yield. The remaining secondary amino groups were modified with chloroacetic acid in the final step. The alkylation was performed in aq. solution maintained at pH 12 by adding LiOH. To reach a high conversion, an excess of chloroacetic acid was added in two portions. Following purifications on a cation exchange resin, H_4**L** was separated in 87% yield.

2.2. Solid-state structures

Precursor **1** crystallized as **1**·4H_2O containing two structurally independent formula units with similar geometries (Fig. S1). Thus, only one of them is shown in Fig. 1. Two amino groups of the macrocycle are protonated, and the pendant arm is fully deprotonated giving a zwitterion. The macrocycle adopts a (3,3,3,3)-B conformation, which is common for double protonated cyclen

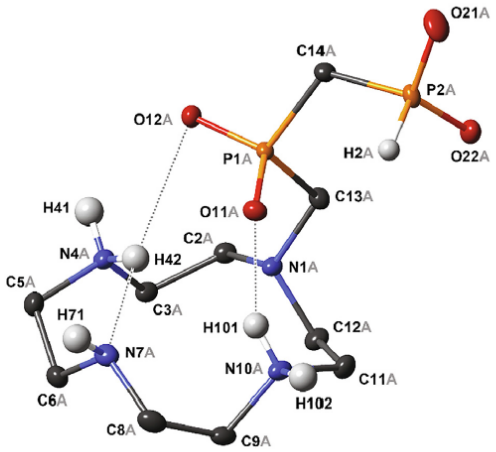

Fig. 1. Molecular structure of **1** found in the crystal structure of **1**·4H_2O. Intramolecular hydrogen bonds are shown as dotted lines. Only one of two structurally independent molecules is shown. Water molecules of crystallization and the carbon-bound hydrogen atoms are not displayed for the sake of clarity. Thermal ellipsoids are set at 65% probability.

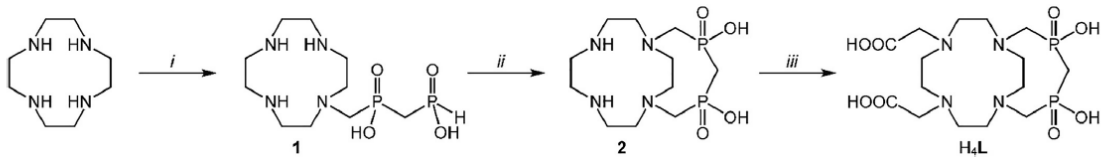

Scheme 1. Synthesis of H_4**L**. (*i*) $CH_2(PO_2H_2)_2$, paraformaldehyde, 6 M aq. HCl, 40 °C, 2 d (75%); (*ii*) paraformaldehyde, 6 M aq. HCl, 90 °C, 24 h (61%); (*iii*) $ClCH_2COOH$, water, pH ~ 12 (LiOH), 60 °C, 3 d (87%).

derivatives [30]. The structure is stabilized by medium-to-weak intramolecular hydrogen bonds between phosphinate oxygen atoms and amino groups of the protonated macrocycle. Such hydrogen bonds between the negatively charged pendant arm and the protonated amine group, which is separated by an ethylene chain within the ring, create a common structural motif in polyazamacrocycle derivatives. Each independent molecule forms a dimer with its neighboring centrosymmetry-related partner (Fig. S2). The crystal structure is stabilized by a system of intermolecular hydrogen bonds between the amino groups, the phosphinate oxygen atoms and water molecules of crystallization. Parameters of selected hydrogen bonds are outlined in Table S1.

The single-crystals of ligand H_4**L** had the formula $Na_{0.5}(H_5\mathbf{L})(H_{3.5}\mathbf{L})Cl{\cdot}20H_2O$. The sodium(I) cation present in the structure presumably originates from glass of the vial used for crystallization. Significant crystallographic disorders of chloride counter-ion and water molecules were found and required squeezing of the related electronic density. Nevertheless, hydrogen atoms of the ligand molecules were located and eventually fully refined, thereby confirming the protonation state suggested above. In the resulting non-trivial formula, Na^I ion occupies a special position with half-occupancy, and the $(H_3\mathbf{L})^-$ unit is connected to its centrosymmetry-related partner by a very strong hydrogen bond, d(O31X···O31X$^{\#}$) = 2.43 Å, through the hydrogen atom H31X, which also occupies the special position, leading to a $[H(H_3\mathbf{L})_2]^- = 2\times(H_{3.5}\mathbf{L})^{0.5-}$ dimer. The basic structural motif consists from head-to-head oriented $(H_5\mathbf{L})^+$ and $(H_{3.5}\mathbf{L})^{0.5-}$ fragments connected by strong hydrogen bonds between protonated and deprotonated pendant arms. In addition to these interactions, the intramolecular hydrogen bonds between protonated amino groups and deprotonated amino groups/pendant oxygen atoms stabilize the (3,3,3,3)-B conformation of the cyclen ring, as commonly found in double protonated cyclen derivatives [30]. Parameters of selected hydrogen bonds are outlined in Table S2. Both ligand molecules are also coordinated to the Na^I ion through the carboxylate oxygen atom O31B of the $(H_5\mathbf{L})^+$ unit and two bis(phosphinate) oxygen atoms O1Y and O2Y of the $(H_{3.5}\mathbf{L})^{0.5-}$ fragment. The centrosymmetric character of the Na^I coordination sphere results in an almost regular octahedron with Na···O distances in the 2.31–2.40-Å range and with *cis*-O···Na···O angles in the 87.1–92.9° range. The coordination to Na^I, together with the strong centrosymmetric hydrogen bond mentioned above, leads to the formation of a 1D-polymeric chain (Fig. 2).

Cu^{II} complex crystallized in the form $Li_2[Cu(\mathbf{L})]{\cdot}4H_2O$. The central Cu^{II} ion is coordinated by all nitrogen atoms of the macrocycle, and the pentacoordinated sphere of the metal ion is closed by one oxygen atom (O11) of the side-cyclic bis(phospinate) moiety (Fig. 3). The coordination sphere is distorted square-pyramid with almost perfectly symmetrical N_4-basal plane (Cu–N distances in a narrow range 2.07–2.12 Å, both *trans*-angles N–Cu–N equal and about 148°, Table 1), with unsymmetrically placed apical oxygen atom O11 due to a short chelate ring (N1–Cu1–O11 ~ 88°), leading to a large range of N–Cu–O angles 88–123° (Table 1). The oxygen atom of one acetate pendant arm (O31) is turner towards the Cu^{II} ion, but the Cu···O31 distance is too long (3.28 Å) to be suggested as semi-coordinative interaction.

In the crystal structure, two (centrosymmetrically related) $[Cu(\mathbf{L})]^{2-}$ species are connected through tetrahedral coordination to one of Li^I counter-ions (Li1) by oxygen atoms O11, O21 and O31 from one complex molecule and by O22$^{\#}$ from the centrosymmetrically-related partner. The second Li^I ion (Li2) is terminally coordinated by oxygen atom O32 of the acetate pendant arm and its coordination sphere is closed with three water molecules (Fig. S3).

Microcrystalline Cu^{II} and Zn^{II} complexes were prepared and their elemental analyses showed stoichiometry Li:M^{II}:L 2:1:1 which is same as was found in the single crystals of $Li_2[Cu(\mathbf{L})]{\cdot}4H_2O$.

2.3. Equilibrium studies

Protonation constants of H_4**L** and stability constants of its complexes with Zn^{II}, Cu^{II}, La^{III}, Gd^{III} and Lu^{III} ions were determined by

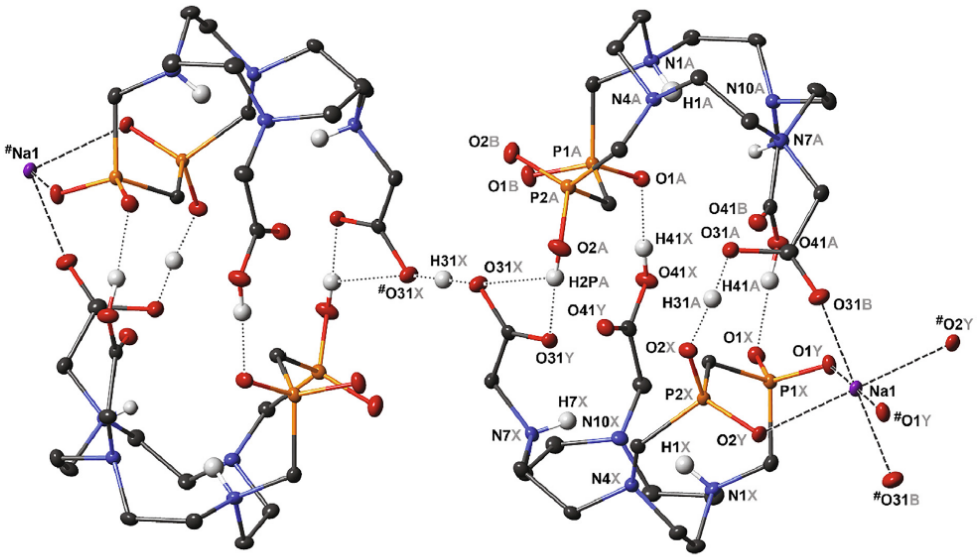

Fig. 2. 1D-polymeric structural motif found in the crystal structure of $Na_{0.5}(H_5\mathbf{L})(H_{3.5}\mathbf{L})Cl{\cdot}20H_2O$. Selected symmetry-related atoms are labelled with an "#". Intramolecular hydrogen bonds are shown as dotted lines, whereas coordination bonds are depicted as dashed lines. The water molecules of crystallization, carbon-bound hydrogen atoms and intramolecular hydrogen bonds are not displayed for the sake of clarity. Thermal ellipsoids are set at 65% probability.

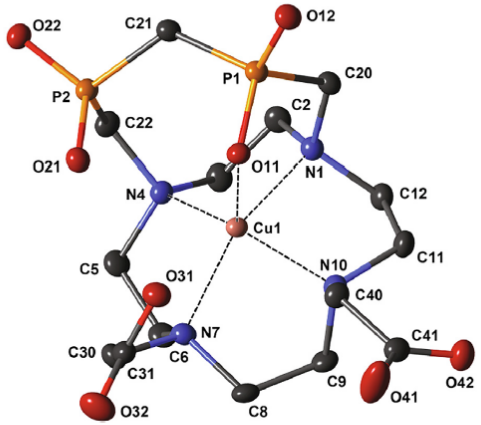

Fig. 3. Molecular structure of $[Cu(\mathbf{L})]^{2-}$ species found in the crystal structure of $Li_2[Cu(\mathbf{L})]\cdot 4H_2O$. The hydrogen atoms are not displayed for sake of clarity.

potentiometry. Five protonation constants of the ligand were found (Table 2). The first two protonations occur in the alkaline region, and the corresponding constants ($\log K_1$ = 12.70 and $\log K_2$ = 9.15) lie within the range typical for ring amine protonations of substituted cyclen derivatives. These values confirm the previously reported observation that introducing a geminal bis (phosphinate) group as a pendant arm does not decrease the basicity of ring amines, in contrast to the presence of a simple phosphinate group [18,29,31]. The protons are likely located at distant ring amine groups, as observed in the solid state (see above). The double protonated species $(H_2\mathbf{L})^{2-}$ is the dominant species in the neutral region. The first carboxylate group is protonated in a weakly acidic region. The other carboxylate group and the bis(phosphinate) group are protonated at pH < 2.5.

The stability constants of the complexes are summarized in Table 3. The systems with Cu^{II} and Zn^{II} ions are mutually similar. The diprotonated species $[M(H_2L)]$ start forming with Cu^{II} and Zn^{II} at pH ~ 1 and pH ~ 2, respectively (Fig. 4). For the system with Cu^{II}, the chemical model was confirmed by UV–VIS spectra at different pH. The intensity of the d-d transition band of the copper(II) complex (Fig. S4) with a maximum at ~650 nm perfectly fits the distribution diagram (Fig. 3A). The initially formed complexes are deprotonated in two steps. The values of the corresponding protonation constants are similar to the $\log K_3$ and $\log K_4$ of the free ligand, thus indicating that the ring amine groups are fully coordinated in all species, as confirmed by the absorption spectra of the Cu(II) species (Fig. S4). Therefore, the (de)protonations occur on the non-coordinated pendant arms. For both metal ions, the diprotonated $[M(H_2\mathbf{L})]$ and monoprotonated $[M(H\mathbf{L})]^-$ species reach the maximum abundance at pH ~ 2 and 3.5, respectively. The dominant species in the neutral region are fully deprotonated complexes $[M(\mathbf{L})]^{2-}$.

All three lanthanide ions, La^{III}, Gd^{III} and Lu^{III}, show similar values of stability constants and distribution diagrams. Their com-

Table 1
Geometric parameters of the Cu^{II} coordination sphere found in crystal structure of $Li_2[Cu(\mathbf{L})]\cdot 4H_2O$.

distances, Å		angles, °			
Cu1–N1	2.068(2)	N1–Cu1–N4	84.07(7)	N4–Cu1–N10	148.50(7)
Cu1–N4	2.120(2)	N1–Cu1–N7	148.31(7)	N4–Cu1–O11	116.52(6)
Cu1–N7	2.072(2)	N1–Cu1–N10	85.36(7)	N7–Cu1–N10	86.29(7)
Cu1–N10	2.073(2)	N1–Cu1–O11	87.56(6)	N7–Cu1–O11	123.33(7)
Cu1–O11	2.194(2)	N4–Cu1–N7	87.32(7)	N10–Cu1–O11	92.53(6)

Table 2
Stepwise protonation constants of the ligands and overall protonation constants logβ (in italics) of the title ligand (25 °C, I = 0.1 M $(NMe_4)Cl$).

Ligand	$H_4\mathbf{L}$	$H_4\mathbf{dota}$ [32]	1,4-$H_2\mathbf{do2a}$ [33]	1,4-$H_2\mathbf{Bn_2do2p^H}$ [34]	1,4-$H_2\mathbf{do2p^{OEt}}$ [34]
$\log K_1$	12.70 *12.70 ± 0.01*	12.90	11.07	11.22	11.38
$\log K_2$	9.15 *21.85 ± 0.01*	9.76	9.76	6.78	8.57
$\log K_3$	4.39 *26.24 ± 0.01*	4.68	3.84	–	1.29
$\log K_4$	2.26 *28.50 ± 0.01*	4.11	1.75	–	–
$\log K_5$	1.08 *29.58 ± 0.02*	2.37	–	–	–

Table 3
Stability constants of [M(L)] species and their protonation constants for $H_4\mathbf{L}$ complexes ($\log K$, 25 °C, I = 0.1 M $(NMe_4)Cl$). Overall stability constants logβ of the corresponding species are given in italics.

Equilibrium[a]	Cu^{II}	Zn^{II}	La^{III}	Gd^{III}	Lu^{III}
M + L ↔ [M(L)]	22.97 *22.97 ± 0.02*	19.59 *19.59 ± 0.01*	14.89 *14.89 ± 0.03*	14.90 *14.90 ± 0.03*	15.60 *15.60 ± 0.03*
[M(L)] + H ↔ [M(HL)]	3.81 *26.78 ± 0.02*	4.22 *23.81 ± 0.01*	–	–	–
[M(HL)] + H ↔ [M(H_2L)]	2.60 *29.38 ± 0.03*	2.18 *25.99 ± 0.02*	–	–	–
[M(L)] + 2H ↔ [M(H_2L)]	–	–	12.16 (2 × 6.08) *27.04 ± 0.02*	13.10 (2 × 6.55) *28.00 ± 0.03*	12.08 (2 × 6.04) *27.68 ± 0.02*

[a] The charges of the species are omitted.

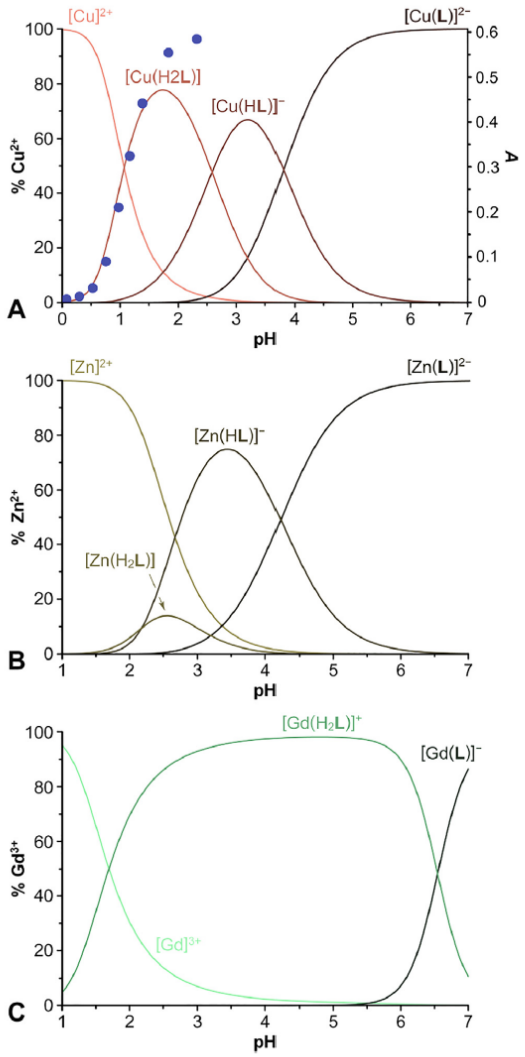

Fig. 4. Distribution diagrams of Cu^{II}-H_4**L** (A), Zn^{II}-H_4**L** (B) and Gd^{III}-H_4**L** (C) systems ($c_M = c_L$ = 4 mM, 25 °C, I = 0.1 M (NMe_4)Cl). The absorption of Cu^{II} complexes at 648 nm is shown as blue dots. The alkaline region is not displayed for Cu^{II} and Zn^{II} ions because $[M(L)]^{2-}$ is the only abundant species. (For interpretation of the references to colour in this figure legend, the reader is referred to the web version of this article.)

plexation occurs at pH 1–2, with the formation of diprotonated species $[M(H_2\mathbf{L})]^+$. The characteristic feature of these systems is the absence of $[M(H\mathbf{L})]$ species in the chemical model, suggesting that both protons are simultaneously lost at pH above 6, in line with models reported for analogous Ln^{III}-ligand systems with DOTA-like ligands. Thus, the diprotonated species can be considered *out-of-cage* complexes in which the metal ion is likely coordinated only through the pendant oxygen atoms, whereas the macrocycle remains protonated [35,36]. The transfer of the metal ions into the macrocyclic cavity (i.e., the formation of the $[M(\mathbf{L})]^-$ species) is accompanied by the simultaneous removal of both protons. The fully deprotonated complexes $[M(\mathbf{L})]^-$ are the dominant species in the neutral region. Metal hydroxides precipitate at pH > ~7.5.

The stability constants of Cu^{II} and Zn^{II} complexes are quite high, similar to those reported for H_4**dota** and 1,4-H_2**do2a** and higher than those of analogous ligands with phosphorus acid pendant arms (Table 4) due to the high basicity of the ring amine groups in H_4**L**. The stability constants follow the Irving-Williams series. In turn, the stability constants of the Ln^{III} complexes are 7–10 orders of magnitude lower than those reported for H_4**dota**. The low thermodynamic stability of the Ln^{III}-H_4**L** complexes led to the precipitation of Ln^{III} hydroxides in the weakly alkaline region, which indicates that the bis(phosphinate) side-bridged cyclen is not suitable for Ln^{III} complexation, most likely for steric reasons. In other words, the steric requirements of the bis(phosphinate) bridge may not allow simultaneous coordination of both phosphinate moieties as occurs in complexes of analogous DOTA-like ligands. In the complexes, all four pendant arms are coordinated and "rotated" in the same direction. In the Ln^{III}-H_4**L** complexes, such a synchronous orientation of all pendant arms is not possible because one phosphinate group must be "turned" in the opposite direction to the other three pendant groups.

3. Conclusions

A macrobicyclic ligand combining cyclen with a geminal bis (phosphinate) side bridge was synthesized in a high yield through a three-step procedure combining Mannich-type reactions and alkylation. The basicity of the ligand and the stabilities of its Cu^{II} and Zn^{II} complexes are similar to those of related DOTA-like ligands. Surprisingly, although the number and type of donor atoms is the same as those of H_4dota, the stability constants of the Ln^{III} complexes with the bis(phosphinate)-bridged ligand are 7–10 orders of magnitude lower than those of H_4dota complexes. These values demonstrate that geometry of the bis(phosphinate) bridge attached to the cyclen core is not suitable for the complexation of lanthanide(III) ions and that the synthesized ligand is not applicable as a carrier of Ln^{III} ions in tracers for molecular imaging or radiotherapy. However, the ligand effectively binds Cu^{II} and Zn^{II} ions. In conclusion, the macrobicycle prepared in this study is the first member of a new class of ligands, and the straightforward synthetic pathway reported here opens new opportunities for syntheses and applications of other ligands of this class in coordination chemistry.

4. Experimental

4.1. General

All commercially available starting materials were used without further purification. Methylene-bis(phosphinic acid) was synthesized from commercial $CH_2(PCl_2)_2$ by careful hydrolysis according to a previously published procedure [40]. ^{1}H (400 MHz), ^{13}C (100 MHz) and ^{31}P (161 MHz) NMR spectra were acquired at 25 °C on a Bruker 400 Avance spectrometer. To perform NMR experiments at a higher temperature, a Varian S300 spectrometer was used to measure ^{1}H (300 MHz) and ^{31}P (121 MHz) NMR spectra. All NMR measurements were performed in D_2O. For ^{1}H and ^{13}C NMR measurements, the methyl signal of *t*-BuOH was used as an internal standard (δ 1.25 and 30.3 ppm for ^{1}H and ^{13}C NMR, respectively); ^{31}P NMR spectra were referenced to external 85% H_3PO_4 (δ 0.0 ppm). All values of chemical shifts are given in ppm and coupling constants in Hz. ESI-MS spectra were recorded on a Bruker Esquire 3000 spectrometer with ion-trap detection in negative or positive modes. Merck aluminum foils with silica gel 60 F_{254} were used for TLC.

Table 4
Comparison of the stability constants $\log K_{ML}$ of the complexes.

Metal ion	Ligand				
	H_4L	**H_4dota** [37,38]	**H_2do2a** [39]	**H_2Bn$_2$do2p^H** [34]	**H_2do2p^{OEt}** [34]
Cu^{II}	22.97	22.3	24.4	–	19.55
Zn^{II}	19.59	20.8	18.0	13.26	15.42
La^{III}	14.89	22.0	–	–	–
Gd^{III}	14.90	24.7	–	–	–
Lu^{III}	15.60	23.9	–	–	–

4.2. Syntheses

Compound 1: The 1,4,7,10-Tetraazacyclododecane (4.79 g; 27.8 mmol; 4 equiv) and methylene-bis(phosphinic acid) (2.00 g; 13.9 mmol; 2 equiv) were dissolved in aq. HCl (6 M; 40 ml). Paraformaldehyde (208 mg; 6.9 mmol; 1 equiv) was added in one portion. The flask was closed and heated at 40 °C for 2 days. After cooling to room temperature, volatiles were removed under vacuum. Excess HCl was removed by repeated co-evaporation with water. Purification of the crude product was performed via chromatography on a strong cation-exchange resin (Dowex 50; ~150 ml; H^+-form; water → 10% aq. pyridine). The excess of methylene-bis(phosphinic acid) was eluted with water. The pyridine fraction containing the product was evaporated to dryness under vacuum. The remaining oil was dissolved in water (250 ml). Lyophilization gave the product as a white fine powder. Yield: 1.85 g (75%). Elem. anal. calcd. for $C_{10}H_{26}N_4O_4P_2{\cdot}1.5H_2O$: C, 33.80; H, 8.23; N, 15.77. Found: C, 33.75; H, 7.91; N, 15.71. NMR (D_2O + CsOD, pD ~ 13): ^{1}H δ 2.02 (P–C*H*$_2$–P, t, 2H, $^2J_{HP}$ = 17 Hz); 2.60 (*cycle*, m, 4H); 2.64 (*cycle*, m, 4H); 2.74 (*cycle*, m, 8H); 2.78 (N–C*H*$_2$–P, d, 2H, $^2J_{HP}$ = 8 Hz); 7.13 (P*H*, d, 1H, $^1J_{HP}$ = 530 Hz); ^{13}C{^{1}H} δ 36.7 (P–C*H*$_2$–P, dd, $^1J_{CP}$ = 77 Hz, $^1J_{CP}$ = 74 Hz); 45.2 (*cycle*, s); 46.0 (*cycle*, s); 46.6 (*cycle*, s); 54.0 (*C*H$_2$–N–CH$_2$–P, d, $^3J_{CP}$ = 7 Hz); 57.1 (N–*C*H$_2$–P, d, $^1J_{CP}$ = 109 Hz); ^{31}P δ 18.8 (*P*H, dtd, 1P, $^1J_{PH}$ = 530-Hz, $^2J_{PH}$ = 17 Hz, $^2J_{PP}$ = 6 Hz); 32.3 (*P*–CH$_2$–N, m, 1P). MS (negative mode) *m*/*z* 327 ([M − H$^+$]$^-$); (positive mode) *m*/*z* 329 ([M + H$^+$]$^+$), 657 ([2 M + H$^+$]$^+$).

Compound 2: The flask was charged with **1** (250 mg; 762 μmol; 1.0 equiv), adding paraformaldehyde (1.15 g; 38.3 mmol; 50.0 equiv) and aq. HCl (6 M; 650 ml). The flask was then closed and heated at 90 °C for 24 h. After cooling to room temperature, the volatiles were removed under vacuum, and the residual HCl was removed by repeated co-evaporation with water. The crude product was purified on a strong cation-exchange resin (Dowex 50; ~50 ml; H^+-form; water → 10% aq. pyridine). The pyridine fraction containing the product was evaporated to dryness under vacuum, and the remaining oil was purified by flash chromatography (SiO_2; *i*PrOH : conc. aq. ammonia : water 7:4:4). The product-containing fractions were combined and evaporated. Ammonia was removed on a cation-exchange resin (Dowex 50; ~30 ml; H^+-form; water → 10% aq. pyridine). The pyridine fraction with the product was evaporated. Traces of pyridine were removed by repeated co-evaporation with water. Lastly, the residue was dissolved in aq. 1% HCl and evaporated. The resulting oil was dissolved in water (250 ml). After lyophilization, the product was isolated as a fine white powder. Yield: 186 mg (63%). Elem. anal. calcd. for $C_{11}H_{26}N_4O_4P_2{\cdot}3.5H_2O0.5HCl$: C, 31.34; H, 8.01; N, 13.29. Found: C, 30.99; H, 7.79; N, 12.96. NMR (D_2O + CsOD, pD ~ 13): ^{1}H δ 1.60–1.79 (P–C*H*$_2$–P, m, 1H); 2.35 (N–C*H*$_2$–P, t, 2H, $^2J_{HP}$ = $^2J_{HH}$ = 15 Hz); 2.43–2.57 (*cycle*, m, 8H); 2.58–2.72 (*cycle*, m, 6H + P–C*H*$_2$–P, m, 1H); 2.73–2.83 (*cycle*, m, 2H); 2.84–2.97 (N–C*H*$_2$–P, m, 2H); ^{13}C{^{1}H} δ 32.6 (P–CH$_2$–P, t, $^1J_{CP}$ = 79 Hz); 43.2 (*cycle*, s); 44.5 (*cycle*, s); 51.6 (*C*H$_2$–N–CH$_2$–P, t, $^3J_{CP}$ = 3 Hz); 53.9 (N–CH$_2$–P, d, $^1J_{CP}$ = 120 Hz); 55.4 (*cycle*, d, $^3J_{CP}$ = 5 Hz); ^{31}P{^{1}H} δ 36.7 (s). MS (negative mode) *m*/*z* 339 ([M − H$^+$]$^-$); (positive mode) *m*/*z* 341 ([M + H$^+$]$^+$), 681 ([2 M + H$^+$]$^+$). TLC (SiO_2, *i*PrOH : conc. aq. ammonia : water 7:4:4): R_f 0.45.

H_4L: Compound **2** (1.00 g, 2.94 mmol, 1.0 equiv) was dissolved in water (25 ml), adding chloroacetic acid (2.23 g, 23.6 mmol, 8.0 equiv) and LiOH·H_2O (1.23 g, 29.3 mmol, 10.0 equiv). The solution was stirred at 60 °C for 5 h and then alkalized to pH 12 with solid LiOH·H_2O. After stirring the mixture overnight, at the same temperature, another portion of chloroacetic acid (2.23 g, 23.6 mmol, 8.0 equiv) was added, stirring the mixture at 60 °C for another 2 days and maintaining the pH at 12 by repeated additions of small amounts of solid LiOH·H_2O. After cooling to room temperature, the mixture was concentrated under vacuum, and the residue was purified by chromatography on a strong cation-exchange resin (Dowex 50; ~100 ml; H^+-form; H_2O → 10% aq. pyridine). The product-containing fractions were combined, and pyridine was removed by repeated evaporation. The product was obtained as a fine white powder from 1% aq. HCl by acetone addition. Yield: 1.14 g (85%). Elem. anal. calcd. for $C_{15}H_{30}N_4O_8P_2{\cdot}5H_2O0.5HCl$: C, 31.90; H, 7.23; N, 9.92; P, 10.97; Cl, 3.14. Found: C, 31.99; H, 6.75; N, 9.65; P, 10.59; Cl, 3.47. NMR (D_2O + CsOD, pD ~ 14): ^{1}H δ 1.74 (P–C*H*$_2$–P, t, 1H, $^2J_{HP}$ = 18 Hz); 2.50 (N–C*H*$_2$–P, t, 2H, $^2J_{HP}$ = $^2J_{HH}$ = 14 Hz); 2.59–3.05 (*cycle*, m, 11*H* + N–C*H*$_2$–P, m, 2H); 3.07–3.57 (*cycle*, m, 5H + P–C*H*$_2$–P, m, 1H); 3.92 (*C*H$_2$–COOH, s, 4H); ^{13}C{^{1}H} δ 31.3 (P–CH$_2$–P, t, $^1J_{CP}$ = 80 Hz); 52.9 (*cycle*, s); 53.6 (*cycle*, s); 57.0 (N–CH$_2$–P, d, $^1J_{CP}$ = 119 Hz); 58.1 (*C*H$_2$–N–CH$_2$–P, t, $^3J_{CP}$ = 5-Hz); 61.5 (*cycle*, s); 62.7 (CH$_2$–COOH, s); 180.3 (*C*O, s); ^{31}P{^{1}H} δ 37.3 (s). MS (negative mode) *m*/*z* 455 ([M − H$^+$]$^-$); (positive mode) *m*/*z* 457 ([M + H$^+$]$^+$), 913 ([2 M + H$^+$]$^+$).

Li$_2$[Cu(L)]·3.7H$_2$O: H_4L·5H_2O·0.5HCl (100 mg, 177 μmol) was dissolved in H_2O (3 ml), and excess of $CuCO_3$·$Cu(OH)_2$ (43 mg, 195 μmol, 1.1 equiv) was added. pH was slowly increased by addition of LiOH solution at pH 8. The mixture was stirred overnight at 90 °C. The solid matter was filtered off and the dark-blue filtrate was concentrated under vacuum. The resulting oil was dissolved in water and an excess of ethanol was added. The dark-blue product was filtered and washed with ethanol. Yield: 83 mg (75%). Elem. anal. calcd. for Li$_2$[Cu(L)]·3.7H_2O: C, 30.21; H, 5.64; N, 9.39; Cu, 10.66; Li, 2.33. Found: C, 30.39; H, 5.90; N, 9.13; Cu, 10.49; Li, 2.13. MS (negative mode) *m*/*z* 515.7 ([Cu(HL)]$^-$); (positive mode) *m*/*z* 517.8 ([Cu(H_3L)]$^+$). UV–VIS λ_{max} = 323 nm ε_{323} = 5025 dm^3·mol^{-1}·cm^{-1}, λ_{max} = 637 nm ε_{323} = 334 dm^3·mol^{-1}·cm^{-1}.

Li$_2$[Zn(L)]·3.5H$_2$O·0.5EtOH: H_4L·5H_2O0.5HCl (100 mg, 177 μmol) was dissolved in water (3 ml) and $ZnCO_3$ (24 mg, 195 μmol, 1.1 equiv) was added. pH was slowly increased by addition of LiOH solution at pH 8. The mixture was stirred overnight at 90 °C. The solid matter was filtered off and the filtrate was concentrated under vacuum. The resulting oil was dissolved in water and an excess of ethanol was added. The white product was filtered and washed with ethanol. Yield: 74 mg (68%). Elem. anal. calcd. for Li$_2$[Zn(L)]·3.5H_2O·0.5EtOH: C, 31.11; H, 5.87; N, 9.07; Zn, 10.58; Li, 2.25. Found: C, 31.27; H, 5.74; N, 8.86; Zn, 10.73; Li, 2.27. NMR (D_2O, pD ~ 8.5): ^{1}H δ 2.48 (P–C*H*$_2$–P, t, 2H, $^2J_{HP}$ 19 Hz); 2.51–2.81 (cycle, m, 10*H*); 2.82–2.95 (*cycle*, m, 4H); 2.96–3.35 (*cycle*, m, 2H + N–C*H*$_2$–P, m, 4H); 3.94 (*C*H$_2$–COOH, s, 4H); ^{13}C{^{1}H} δ 31.0

(P–CH_2–P, t, $^1J_{CP}$ 79 Hz); 47.9 (*cycle*, bs); 48.4 (*cycle*, bs); 52.3 (N–CH_2–P, bm); 53.5 (*cycle*, bs); 54.1 (*cycle*, s); 56.4 (CH_2–COOH, s); 172.8 (*CO*, s); $^{31}P\{^1H\}$ δ 30.3 (s). MS (positive mode) *m/z* 519.7 ($[Zn(H_3L)]^+$).

4.3. Potentiometric titrations

Potentiometry was performed according to previously published procedures; for further details on equipment, electrode system calibration, titration procedures and data treatment, see refs. [41,42]. Throughout the manuscript, pH means –log[H^+]. Protonation and stability constants were determined in 0.1 M (NMe_4)Cl at 25.0 °C with pK_w = 13.81. The stability constants of the Zn^{II} and Cu^{II} complexes were determined based on in-cell titrations from data collected in the pH range of 1.6–12 with ~ 30 points per titration and three parallel titrations (c_L = c_M = 4 mM). The stability constants of the La^{III}, Gd^{III} and Lu^{III} complexes were assessed using the out-of-cell method. The batches (starting volume 1 ml) were prepared under an argon stream in tubes with ground joints from the ligand, metal ion and HCl / (NMe_4)Cl stock solutions and water (molar ratio L : M = 1 : 0.95, c_L = 0.4 mM). Then, a known amount of the (NMe_4)OH stock solution was added under Ar. The tubes were firmly closed with stoppers, and the solutions were equilibrated at room temperature for 4 weeks. The titrations were performed in the pH range of 1.6–7 (the final pH values) with approximately 20 data points per titration and three titrations per system. The titration data were treated using the program OPIUM [43].

4.4. Crystal structure determination

Single crystals of **1**·4H_2O and $Na_{0.5}(H_5\mathbf{L})(H_{3.5}\mathbf{L})Cl{\cdot}20H_2O$ were obtained by slow evaporation of an aq. solution of the ligand (**1**) or ligand hydrochloride ($H_4\mathbf{L}$), respectively. The sodium(I) cation present in the later compound presumably originates from the glass. Single crystals of $Li_2[Cu(\mathbf{L})]{\cdot}4H_2O$ were obtained by ethanol addition into aqueous solution of complex. The Bruker D8 VENTURE Kappa Duo PHOTON100 diffractometer with IμS micro-focus sealed tube was used to collect diffraction data on **1**·4H_2O and $Li_2[Cu(\mathbf{L})]{\cdot}4H_2O$ using Cu-Kα (λ 1.54178 Å) radiation and on $Na_{0.5}(H_5\mathbf{L})(H_{3.5}\mathbf{L})Cl{\cdot}20H_2O$ using Mo-*K*α (λ 0.71073 Å) radiation at 120 K (Cryostream Cooler, Oxford Cryosystem). The data were analyzed using the SAINT (Bruker AXS Inc.) software package and corrected for absorption effects using the multi-scan method (SADABS). The structures were solved using direct methods (SHELXT2014) [44] and refined using full-matrix least-squares techniques (SHELXL2014) [45]. All non-hydrogen atoms were refined anisotropically. In the crystal structure of **1**··4H_2O, two formula units form the structurally independent part. All hydrogen atoms were found in the difference density map. However, hydrogen atoms bound to carbon atoms were fixed in theoretical positions using U_{eq}(H) = 1.2 U_{eq}(C) to keep a number of parameters low, and only hydrogen atoms bound to heteroatoms (N, O, P) were fully refined. In the crystal structure of $Na_{0.5}(H_5\mathbf{L})(H_{3.5}\mathbf{L})Cl{\cdot}20H_2O$, one formula unit forms the structurally independent part. A complicated crystallographic disorder of chloride counter ion and water molecules of crystallization was found and could not be reliably modelled, thereby requiring density-dependent squeezing using PLATON [46]. The removed electron density corresponded to one chloride anion and 20 water molecules (fully matching refinement trials with crystallographic disorder modelling). The hydrogen atoms of the nitrogen, oxygen and phosphorus atoms of the ligand molecules were located in difference density maps and fully refined, whereas hydrogen atoms bound to carbon atoms were fixed in theoretical positions, as stated above.

In the structure of $Li_2[Cu(\mathbf{L})]{\cdot}4H_2O$, all hydrogen atoms were found in the difference density map, but those bound to the carbon atoms were fixed in theoretical positions using U_{eq}(H) = 1.2 U_{eq}(C) to keep a number of parameters low. In addition, few hydrogen atoms belonging to the water molecules were fixed in the original position as their refinement led to unrealistically short/long bonds; but, most of the water hydrogen atoms were fully refined.

Selected experimental data on the refinement of individual structures are outlined in Table S3.

Declaration of Competing Interest

The authors declare that they have no known competing financial interests or personal relationships that could have appeared to influence the work reported in this paper.

Acknowledgement

The thank the funding from the Grant Agency of the Czech Republic (19-17380S). This work was conducted within the framework COST Action CA18202 (NECTAR) and the Inter-COST project MSMT (LTC 20044). The authors also thank I. Císařová (Charles University) for X-ray data acquisition.

Appendix A. Supplementary data

CCDC 2031495, 2031496 and 2049264 contains the supplementary crystallographic data for **1**·4H_2O, $Na_{0.5}(H_5\mathbf{L})(H_{3.5}\mathbf{L})Cl{\cdot}20H_2O$ and $Li_2[Cu(\mathbf{L})]{\cdot}4H_2O$, respectively. These data can be obtained free of charge via http://www.ccdc.cam.ac.uk/conts/retrieving.html, or from the Cambridge Crystallographic Data Centre, 12 Union Road, Cambridge CB2 1EZ, UK; fax: (+44) 1223-336-033; or e-mail: deposit@ccdc.cam.ac.uk. Supplementary data to this article can be found online at https://doi.org/10.1016/j.poly.2020.114994.

References

[1] Contrast Agents for MRI: Experimental Methods; V. C. Pierre, M. J. Allen, Eds.; RSC: London, 2018.
[2] P. Hermann, J. Kotek, V. Kubíček, I. Lukeš, Dalton Trans (2008) 3027–3047.
[3] H. Li, T.J. Meade, J. Am. Chem. Soc. 141 (2019) 17025–17041.
[4] T.J. Clough, L. Jiang, K.-L. Wong, N.J. Long, Nat. Commun. 10 (2019) 1420.
[5] J. Wahsner, E.M. Gale, A. Rodríguez-Rodríguez, P. Caravan, Chem. Rev. 119 (2019) 957–1057.
[6] C.F. Ramogida, C. Orvig, Chem. Commun. 49 (2013) 4720–4739.
[7] B.M. Zeglis, J.L. Houghton, M.J. Evans, N. Viola-Villegas, J.S. Lewis, Inorg. Chem. 53 (2014) 1880–1899.
[8] T.W. Price, J. Greenman, G.J. Stasiuk, Dalton Trans. 45 (2016) 15702–15724.
[9] L.E. McInnes, S.E. Rudd, P.S. Donnelly, Coord. Chem. Rev. 352 (2017) 499–516.
[10] A.J. Amoroso, I.A. Fallis, S.J.A. Pope, Coord. Chem. Rev. 340 (2017) 198–219.
[11] E. Boros, A.B. Packard, Chem. Rev. 119 (2019) 70–901.
[12] T.I. Kostelnik, C. Orvig, Chem. Rev. 119 (2019) 902–956.
[13] N.M. Di Bartolo, A.M. Sargeson, T.M. Donlevy, S.V. Smith, J. Chem. Soc., Dalton Trans. (2001) 2303–2309.
[14] E.H. Wong, G.R. Weisman, D.C. Hill, D.P. Reed, M.E. Rogers, J.P. Condon, M.A. Fagan, J.C. Calabrese, K.-C. Lam, I.A. Guzei, A.L. Rheingold, J. Am. Chem. Soc. 122 (2000) 10561–10572.
[15] C.A. Boswell, X. Sun, W. Niu, G.R. Weisman, E.H. Wong, A.L. Rheingold, C.J. Anderson, J. Med. Chem. 47 (2004) 1465–1474.
[16] A. Rodríguez-Rodríguez, M. Regueiro-Figueroa, D. Esteban-Gómez, R. Tripier, G. Tircsó, F. K. Kálmán, A. C. Bényei, I. Tóth, A. de Blas, T. Rodríguez-Blas, C. Platas-Iglesias, Inorg. Chem. 2016, 55, 2227−2239.
[17] R. Pujales-Paradela, T. Savić, I. Brandariz, P. Pérez-Lourido, G. Angelovski, D. Esteban-Gómez, C. Platas-Iglesias, Chem. Commun. 55 (2019) 4115–4118.
[18] T. David, V. Kubíček, O. Gutten, P. Lubal, J. Kotek, H.J. Pietzsch, L. Rulíšek, P. Hermann, Inorg. Chem. 54 (2015) 11751–11766.
[19] S. Füzerová, J. Kotek, I. Císařová, P. Hermann, K. Binnemans, I. Lukeš, Dalton Trans. (2005) 2908–2915.
[20] J. Kotek, P. Lubal, P. Hermann, I. Císařová, I. Lukeš, T. Godula, I. Svobodová, P. Táborský, J. Havel, Chem. Eur. J. 9 (2003) 233–248.
[21] I. Lukeš, J. Kotek, P. Vojtíšek, P. Hermann, Coord. Chem. Rev. 216–217 (2001) 287–312.
[22] I. Svobodová, J. Havlíčková, J. Plutnar, P. Lubal, J. Kotek, P. Hermann, Eur. J. Inorg. Chem. (2009) 3577–3592.

[23] M. Paúrová, T. David, I. Císařová, P. Lubal, P. Hermann, J. Kotek, New J. Chem. 42 (2018) 11908–11929.
[24] S. Aime, C. Cavallotti, E. Gianolio, G.B. Giovenzana, G. Palmisano, M. Sisti, Tetrahedron Lett. 43 (2002) 8387–8389.
[25] Y.G. Lee, S.T. Kim, D.I. Jung, J.T. Hanh, Asian J. Chem. 27 (2015) 1481–1483.
[26] D.M. Weekes, M. de Guadalupe Jaraquemada-Peláez, T.I. Kostelnik, B.O. Patrick, C. Orvig, Inorg. Chem. 2017, 56, 10155−10161.
[27] S. Procházková, V. Kubíček, J. Kotek, A. Vágner, J. Notni, P. Hermann, Dalton Trans. 47 (2018) 13006–13015.
[28] T. David, V. Hlinová, V. Kubíček, R. Bergmann, F. Striese, N. Berndt, D. Szöllősi, T. Kovács, D. Máthé, M. Bachmann, H.-J. Pietzsch, P. Hermann, J. Med. Chem. 61 (2018) 8774–8796.
[29] L. Pazderová, T. David, V. Hlinová, J. Plutnar, J. Kotek, P. Lubal, V. Kubíček, P. Hermann, Inorg. Chem. 59 (2020) 8432–8443.
[30] M. Meyer, V. Dahaoui-Gindrey, C. Lecomte, R. Guilard, Coord. Chem. Rev. 178–180 (1998) 1313–1405.
[31] T. David, S. Procházková, J. Havlíčková, J. Kotek, V. Kubíček, P. Hermann, I. Lukeš, Dalton Trans. 42 (2013) 2414–2422.
[32] M. Pniok, V. Kubíček, J. Havlíčková, J. Kotek, A. Sabatie-Gogová, J. Plutnar, S. Huclier-Markai, P. Hermann, Chem. Eur. J. 20 (2014) 7944–7955.
[33] A. Bianchi, L. Calabi, C. Giorgi, P. Losi, P. Mariani, D. Palano, P. Paoli, P. Rossi, B. Valtancoli, J. Chem. Soc., Dalton Trans. (2001) 917–922.
[34] J. Bárta, P. Hermann, J. Kotek, Molecules 24 (2019) 3324.
[35] J. Šimeček, P. Hermann, J. Havlíčková, E. Herdtweck, T.G. Kapp, N. Engelbogen, H. Kessler, H.-J. Wester, J. Notni, Chem. Eur. J. 19 (2013) 7748–7757.
[36] P.A. Stenson, A.L. Thompson, D. Parker, Dalton Trans. (2006) 3291–3293.
[37] (a) A.E. Martell, R.M. Smith, Critical Stability Constants, Vols. 1–6. Plenum Press, New York, USA, 1974–1989. (b) NIST Standard Reference Database 46 (Critically Selected Stability Constants of Metal Complexes), Version 7.0, 2003. (c) C.F. Baes, Jr.; R.E. Mesmer, The Hydrolysis of Cations, Wiley, New York, USA, 1976.
[38] G. Anderegg, F. Arnaud-Neu, R. Delgado, J. Felcman, K. Popov, Pure Appl. Chem. 77 (2005) 1445–1495.
[39] A. Forgács, L. Tei, Z. Baranyai, I. Tóth, L. Zékány, M. Botta, Eur. J. Inorg. Chem. (2016) 1165–1174.
[40] C. King, D.M. Roundhill, F.R. Fronczek, Inorg. Chem. 25 (1986) 1290–1292.
[41] V. Kubíček, J. Havlíčková, J. Kotek, G. Tircsó, P. Hermann, É. Tóth, I. Lukeš, Inorg. Chem. 49 (2010) 10960–10969.
[42] M. Försterová, I. Svobodová, P. Lubal, P. Táborský, J. Kotek, P. Hermann, I. Lukeš, Dalton Trans. (2007) 535–549.
[43] a) M. Kývala, I. Lukeš, International Conference Chemometrics '95, Pardubice, Czech Republic, 1995, p. 63; b) M. Kývala, P. Lubal, I. Lukeš, IX. Spanish-Italian and Mediterranean Congress on Thermodynamics of Metal Complexes (SIMEC 98), Girona, Spain, 1998. The full version of the OPIUM program is available (free of charge) on http://www.natur.cuni.cz/_kyvala/opium.html.
[44] (a) G. M. Sheldrick, SHELXT2014/5. Program for Crystal Structure Solution from Diffraction Data, University of Göttingen, Göttingen, 2014.;
(b) G.M. Sheldrick, Acta Crystallogr. Sect. A. A64 (2008) 112–122.
[45] (a) C.B. Hübschle, G.M. Sheldrick, B. Dittrich, ShelXle: A Qt Graphical User Interface for SHELXL, University of Göttingen, Göttingen, 2014;
(b) C.B. Hübschle, G.M. Sheldrick, B. Dittrich, J. Appl. Cryst. 44 (2011) 1281–1284;
(c) G.M. Sheldrick, SHELXL-2014/7. Program for Crystal Structure Refinement from Diffraction Data, University of Göttingen, Göttingen, 2017;
(d) G.M. Sheldrick, Acta Crystallogr. Sect. C C71 (2015) 3–8.
[46] (a) A.L. Spek, PLATON. A Multipurpose Crystallographic Tool, Utrecht University, Utrecht, 2005;
(b) A.L. Spek, Acta Crystallogr. Sect. C C71 (2015) 9–18.

Complexes of cyclen side-bridged with a methylene-bis(phosphinate) group

Lucia Pazderová, Tomáš David, Jan Kotek, Vojtěch Kubíček,* Petr Hermann

Department of Inorganic Chemistry, Faculty of Science, Charles University, Hlavova 8, 128 40 Prague 2, Czech Republic. Tel.: +420221951436; fax: +420221951253; e-mail: kubicek@natur.cuni.cz

Table of contents

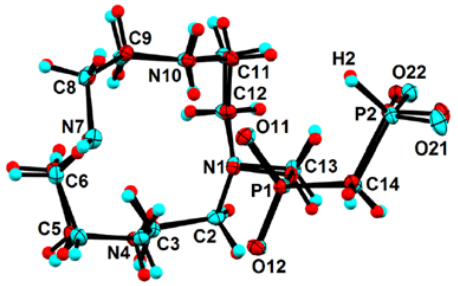

Figure S1. Overlay of two structurally independent molecules of **1** found in the crystal structure of **1**·4H$_2$O

Table S1. Parameters of selected hydrogen bonds involving hydrogen atoms of the amino groups found in the crystal structure of **1**·4H$_2$O

D–H	*d*(D–H), Å	*d*(H···A), Å	<DHA, °	*d*(D···A), Å	A [symmetry code]
N4A-H41	0.89(2)	1.91(2)	158(2)	2.753(1)	O1W
N4A-H42	0.89(2)	2.37(2)	113(1)	2.841(2)	N7A
N7A-H71	0.85(2)	2.37(2)	157(2)	3.166(1)	O12A [−*x*+2, −*y*+1, −*z*+2]
N10A-H101	0.88(2)	2.05(2)	149(1)	2.845(1)	O11A
N10A-H102	0.92(2)	1.81(2)	170(2)	2.729(1)	O22A [−*x*+2, *y*+1/2, −*z*+3/2]
N4X-H43	0.87(2)	1.87(2)	159(2)	2.698(1)	O8W
N4X-H44	0.87(2)	2.43(2)	112(1)	2.871(1)	N1X
N4X-H44	0.87(2)	2.38(2)	114(1)	2.839(2)	N7X
N7X-H73	0.85(2)	2.28(2)	147(1)	3.030(1)	O12X [−*x*+1, −*y*+1, −*z*+1]
N10X-H103	0.89(2)	1.95(2)	145(1)	2.737(1)	O11X
N10X-H104	0.92(2)	1.83(2)	169(1)	2.745(1)	O22X [−*x*+1, *y*−1/2, −*z*+1/2]

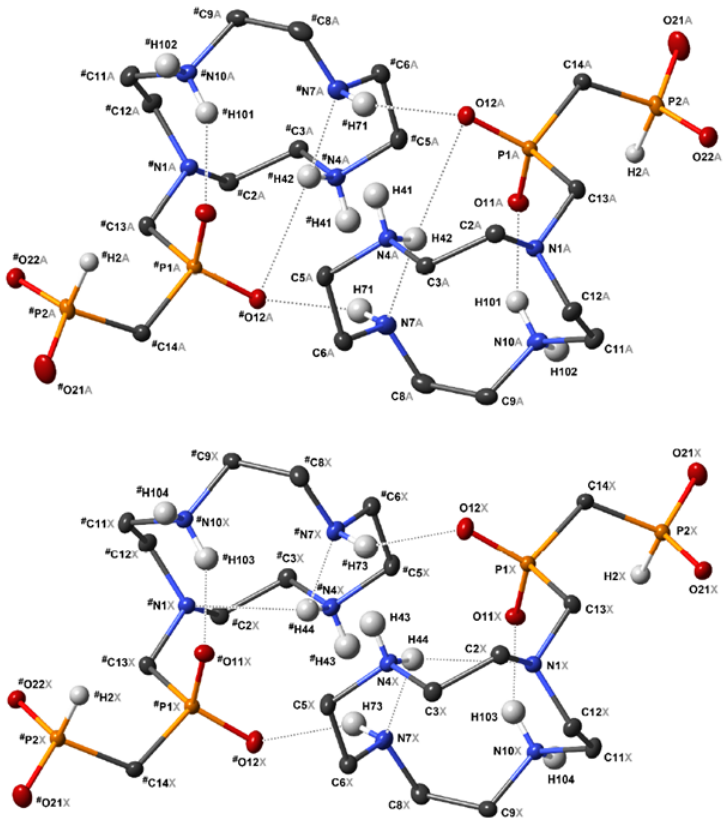

Figure S2. Centrosymmetric hydrogen-bond-bound dimers of **1** found in the crystal structure of **1**·4H_2O. Symmetry-related atoms are labelled with an "#". Hydrogen bonds are shown as turquoise lines. The water molecules of crystallization and carbon-bound hydrogen atoms are not displayed for the sake of clarity. Thermal ellipsoids are set at 65% probability.

Table S2. Parameters of selected hydrogen bonds involving protonated ligand pendant arms found in the crystal structure of $Na_{0.5}(H_5\mathbf{L})(H_{3.5}\mathbf{L})Cl{\cdot}20H_2O$.

D–H	*d*(D–H), Å	*d*(H···A), Å	<DHA, °	*d*(D···A), Å	A [symmetry code]
N1A-H1A	0.92(2)	2.33(2)	114(1)	2.829(2)	N4A
N1A-H1A	0.92(2)	2.34(2)	116(1)	2.864(2)	N10A
N7A-H7A	0.87(2)	2.55(2)	113(1)	2.998(2)	N10A
N7A-H7A	0.87(2)	2.44(2)	133(1)	3.100(2)	O41B
O2A-H2PA	0.80(3)	2.58(3)	124(2)	3.102(1)	O31X
O2A-H2PA	0.80(3)	1.77(3)	176(3)	2.568(1)	O31Y
O31A-H31A	1.17(3)	1.29(2)	176(3)	2.461(1)	O2X
O41A-H41A	0.88(2)	1.70(2)	171(2)	2.572(1)	O1X
N1X-H1X	0.85(2)	2.35(2)	115(1)	2.823(2)	N4X
N1X-H1X	0.85(2)	2.41(2)	116(1)	2.891(2)	N10X
N7X-H7X	0.84(2)	2.52(2)	113(1)	2.957(2)	N10X
N7X-H7X	0.84(2)	2.47(2)	128(1)	3.064(1)	O41Y
O31X-H31X	1.216(1)	1.216(1)	180	2.431(2)	O31X [−*x*+1, −*y*+2, −*z*+1]
O41X-H41X	0.90(2)	1.71(2)	169(2)	2.601(1)	O1A

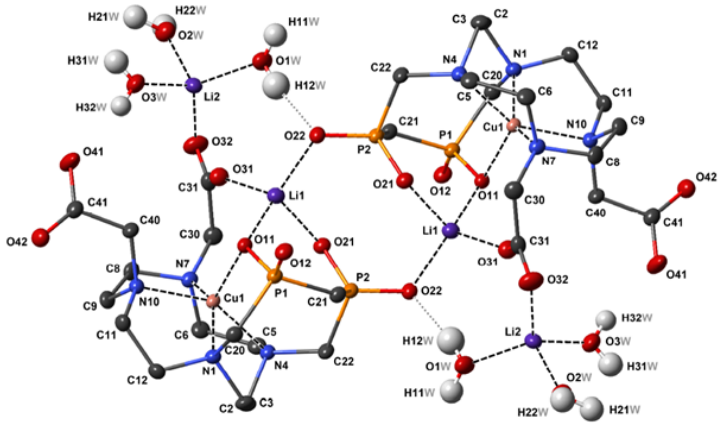

Figure S3. Dimeric species $\{Li[Li(H_2O)_3][Cu(\mathbf{L})]\}_2$ found in the crystal structure of $Li_2[Cu(\mathbf{L})]\cdot 4H_2O$. The carbon-bound hydrogen atoms and one water molecule of crystallization are not displayed for sake of clarity.

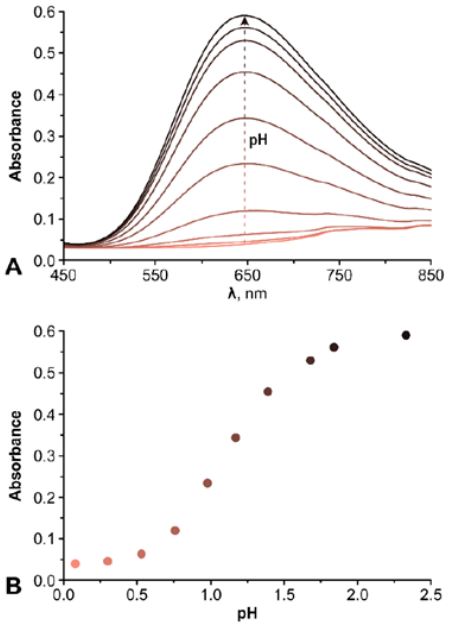

Figure S4. UV-VIS spectra of Cu^{II}- $H_4\mathbf{L}$ in the pH range of 0.08–2.33 (A) and absorbance at 648 nm as function of pH (B); $c_M = c_L = 3$ mM, 25 °C

Table S3. Experimental crystallographic data for reported crystal structures

Parameter	**1**·4H_2O	$Na_{0.5}(H_5\mathbf{L})(H_{3.5}\mathbf{L})Cl{\cdot}20H_2O$	$Li_2[Cu(\mathbf{L})]{\cdot}4H_2O$
Formula	$C_{10}H_{34}N_4O_8P_2$	$C_{30}H_{100.5}ClN_8Na_{0.5}O_{36}P_4$	$C_{15}H_{34}CuLi_2N_4O_{12}P_2$
M_r	400.35	1320.50	601.82
Habit	bar	prism	prism
Colour	colourless	colourless	blue
Crystal system	monoclinic	monoclinic	monoclinic
Space group	$P2_1/c$	$P2_1/c$	$P2_1/c$
a, Å	19.9061(5)	17.1349(8)	14.8039(4)
b, Å	8.6279(2)	19.9438(9)	9.8436(3)
c, Å	23.6948(6)	19.0868(8)	15.9403(5)
α, °	90	90	90
β, °	111.617(1)	111.916(1)	92.739(1)
γ, °	90	90	90
U, Å^3	3783.31(16)	6051.2(5)	2320.23(12)
Z	8	4	4
D_{calc}, g cm^{-3}	1.406	1.449	1.723
μ, mm^{-1}	2.496	0.272	3.267
Unique refl.	7452	13928	4527
Obsd. refl. ($I>2\sigma(I)$)	7107	12452	4053
$R(I>2\sigma(I))$	0.0258	0.0349	0.0334
R'(all)	0.0270	0.0392	0.0380
$wR(I>2\sigma(I))$	0.0691	0.0911	0.0882
wR'(all)	0.0701	0.0939	0.0918
CCDC number	2031495	2031496	2049264

Appendix 3

Pazderová, L., David, T., Hlinová, V., Plutnar, J., Kotek, J., & Lubal, P. et al. (2020). Cross-Bridged Cyclam with Phosphonate and Phosphinate Pendant Arms: Chelators for Copper Radioisotopes with Fast Complexation. *Inorganic Chemistry*, *59*(12), 8432-8443. https://doi.org/10.1021/acs.inorgchem.0c00856

Inorganic Chemistry

pubs.acs.org/IC Article

Cross-Bridged Cyclam with Phosphonate and Phosphinate Pendant Arms: Chelators for Copper Radioisotopes with Fast Complexation

Lucia Pazderová, Tomáš David, Veronika Hlinová, Jan Plutnar, Jan Kotek, Přemysl Lubal, Vojtěch Kubíček,* and Petr Hermann

Cite This: *Inorg. Chem.* 2020, 59, 8432−8443 Read Online

ACCESS | Metrics & More | Article Recommendations | Supporting Information

ABSTRACT: Cross-bridged cyclam derivatives bearing two phosphonate (H_4L^1), bis(phosphinate) (H_4L^2), or phosphinate (H_2L^3) pendant arms were synthesized and studied with respect to their application as copper radioisotope carriers in nuclear medicine. The ligands show high macrocycle basicity ($pK_1 > 14$) and high Cu(II) complex stability (log K = 20−24). The complexation and dissociation kinetics of the Cu(II) complexes were studied by ultraviolet−visible spectroscopy. Phosphonate Cu(II)-H_4L^1 and bis(phosphinate) Cu(II)-H_4L^2 complexes form very quickly, reaching quantitative formation within 1 s at pH ∼6 and millimolar concentrations. Conversely, the formation of the phosphinate complex Cu(II)-H_2L^3 is much slower (9 min at pH ∼6) due to the low stability of the *out-of-cage* reaction intermediate. All studied complexes are highly kinetically inert, showing half-lives of 120, 11, and 111 h for Cu(II)-H_4L^1, Cu(II)-H_4L^2, and Cu(II)-H_2L^3 complexes, respectively, in 1 M $HClO_4$ at 90 °C. The high thermodynamic stability, fast formation, and extreme kinetic inertness of Cu(II) complexes indicate that phosphonate and bis(phosphinate) derivatives are promising ligands for nuclear medicine.

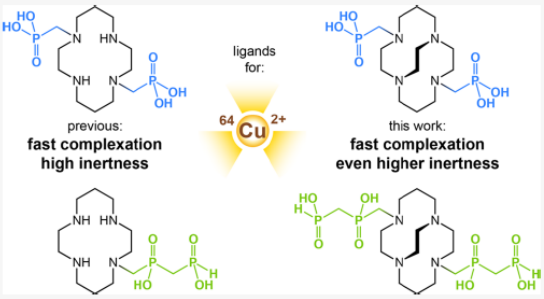

INTRODUCTION

Copper radioisotopes are increasingly being used in radiopharmaceuticals and applied in nuclear medicine.[1−3] The nuclides ^{61}Cu (100% β^+; $t_{1/2}$ = 3.3 h) and ^{64}Cu (61% β^+, 39% β^-; $t_{1/2}$ = 12.7 h) are promising imaging radioisotopes for positron emission tomography, whereas nuclides ^{64}Cu and ^{67}Cu (100% β^-; $t_{1/2}$ = 62 h) are studied as radiotherapeutics. These radioisotopes have become increasingly available in recent years, and several copper-based radiopharmaceuticals are currently at different phases of clinical trials. Imaging and therapeutic radionuclides can be combined into theranostics, and radiopharmaceuticals containing ^{64}Cu and ^{67}Cu are considered the first, usable, single-element theranostics.

For *in vivo* applications, any metal ion must be bound in a thermodynamically stable and kinetically inert complex to avoid nonspecific radioisotope deposition in tissues. Macrocyclic ligands with coordinating pendant arms are preferentially used to ensure that complexes reach sufficient kinetic inertness. The ligands are mostly derivatives of 1,4,7-triazacyclononane (H_3**nota** analogues), 1,4,7,10-tetraazacyclododecane (H_4**dota** analogues), or 1,4,8,11-tetraazacyclotetradecane (H_4**teta** analogues) (Chart 1). In recent years, macrobicyclic ligands have been studied to further improve the kinetic inertness of complexes.[4] Among the most promising ligands, derivatives of cross-bridged cyclam stand out [cb-cyclam (Chart 1)]. The parent macrocycle was first modified with two acetates [e.g., H_2**cb-te2a** (Chart 1)] or acetate/acetamide pendants.[5−8] Subsequently, two methylphosphonate [e.g., H_4**cb-te2p** (Chart 1)] or methylphosphonate/acetamide groups were added to the macrocycle,[9−13] thereby improving radiolabeling efficacy with these pendant arms. Cross-bridged cyclams with picolinate pendant(s) have also been identified as good chelators for copper(II) complexation.[14] However, in general, the use of cross-bridged macrocyclic ligands is mainly limited by the rather slow, i.e., inefficient complexation of Cu(II) ions, and the complexation rate is strongly affected by pendant arms attached to the macrocycle amine groups. Among the cb-cyclam derivatives, the cb-cyclam with two phosphonate pendants shows the best labeling efficiency.[10,12,13] However, most studies have focused on only the use of the chelators, overlooking thermodynamic and kinetic parameters of complexes of these ligands.[5,6,14,15] Similarly, only a few

Received: March 22, 2020
Published: May 21, 2020

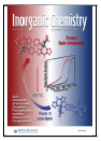

https://dx.doi.org/10.1021/acs.inorgchem.0c00856
Inorg. Chem. 2020, 59, 8432−8443

Chart 1. Structures of the Ligands Discussed in the Text

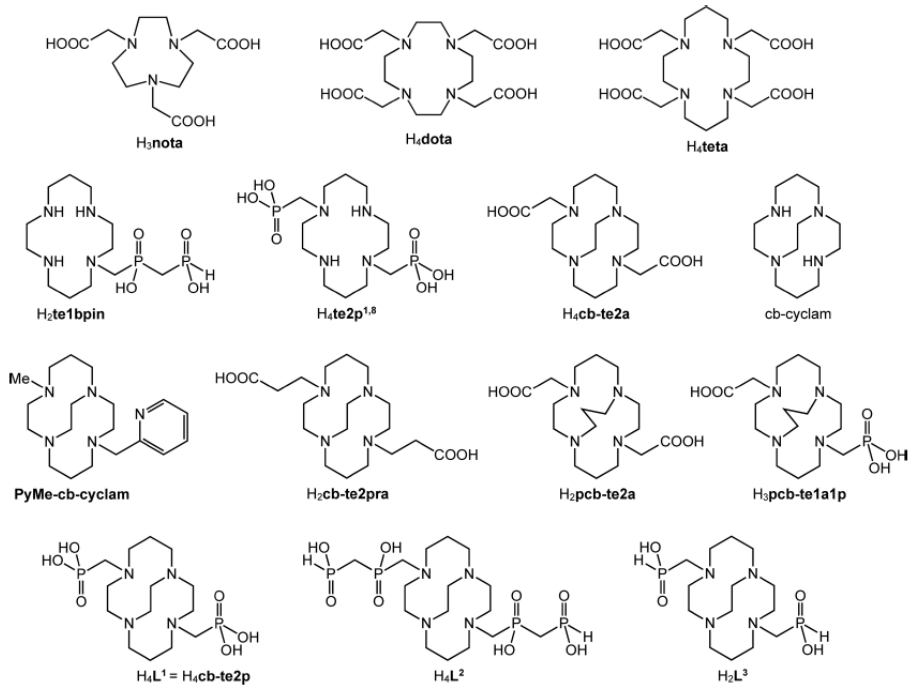

structural studies of complexes of cb-cyclams with coordinating pendant arms have been published thus far.[5,9,10,16−18]

In our previous studies, we have shown that Cu(II) is very efficiently complexed by phosphonic acid derivatives of cyclam.[19−24] Their Cu(II) complexes have a high thermodynamic stability, as well as high thermodynamic and kinetic selectivity for Cu(II) over other divalent metal ions.[25,26] Complexes of ligands without fully substituted cyclam ring amine groups are also kinetically inert. The rate of complexation of the Cu(II) ion with these phosphonate cyclam derivatives is generally higher than that of cyclam itself or the rates with their acetate analogues. However, for radiopharmaceutical purposes, the complexation rate must be even higher. Metal ion complexation by macrocyclic ligands is described as a two-step process. The first equilibrium step is the immediate formation of an *out-of-cage* intermediate in which the metal ion is coordinated by the pendant donor groups while the amine groups of the macrocycle remain protonated. This step is followed by the rate-determining step in which the intermediate rearranges into the final *in-cage* complex with the metal ion coordinated by all nitrogen atoms of the macrocycle and by donor atoms of the pendants. Thus, the overall complexation rate is affected by two factors: the abundance of *out-of-cage* intermediates and the rate of *out-of-cage*-to-*in-cage* complex transformation.

On the basis of the information presented above, complexation (and thus radiolabeling) can be accelerated by increasing the *out-of-cage* complex stability or by improving the rate of the final *in-cage* complex formation, as we have already shown for the complexation of trivalent gallium[27,28] and lanthanides.[29] Upon application of the same principles to the complexation of Cu(II), the rate of formation and radiolabeling of cyclam-based ligands should be significantly enhanced when introducing bis(phosphinate) pendant arms [e.g., H_2**te1bpin** (Chart 1)] because these groups can form an *out-of-cage* complex with a relatively high stability.[30,31] Most importantly, the selectivity of ligands for divalent copper over other metal ions, the high thermodynamic stability of Cu(II) complexes, and their high kinetic inertness are preserved upon this functionalization.[30] Moreover, a bifunctional derivative of such a complex was conjugated to an antibody, and the resulting conjugate was quickly labeled with ^{64}Cu at 37 °C to prepare a radiolabeled antibody with high specific activity, which was fully stable *in vivo* for days.[32]

Detailed thermodynamic and kinetic studies of cross-bridged cyclam derivatives and their complexes are rather rare. Knowledge of these parameters is important for successfully developing new, more efficient ligands for radiochemical applications. Thus, we report here a detailed study of Cu(II) complexes with cb-cyclam derivatives bearing phosphorus acid pendant arms (Chart 1). We assessed the effect of a phosphorus acid pendant arm structure on the complexation and decomplexation rates. The pendants are expected to differently stabilize the *out-of-cage* intermediate because they differ in their complexation ability. The compounds H_4L^1 (H_4**cb-te2p**) bearing two phosphonate pendants, H_4L^2 bearing two bis(phosphinate) pendants, and H_2L^3 bearing two phosphinate pendants were prepared, and the thermodynamic and kinetic properties of their Cu(II) complexes were evaluated in this study.

RESULTS AND DISCUSSION

Ligand Synthesis. All ligands were synthesized in a one-step phospha-Mannich reaction from cb-cyclam, paraformalde-

https://dx.doi.org/10.1021/acs.inorgchem.0c00856
Inorg. Chem. 2020, 59, 8432−8443

Scheme 1. Syntheses of the Studied Ligands and the Respective Isolated Yields[a]

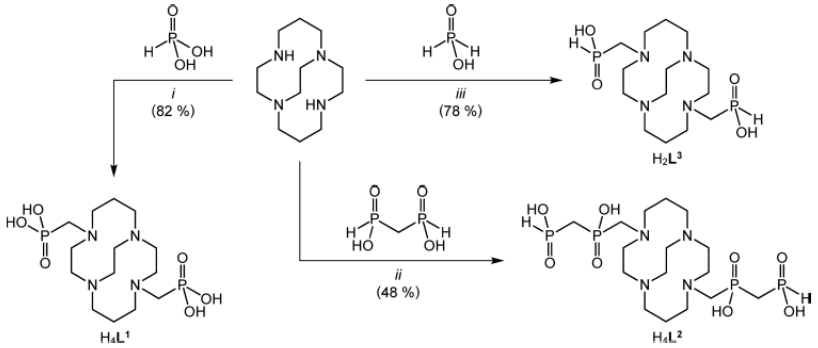

[a](*i*) $(CH_2O)_n$, 12 M aqueous HCl, 35 °C, 7 days; (*ii*) $(CH_2O)_n$, 6 M aqueous HCl, 60 °C, 2 days; (*iii*) $(CH_2O)_n$, 50% aqueous H_3PO_2, 60 °C, 3 h.

hyde, and the corresponding phosphorus precursor (Scheme 1). The phosphonate derivative H_4L^1 was synthesized using phosphorous acid as the phosphorus source at 35 °C because using higher temperatures leads to the formation of side products (Figure S1). As the reaction at 35 °C is rather slow, a large excess of both H_3PO_3 and paraformaldehyde (15 equiv) and a long reaction time (7 days) were utilized to quantitatively and clearly form H_4L^1. Simple purification of the reaction mixture on a strong cation exchange resin afforded pure H_4L^1 on a gram scale and in a high yield [82% (Figure S2)]. A previously described two-step procedure using triethylphosphite in phospha-Mannich synthesis followed by hydrolysis of the esterified intermediate resulted in a 60% overall yield.[9,10]

The ligand H_4L^2 bearing bis(phosphinate) pendants was synthesized from methylene-bis(phosphinic acid) as previously reported for the cyclam derivatives.[30,32] Disubstitution was controlled using an excess of methylene-bis(phosphinic acid) and paraformaldehyde over cb-cyclam. However, the reaction does not proceed quantitatively, thus requiring chromatographic purification to separate monosubstituted and *N*-methylated derivatives. Thus, H_4L^2 was isolated in a moderate yield [48% (Figure S3)]. Surprisingly, no *P*-hydroxomethylation was observed despite using an excess of paraformaldehyde, thus showing the unexpectedly low reactivity of the geminal bis(phosphinate) fragment in the *P*-hydroxomethylation reaction.

The phosphinate derivative H_2L^3 was synthesized using an excess of hypophosphorous acid at a high temperature (60 °C). The reaction is fast, reaching an almost quantitative conversion within 3 h. H_2L^3 does not undergo hydroxomethylation or oxidation of the phosphinate pendant arms under the applied conditions. Small quantities (<5%) of the *N*-methylated monophosphinate derivative that formed during the reaction were removed on a strong cation exchange resin, isolating the product in a high yield [78% (Figure S4)].

Crystal Structures. The ligand H_2L^3 crystallizes in pentahydrate form (Figure 1A). The N4 and N11 atoms bearing the methylphosphinate groups are both protonated. The protons are turned inside the macrocyclic cavity and participate in the intramolecular hydrogen bond system involving all nitrogen atoms of the macrocycle and one oxygen atom of each methylphosphinate groups. The remaining phosphinate oxygen atoms participate in the intermolecular system of hydrogen bonds together with water molecules of

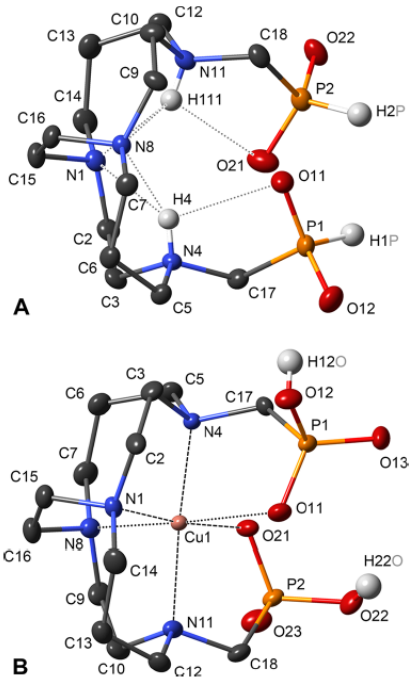

Figure 1. Molecular structure of H_2L^3 (A) found in the crystal structure of $H_2L^3 \cdot 5H_2O$ (intramolecular hydrogen bonds are shown as dotted lines) and of $[Cu(H_2L^1)]$ (B) found in the crystal structure of $[Cu(H_2L^1)] \cdot 2H_2O$ (axial bonds are displayed as dotted lines). Water molecules of crystallization and carbon-bound hydrogen atoms are not displayed.

crystallization. The hydrogen bond parameters (lengths and angles) are listed in Table S1. The P−O distances in the methylphosphinate groups suggest delocalization of the negative charge over both oxygen atoms of each HPO_2^- moiety (P1−O11, 1.490 Å; P1−O12, 1.505 Å; P2−O21, 1.492 Å; P2−O22, 1.508 Å). The geometry, bond lengths, and structure of hydrogen bonds are similar to those reported previously for the crystal structure of $H_2L^1 \cdot HCl \cdot 4H_2O$.[9]

Upon exposure of the $[Cu(L^3)]$ complex aqueous solutions to air for a long time, the coordinated diphosphinate ligand

https://dx.doi.org/10.1021/acs.inorgchem.0c00856
Inorg. Chem. 2020, 59, 8432−8443

Table 1. Protonation Constants of the Studied Ligands and Related Compounds and Stability Constants of Their Cu(II) Complexes (25 °C, I = 0.1 M NMe_4Cl)[a]

	ligand protonation constants (log K_a)					
	H_4L^1	H_4L^2	H_2L^3	cb-cyclam[c]	H_4te2p[1,8,d]	H_2te1bpin[e]
HL	~15[b]	~15[b]	~15[b]	12.42	–	12.18
H_2L	11.22	6.89	6.35	10.20	26.41[h]	10.75
H_3L	7.34	2.60	–	–	6.78	2.94
H_4L	4.63	1.35	–	1.39[g]	5.36	1.61
	stability constants of the complexes (log K)					
	H_4L^1	H_4L^2	H_2L^3	cb-cyclam[c]	H_4te2p[1,8,e]	H_2te1bpin[f]
Cu + L ↔ [Cu(L)]	23.97	20.21	21.28	27.1	25.40[i]/26.50[j]	25.83
[Cu(L)] + H ↔ [Cu(HL)]	8.26	2.63	–	–	7.05[i]/6.53[j]	–
[Cu(HL)] + H ↔ [Cu(H_2L)]	4.63	–	–	–	5.10[i]/5.39[j]	–
pCu[k]	7.80	7.45	8.02	12.24	8.13[i]/8.62[j]	10.05

[a]Charges have been omitted. [b]The value could not be determined and was, thus, fixed at log K_1 = 15. Stability constants of the complexes are related to this value. [c]From ref 5. [d]From ref 38. [e]From ref 19. [f]From ref 30. [g]The value corresponds to the protonation over two steps (log K_3 + log K_4). [h]The value corresponds to the protonation over two steps (log K_1 + log K_2). [i]Values determined for the pentacoordinated isomer. [j]Values determined for the hexacoordinated *trans* isomer. [k]pCu = −log[Cu(II)] calculated for c_L = c_{Cu} = 0.004 M at pH 7.4.

was oxidized, and the [Cu(H_2L^1)]·2H_2O complex crystallized out of the system (Figure 1B). In this complex, the copper central atom is surrounded by six donor atoms in a distorted octahedral coordination sphere, and two oxygen atoms from the phosphonate groups are located in *cis* positions as a result of ligand preorganization. The Jahn−Teller distortion of the octahedron toward one of the phosphonate moieties is relatively large. The axial Cu−O11 distance (2.716 Å) is approximately 0.7 Å longer than the equatorial Cu−O21 distance (1.981 Å), thus suggesting only a weak interaction between the N4-bound methylphosphonate group and the central Cu(II) ion. The difference in the coordination binding strength of the respective phosphonate groups is also shown by the bond parameters of the phosphonate groups (Table S2). The Cu−N distances in the equatorial plane range from 2.045 to 2.104 Å, whereas the Cu−N8 bond coordinated in the axial position is 2.207 Å (Table S3). In the neutral complex, the ligand is present in its doubly deprotonated form, and each of the methyl(hydrogenphosphonate) pendant arms bears one negative charge. In the crystal lattice, the molecules are interconnected by a system of hydrogen bonds, either between two phosphonate groups from different ligand molecules or involving the solvate water molecules (Table S4).

The previously reported structure of [Cu(H_2L^1)] shows a similar coordination motif, primarily differing in the coordination distance of axially bound phosphonate [d(Cu−O_{ax}) = 2.44−2.58 Å (Table S3)][9,10] due to the differences in the hydrogen bond networks. A similar coordination motif and bond lengths have also been reported for Cu(II) complexes with H_2cb-te2a (Table S3).[5,6,33] In turn, the cyclam-diphosphonate complex *trans*-[Cu(H_2te2p[1,8])] has all four nitrogen atoms in equatorial positions, which shows slightly shorter bond lengths [d(Cu−N_{eq}) = 2.01−2.08 Å],[19] which indicates optimal preorganization of the cyclam cavity for the Cu(II) ion.

Protonation and Stability Constants. Protonation constants of the ligands and stability constants of their Cu(II) complexes were determined by potentiometry (Table 1). The cavity of cb-cyclam is well preorganized for proton binding, and thus, the compounds show extremely high affinity for the first proton in the cage and behave as a proton sponge. Consequently, the first protonation constant (log K_1) could not be determined by potentiometry. The NMR titration also showed no changes in the spectra in the alkaline region [pH 12−14 (Figure S5)], hence indicating a very high value of the first protonation constant log K_1 > 14.5. On the other hand, on the basis of comparison with other macrocyclic ligands, we do not expect the constant to exceed this value by several orders of magnitude. Thus, it was estimated and fixed in calculations at log K_1 = 15. The high value of log K_1 was expected for H_4L^1 because phosphonate groups increase the basicity of the ring amines.[34] It is surprising for H_4L^2 and H_2L^3 because phosphinate pendants generally decrease the basicity of macrocyclic amine groups.[34] Similarly, the high basicity of the cb-cyclam core has been previously described.[14,35,36]

The expected influence of different pendant arms is markedly expressed in the second protonation constant, which is rather high (pK_2 = 11.22) for H_4L^1 but more than 4 orders of magnitude lower for H_4L^2 and H_2L^3 (6.89 and 6.35, respectively). The remaining protonation constants of each ligand correspond to the protonation of phosphonate or phosphinate groups, and the values are in the expected range.

The H_4L^2 complexation of Cu(II) was fast enough for in-cell potentiometry, whereas the Cu(II)-H_4L^1 and Cu(II)-H_2L^3 systems required out-of-cell analysis at pH <7.[37] Distribution diagrams are shown in Figure 2. In the Cu(II)-H_4L^1 system, [Cu(L)] is the dominant species only in the alkaline region, whereas [Cu(HL)] and [Cu(H_2L)] are dominant in neutral and acidic regions, respectively. The protonations occur on the noncoordinated phosphonate oxygen atom of each phosphonate group, and the values are in line with those reported for analogous systems.[19−24] In the Cu(II)-H_4L^2 system, [Cu(L)] is the dominant species at pH >4. The [Cu(HL)] species is formed at pH <4, and the proton is more likely localized on the noncoordinated terminal phosphinate. H_2L^3 does not form a protonated Cu(II) complex, and [Cu(L)] is the dominant species along the whole studied pH range. The stability constants of the [Cu(L)] species are rather high for all ligands. However, the values are lower than those determined for cyclam derivatives (Table 1 and Table S5), although the macrocycle basicity is higher for cb-cyclam derivatives. This difference results from the high rigidity of the cb-cyclam core, which precludes the coordination of all four nitrogen atoms in the equatorial plane of the square pyramidal or bipyramidal

https://dx.doi.org/10.1021/acs.inorgchem.0c00856
Inorg. Chem. 2020, 59, 8432−8443

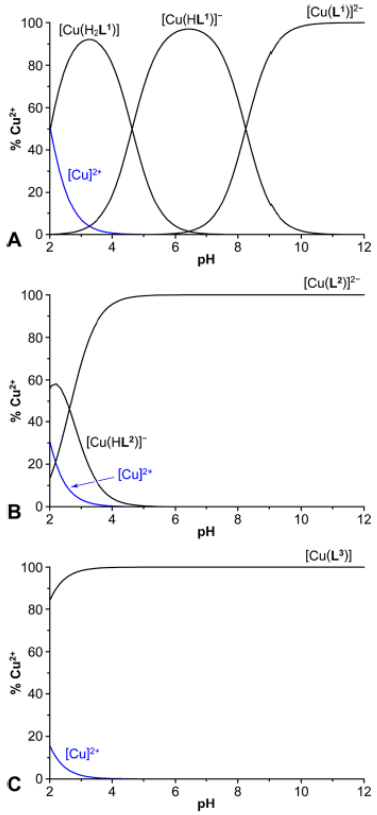

Figure 2. Distribution diagrams of (A) Cu(II)-H_4L^1, (B) Cu(II)-H_4L^2, and (C) Cu(II)-H_2L^3 systems ($c_M = c_L = 4$ mM, 25 °C, $I = 0.1$ M NMe_4Cl).

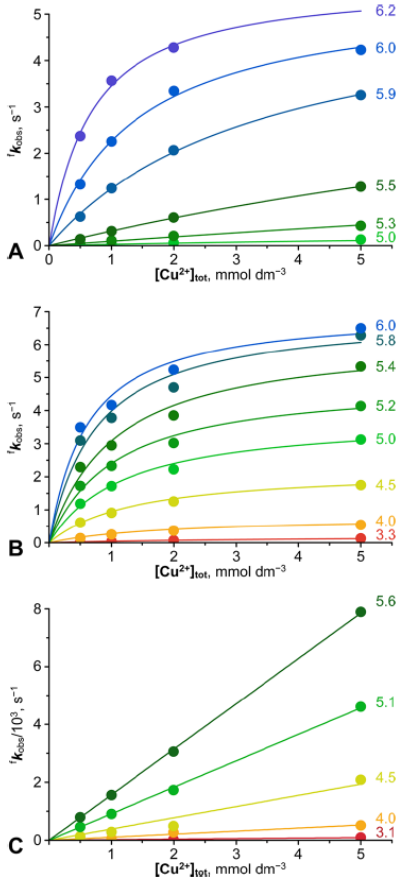

Figure 3. Formation of Cu(II) complexes: $^fk_{obs}$ values of (A) H_4L^1, (B) H_4L^2, and (C) H_2L^3 as a function of copper(II) concentration (c_L = 0.1 mM, 25 °C) at various pH values (given in the figures). Only selected curves are displayed. Solid lines represent the best fits according to eq 2 or 6.

coordination spheres (see Crystal Structures). The highest stability constant of [Cu(L)] was found for H_4L^1 due to the high amine basicity. The protonation constants of H_4L^2 and H_2L^3 complexes show the reverse order compared to their stability constants. The calculated values of pCu [negative logarithm of the free Cu(II) ion concentration (Table 1)] confirm the high stability of the studied complexes under physiological conditions.

Formation Kinetics. The complexation kinetics of Cu(II) with H_4L^1, H_4L^2, and H_2L^3 were investigated by ultraviolet−visible (UV−vis) measurements under pseudo-first-order conditions and Cu(II) excess in the weakly acidic region. Cu(II)-H_4L^1 and Cu(II)-H_4L^2 complexes formed quickly and were, thus, measured using the stopped-flow technique.

The rate of complexation under pseudo-first-order conditions is expressed by eq 1

$$v = {}^fk_{obs}[L]_{tot} \quad (1)$$

where $^fk_{obs}$ is the observed reaction rate constant and $[L]_{tot}$ is the total concentration of the ligand. The plot of $^fk_{obs}$ as a function of Cu(II) concentration at various pH values is shown in Figure 3 and Figure S6. H_4L^1 [at pH >5.5 (Figure 3A)] and H_4L^2 [over the entire pH range tested (Figure 3B)] show saturation curves, indicating the formation of a stable reaction intermediate. According to the generally accepted complexation mechanism (Scheme 2), the intermediate is the *out-of-cage* complex (further labeled with an asterisk) in which the metal ion is bound only through pendant oxygen atoms and the macrocycle amine groups are still protonated. Then, the rate of *in-cage* complexation is proportional to the concentration of the *out-of-cage* intermediate, and $^fk_{obs}$ is expressed by eq 2

$$ {}^fk_{obs} = \frac{{}^fkK^*[Cu]_{tot}}{1 + K^*[Cu]_{tot}} \quad (2)$$

where ^fk is the rate constant describing the formation of the *in-cage* complex, K^* is the conditional thermodynamic stability

Scheme 2. Two-Step Complexation Mechanism of Tetraazamacrocyclic Ligands with Pendant Arms Containing Coordinating Pendant Arms

$$Cu^{2+} + H_xL \overset{K^*}{\rightleftharpoons} [Cu(H_nL)]^* \xrightarrow{{}^fk} [Cu(H_{n-2}L)]$$

out-of-cage in-cage

https://dx.doi.org/10.1021/acs.inorgchem.0c00856
Inorg. Chem. 2020, 59, 8432−8443

constant of the *out-of-cage* intermediate, and $[Cu]^*_{tot}$ is the overall concentration of Cu(II) ions.

The ^fk and K^* values of Cu(II)-H_4L^2 were calculated individually for each solution pH, and the results are shown in Figure 4. The *out-of-cage* species are formed quantitatively under a large excess of metal ions, and the overall complexation rate can be expressed as the contribution of individual *out-of-cage* species, $[Cu(H_nL)]^*$, differing in protonation state (eq 3)

$$v = {}^fk[CuL]^*_{tot} = \sum_{n=0-x} \{{}^fk_n[Cu(H_nL)]^*\} \quad (3)$$

where $[CuL]_{tot}$ is the overall concentration of *out-of-cage* species, $[Cu(H_nL)]^*$ is the concentration of the individual differently protonated *out-of-cage* species, and ^fk_n values are their "isomerization" rate constants. Upon inclusion of the overall protonation constants, the β_n^* of the *out-of-cage* species and the rate constants ^fk can be expressed by eq 4

$$ {}^fk = \frac{{}^fk_0 + \sum_{n=1-x}({}^fk_n\beta_n^*[H]^n)}{1 + \sum_{n=1-x}(\beta_n^*[H]^n)} \quad (4)$$

Contributions of the nonprotonated and diprotonated *out-of-cage* complexes are negligible in the studied pH range, and thus, $^fk_0$ and $^fk_2$ can be omitted. Considering the values of the ligand protonation constants, the *out-of-cage* complex is present in the measured pH range as a mixture of monoprotonated and diprotonated forms. Thus, eq 4 was simplified (see the Supporting Information) and ^fk values were fitted by eq 5

$$ {}^fk \approx \frac{{}^fk_1}{1 + K^*_{p2}[H]} \quad (5)$$

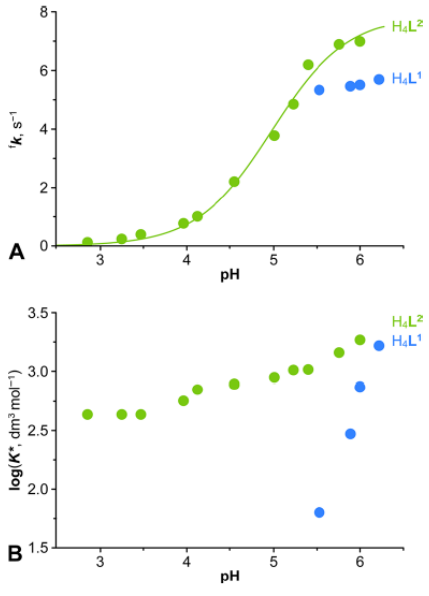

Figure 4. Comparison of the formation rate constants ^fk (A; the line represents the best fit according to eq 5) and the *out-of-cage* complex conditional stability constants K^* (B) as a function of pH for Cu(II)-H_4L^1 (blue) and Cu(II)-H_4L^2 (green) at 25 °C.

where K^*_{p2} is the second consecutive protonation constant of the *out-of-cage* species. The calculated values are as follows: $^fk_1$ = 7.9 ± 0.2 s^{-1} and log K^*_{p2} = 4.98 ± 0.05. The protonation constant K^*_{p2} (in M^{-1}) describes the second protonation of macrocycle nitrogen atoms to form the *out-of-cage* complex $[Cu(H_2L^2)]^*$. The value is ~2 orders of magnitude lower than that of the free ligand H_4L^2. This difference can be explained by the absence of intramolecular hydrogen bonds that are typical of free ligand forms [see the crystal structure of H_4L^1 (ref 9) or H_2L^3 above], which are broken upon coordination of the Cu(II) ion by the pendant arms.[38] The values of conditional stability constants, log K^*, do not change significantly, as expected, because the coordinated bis-(phosphinate) groups do not undergo any protonation/deprotonation in the studied pH range. The observed increase in log K^* between pH 2.5 and 6.5 is smaller than one logarithmic unit and is most likely associated with macrocycle deprotonation.

The Cu(II)-H_4L^1 system shows a saturation curve of k_{obs} as a function of Cu(II) concentration only in a very narrow pH range, thus precluding a detailed analysis. However, the significant change in log K^* can be attributed to proton dissociation from the monoprotonated phosphonate group, which increases the negative charge and, consequently, the *out-of-cage* complex stability. In addition, the $^fk_1$ value of approximately 5 s^{-1} for the H_4L^1 ligand, describing the transformation of the *out-of-cage* complex into an *in-cage* complex, is slightly lower than that for H_4L^2 (Figure 4A).

H_4L^1, at pH <5.5, and H_2L^3, at all pH values, show a linear curve of $^fk_{obs}$ as a function of Cu(II) concentration (Figure 3A,C), thus indicating the low stability of the *out-of-cage* intermediates and the low values of the stability constants K^*. For this reason, the ^fk and K^* values cannot be separated, and $^fk_{obs}$ is expressed as in eq 6

$$ {}^fk_{obs} = {}^fkK^*[Cu]_{tot} = k_{2,f}[Cu]_{tot} \quad (6)$$

where $k_{2,f}$ is the reaction rate of the bimolecular reaction, which is expressed as $k_{2,f} = {}^fkK^*$.

The results show considerable differences between ligands. These differences are mainly reflected in the stability of the *out-of-cage* complexes and in the pH profile of the formation rate. In the *out-of-cage* intermediates, double protonation of amine groups of the ligand cage is supposed and their basicity should follow the markedly different basicity of the ligands [log K_2 (see above)]. The complex of H_4L^2 shows the highest conditional stability constants among the studied complexes due to the chelating bidentate coordination of each bis-(phosphinate) moiety. The conditional stability constants of the H_4L^1 complex are significantly lower at pH <5, where an additional protonation of the phosphonate groups can be expected.[19−24] The conditional stability constants of complexes of both ligands increase close to neutral pH due to phosphonate {in $[Cu(H_2L^1)]^*$} or macrocycle {in $[Cu(H_2L^2)]^*$} deprotonation (Figure 4). The conditional stability constants of the H_2L^3 *out-of-cage* complex are very low, due to the weak monodentate coordination of the phosphinate group, and therefore, they could not be determined.

The complexation rate of the studied ligands was nevertheless compared in terms of constant $k_{2,f}$. The constant $k_{2,f}$ ($k_{2,f} = {}^fkK^*$) is highly relevant for radiochemical labeling because it is decisive for the complexation rate (i.e., radiolabeling efficacy) at very low Cu(II) concentrations.

https://dx.doi.org/10.1021/acs.inorgchem.0c00856
Inorg. Chem. 2020, 59, 8432−8443

The formation constants $k_{2,f}$ were plotted as a function of pH, as shown in Figure 5. The analysis of $k_{2,f}$ as a function of pH allows us to estimate the reactivity of differently protonated ligand species. Because this approach has been previously reported in the literature,[39,40] we can directly compare the results with previously published data. Considering that H_2L and HL are dominantly reacting ligand species and that the ligand species are highly abundant in the studied pH region, the reaction scheme shown in Scheme S1 is suggested, giving the rate law expressed by eq 7.

$$k_{2,f} \approx \frac{k_{HL} + k_{H2L}K_2[H^+]}{1 + K_2[H^+] + K_2K_3[H^+]^2 + K_2K_3K_4[H^+]^3} \quad (7)$$

where K_n terms are the ligand protonation constants and k_{HL} and k_{H2L} are rate constants describing the $\{Cu^{2+} + HL\}$ and $\{Cu^{2+} + H_2L\}$ reaction pathways, respectively. The results (Table 2) show that the HL species are significantly more reactive than the H_2L species for all ligands and that the $\{Cu^{2+} + H_2L\}$ reaction pathway weakly contributes to the overall reaction rate. Thus, all analyses of data show that the dominant reactive species are the monoprotonated ligands HL and the monoprotonated *out-of-cage* complexes [Cu(HL)]*.

The formation constants $^fk_{obs}$ were plotted as a function of pH, as shown in Figure S7. The logarithms of the constants show an almost linear trend for all studied ligands, but the lines have a significantly different slope. The reaction rates of the phosphinate ligands H_4L^2 and H_2L^3 linearly increase with the decrease in proton concentration (i.e., the reaction is base-catalyzed). The complexation of H_2L^3 is almost 4 orders of magnitude slower than that of H_4L^2 throughout the pH range. This difference could be ascribed to the much lower *out-of-cage* complex stability and/or the less efficient proton transfer ability of H_2L^3. The line for the phosphonate ligand H_4L^1 is much steeper, thus showing that the reaction rate likely increases with $[H^+]^{-2}$ (i.e., $[OH^-]^2$). This difference results from the different protonation schemes. *Out-of-cage* complexes of tetraazamacrocyclic ligands with metal ions are mostly diprotonated on the macrocycle nitrogen atoms. The rate-determining step of complexation is the removal of the first proton from the *out-of-cage* intermediate and the simultaneous formation of the *in-cage* complex. The H_4L^1 *out-of-cage* complexes can also bear additional protons on the phosphonate groups. Thus, *in-cage* coordination must be initiated by multiple deprotonations. As a consequence, the rate of formation of H_4L^1 is comparable to that of H_2L^3 at pH <3 and to that of H_4L^2 at pH ≈6.

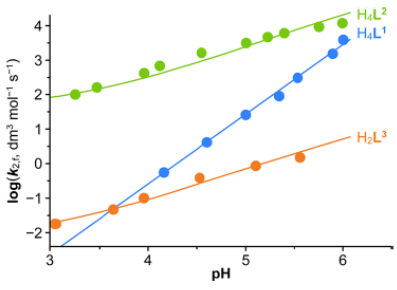

Figure 5. Comparison of the formation rate constant $k_{2,f}$ as a function of pH for Cu(II)-H_4L^1 (blue), Cu(II)-H_4L^2 (green), and Cu(II)-H_2L^3 (orange) systems at 25 °C. The lines represent the best fits according to eq 7.

Table 2. Comparison of the Reactivity of Differently Protonated Ligand Species in the Formation of Cu(II) Complexes (t = 25 °C)[a]

ligand	k_{HL}	k_{H2L}	k_{HL}/k_{H2L}
H_4L^1	(1.1 ± 0.1) × 10^{10}	(2.4 ± 0.7) × 10^3	(4.6 ± 1.4) × 10^6
H_4L^2	(1.9 ± 0.3) × 10^5	100 ± 40	(1.9 ± 0.8) × 10^3
H_2L^3	17 ± 3	(1.1 ± 0.6) × 10^{-2}	(1.5 ± 0.8) × 10^3

[a]The rate constants are expressed in M^{-1} s^{-1}.

The rate of formation of H_4L^2 is comparable to that of the related nonbridged cyclam ligands H_2**te1bpin** and H_4**te2p**[1,8] (Chart 1) throughout the pH range (Figure S7). All of these ligands show full complexation in a few seconds at pH 4 or within 1 s at pH 6 (Table 3) and at millimolar concentrations. These results show that H_4L^2 is a very promising ligand for the complexation of copper radioisotopes. H_4L^1 shows a similar complexation rate only at pH ∼6, whereas the complexation time is rather prolonged at a lower pH. The combination of cb-cyclam with monophosphinate pendant arms in H_2L^3 is unsuitable for the complexation of copper radionuclides because its complexation times are on the scale of hours and minutes at pH 4 and 6, respectively.

Dissociation Kinetics. The kinetic inertness of the Cu(II) complexes was evaluated by acid-assisted dissociation experiments in 0.1−4.0 M $HClO_4$ at I = 5 M (H,Na)ClO_4 and followed by UV−vis spectroscopy. The complexes are extremely kinetically inert, and thus, the experiments were performed at 90 °C; these long experiments were performed using the batch method with solutions incubated in sealed ampules.[19]

The curves of the dissociation rate constant ($^dk_{obs}$) as function of acid concentration [i.e., dissociation profile (Figure 6 and Figure S8)] of each complex, Cu(II)-H_4L^1, Cu(II)-H_4L^2, and Cu(II)-H_2L^3, show different shapes. The dissociation rate can be expressed according to the following general function (eq 8)

$$^dk_{obs} = \frac{^dk_{n+1}K_{Hn+1}[H] + {}^dk_{n+2}K_{Hn+1}K_{Hn+2}[H]^2}{1 + K_{Hn+1}[H] + K_{Hn+1}K_{Hn+2}[H]^2} \quad (8)$$

where $^dk_{n+1}$ and $^dk_{n+2}$ are the rate constants that correspond to the dissociation of species bearing more protons (by one or two) than the thermodynamically stable species and $^dK_{Hn+1}$ and $^dK_{Hn+2}$ are the corresponding consecutive protonation

Table 3. Estimated Formation Rate Constants $^fk_{obs}$ and Complexation Times (99% formation) of the Studied Cu(II) Complexes of H_4L^1, H_4L^2, and H_2L^3 and Their Related Ligands (c_L = 0.1 mM, 10-fold metal ion excess, 25 °C)

ligand	pH 4		pH 6	
	$^fk_{obs}$ (s^{-1})	$t_{99\%}$	$^fk_{obs}$ (s^{-1})	$t_{99\%}$
H_4L^1	2.7 × 10^{-4}	4.7 h	2.9	1.6 s
H_4L^2	0.33	13.9 s	21.8	0.2 s
H_2L^3	8.7 × 10^{-5}	14.7 h	5.3 × 10^{-3}	14.5 min
H_2**te1bpin**[30,a]	0.55	8.4 s	50.9	0.1 s
H_4**te2p**[1,8,19]	7.2 × 10^{-2}	64.5 s	24.4	0.2 s

[a]Formation of the first *in-cage* Cu(II) complex.

https://dx.doi.org/10.1021/acs.inorgchem.0c00856
Inorg. Chem. 2020, 59, 8432−8443

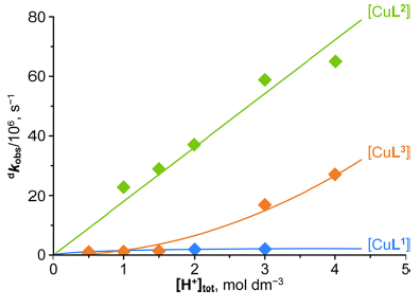

Figure 6. Comparison of dissociation rate constants $^{d}k_{obs}$ of [CuL^1] (blue), [CuL^2] (green), and [CuL^3] (orange) (c_{CuL} = 1 mM, 90 °C). The lines represent the best fits according to eq 8 or 9.

constants (Scheme 3). If logarithms of protonation constants of the complex are log $K \ll 0$, eq 8 can be simplified (see the Supporting Information), expressing $^{d}k_{obs}$ according to eq 9

$$^{d}k_{obs} = {}^{d}k_{Hn+1}[H] + {}^{d}k_{Hn+2}[H]^2 \quad (9)$$

where $^{d}k_{Hn+1} = {}^{d}k_{n+1}K_{Hn+1}$ and $^{d}k_{Hn+2} = {}^{d}k_{n+2}K_{Hn+1}K_{Hn+2}$. The dissociation profile of Cu(II)-H_4L^1 shows a saturation curve (Figure S8A), thus indicating protonation in the studied pH region. Monoprotonated and diprotonated complex species are thermodynamically stable, and the two protons are localized on the noncoordinated phosphonate oxygen atoms (see Figure 1). Accordingly, the protonation observed in the dissociation experiments most likely corresponds to the formation of a triprotonated complex that should be the dominant species in the dissociation pathway. The values of rate constant $^{d}k_3$ and protonation constant K_{H3} were calculated by fitting the curve according to eq 8. The results are summarized in Table 4.

The terminal phosphinate groups of the bis(phosphinate) pendants could be protonated without affecting the stability of the coordination cage. Therefore, the dissociation scheme of Cu(II)-H_4L^2 is the same as that of Cu(II)-H_4L^1, and the observed protonation also corresponds to the formation of the triprotonated complex that is the dominant species in the dissociation pathway, as well. The linear shape of the dissociation profile of Cu(II)-H_4L^2 (Figure S8B) indicates a very low value of the third protonation constant of the complex (log $K_3 < 0$). As a result, the protonation constant cannot be determined experimentally. Hence, only the $^{d}k_{H3}$ value was calculated by fitting the curve according to eq 9.

The dissociation profile of Cu(II)-H_2L^3 (Figure S8C) shows a parabolic shape, and only the $^{d}k_{H2}$ value could be determined when fitting this curve according to eq 9. This indicates that two protonations are required to generate the reactive species and corresponding protonation constants are very low (negative values of log K_1 and log K_2). Because the thermodynamically stable species is the nonprotonated complex [ML], the kinetically active species should be diprotonated. However, protonation sites cannot be suggested

Scheme 3. Dissociation Mechanism of the Studied Complexes

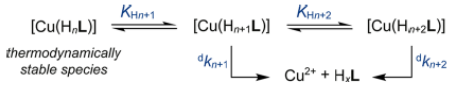

Table 4. Dissociation Rate Constants and Protonation Constants of the Studied Cu(II) Complexes

complex	rate and protonation constants
[CuL^1]	$^{d}k_3 = (2.6 \pm 0.7) \times 10^{-6}$ s^{-1}; $K_{H3} = 1.6 \pm 0.4$ M^{-1}
	$^{d}k_{H3} = (4.2 \pm 0.4) \times 10^{-6}$ M^{-1} s^{-1}
[CuL^2]	$^{d}k_{H3} = (1.8 \pm 0.1) \times 10^{-5}$ M^{-1} s^{-1}
[CuL^3]	$^{d}k_{H2} = (1.74 \pm 0.08) \times 10^{-6}$ M^{-2} s^{-1}

because both the macrocycle nitrogen atom and the phosphinate oxygen atom might be protonated in the strongly acidic solution.

A direct comparison of Cu(II) complexes in terms of dissociation parameters is difficult due to the different mechanisms found for the studied systems. Thus, differences between complexes are expressed as dissociation half-lives in 1 M $HClO_4$ at 90 °C (Table 5) and $^{d}k_{H1}$ parameters. Cu(II)-H_4L^1 is the most inert among the studied complexes, showing extremely high kinetic inertness, with a half-life of 120 h. The half-life of Cu(II)-H_2L^3 (111 h) is comparable to that of Cu(II)-H_4L^1 in 1 M acid; however, it becomes shorter with an increase in acid concentration. The difference is ascribed to the different protonation scheme of this complex. The half-life of Cu(II)-H_4L^2 (10.7 h) is 1 order of magnitude shorter than that of Cu(II)-H_4L^1 and similar to the half-life of the *trans* isomer of Cu(II)-H_4**te2P**^{1,8} (13.4 h).[19] The accelerated dissociation of Cu(II)-H_4L^2 might be explained by the relatively strong chelating ability of bis(phosphinate) pendants even in very acidic solutions, which helps the Cu(II) ion be released from the macrocyclic cavity.

The dissociation experiments carried out with Cu(II)-H_4L^2 in 5 M H/NaCl have shown a negligible effect of chloride anions on the dissociation rate (Figure S9). Thus, our results could be compared with those reported previously for dissociation of related ligands in HCl (Table 5). The inertness of Cu(II)-H_4L^1 is similar to that of its diacetate analogue Cu(II)-H_2**cb-te2a** and its propionate analogue, which have half-lives of 155 and 100 h, respectively, in 5 M HCl at 90 °C.[6] The important role of the coordinated pendant arms can be documented for Cu(II) complexes of unsubstituted cb-cyclam derivatives ($t_{1/2}$ = 11.8 min in 5 M HCl at 90 °C)[6] or derivatives bearing a weakly coordinating pyridine pendant ($t_{1/2}$ < 2 min in 5 M HCl at 90 °C).[41] However, the kinetic

Table 5. Dissociation Half-Times of the Discussed Cu(II) Complexes (90 °C)

ligand	condition	$t_{1/2}$	ref
H_4L^1	1 M $HClO_4$	120 h	this work
H_4L^2	1 M $HClO_4$	10.7 h	this work
H_2L^3	1 M $HClO_4$	111 h	this work
H_2**te1bpin**[a]	1 M $HClO_4$	40 s	30
H_4**te2p**^{1,8a}	1 M $HClO_4$	49 s	19
H_4**te2p**^{1,8b}	1 M $HClO_4$	13.4 h	19
H_2**cb-te2a**	5 M HCl	155 h	6
H_2**cb-te2pra**	5 M HCl	~100 h	15
cb-cyclam	5 M HCl	11.8 min	6
PyMe-cb-cyclam	5 M HCl	<2 min	41
H_2**pcb-te2a**	12 M HCl	≫7 days	42
H_3**pcb-te1a1p**	12 M HCl	≫7 days	13

[a]Pentacoordinated isomer, recalculated from original data. [b]Hexacoordinated *trans* isomer, recalculated from original data.

https://dx.doi.org/10.1021/acs.inorgchem.0c00856
Inorg. Chem. 2020, 59, 8432−8443

inertness of the cyclam-based complexes can be improved by designing the bridge as even a higher kinetic inertness was observed for propylene-cross-bridged cyclam derivatives showing no sign of dissociation even after several days in 12 M HCl at 90 °C.[13,42]

■ CONCLUSIONS

Cross-bridged cyclam derivatives with phosphonate, bis(phosphinate), or phosphinate pendants were synthesized and studied as potential carriers of copper radioisotopes in nuclear medicine. The protonation constants of the ligands and the stability constants of their complexes were determined by potentiometry. The macrocycles show very high basicity because the values of the first protonation constant are log K_1 > 14. The thermodynamic stability of the studied Cu(II) complexes is high and sufficient for biomedical applications. However, despite the high ligand basicity, the thermodynamic stability of Cu(II) complexes is lower than that of the complexes of nonbridged cyclam analogues. The lower stability results from the geometry of the cb-cyclam ligand cavity, which prevents the equatorial coordination of all four nitrogen atoms.

The formation of Cu(II) complexes is slower than that of the nonbridged cyclam analogues. However, the formation is still fast, mainly for phosphonate and bis(phosphinate) derivatives (quantitative formation in <2 s at pH 6 at a millimolar scale). Copper(II) ion complexation with derivatives bearing monophosphinate pendants is significantly slower due to the significantly lower stability of the *out-of-cage* complex and/or the less effective proton transfer out of the ligand cavity. All studied complexes are extremely kinetically inert. Consequently, the dissociation kinetics had to be measured at a high temperature over several days or weeks. The complexes decompose with half-lives in the range of hours in 1 M $HClO_4$ at 90 °C.

Fast complexation and outstanding kinetic inertness indicate that cross-bridged cyclam derivatives with phosphonate and bis(phosphinate) pendants are suitable ligand systems for the complexation of copper radionuclides. Conversely, the phosphinate derivative suffers from slow complexation.

■ EXPERIMENTAL SECTION

General. The commercially available (Fluka, Aldrich, Chematech, and Strem) chemicals were synthetically pure and were used as received. Paraformaldehyde was filtered from an aged aqueous formaldehyde solution and dried over P_2O_5 in a vacuum desiccator. Methylene-bis(phosphinic acid) was prepared by careful hydrolysis of commercial $CH_2(PCl_2)_2$ according to the published procedure.[43] cb-cyclam was synthesized according to the previously published procedure.[8] NMR experiments were performed on a Bruker Avance III 600 instrument with a cold probe (^{1}H and ^{13}C{^{1}H}) or on Varian S300 (^{31}P and ^{31}P{^{1}H}) spectrometers (chemical shift in parts per million, coupling constants in hertz; *mc* stands for macrocycle). The ^{31}P NMR spectra were referenced to external 85% H_3PO_4 (δ_P 0.0), and ^{1}H and ^{13}C NMR spectra were referenced to external or internal *t*-BuOH (δ_H 1.25, δ_C 30.29). The ESI-MS spectra were recorded on a Bruker Esquire 3000 spectrometer with ion-trap detection in negative or positive modes. Merck aluminum foils with silica gel 60 F_{254} were used for TLC. Elemental analyses are presented in the format calculated (found).

H_4L^1 Synthesis. In a 100 mL glass flask, H_3PO_3 (13.4 g, 163 mmol, 15 equiv), cb-cyclam (2.46 g, 10.9 mmol, 1.0 equiv), and paraformaldehyde (4.88 g, 163 mmol, 15 equiv) were suspended in concentrated aqueous HCl (60 mL), and the flask was immediately closed with a stopper. The reaction mixture was stirred at 35 °C for 7 days. After cooling to room temperature, the mixture was evaporated to dryness and co-evaporated several times with H_2O. The residue was purified on a strong cation exchange resin (Dowex 50, ~200 mL, H^+ form, H_2O → 10% aqueous pyridine). The pyridine fraction with the product was evaporated to dryness and co-evaporated with water several times to remove pyridine quantitatively. The residue was dissolved in water (250 mL) and lyophilized. The product was obtained in zwitterionic form ($H_4L^1{\cdot}4H_2O$) as a white foam: yield 4.17 g (82%); ^{1}H NMR (D_2O + CsOD, pD ~5) δ 1.76 (*mc*, d, 2H, $^2J_{HH}$ = 17), 2.32 (*mc*, m, 2H), 2.50 (*mc*, d, 2H, $^2J_{HH}$ = 14), 2.76−3.00 (*mc*, N−CH_2−P, m, 8H), 3.02−3.18 (*mc*, m, 4H), 3.24 (*mc*, d, 2H, $^2J_{HH}$ = 13), 3.50 (*mc*, td, 2H, $^2J_{HH}$ = 14, $^3J_{HH}$ = 4), 3.74 (*mc*, tt, 2H, $^2J_{HH}$ = 14, $^3J_{HH}$ = 4), 4.07 (*mc*, m, 2H, $^2J_{HH}$ = 13, $^3J_{HH}$ = 4), 4.29 (N−CH_2−P, t, 2H, $^2J_{HP}$ = $^2J_{HH}$ = 14); ^{13}C{^{1}H} NMR (D_2O + CsOD, pD ≥12) δ 20.4 (*mc*, s), 49.0 (*mc*, s), 52.4 (*mc*, s), 52.7 (N−CH_2−P, d, $^1J_{CP}$ = 133), 52.7 (*mc*, d, $^3J_{CP}$ = 9), 58.1 (*mc*, d, $^3J_{CP}$ = 2), 58.5 (*mc*, s); ^{31}P{^{1}H} NMR (D_2O + CsOD, pD ≥12) δ 8.7 (s); ESI-HRMS (−) 413.1721 [M − H^+]$^-$ (theor. [$C_{14}H_{31}N_4O_6P_2$]$^-$ = 413.1724); TLC (7:3:3 *i*-PrOH/concentrated aqueous NH_4OH/H_2O) R_f ~ 0.2. EA ($C_{14}H_{32}N_4O_6P_2{\cdot}4H_2O$): C 34.6 (34.4), H 8.3 (8.1), N 11.5 (11.3).

H_4L^2 Synthesis. In a 100 mL flask, cb-cyclam (2.00 g, 8.84 mmol, 1.0 equiv), metylene-bis(phosphinic acid) (7.62 g, 52.9 mmol, 6.0 equiv), and paraformaldehyde (594 mg, 19.8 mmol, 2.2 equiv) were suspended in aqueous HCl (6 M, 50 mL), and the flask was quickly closed with a stopper. The resulting suspension was stirred at 60 °C for 2 days. After cooling to room temperature, the reaction mixture was evaporated to dryness and further co-evaporated with H_2O to remove most of the HCl. The residue was purified on a strong cation exchange resin (Dowex 50, ~300 mL, H^+ form, H_2O). Unreacted methylene-bis(phosphinic acid) was eluted first, and the product was eluted in later fractions. Fractions with the pure product were combined, evaporated to dryness, and further co-evaporated several times with water. The residue was redissolved in water (~250 mL) and lyophilized. The product was obtained in zwitterionic form ($H_4L^2{\cdot}2H_2O$) as a colorless hygroscopic powder: yield 2.44 g (48%); ^{1}H NMR (D_2O + CsOD, pD ≥12) δ 1.67 (*mc*, m, 2H), 1.82 (*mc*, m, 2H), 1.99 (P−CH_2−P, t, 4H, $^2J_{HP}$ = 17), 2.78−3.19 (N−CH_2−P, *mc*, bm, 20H), 3.26 (*mc*, m, 2H), 3.62 (*mc*, m, 2H), 7.14 (P*H*, d, 2H, $^1J_{HP}$ = 530), ^{13}C{^{1}H} NMR (D_2O + CsOD, pD ≥12) δ 24.4 (*mc*, s), 37.1 (P−CH_2−P, t, $^1J_{CP}$ = $^1J_{CP}$ = 74), 52.4 (*mc*, s), 52.8 (*mc*, s), 53.8 (*mc*, d, $^3J_{CP}$ = 4), 53.8 (N−CH_2−P, d, $^1J_{CP}$ = 100), 56.5 (*mc*, s), 57.1 (*mc*, d, $^3J_{CP}$ = 3); ^{31}P{^{1}H} NMR (D_2O + CsOD, pD ≥12) δ 19.8 (*PH*, dtd, 2P, $^1J_{PH}$ = 530, $^2J_{PH}$ = 18, $^2J_{PP}$ = 2), 32.5 (P−CH_2−N, tm, 2P, $^2J_{PH}$ = 16); ESI-HRMS (−) 537.1566 [M − H^+]$^-$ (theor. [$C_{16}H_{37}N_4O_8P_4$]$^-$ 537.1567); TLC (7:3:3 *i*-PrOH/NH_4OH/H_2O) R_f ~ 0.4. EA ($C_{16}H_{38}N_4O_8P_4{\cdot}2H_2O$): C 33.5 (33.5), H 7.4 (7.3), N 9.8 (9.7).

H_2L^3 Synthesis. In a 20 mL glass vial, cb-cyclam (2.66 g, 11.8 mmol, 1.0 equiv) was dissolved in 50% aqueous H_3PO_2 (18.0 mL, 164 mmol, 14 equiv) followed by the addition of paraformaldehyde (850 mg, 28.3 mmol, 2.4 equiv). The resulting suspension was stirred at 60 °C for 3 h. Then, the reaction mixture was loaded on a strong cation exchange resin (Dowex 50, H^+ form, ~300 mL). The excess of H_3PO_2 (together with H_3PO_3 and $HOCH_2PO_2H_2$) was washed out with water (~2.5 L). The product was then eluted with 10% aqueous pyridine. The latter fractions with insufficient purity were repurified similarly. Then, all pyridine fractions with a product of ≥95% purity (determined by ^{31}P NMR) were combined and evaporated to dryness. The residue was co-evaporated with H_2O once to remove pyridine quantitatively. The residue (~4 g, ~98% purity determined by ^{31}P NMR) was dissolved in water (~50 mL), and the resulting yellowish solution was filtered through a short column of a strong cation exchange resin (Dowex 50, H^+ form, ~15 mL). The remaining impurities were concentrated on the column, whereas the product of high purity (≥99%) eluted with water (~50 mL). The solution was evaporated to yield a colorless oil, which subsequently crystallized spontaneously. The crystals were crushed and dried under vacuum overnight to yield the product in zwitterionic form ($H_2L^3{\cdot}1.5H_2O$) as a white hygroscopic powder: yield 3.76 g (78%); ^{1}H NMR (D_2O, pD ~2) δ 1.73 (*mc*, d, 2H, $^2J_{HH}$ = 17), 2.32 (*mc*, m, 2H), 2.51 (*mc*, d, 2H,

https://dx.doi.org/10.1021/acs.inorgchem.0c00856
Inorg. Chem. 2020, 59, 8432−8443

$^2J_{HH}$ = 13), 2.71 (*mc*, m, 2H), 2.84 (*mc*, m, 2H), 2.94−3.22 (*mc*, CH_2−P, bm, 8H), 3.28−3.47 (*mc*, m, 4H), 3.69 (*mc*, m, 4H), 3.78 (CH_2−P, m, 2H), 7.22 (P*H*, d, 1H, $^1J_{HP}$ = 550); $^{13}C\{^1H\}$ NMR (D_2O, pD ∼2) δ 19.6 (*mc*, s), 48.0 (*mc*, s), 51.0 (*mc*, d, $^3J_{CP}$ = 7), 52.7 (*mc*, s), 53.2 (CH_2−P, d, $^1J_{CP}$ = 85 Hz), 57.7 (*mc*, s), 58.6 (*mc*, d, $^3J_{CP}$ = 3); ^{31}P NMR (D_2O, pD ∼2) δ 14.0 (dm, $^1J_{PH}$ = 550 Hz); ESI-HRMS (−) 413.1721 $[M - H^+]^-$ (theor. $[C_{14}H_{31}N_4O_6P_2]^-$ 413.1724). EA ($C_{14}H_{32}N_4O_4P_2 \cdot 1.5H_2O$): C 41.1 (40.9), H 8.6 (8.5), N 13.7 (13.6), P 15.1 (14.9).

$[Cu(H_2L^1)]\cdot 2H_2O$ Synthesis. $H_2L^3 \cdot 1.5H_2O$ (200 mg) was dissolved in MeOH (5 mL), and $CuCl_2 \cdot 2H_2O$ (72 mg) was added. The blue-green solution was refluxed for 5 h, and the solvent was evaporated under reduced pressure. The light-blue glassy residue was dissolved in water (2 mL), and the solution was left standing for crystallization. Six months of crystallization attempts consisting of repeated evaporation and dissolving in a minimum amount of water led to the oxidation of the phosphinate groups by air. The final crystallization yielded single crystals suitable for X-ray structure determination.

Potentiometry. The methods for potentiometric titration and experimental data processing used in this study were similar to those previously reported.[44] Titrations were performed in a vessel thermostated at 25 ± 0.1 °C at ionic strength I = 0.1 M $(NMe_4)Cl$. The ligand:metal ratio was 1:1 with a c_L of 0.004 M, and the pH range was 1.7−12.1. Titrations were performed at least three times, each consisting of approximately 40 points. The water ion product (pK_w = 13.81) and stability constants of the Cu(II)−OH^- systems were retrieved from ref 45. The overall protonation constants β_n are concentration constants defined as $\beta_n = [H_nL]/([H]^n[L])$ (stepwise protonation constants are defined as $\log K_1 = \log \beta_1$ and $\log K_n = \log \beta_n - \log \beta_{n-1}$). The overall stability constants are defined as $\beta_{hlm} = [Cu_mH_hL_l]/([Cu]^m[H]^h[L]^l)$. The constants (and their standard deviations) were calculated using the program OPIUM.[46] Equilibrium was established slowly in the Cu(II)-H_4L^1 and Cu(II)-H_2L^3 systems in the acid region. Therefore, the corresponding stability constants of the complexes were determined using the "out-of-cell" method.[37] The solutions, each corresponding to one titration point of a common titration, were prepared under an argon stream in tubes with ground joints from ligand, metal ion and HCl/$(NMe_4)Cl$ stock solutions, and water (1 mL starting volume, 0.95:1 Cu:L molar ratio, c_L = 0.004 M). Then, a known amount of a $(NMe_4)OH$ standard solution was added under argon. The tubes were firmly closed with stoppers, and the solutions were left to equilibrate at room temperature for 1 week. After this time, the pH was measured with a freshly calibrated combined glass electrode in each tube and/or ampule. These titrations were performed in the pH range of 1.8−5.0 (the final pH values) with 20 data points per titration and three titrations per system.

Formation and Dissociation Kinetics. Experiments were performed on a Bio Sequential SX-20 stopped-flow spectrophotometer (Applied Photophysics) equipped with a 150 W xenon lamp and with a diode-array accessory detector or on a Specord 50 Plus spectrophotometer (Analytik Jena AG).

Formation kinetics were studied under the following conditions: c_L = 0.1 mM c_{Cu} = 0.5−5 mM, pH ∼3−6, 25 ± 0.1 °C, I = 0.1 M KCl, and a 50-fold molar excess of the appropriate buffers [chloroacetic acid, acetic acid, or 2-(*N*-morpholino)ethanesulfonic acid (MES)]. The pH of the solution was checked after the measurement and remained unchanged.

Dissociation kinetics were studied using stock solutions of complexes prepared by mixing an equimolar amount of Cu(II) and ligand solutions, subsequently adding a NaOH solution to reach a pH of ∼5. The measurements were performed at I = 5.0 M $(H,Na)ClO_4$ and 90 °C. Long-lasting experiments were performed using a batch method in which the solution for each time point of the measurement was prepared as a separate sample sealed in an ampule. The ampules were incubated in an oven at 90 °C.

Formation ($^fk_{obs}$) and dissociation ($^dk_{obs}$) rate constants were fitted from the absorbance at the maximum of the absorption band of the complexes (H_4L^1 λ = 278 nm; H_4L^2 λ = 277 nm; H_2L^3 λ = 272 nm) as a function of time using the Pro-KII software (Applied Photophysics) or the Scientist program, version 2.0 (Micromath), with the following general exponential function (eq 10):

$$A_t = A_f + (A_0 - A_f)e^{-k_{obs}t} \quad (10)$$

Crystal Structure Determination. Single crystals of $H_2L^3 \cdot 5H_2O$ and $[Cu(H_2L^1)]\cdot 2H_2O$ were obtained by slow evaporation from an aqueous solution. The selected crystals were mounted on a glass fiber in a random orientation, and diffraction data were collected on a Nonius KappaCCD diffractometer equipped with a Bruker APEX-II CCD detector at 150 K (Cryostream Cooler, Oxford Cryosystem) using monochromatized Mo Kα radiation (λ = 0.71073 Å). Data were analyzed using the HKL DENZO program package.[47] All structures were determined using direct methods (SIR92)[48] and refined using the full-matrix least-squares technique (SHELXL2017).[49]

All non-hydrogen atoms were refined anisotropically. Two structurally independent molecules were found in the crystal structure of cb-cyclam. All hydrogen atoms were localized in the difference density map and fully refined. In the crystal structures of $H_2L^3 \cdot 5H_2O$ and $[Cu(H_2L^1)]\cdot 2H_2O$, the formula unit is equal to the independent part of the unit cell. All hydrogen atoms were also localized in the difference density map; however, those bound to the carbon atoms were placed in theoretical positions using $U_{eq}(H) = 1.2U_{eq}(C)$ to keep the number of refined parameters low, and only hydrogen atoms bound to heteroatoms (N, O, and P) were fully refined. Details about data collection and structure refinement are given in Table S6. Single crystals of a key starting compound, *N*,*N*″-dibenzyl-cb-cyclam, were obtained by slow evaporation from acetone. Its crystal structure is reported in Figure S10. The data for the structures reported here were deposited at the Cambridge Crystallographic Data Centre under numbers 1975656−1975658.

■ ASSOCIATED CONTENT

Supporting Information

The Supporting Information is available free of charge at https://pubs.acs.org/doi/10.1021/acs.inorgchem.0c00856.

Details of syntheses, NMR spectra, parameters of crystal structures, overall protonation and stability constants, figures, and schemes of complex formation and dissociation kinetics (PDF)

Accession Codes

CCDC 1975656−1975658 contain the supplementary crystallographic data for this paper. These data can be obtained free of charge via www.ccdc.cam.ac.uk/data_request/cif, or by emailing data_request@ccdc.cam.ac.uk, or by contacting The Cambridge Crystallographic Data Centre, 12 Union Road, Cambridge CB2 1EZ, UK; fax: +44 1223 336033.

■ AUTHOR INFORMATION

Corresponding Author

Vojtěch Kubíček − *Department of Inorganic Chemistry, Faculty of Science, Charles University, 128 40 Prague, Czech Republic;* orcid.org/0000-0003-0171-5713; Phone: +420221951436; Email: kubicek@natur.cuni.cz; Fax: +420221951253

Authors

Lucia Pazderová − *Department of Inorganic Chemistry, Faculty of Science, Charles University, 128 40 Prague, Czech Republic*

Tomáš David − *Department of Inorganic Chemistry, Faculty of Science, Charles University, 128 40 Prague, Czech Republic*

Veronika Hlinová − *Department of Inorganic Chemistry, Faculty of Science, Charles University, 128 40 Prague, Czech Republic*

https://dx.doi.org/10.1021/acs.inorgchem.0c00856
Inorg. Chem. 2020, 59, 8432−8443

Jan Plutnar − *Department of Inorganic Chemistry, Faculty of Science, Charles University, 128 40 Prague, Czech Republic*
Jan Kotek − *Department of Inorganic Chemistry, Faculty of Science, Charles University, 128 40 Prague, Czech Republic;* orcid.org/0000-0003-1777-729X
Přemysl Lubal − *Department of Chemistry, Masaryk University, 611 37 Brno, Czech Republic*
Petr Hermann − *Department of Inorganic Chemistry, Faculty of Science, Charles University, 128 40 Prague, Czech Republic;* orcid.org/0000-0001-6250-5125

Complete contact information is available at: https://pubs.acs.org/10.1021/acs.inorgchem.0c00856

Notes

The authors declare no competing financial interest.

■ ACKNOWLEDGMENTS

The authors thank Ivana Císařová for X-ray diffraction measurements and are thankful for the funding from the Grant Agency of Czech Republic (19-17380S) and Masaryk University (MUNI/A/1424/2019). This study was conducted within the framework of COST Action CA18202 (NECTAR).

■ REFERENCES

(1) Boros, E.; Packard, A. B. Radioactive Transition Metals for Imaging and Therapy. *Chem. Rev.* **2019**, *119*, 870−901.
(2) Ahmedova, A.; Todorov, B.; Burdzhiev, N.; Goze, C. Copper radiopharmaceuticals for theranostic applications. *Eur. J. Med. Chem.* **2018**, *157*, 1406−1425.
(3) Paterson, B. M.; Donnelly, P. S. Macrocyclic Bifunctional Chelators and Conjugation Strategies for Copper-64 Radiopharmaceuticals. *Adv. Inorg. Chem.* **2016**, *68*, 223−251.
(4) Boschi, A.; Martini, P.; Janevik-Ivanovska, E.; Duatti, A. The emerging role of copper-64 radiopharmaceuticals as cancer theranostics. *Drug Discovery Today* **2018**, *23*, 1489−1501.
(5) Sun, X.; Wuest, M.; Weisman, G. R.; Wong, E. H.; Reed, D. P.; Boswell, C. A.; Motekaitis, R.; Martell, A. E.; Welch, M. J.; Anderson, C. J. Radiolabeling and In Vivo Behavior of Copper-64-Labeled Cross-Bridged Cyclam Ligands. *J. Med. Chem.* **2002**, *45*, 469−477.
(6) Woodin, K. S.; Heroux, K. J.; Boswell, C. A.; Wong, E. H.; Weisman, G. R.; Niu, W.; Tomellini, S. A.; Anderson, C. J.; Zakharov, L. N.; Rheingold, A. L. Kinetic Inertness and Electrochemical Behavior of Copper(II) Tetraazamacrocyclic Complexes: Possible Implications for in Vivo Stability. *Eur. J. Inorg. Chem.* **2005**, *2005*, 4829−4833.
(7) Boswell, C. A.; Sun, X.; Niu, W.; Weisman, G. R.; Wong, E. H.; Rheingold, A. L.; Anderson, C. J. Comparative in Vivo Stability of Copper-64-Labeled Cross-Bridged and Conventional Tetraazamacrocyclic Complexes. *J. Med. Chem.* **2004**, *47*, 1465−1474.
(8) Wong, E. H.; Weisman, G. R.; Hill, D. C.; Reed, D. P.; Rogers, M. E.; Condon, J. P.; Fagan, M. A.; Calabrese, J. C.; Lam, K.-C.; Guzei, I. A.; Rheingold, A. L. Synthesis and Characterization of Cross-Bridged Cyclams and Pendant-Armed Derivatives and Structural Studies of Their Copper(II) Complexes. *J. Am. Chem. Soc.* **2000**, *122*, 10561−10572.
(9) Stigers, D. J.; Ferdani, R.; Weisman, G. R.; Wong, E. H.; Anderson, C. J.; Golen, J. A.; Moore, C.; Rheingold, A. L. A new phosphonate pendant-armed cross-bridged tetraamine chelator accelerates copper(II) binding for radiopharmaceutical applications. *Dalton Trans.* **2010**, *39*, 1699−1701.
(10) Ferdani, R.; Stigers, D. J.; Fiamengo, A. L.; Wei, L.; Li, B. T. Y.; Golen, J. A.; Rheingold, A. L.; Weisman, G. R.; Wong, E. H.; Anderson, C. J. Synthesis, Cu(II) complexation, ^{64}Cu-labeling and biological evaluation of cross-bridged cyclam chelators with phosphonate pendant arms. *Dalton Trans.* **2012**, *41*, 1938−1950.
(11) Zeng, D.; Ouyang, Q.; Cai, Z.; Xie, X.-Q.; Anderson, C. J. New cross-bridged cyclam derivative CB-TE1K1P, an improved bifunctional chelator for copper radionuclides. *Chem. Commun.* **2014**, *50*, 43−45.
(12) Cai, Z.; Li, B. T. Y.; Wong, E. H.; Weisman, G. R.; Anderson, C. J. Cu(I)-assisted click chemistry strategy for conjugation of non-protected cross-bridged macrocyclic chelators to tumour-targeting peptides. *Dalton Trans.* **2015**, *44*, 3945−3948.
(13) Dale, A. V.; An, G. I.; Pandya, D. N.; Ha, Y. S.; Bhatt, N.; Soni, N.; Lee, H.; Ahn, H.; Sarkar, S.; Lee, W.; Huynh, P. T.; Kim, J. Y.; Gwon, M.-R.; Kim, S. H.; Park, J. G.; Yoon, Y.-R.; Yoo, J. Synthesis and evaluation of new generation of cross-bridged bifunctional chelator for ^{64}Cu radiotracers. *Inorg. Chem.* **2015**, *54*, 8177−8186.
(14) Lima, L. M. P.; Halime, Z.; Marion, R.; Camus, N.; Delgado, R.; Platas-Iglesias, C.; Tripier, R. Monopicolinate cross-bridged cyclam combining very fast complexation with very high stability and inertness of its copper(II) complex. *Inorg. Chem.* **2014**, *53*, 5269−5279.
(15) Heroux, K. J.; Woodin, K. S.; Tranchemontagne, D. J.; Widger, P. C. B.; Southwick, E.; Wong, E. H.; Weisman, G. R.; Tomellini, S. A.; Wadas, T. J.; Anderson, C. J.; Kassel, S.; Golen, J. A.; Rheingold, A. L. The long and short of it: the influence of *N*-carboxyethyl *versus* *N*-carboxymethyl pendant arms on *in vitro* and *in vivo* behavior of copper complexes of cross-bridged tetraamine macrocycles. *Dalton Trans.* **2007**, 2150−2162.
(16) Rodríguez-Rodríguez, A.; Esteban-Gomez, D.; Tripier, R.; Tircsó, G.; Garda, Z.; Tóth, I.; de Blas, A.; Rodriguez-Blas, T.; Platas-Iglesias, C. Lanthanide(III) Complexes with a Reinforced Cyclam Ligand Show Unprecedented Kinetic Inertness. *J. Am. Chem. Soc.* **2014**, *136*, 17954−17957.
(17) Rodríguez-Rodríguez, A.; Regueiro-Figueroa, M.; Esteban-Gómez, D.; Tripier, R.; Tircsó, G.; Kálmán, F. K.; Bényei, A. C.; Tóth, I.; de Blas, A.; Rodríguez-Blas, T.; Platas-Iglesias, C. Complexation of Ln^{3+} Ions with Cyclam Dipicolinates: A Small Bridge that Makes Huge Differences in Structure, Equilibrium, and Kinetic Properties. *Inorg. Chem.* **2016**, *55*, 2227−2239.
(18) Grenier, L.; Beyler, M.; Platas-Iglesias, C.; Closson, T.; Gómez, D. E.; Seferos, D. S.; Liu, P.; Ornatsky, O. I.; Baranov, V.; Tripier, R. Highly Stable and Inert Complexation of Indium(III) by Reinforced Cyclam Dipicolinate and a Bifunctional Derivative for Bead Encoding in Mass. *Chem. - Eur. J.* **2019**, *25*, 15387−15400.
(19) Kotek, J.; Lubal, P.; Hermann, P.; Císařová, I.; Lukeš, I.; Godula, T.; Svobodová, I.; Táborský, P.; Havel, J. High Thermodynamic Stability and Extraordinary Kinetic Inertness of Copper(II) Complexes with 1,4,8,11-Tetraazacyclotetradecane-1,8-bis-(methylphosphonic acid): Example of a Rare Isomerism between Kinetically Inert Penta- and Hexacoordinated Copper(II) Complexes. *Chem. - Eur. J.* **2003**, *9*, 233−248.
(20) Füzerová, S.; Kotek, J.; Císařová, I.; Hermann, P.; Binnemans, K.; Lukeš, I. Cyclam (1,4,8,11-tetraazacyclotetradecane) with one methylphosphonate pendant arm: a new ligand for selective copper(II) binding. *Dalton Trans.* **2005**, 2908−2915.
(21) Svobodová, I.; Lubal, P.; Plutnar, J.; Havlíčková, J.; Kotek, J.; Hermann, P.; Lukeš, I. Thermodynamic, kinetic and solid-state study of divalent metal complexes of 1,4,8,11-tetraazacyclotetradecane (cyclam) bearing two *trans*(1,8-)methylphosphonic acid pendant arms. *Dalton Trans.* **2006**, 5184−5197.
(22) Havlíčková, J.; Medová, H.; Vitha, T.; Kotek, J.; Císařová, I.; Hermann, P. Coordination properties of cyclam (1,4,8,11-tetraazacyclotetradecane) endowed with two methylphosphonic acid pendant arms in the 1,4-positions. *Dalton Trans.* **2008**, 5378−5386.
(23) Svobodová, I.; Havlíčková, J.; Plutnar, J.; Lubal, P.; Kotek, J.; Hermann, P. Metal Complexes of 4,11-Dimethyl-1,4,8,11-tetraazacyclotetradecane-1,8-bis(methylphosphonic acid) − Thermodynamic and Formation/Decomplexation Kinetic Studies. *Eur. J. Inorg. Chem.* **2009**, *2009*, 3577−3592.
(24) Paúrová, M.; Havlíčková, J.; Pospíšilová, A.; Vetrík, M.; Císařová, I.; Stephan, H.; Pietzsch, H.-J.; Hrubý, M.; Hermann, P.; Kotek, J. Bifunctional cyclam-based ligands with phosphorus pendant

moieties for radiocopper separation − Thermodynamic and kinetic studies. *Chem. - Eur. J.* **2015**, *21*, 4671−4687.
(25) Svobodová, I.; Lubal, P.; Hermann, P.; Kotek, J.; Havel, J. Selective Kinetic Determination of Cu^{2+} with Tetraazamacrocyclic Bis(Methylphosphonate) Ligand (Dipon). *Microchim. Acta* **2004**, *148*, 21−26.
(26) Svobodová, I.; Lubal, P.; Hermann, P.; Kotek, J.; Havel, J. Application of Dipon, 1,4,8,11-Tetraazacyclotetradecane-4,11-bis-(methylphosphonic acid) as Selective Complexing Agent for Determination of Copper(II). *J. Inclusion Phenom. Mol. Recognit. Chem.* **2004**, *49*, 11−15.
(27) Notni, J.; Hermann, P.; Havlíčková, J.; Kotek, J.; Kubíček, V.; Plutnar, J.; Loktionova, N.; Riss, P. J.; Rösch, F.; Lukeš, I. A triazacyclononane based bifunctional phosphinate ligand for preparation of multimeric ^{68}Ga PET tracers. *Chem. - Eur. J.* **2010**, *16*, 7174−7185.
(28) Šimeček, J.; Zemek, O.; Hermann, P.; Notni, J.; Wester, H.-J. Tailored gallium(III) chelator NOPO: Synthesis, characterization, bioconjugation, and application in preclinical Ga-68 PET imaging. *Mol. Pharmaceutics* **2014**, *11*, 3893−3903.
(29) Procházková, S.; Kubíček, V.; Kotek, J.; Vágner, A.; Notni, J.; Hermann, P. Lanthanide(III) complexes of monophosphinate/monophosphonate DOTA-analogues: effects of the substituents on the formation rate and radiolabelling yield. *Dalton Trans.* **2018**, *47*, 13006−13015.
(30) David, T.; Kubíček, V.; Gutten, O.; Lubal, P.; Kotek, J.; Pietzsch, H.-J.; Rulíšek, L.; Hermann, P. Cyclam derivatives with a bis(phosphinate) or a phosphinato-phosphonate pendant arm: ligands for fast and efficient copper(II) complexation for nuclear medical applications. *Inorg. Chem.* **2015**, *54*, 11751−11766.
(31) Paúrová, M.; David, T.; Císařová, I.; Lubal, P.; Hermann, P.; Kotek, J. Optimization of the selectivity and rate of copper radioisotope complexation: formation and dissociation kinetic studies of 1,4,8-trimethylcyclam-based ligands with different coordinating pendant arms. *New J. Chem.* **2018**, *42*, 11908−11929.
(32) David, T.; Hlinová, V.; Kubíček, V.; Bergmann, R.; Striese, F.; Berndt, N.; Szöllősi, D.; Kovács, T.; Máthé, D.; Bachmann, M.; Pietzsch, H.-J.; Hermann, P. Improved conjugation, 64-Cu radiolabeling, in vivo stability and imaging using non-protected bifunctional macrocyclic ligands: Bis(phosphinate) cyclam (BPC) chelators. *J. Med. Chem.* **2018**, *61*, 8774−8796.
(33) Day, M. W.; Meade, T. J.; Hubin, T. J. CSD Communication (Private Communication) IXOKIP, 2004.
(34) Lukeš, I.; Kotek, J.; Vojtíšek, P.; Hermann, P. Tetraazacycles with Methylphosphinic/ phosphonic Acid Pendant Arms. A Comparison with their Acetic Acid Analogues. *Coord. Chem. Rev.* **2001**, *216−217*, 287−312.
(35) Weisman, G. R.; Rogers, M. E.; Wong, E. H.; Jasinski, J. P.; Paight, E. S. Cross-Bridged Cyclam. Protonation and Li^{+} Complexation in a Diamond-Lattice Cleft. *J. Am. Chem. Soc.* **1990**, *112*, 8604−8605.
(36) Hubin, T. J.; McCormick, J. M.; Collinson, S. R.; Buchalova, M.; Perkins, Ch. M.; Alcock, N. W.; Kahol, P. K.; Raghunathan, A.; Busch, D. H. New Iron(II) and Manganese(II) Complexes of Two Ultra-Rigid, Cross-Bridged Tetraazamacrocycles for Catalysis and Biomimicry. *J. Am. Chem. Soc.* **2000**, *122*, 2512−2522.
(37) Šimeček, J.; Schulz, M.; Notni, J.; Plutnar, J.; Kubíček, V.; Havlíčková, J.; Hermann, P. Complexation of metal ions with TRAP (1,4,7-triazacyclononane phosphinic acid) ligands and 1,4,7-triazacyclononane-1,4,7-triacetic acid: Phosphinate-containing ligands as unique chelators for trivalent galium. *Inorg. Chem.* **2012**, *51*, 577−590.
(38) Kotek, J.; Vojtíšek, P.; Císařová, I.; Hermann, P.; Jurečka, P.; Rohovec, J.; Lukeš, I. Bis(methylphosphinic acid) Derivatives of 1,4,8,11-tetraazacyclododecane (cyclam). Synthesis, Crystal and Molecular Structures, and Solution Properties. *Collect. Czech. Chem. Commun.* **2000**, *65*, 1289−1316.
(39) Kasprzyk, S. P.; Wilkins, R. G. Kinetics of interaction of metal ions with two tetraaza tetraacetate macrocycles. *Inorg. Chem.* **1982**, *21*, 3349−3352.
(40) Wang, X.; Jin, T.; Comblin, V.; Lopez-Mut, A.; Merciny, E.; Desreux, J. F. A kinetic investigation of the lanthanide DOTA chelates. Stability and rates of formation and of dissociation of a macrocyclic gadolinium(III) polyaza polycarboxylic MRI contrast agent. *Inorg. Chem.* **1992**, *31*, 1095−1099.
(41) Jones, D. G.; Wilson, K. R.; Cannon-Smith, D. J.; Shircliff, A. D.; Zhang, Z.; Chen, Z.; Prior, T. J.; Yin, G.; Hubin, T. J. Synthesis, Structural Studies, and Oxidation Catalysis of the Late- First-Row-Transition-Metal Complexes of a 2-Pyridylmethyl Pendant-Armed Ethylene Cross-Bridged Cyclam. *Inorg. Chem.* **2015**, *54*, 2221−2234.
(42) Pandya, D. N.; Dale, A. V.; Kim, J. Y.; Lee, H.; Ha, Y. S.; An, G. I.; Yoo, J. New Macrobicyclic Chelator for the Development of Ultrastable ^{64}Cu-Radiolabeled Bioconjugate. *Bioconjugate Chem.* **2012**, *23*, 330−335.
(43) King, C.; Roundhill, D. M.; Fronczek, F. R. Synthesis and structural characterization of methylenebisphosphinic acid, $CH_2[PH(O)OH]_2$. *Inorg. Chem.* **1986**, *25*, 1290−1292.
(44) (a) Táborský, P.; Lubal, P.; Havel, J.; Kotek, J.; Hermann, P.; Lukeš, I. Thermodynamic and Kinetic Studies of Lanthanide(III) Complexes with H_5do3ap (1,4,7,10-tetraazacyclododecane-1,4,7-triacetic-10-(methylphosphonic acid)), a monophosphonate Analogue of H_4dota. *Collect. Czech. Chem. Commun.* **2005**, *70*, 1909−1942. (b) Försterová, M.; Svobodová, I.; Lubal, P.; Táborský, P.; Kotek, J.; Hermann, P.; Lukeš, I. Thermodynamic Study of Lanthanide(III) Complexes with Bifunctional Monophosphinic Acid Analogues of H_4dota and Comparative Kinetic Study of Yttrium(III) Complexes. *Dalton Trans.* **2007**, 535−549.
(45) Baes, C. F., Jr.; Mesmer, R. E. *The Hydrolysis of Cations*; Wiley: New York, 1976.
(46) Kývala, M.; Lukeš, I. International Conference, Chemomotrics '95, Pardubice, Czech Republic, 1995; p 63, full version of "OPIUM" available (free of charge) from http://www.natur.cuni.cz/~kyvala/opium.html.
(47) (a) Otwinowski, Z.; Minor, W. *HKL Denzo and Scalepack Program Package*; Nonius BV: Delft, The Netherlands, 1997. (b) Otwinowski, Z.; Minor, W. Processing of X-ray diffraction data collected in oscillation mode. *Methods Enzymol.* **1997**, *276*, 307−326.
(48) Altomare, A.; Burla, M. C.; Camalli, M.; Cascarano, G.; Giacovazzo, C.; Guagliardi, A.; Polidori, G. SIR92 - a program for automatic solution of crystal structures by direct methods. *J. Appl. Crystallogr.* **1994**, *27*, 435−435.
(49) (a) Hübschle, C. B.; Sheldrick, G. M.; Dittrich, B. *ShelXle: a Qt graphical user interface for SHELXL*; University of Göttingen: Göttingen, Germany, 2014. (b) Hübschle, C. B.; Sheldrick, G. M.; Dittrich, B. ShelXle: a Qt graphical user interface for SHELXL. *J. Appl. Crystallogr.* **2011**, *44*, 1281−1284. (c) Sheldrick, G. M. *SHELXL-2017/1. Program for Crystal Structure Refinement from Diffraction Data*; University of Göttingen: Göttingen, Germany, 2017. (d) Sheldrick, G. M. Crystal structure refinement with SHELXL. *Acta Crystallogr., Sect. C: Struct. Chem.* **2015**, *C71*, 3−8.

https://dx.doi.org/10.1021/acs.inorgchem.0c00856
Inorg. Chem. 2020, 59, 8432−8443

Cross-bridged cyclam with phosphonate and phosphinate pendant arms: chelators for copper radioisotopes with fast complexation kinetics

Lucia Pazderová,[a] Tomáš David,[a,&] Veronika Hlinová,[a] Jan Plutnar,[a,#] Jan Kotek,[a] Přemysl Lubal,[b] Vojtěch Kubíček*[a] and Petr Hermann[a]

[a] Department of Inorganic Chemistry, Faculty of Science, Charles University, Hlavova 8, 128 40 Prague 2, Czech Republic. Tel.: +420221951436; fax: +420221951253; e-mail: kubicek@natur.cuni.cz

[b] Department of Chemistry, Masaryk University, Kotlářská 2, 611 37, Brno, Czech Republic.

[&] current address: Institute of Organic Chemistry and Biochemistry of the Czech Academy of Sciences, Flemingovo nám. 2, 16610, Prague 6, Czech Republic.

[#] current address: Center for Advanced Functional Nanorobots, Department of Inorganic Chemistry, Faculty of Chemical Technology, University of Chemistry and Technology, Technická 5, Prague 6, 16000, Czech Republic.

Table of content page

Figure S1. Typical ^{31}P NMR spectrum of the reaction mixture obtained after heating cb-cyclam, H_3PO_3 (*a*) and paraformaldehyde at 60–80 °C. In addition to the product H_4L^1 (**light blue circle**) and to the expected side products – i.e., phosphoric acid (*b*) and hydroxymethylphosphonic acid (*c*) – undesired monomethylphosphonate cb-cyclam (**red circle**) and other species (#) also formed during the reaction (**A**). However, at a lower temperature (35 °C) and with a large excess of both H_3PO_3 (*a*) and paraformaldehyde (15 eq. each), a prolonged reaction time (7 days) quantitatively afforded H_4L^1 (**B**). When such a mixture was purified on a strong cation exchange resin (H^+-form), compounds *a*–*c* were quantitatively removed by washing with distilled H_2O. Subsequent washing with 10% aqueous pyridine led (after removing pyridine through repeated evaporation with H_2O) to pure H_4L^1 in zwitterionic form (**C**).

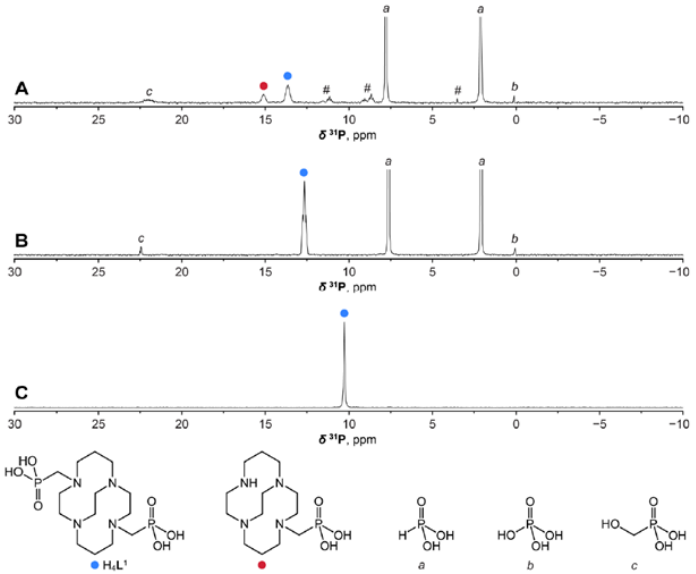

Figure S2. Characterization $^{31}P\{^{1}H\}$ (**A**), ^{1}H (**B**) and $^{13}C\{^{1}H\}$ (**C**) NMR spectra of $H_4\mathbf{L}^1$ in D_2O+CsOD (pD ~5)

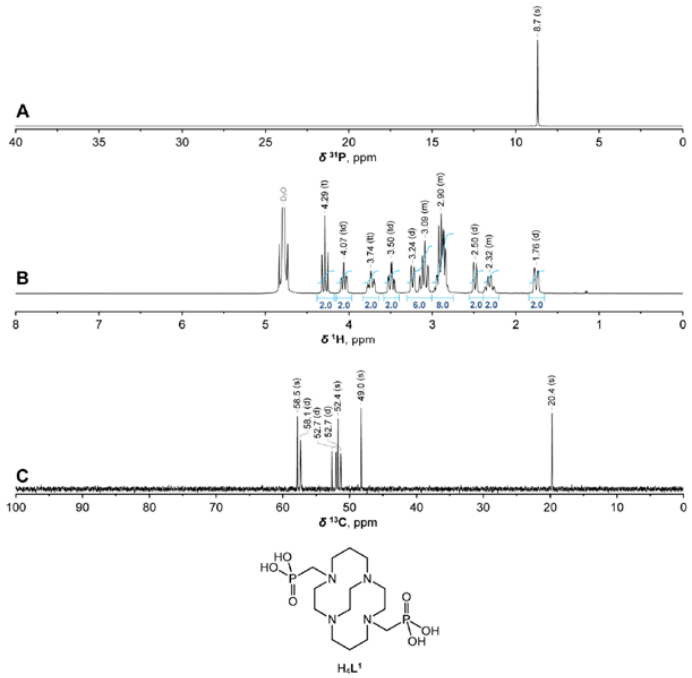

Figure S3. Characterization ^{31}P (**A**), ^{1}H (**B**) and $^{13}C\{^{1}H\}$ (**C**) NMR spectra of $H_4\mathbf{L}^2$ in D_2O+CsOD (pD ≥12). Partial deuteration of P–H bond is denoted by a grey double arrow (**A**)

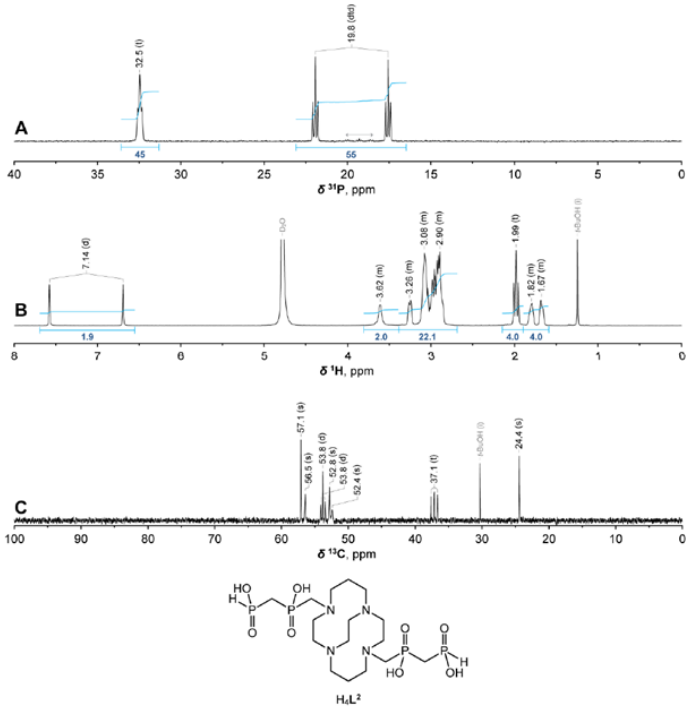

Figure S4. Characterization ^{31}P (**A**), ^{1}H (**B**) and $^{13}C\{^{1}H\}$ (**C**) NMR spectra of H_2L^3 in D_2O+CsOD (pD ≥12)

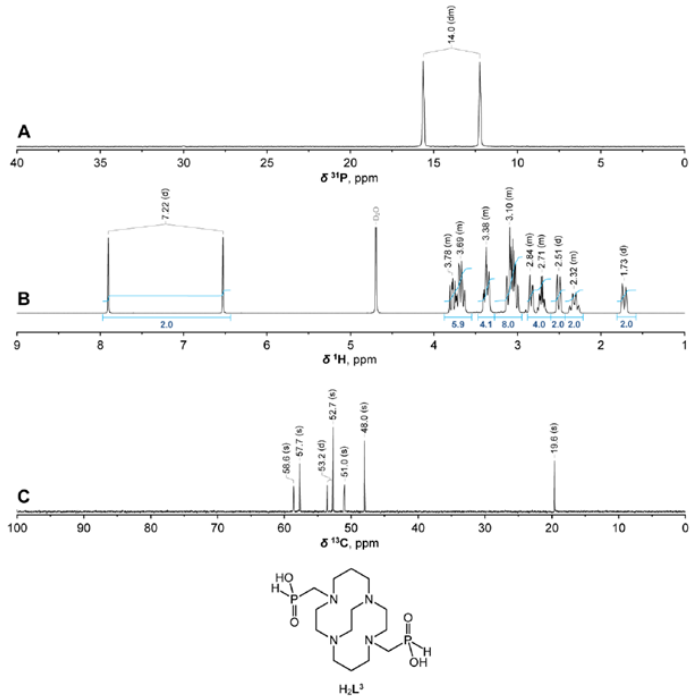

Table S1: Parameters of intramolecular hydrogen bonds found in the crystal structure of $H_2L^3 \cdot 5H_2O$

D–H	*d*(D–H) (Å)	*d*(H···A) (Å)	<DHA (°)	*d*(D···A) (Å)	A
N4–H41	0.87(2)	2.04(2)	146(1)	2.800(1)	N8
N4–H41	0.87(2)	2.59(1)	113(1)	3.045(1)	N1
N4–H41	0.87(2)	2.57(1)	105(1)	2.928(1)	O11
N11–H111	0.86(2)	2.02(2)	147(1)	2.780(2)	N1
N11–H111	0.86(2)	2.63(2)	112(1)	3.053(1)	N8
N11–H111	0.86(2)	2.68(2)	105(1)	3.008(2)	O21

Table S2. Geometry of the phosphonate moieties in the $[Cu(H_2L^1)]\cdot 2H_2O$ complex

Distances (Å)			
P1–O11	1.505(2)	P2–O21	1.520(2)
P1–O12	1.580(2)	P2–O22	1.580(2)
P1–O13	1.501(2)	P2–O23	1.487(2)
P1–C17	1.814(3)	P2–C18	1.821(3)
Angles (°)			
O11–P1–O1	107.7(1)	O21–P1–O22	110.7(1)
O11–P1–O1	117.6(1)	O21–P1–O23	117.5(1)
O11–P1–C1	108.9(1)	O21–P1–C18	102.8(1)
O12–P1–O1	110.6(1)	O22–P1–O23	107.6(1)
O12–P1–C1	105.3(1)	O22–P1–C18	105.0(1)
O13–P1–C1	106.0(1)	O23–P1–C18	112.6(1)

Table S3. Coordination geometry of the [Cu(H_2**L**^{1})] found in [Cu(H_2**L**^{1})]·2H_2O and its comparison with relevant structures deposited in CCDC

Parameter	[Cu(H_2**L**^{1})] ·2H_2O[a]	[Cu(H_2**L**^{1})] ·0.5NaCl·4H_2O[b]		[Cu(H**cb-te2a**)] (ClO_4)	[Cu(**cb-te2a**)] ·NH_4PF_6·H_2O	[Cu(**cb-te2a**)] $NaClO_4$·1.5H_2O	
CCDC code		KUPHEJ		RAZGOP	IXOKIP	VIQKEL[c]	
Distances (Å)							
Cu–N1	2.045(2)	2.036	2.104/1.985	2.016	2.071	2.073	2.067
Cu–N4	2.051(2)	2.041	2.033/2.096	2.046	2.053	2.034	2.050
Cu–N8	2.207(2)	2.204	2.188	2.216	2.218	2.223	2.244
Cu–N11	2.104(2)	2.087	2.094	2.057	2.048	2.027	2.042
Cu–O11	2.716(2)	2.444	2.575/2.338	2.525	2.271	2.301	2.327
Cu–O21	1.981(2)	1.998	1.992	1.966	2.018	2.008	1.998
Angles (°)							
N1–Cu–N4	85.55(9)	85.57	82.55/85.33	87.25	88.22	88.26	88.04
N1–Cu–N8	86.07(9)	86.19	80.98/94.88	86.37	84.83	84.82	84.53
N1–Cu–N11	97.72(9)	98.12	96.27/98.98	98.58	93.38	94.27	93.76
N1–Cu–O11	87.81(8)	91.85	91.09/92.93	93.07	90.65	88.13	88.87
N1–Cu–O21	173.30(9)	174.43	172.14/170.68	177.02	177.49	178.38	178.43
N4–Cu–N8	98.84(9)	99.69	92.62/106.08	99.44	91.78	93.01	91.24
N4–Cu–N11	176.03(9)	174.74	176.98/168.35	172.93	177.69	177.46	176.45
N4–Cu–O11	79.94(7)	83.81	86.14/82.28	76.06	81.07	81.31	80.29
N4–Cu–O21	88.43(8)	88.87	93.46/87.16	90.05	93.79	91.84	93.49
N8–Cu–N11	83.69(9)	84.35	84.44	85.00	86.72	86.96	85.89
N8–Cu–O11	173.84(8)	175.83	172.06/168.98	175.49	171.67	171.09	169.44
N8–Cu–O21	97.76(9)	94.46	92.49	95.31	93.58	93.55	95.12
N11–Cu–O11	97.87(7)	92.30	96.67/86.67	99.51	100.56	99.03	102.79
N11–Cu–O21	88.19(9)	87.44	87.38	84.03	84.57	85.63	84.69
O11–Cu–O22	88.26(7)	87.84	95.40/80.58	85.07	91.16	93.49	91.69

[a] This work. [b] Two independent complex molecules are present, finding partial disorder of one of them. [c] Two independent complex molecules were found.

Table S4. Parameters of hydrogen bonds found in the crystal structure of [Cu(H_2**L**^{1})]·2H_2O

D–H	*d*(D–H) (Å)	*d*(H···A) (Å)	<DHA (°)	*d*(D···A) (Å)	A
O12–H12O	0.84(6)	1.76(6)	164(6)	2.573(3)	O11 [*x*, −*y*+2, *z*+1/2]
O22–H22O	0.94(6)	1.69(6)	163(5)	2.600(3)	O1W
O1W–H11W	0.83(5)	1.95(5)	167(4)	2.762(3)	O13
O1W–H12W	0.91(5)	1.92(5)	173(4)	2.819(3)	O13 [*x*, −*y*+2, *z*−1/2]
O2W–H21W	0.89(7)	1.99(7)	155(6)	2.823(3)	O23
O2W–H22W	0.78(5)	2.22(5)	151(5)	2.927(3)	O23 [*x*, −*y*+1, *z*+1/2]

Table S5. Overall protonation constants logβ of ligands and overall stability constants logβ of Cu(II) complexes (25 °C, *I* = 0.1M NMe_4Cl). Charges are omitted.

Species	H_4**L**^{1}	H_4**L**^{2}	H_2**L**^{3}
HL	15 [a]	15 [a]	15 [a]
H_2L	26.22(1)	21.89(1)	21.35(1)
H_3L	33.56(1)	24.49(1)	–
H_4L	38.19(1)	25.84(1)	–
[Cu(L)]	23.97(13)	20.21(1)	21.28(3)
[Cu(HL)]	32.23(13)	22.84(1)	–
[Cu(H_2L)]	36.86(6)	–	–

[a] The value cannot be determined and was, thus, fixed at logβ = 15.

Figure S5. ^{31}P NMR titration of ligands in the alkaline region. Signal shifts of $H_4\mathbf{L}^1$ (**A**), $H_4\mathbf{L}^2$ (**B**) and $H_2\mathbf{L}^3$ (**C**) as a function of pH, adjusting the pH with $(NMe_4)OH$.

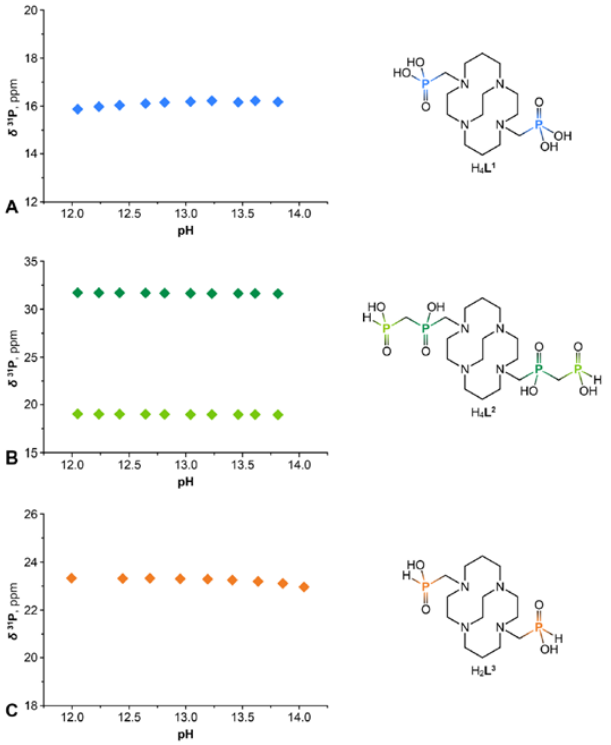

Figure S6. Formation of Cu(II) complexes: $^{f}k_{obs}$ of $H_4\mathbf{L}^1$ (**A**), $H_4\mathbf{L}^2$ (**B**) and $H_2\mathbf{L}^3$ (**C**) as function of copper(II) concentration (c_L = 0.1 mM, 25 °C) at various pH values (given in the figures). Only selected curves are displayed. The solid lines represent the best fits according to Equations 2 or 6.

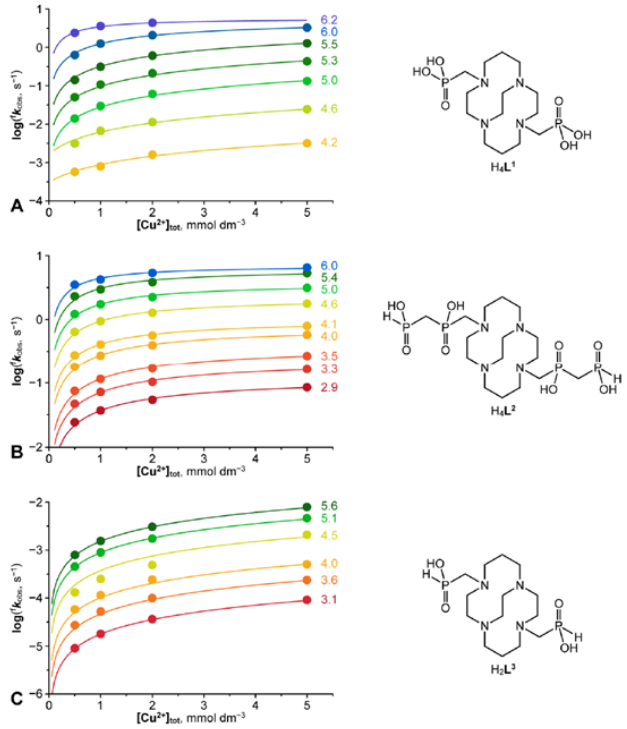

Description of complexation kinetics

According to the generally accepted complexation mechanism (Scheme 2), complexation of metal ions by macrocyclic ligands with pendant arms containing functional groups with coordinating ability proceeds as a two-step process. The *out-of-cage* complex (further labeled with an asterisk) is formed in the first equilibrium step. The metal ion in the *out-of-cage* complex is bound only through pendant oxygen atoms and the macrocycle amin groups are still protonated. The second step is metal binding into the macrocyclic cavity and formation of the *in-cage* complex. The rate of *in-cage* complexation is proportional to the concentration of the *out-of-cage* intermediate, and observed reaction rate ($^{f}k_{obs}$) is expressed by Equation 2[†]

$$^{f}k_{obs} = \frac{^{f}k \cdot K^{*} \cdot [Cu]_{tot}}{1 + K^{*} \cdot [Cu]_{tot}} \quad (2)$$

where ^{f}k is the rate constant describing the formation of the *in-cage* complex, K^{*} is the conditional thermodynamic stability constant of the *out-of-cage* intermediate, and $[Cu]_{tot}$ is the overall concentration of Cu(II) ions.

At any particular pH, the rate of *in-cage* complexation is proportional to the overall concentration of *out-of-cage* species and it can be expressed as sum of contributions of differently protonated *out-of-cage* species (only non-protonated, monoprotonated and diprotonated species are mentioned in the equation)

$$v = {}^{f}k \cdot ([CuL]^{*} + [CuHL]^{*} + [CuH_2L]^{*}) = {}^{f}k_0 \cdot [CuL]^{*} + {}^{f}k_1 \cdot [CuHL]^{*} + {}^{f}k_2 \cdot [CuH_2L]^{*}$$

where $^{f}k_n$ are the rate constants describing the contribution of individual (differently protonated) species. Considering the values of the ligand protonation constants, the *out-of-cage* complex is present in noticeable concentration in the measured pH range 3–6 as a mixture of monoprotonated and diprotonated forms (i.e. concentration of $[CuL]^{*}$ can be neglected when compared to $[CuHL]^{*}$ and $[CuH_2L]^{*}$, leading to simplification of denominator in the following equation):

$$^{f}k \approx \frac{^{f}k_0 + {}^{f}k_1 \cdot K^{*}_{p1} \cdot [H] + {}^{f}k_2 \cdot K^{*}_{p1} \cdot K^{*}_{p2} \cdot [H]^2}{K^{*}_{p1} \cdot [H] + K^{*}_{p1} \cdot K^{*}_{p2} \cdot [H]^2}$$

where K^{*}_{p1} and K^{*}_{p2} are consecutive protonation constants of the mono- and di- protonated *out-of-cage* species.

Analysis of data has shown that contributions of the non-protonated and diprotonated *out-of-cage* complexes to whole reaction rate (i.e. in numerator of the above equation) are

[†] Numbering of equations corresponds to the main text.

negligible in the studied pH range and, thus, $^{f}k_0$ and $^{f}k_2$ can be omitted. It leads to the simplified formulation of ^{f}k as is expressed by Equation 5

$$^{f}k \approx \frac{^{f}k_1}{1 + K^{*}_{p2} \cdot [H]} \quad (5)$$

Description of dissociation kinetics

Dissociation rate at particular pH is proportional to the overall concentration of the complex and it could be also expressed as sum of contributions of kinetically active protonated species

$$v = {}^{d}k_{obs} \cdot [CuL]_{tot} = {}^{d}k_{n+1} \cdot [CuHL] + {}^{d}k_{n+2} \cdot [CuH_2L]$$

where $^{d}k_{n+1}$ and $^{d}k_{n+2}$ are the rate constants that correspond to the dissociation of species bearing more protons (by one and two) than is present in thermodynamically stable species. Then, the observed rate constant is expressed by Equation 8[‡]

$$^{d}k_{obs} = \frac{^{d}k_{n+1} \cdot K_{Hn+1} \cdot [H] + {}^{d}k_{n+2} \cdot K_{Hn+1} \cdot K_{Hn+2} \cdot [H]^2}{1 + K_{Hn+1} \cdot [H] + K_{Hn+1} \cdot K_{Hn+2} \cdot [H]^2} \quad (8)$$

where K_{Hn+1} and K_{Hn+2} are consecutive protonation constants of the complex. If protonation takes place only in very acidic solutions, i.e. logarithms of protonation constants of the complex are $\log K_n << 0$, then complex is present only in the nonprotonated state and $K_{Hn+1} \cdot [H] + K_{Hn+1} \cdot K_{Hn+2} \cdot [H]^2 << 1$. Thus, Equation 8 can be simplified, expressing $^{d}k_{obs}$ according to Equation 9

$$^{d}k_{obs} = {}^{d}k_{Hn+1} \cdot [H] + {}^{d}k_{Hn+2} \cdot [H]^2 \quad (9)$$

where $^{d}k_{Hn+1} = {}^{d}k_{n+1} \cdot K_{Hn+1}$ and $^{d}k_{Hn+2} = {}^{d}k_{n+2} \cdot K_{Hn+1} \cdot K_{Hn+2}$.

[‡] Numbering of equations corresponds to the main text.

Scheme S1. Formal reaction scheme for the formation of the *in-cage* Cu(II) complexes. Charges of ligand and complex species are omitted.

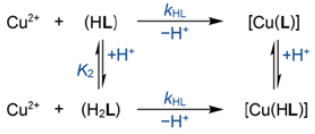

Figure S7. Comparison of the determined formation rate constants $^{f}k_{obs}$ (c_L = 0.1 mM, c_{Cu} = 1 mM, 25 °C) of $H_4\mathbf{L}^1$ (**blue**), $H_4\mathbf{L}^2$ (**light green**), $H_2\mathbf{L}^3$ (**orange**), H_2**te1bpin** (**dark green**, adopted from ref. 1; it corresponds to the formation of the initially formed *in-cage* complex) and H_4**te2p**^{1,8} (**red line**, calculated from data in ref. 2).

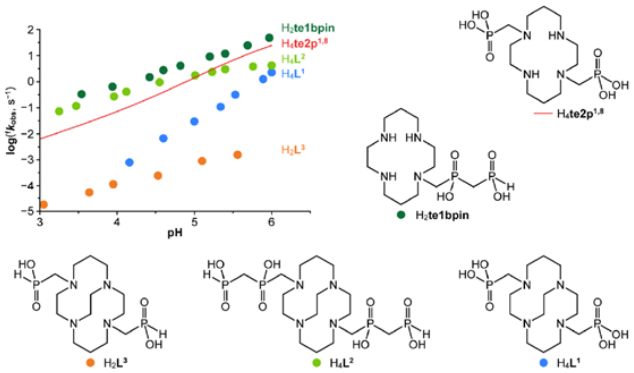

Figure S8. Dissociation rate constants $^{d}k_{obs}$ of Cu(II)-$H_4\mathbf{L}^1$ (**A**, **blue**), Cu(II)-$H_4\mathbf{L}^2$ (**B**, **green**) and Cu(II)-$H_2\mathbf{L}^1$ (**C**, **orange**) (c_{CuL} = 1 mM, 90 °C, I = 5M H/$NaClO_4$). The lines represent the best fits according to Equations 8 or 9.

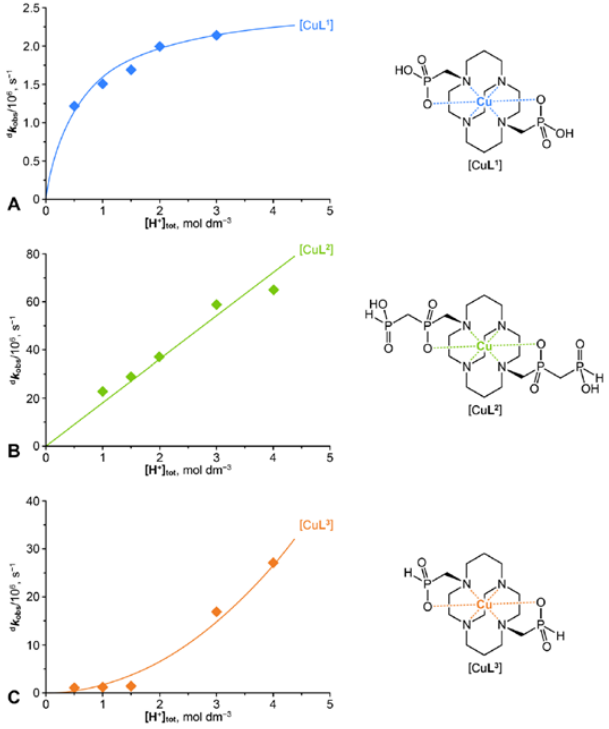

Figure S9. Comparison of dissociation rate constants $^{d}k_{obs}$ of Cu(II)-$H_4\mathbf{L}^2$ in $HClO_4$ (**light green**) and in HCl (**dark green**) (c_{CuL} = 1 mM, 90 °C, I = 5M H/$NaClO_4$ or H/NaCl).

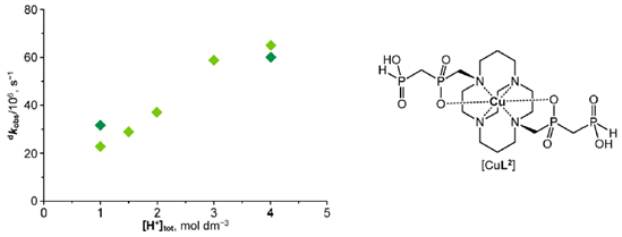

[CuL^2]

Table S6. X-ray crystal data collection and refinement details

Parameter	$H_2\mathbf{L}^3\cdot 5H_2O$	$[Cu(H_2\mathbf{L}^1)]\cdot 2H_2O$	*N*,*N*′-Dibenzyl-cb-cyclam
Formula	$C_{14}H_{42}N_4O_9P_2$	$C_{14}H_{34}CuN_4O_8P_2$	$C_{26}H_{38}N_4$
M_r	472.45	511.93	406.60
Habit	plate	prism	prism
Color	colorless	blue	colorless
Crystal system	triclinic	monoclinic	triclinic
Space group	*P*−1	*Cc*	*P*−1
a (Å)	8.25370(10)	15.0444(3)	11.8352(3)
b (Å)	12.0387(3)	14.8121(3)	12.1285(2)
c (Å)	12.3127(3)	9.1358(2)	17.4415(4)
α (°)	104.7529(10)	90	77.6745(12)
β (°)	90.9996(13)	100.3615(12)	89.8743(9)
γ (°)	107.1201(13)	90	75.0877(11)
U, Å^3	1125.01(4)	2002.61(7)	2359.84(9)
Z	2	4	4
D_{calc}, g cm^{-3}	1.395	1.698	1.144
μ, mm^{-1}	0.245	1.302	0.068
Unique refl.	5107	4426	10840
Obsd. refl. (I>2σ(I))	4545	4368	7954
$R(I>2\sigma(I))$	0.0319	0.0209	0.0431
R'(all)	0.0369	0.0213	0.0671
$wR(I>2\sigma(I))$	0.0840	0.0513	0.0962
wR'(all)	0.0876	0.0516	0.1081

Figure S10: Single crystals of a key starting compound – *N,N″*-dibenzyl-cb-cyclam – enabled the determination of its crystal structure. The structural parameters differ from a recently published structure of this compound.[3] In the present case, two independent molecules were found (one of them is shown in **A**; hydrogen atoms are not displayed). However, both units have very similar geometry (overlay of both independent molecules is shown in **B**). Furthermore, both independent units are very similar to that in the recently published structure – only slightly differing in the position of the benzyl groups. Overlay of the present structure (red and blue) with the recently reported crystal structure (green, miwpeq, CCDC-1555222)3 is shown in **C**.

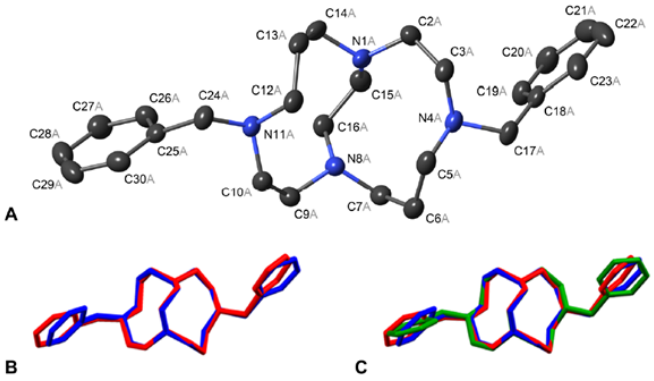

References

[1] David, T.; Kubíček, V.; Gutten, O.; Lubal, P.; Kotek, J.; Pietzsch, H.-J.; Rulíšek, L.; Hermann, P. Cyclam Derivatives with a Bis(phosphinate) or a Phosphinato–Phosphonate Pendant Arm: Ligands for Fast and Efficient Copper(II) Complexation for Nuclear Medical Applications. *Inorg. Chem.* **2015**, *54*, 11751–11766.

[2] Kotek, J.; Lubal, P.; Hermann, P.; Císařová, I.; Lukeš, I.; Godula, T.; Svobodová, I.; Táborský, P.; Havel, J. Unusually High Thermodynamic Stability and Extraordinary Kinetic Inertness of Copper(II) Complexes with 1,4,8,11-Tetraazacyclotetradecane-1,8-bis(methylphosphonic Acid). Example of a Rare Isomerism Between Kinetically Inert Penta- and Hexacoordinated Copper(II) Complexes. *Chem. Eur. J.* **2003**, *9*, 233–248.

[3] Hubin, T. J.; Walker, A. N.; Davilla; D. J.; Freeman, T. N. C.; Epley, B. M.; Hasley, T. R.; Amoyaw, P. N. A.; Jain, S.; Archibald, S. J.; Prior, T. J.; Krause, J. A.; Oliver, A. G.; Tekwani, B. L.; Khan, M. O. F. Tetraazamacrocyclic derivatives and their metal complexes as antileishmanial leads. *Polyhedron* **2019**, *163*, 42–53.

Appendix 4

Pazderová, L., Benešová, M., Havlíčková, J., Vojtíčková, M., Kotek, J., Lubal, P., Ullrich, M., Walther, M., Schulze, S., Neuber, Ch., Rammelt, S., Pietzsch, H., Pietzsch, J., Kubíček, V., & Hermann, P. (2021). Cyclam with a phosphinate-bis(phosphonate) pendant arm: a bone-targeting carrier of copper radionuclides. *Journal of Medicinal Chemistry*, submitted for publication

Cyclam with a phosphinate-bis(phosphonate) pendant arm: a bone-targeting carrier of copper radionuclides

Lucia Pazderová,[a] Martina Benešová,[a,b] Jana Havlíčková,[a] Margareta Vojtíčková,[a] Jan Kotek,[a] Přemysl Lubal,[c] Martin Ullrich,[d] Martin Walther,[d] Sabine Schulze,[e] Christin Neuber,[d] Stefan Rammelt,[f] Hans-Jürgen Pietzsch,[d,g] Jens Pietzsch,[d,g] Vojtěch Kubíček,[a] and Petr Hermann[a]*

[a]Department of Inorganic Chemistry, Faculty of Science, Charles University, Hlavova 8, 128 40 Prague 2, Czech Republic. Tel.: +420221951436; e-mail: kubicek@natur.cuni.cz

[b]Research Group Molecular Biology of Systemic Radiotherapy, German Cancer Research Center, Im Neuenheimer Feld 223, 69120 Heidelberg, Germany

[c]Department of Chemistry, Faculty of Science, Masaryk University, Kamenice 5, 625 00 Brno, Czech Republic

[d]Helmholtz-Zentrum Dresden-Rossendorf, Institute of Radiopharmaceutical Cancer Research, Bautzner Landstrasse 400, 01328 Dresden, Germany

[e]Technische Universität Dresden, Faculty of Medicine, Centre for Translational Bone, Joint and Soft Tissue Research, Fetscherstrasse 74, 01307 Dresden, Germany

[f]Technische Universität Dresden, University Hospital Carl Gustav Carus, University Center for Orthopaedics and Traumatology, Fetscherstrasse 74, 01307 Dresden, Germany

[g]Technische Universität Dresden, School of Science, Faculty of Chemistry and Food Chemistry, 01069 Dresden, Germany

Abstract

Ligands combining a bis(phosphonate) group with a macrocycle are studied as metal isotope carriers for radionuclide-based imaging and for treating bone metastases associated with several cancers. However, bis(phosphonate) pendant arms often slow down complex formation and decrease radiochemical yields. Nevertheless, their negative effect on complexation rates could be mitigated by using a suitable spacer between bis(phosphonate) and the macrocycle. To demonstrate the potential of bis(phosphonate) bearing macrocyclic ligands as carriers of copper radioisotopes, we report the synthesis of a new cyclam derivative bearing a phosphinate-bis(phosphonate) pendant (H_5te1P^{BP}). The ligand showed a high selectivity to Cu^{II} over Zn^{II} and Ni^{II} ions, and the bis(phosphonate) group was not coordinated in the Cu^{II} complex, strongly interacting with other metal ions in solution. The Cu^{II} complex formed quickly, in 1 s, at pH 5 and at a millimolar scale. The complexation rates significantly differed under a ligand or metal ion excess due to the formation of reaction intermediates differing in metal-to-ligand ratio and protonation state, respectively. The Cu^{II}-te1P^{BP} complex also showed a high resistance to acid-assisted hydrolysis ($t_{1/2}$ 4.2 min; 1 M $HClO_4$, 70 °C) and was effectively adsorbed on the hydroxyapatite surface. H_5te1P^{BP} radiolabeling with [^{64}Cu]$CuCl_2$ was fast and efficient, with specific activities of approximately 30 GBq ^{64}Cu per 1 μmol of ligand (pH 5.5, room temperature, 30 min). In a pilot experiment, we further demonstrated the excellent suitability of [^{64}Cu]Cu^{II}-te1P^{BP} for imaging active bone compartments by dedicated small animal PET/CT in healthy mice and subsequently in a rat femoral defect model, in direct comparison with [^{18}F]fluoride. Moreover, [^{64}Cu]Cu^{II}-te1P^{BP} showed higher uptake in critical bone defect regions. Therefore, our study shows the high potential of [^{64}Cu]Cu^{II}-te1P^{BP} as a PET radiotracer

for evaluating bone healing in preclinical and clinical settings with a diagnostic value similar to that of [^{18}F]fluoride, albeit with a longer half-life (12.7 h) than ^{18}F (1.8 h), thereby enabling extended observation times.

Introduction

Bone is a common target for imaging and therapy in oncology because bone metastases are frequently associated with prostate and breast cancers. For this reason, tracers or drugs are often applied in combination with imaging, treatment and palliation of bone metastases, but bone imaging also helps to diagnose other disorders, such as osteoarthritis, osteomyelitis or microfractures. Radiomedical imaging techniques – positron emission tomography (PET) and single-photon emission computed tomography (SPECT) – play a key role in the diagnosis of bone disorders. [^{18}F]fluoride and [^{99m}Tc]Tc-methylene diphosphonate ([^{99m}Tc]Tc-MDP) stand out as the most commonly used imaging agents (in PET and SPECT, respectively). Yet, in recent years, research efforts have focused on other radioisotopes and radiotracers to improve image quality and to collect more specific information. In addition, other radioisotopes are used as therapeutic or palliative agents.[1-2]

Among such radiotracers, the most relevant are those based on metallic radioisotopes. Metallic radioisotopes must be administered as thermodynamically stable and kinetically inert complexes to avoid non-specific deposition of metal ions in tissues. Another crucial parameter of the complexes used in radiomedicine is their formation rate. Fast formation is necessary to shorten the time required for radiotracer synthesis and to maintain tracer specific activity as high as possible. Among the metallic radioisotopes, the most common carriers are polyazamacrocyclic ligands bearing coordinating pendant arms, mostly derivatives of 1,4,7-triazacyclonane (tacn), 1,4,7,10-tetraazacyclododecane (cyclen) and 1,4,8,11-tetraazacyclotetradecane (cyclam).

Nuclear medicine is primarily aimed at imaging bone disorders, such as arthritis or tumors, and at palliative treatments of bone metastases. For bone imaging and therapy, ligands are often decorated with the pendant arms bearing the bis(phosphonate) group. The bis(phosphonate) group shows a high affinity to hydroxyapatite, which is the major inorganic component of bone tissue and has been used in several conjugates for bone disease targeting.[1-5] In our laboratory, we have previously synthesized and studied tacn and cyclen derivatives bearing bis(phosphonate) pendant arms (Chart 1).[6-11] The attached bis(phosphonate) groups provide a very good bone uptake, and several ligands combining macrocycle and bis(phosphonate) have been successfully tested as bone targeting radioisotope carriers.[1,12,13] Some of these radiotracer have also been successfully applied in patients for both imaging and therapy.[14-16] However, complexation and radiolabeling studies performed with gallium(III) or lanthanide(III) ions have shown that the bis(phosphonate) pendant arms often slow down complex formation and decrease radiochemical yields. The complexation rate decreases even more among ligands bearing more than one bis(phosphonate) group.[10,11,17,18] Nevertheless, the negative effect of bis(phosphonate) group on the complexation rate could be partly compensated for by using a suitable spacer between bis(phosphonate) and the macrocycle, as shown in macrocycles bearing a phosphinate-bis(phosphonate) pendant arm.[17]

In this context, copper radioisotopes are increasingly garnering research interest because copper is considered a promising theranostic element, i.e., an element with both therapeutic and diagnostic radioisotopes.[19-21] The nuclides ^{61}Cu (β^+ (61.4 %), EC (38.6 %); $t_{1/2}$ 3.3 h) and ^{64}Cu (β^+ (18 %), EC (44 %), β^- (38 %), γ (0.5 %); $t_{1/2}$ 12.8 h) are promising imaging radioisotopes for PET, whereas the nuclides ^{64}Cu and ^{67}Cu (100% β^-; $t_{1/2}$ 62 h) are studied as radiotherapeutics. As such, copper isotopes are promising single-element theranostics. However, these bone-targeting chelators are mostly based on tacn or cyclen cores, which are unsuitable carriers of Cu^{II} ions.[22] The first-choice ligands are cyclam derivatives for their high

thermodynamic selectivity to Cu^{II} ions and for the high kinetic inertness of their Cu(II) complexes.[23]

Considering the above, we present a new cyclam chelator bearing one phosphinato-bis(phosphonate) pendant arm, H_5te1P^{BP} (Chart 1). In this contribution, we report and discuss its synthesis, the acid-base properties and thermodynamic stabilities of its complexes, and the formation and dissociation kinetics of its Cu^{II} complex regarding potential applications in nuclear medicine. Moreover, we assess the *in vitro* and *in vivo* behavior of the [^{64}Cu]Cu-H_5te1P^{BP} tracer. Ultimately, our study highlights the properties of H_5te1P^{BP} as a quickly synthesized bone-targeting carrier of copper radioisotopes suitable for long observation times.

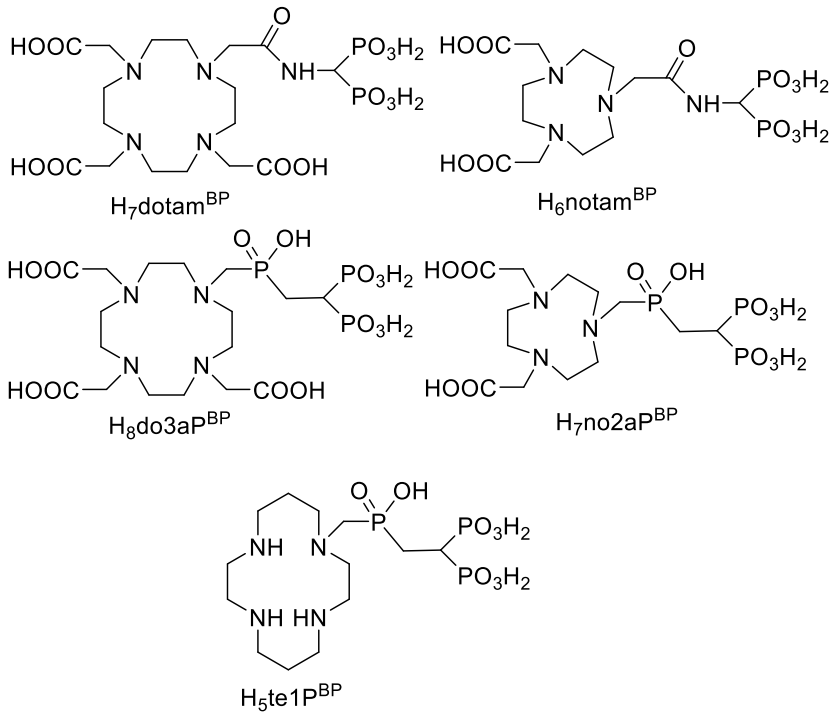

Chart 1. Discussed bis(phosphonate)-bearing macrocyclic ligands

Results and Discussion

Ligand synthesis

The key reaction in the synthesis of H_5te1P^{BP} is the fusion of triprotected cyclam (**1**)[24] with the bis(phosphonate)-phosphinate pendant arm (**2**)[8] via Kabachnik-Fields (also known as phospha-Mannich) reaction. Using pyridine as a novel solvent in the reaction, together with two

equivalents of a strong acid (HBr) as a catalyst led to an almost quantitative conversion under mild conditions and enabled us to isolate the protected intermediate (**3**) in a high yield (79%). Subsequent simultaneous removal of protecting groups under acidic conditions (6 M aq. HCl) yielded the target ligand. The zwitter-ionic form of H_5te1P^{BP} was obtained after ion-exchange treatment in 74% yield. The solubility of the zwitterionic form in water is low, thus requiring acid or base additions when preparing stock solutions for the subsequent experiments.

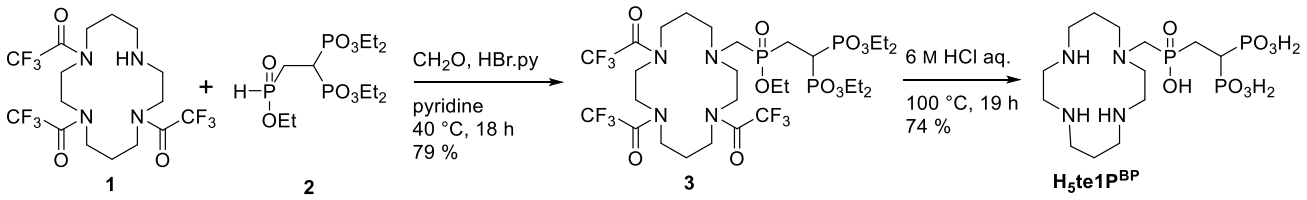

Scheme 1. H_5te1P^{BP} synthesis

Protonation and stability constants

We determined six protonation constants of H_5te1P^{BP} (Tables 1 and S1). As expected,[25] the first two protonation constants of cyclam derivatives were very high, laying outside the pH range accessible by potentiometric titrations and thus requiring using NMR for their determination. The ^{31}P NMR signal of the phosphinate group was quite sensitive to protonation of the neighboring amino groups. For this reason, its chemical shift as function of pH was used to determine the corresponding constant (Figure S1). However, the two protonation constants were close to each other (or have the reverse order)[26] and, thus, could not be distinguished without using the chemical model involving simultaneous diprotonation for data fitting. The overall protonation constant logβ_2 was even higher than those reported for related cyclam-based phosphonate/phosphinate ligands (Table 1). This difference may be explained by the high negative charge of the fully deprotonated pendant arm in $(H_2$te1P$^{BP})^{3-}$ anion. In turn, the protonation constants K_3–K_6 were determined by potentiometry. The constants K_3 and pK_4 should correspond to protonations of the bis(phosphonate) group. They were somewhat higher

than the range typical of protonations of the bis(phosphonate) group (logK_1 = 10.3–11.1, logK_2 = 5.8–7.1),[27] most likely due to the neighboring doubly protonated macrocycle. The other ligand protonation constants, K_5 and K_6, can be attributed to the third protonation of macrocycle and/ or to another protonation of the bis(phosphonato)-phosphinate pendant arm.

Indirect evidence of the protonation scheme suggested above is found in the solid-state structure of the ligand zwitterionic form H_5te1p^{BP} (Figure 1). One phosphonate group is disordered into two positions sharing carbon and phosphorus atoms and differing in the positions of the oxygen atoms and in their protonation, resulting in two forms differing in their hydrogen bond system. Three protons are bound to secondary macrocyclic nitrogen atoms. Such a protonation is rather uncommon in cyclam derivatives and leads to the unusual Dale's (3,3,4,4) ring conformation.[28] The protonated amine nitrogen atom N4 forms a short intramolecular hydrogen bond to the phosphinate oxygen atom (N4–H···O11, $d_{D\cdots A}$ = 2.720 Å), and each phosphonate group is monoprotonated. In one form, the disordered phosphonate group forms an intramolecular hydrogen bond to the phosphinate oxygen atom (O31–H···O11, $d_{D\cdots A}$ = 2.506 Å). In contrast, the second form shows an intramolecular hydrogen bond (O34–H···O21, $d_{D\cdots A}$ = 2.867 Å) to the other phosphonate group. These differences highlight the involvement of all groups of the ligand molecule in hydrogen bonding, which is important for describing not only the ligand protonation scheme but also proton transfer from the macrocycle cage to bulk water, one of the crucial parameters in both metal ion complexation and complex dissociation.

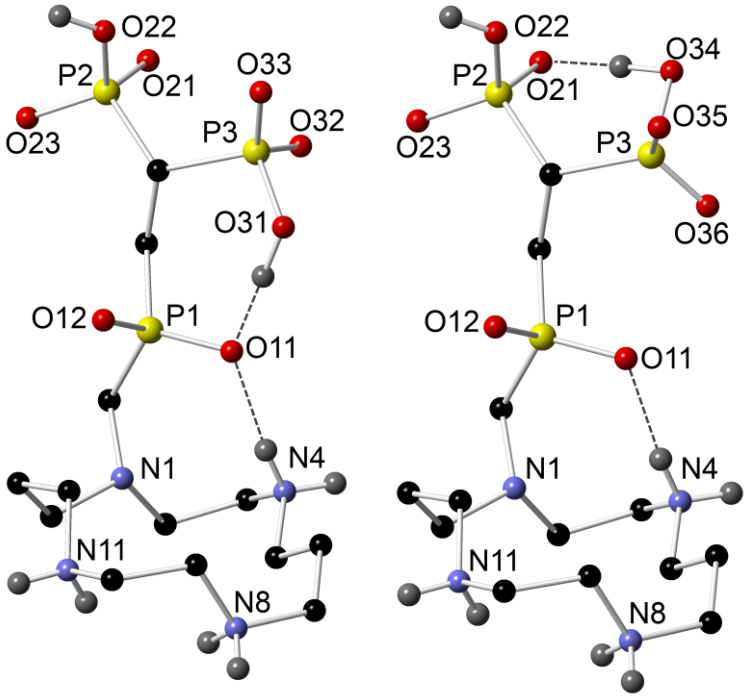

Figure 1. Molecular structure of H_5te1P^{BP} in the crystal structure of $H_5te1P^{BP}\cdot 6H_2O$. The structures highlight the different positions of the disordered bis(phosphonate) group and related hydrogen bonds. Hydrogen bonds are shown as dashed lines.

Stability constants and protonation constants of H_5te1P^{BP} complexes with Cu^{II}, Ni^{II} and Zn^{II} ions were determined by combining in-cell with out-of-cell potentiometry. Out-of-cell potentiometry was used in the acidic region (pH ~ 2 to 5) due to slow complex formation. In-cell potentiometry was performed from the slightly acidic to the strongly alkaline range on pre-formed *in-cage* complexes to determine their protonation constants. In addition, by UV-VIS out-of-cell titration, we evaluated the Cu^{II}-H_5te1P^{BP} system in the strongly acidic region (Figure S2) as the complex is fully formed at pH 1.6, i.e., at the starting point of potentiometric titrations. The results from the simultaneous treatment of all data are summarized in Tables 1 and S2. As reported in the literature, complexes of cyclam derivatives can exist in several isomeric forms differing in the conformation of the macrocycle chelate rings and, therefore, in the mutual orientation of substituents on the ring nitrogen atoms.[28,29] The maximum of the

absorption band at 580 nm indicates that the resulting species formed in this reaction is pentacoordinated I-isomer.[30,31]

The Cu^{II}-te1P^{BP} complex is highly stable. and the ligand is highly selective to Cu^{II} over Ni^{II} or Zn^{II} ions, as usual for cyclam-based ligands. The stability of the Cu^{II} complex is the highest among related ligands (Table 2) because this complex has the highest macrocycle basicity. The values of the stability constants also confirm that the metal ions are bound in the macrocyclic cavity (Table 1).[30,31] The protonation constants of the complexes (e.g., logK_1 12.69, logK_2 7.44 and logK_3 3.46 for Cu^{II}-te1P^{BP}; Table S3) are typical of the bis(phosphonate) group[27] and indicate that the bis(phosphonate) moiety is not coordinated to the metal ion bound in the cavity of the macrocycle. The selected distribution diagrams (Figure 2A,B) show that the Cu^{II} complex is fully formed at pH 1.5, whereas the Zn^{II} complex requires pH ~ 5. Both complexes are present as a mixture of mono and diprotonated species in the neutral region.

Table 1. Comparison of protonation constants of the ligands (Charts 1 and 2) and stability constants of their complexes (I = 0.1M NMe_4Cl, 25 °C); the full set of constants is given in Tables S1 and S2.

Constant	H_5te1P^{BP}	H_2te1P [a]	H_4te2P [b]	H_2te1P^{PIN} [c]	H_3te1P^{PON} [c]
logK_1	2×"13.38" [d,e]	12.49	2×"13.20" [d]	12.18	12.88
logK_2		11.76		10.75	11.68
logK_3	11.83	6.05	6.78	2.94	7.12
logK_4	7.32	2.42	5.36	1.61	3.17
logK_5	3.29	2×"1.08" [d,e]	1.15	–	1.84
logK_6	2.07		–	–	–
logK_{CuL}	29.11	27.34	25.40	25.83	27.66
logK_{ZnL}	20.74	21.03	20.35	18.12	19.84
logK_{NiL}	25.92	–	21.99	21.94	24.01

[a]Ref. 32, I = 0.1 M KNO_3; [b]Refs. 26,30,33, I = 0.1 M KNO_3; [c]Ref. [31]; [d]Protonation over two steps; [e]Determined by ^{31}P NMR titration

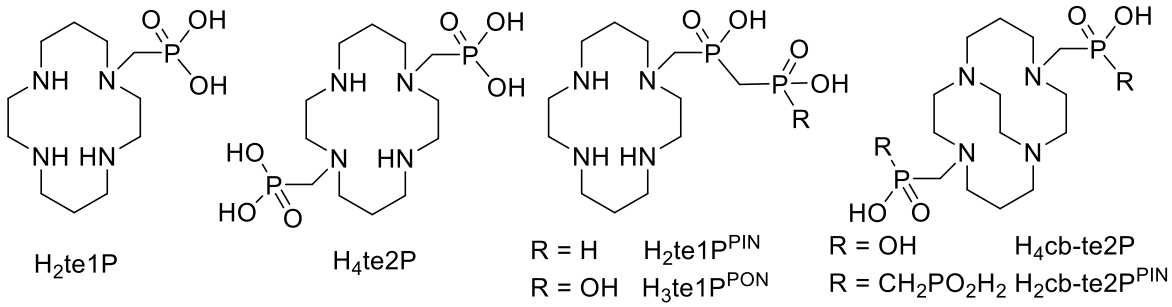

Chart 2. Related cyclam-based ligands

The free bis(phosphonate) group interacted with other metal ions present in solution. This interaction is important for complex speciation in body fluids. The macrocyclic Cu^{II} complex also enables us to investigate its ternary complexes (in which Cu^{II} ion is bound inside the macrocyclic cavity) as any transmetallation can be ruled out due to its high thermodynamic stability and selectivity, as well as kinetic inertness (see below). Thus, we studied ternary complexes of the Cu^{II}-te1P^{BP} with Cu^{II}, Zn^{II}, Ca^{II} and Mg^{II} ions.

After our statistical treatment of the experimental data, were generated rich chemical models with 1:1, 1:2 and 2:1 (Cu^{II}-te1P^{BP}-to-M^{II} ratio) species (Tables 2, S4 and S5) and found various protonated and hydroxido species. As in other simple bis(phosphonates), the {M[Cu(L)]} species, in which one bis(phosphonate) binds one metal ion, shows a high stability, whereas coordination of the second bis(phosphonate) molecule or metal ion in {M[Cu(L)]$_2$} and {M$_2$[Cu(L)]} species, respectively, is significantly weaker (Tables 2, S4 and S5).

The complexes are bound to bones *in vivo*. However, speciation is crucial for their pharmacokinetics. The *in-cage* Cu^{II}-te1P^{BP} complex should circulate in body fluids in the form of Ca^{II} and Mg^{II} ternary complexes given the high concentration of the Ca^{II} and Mg^{II} ions. However, the significant abundance of the ternary complex with Zn^{II} may be also expected in regions with a high Zn^{II} concentration. Conversely, other biogenic metal ions – Cu^{II} and Fe^{III} –

are not present in body fluids in the free form and, thus, their ternary complexes cannot be formed. By comparison with previously published results, the *in-cage* Cu^{II}-cyclam complex does not significantly alter the coordination properties of the bis(phosphonate) group and, thus, the speciation of the Cu^{II}-te1P^{BP} complex in body fluids is likely similar to that of "simple" bis(phosphonates).[26] The example of the distribution diagram of the ternary Cu^{II}-te1p^{BP} – Ca^{II} system (Figure 2C) shows the significant abundance of ternary species, even at a 1:1 Ca-to-{Cu^{II}-te1P^{BP}} ratio. Ternary species with Ca^{II} are predominantly monoprotonated at physiological pH.

Table 2. Consecutive stability constants, log*K*, of equilibria in the *in-cage* Cu^{II}-te1p^{BP} systems with divalent metal ions (*I* = 0.1 M NMe_4Cl, 25 °C); the full set of overall stability constants and protonation constants of the ternary complexes is given in Tables S4 and S5, respectively.

Equilibrium[a]	Cu^{II}	Zn^{II}	Ca^{II}	Mg^{II}
M + [Cu(L)] → {M[Cu(L)]}	15.19	13.56	7.15	7.89
M + {M[Cu(L)]} → {M_2[Cu(L)]}	5.39	4.98	4.67	4.04
[Cu(L)] + {M[Cu(L)]}→ {M[Cu(L)]$_2$}	8.31	7.43	4.33	–

[a]Charges are omitted

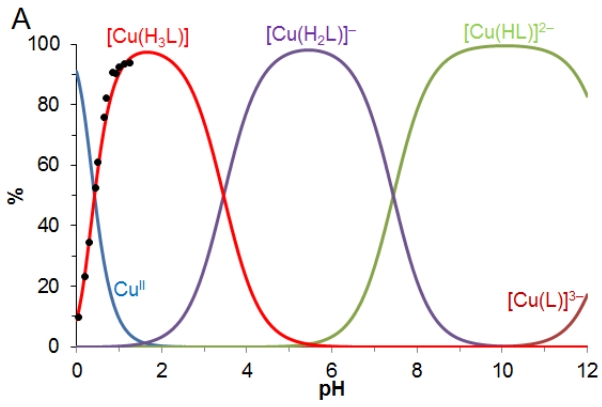

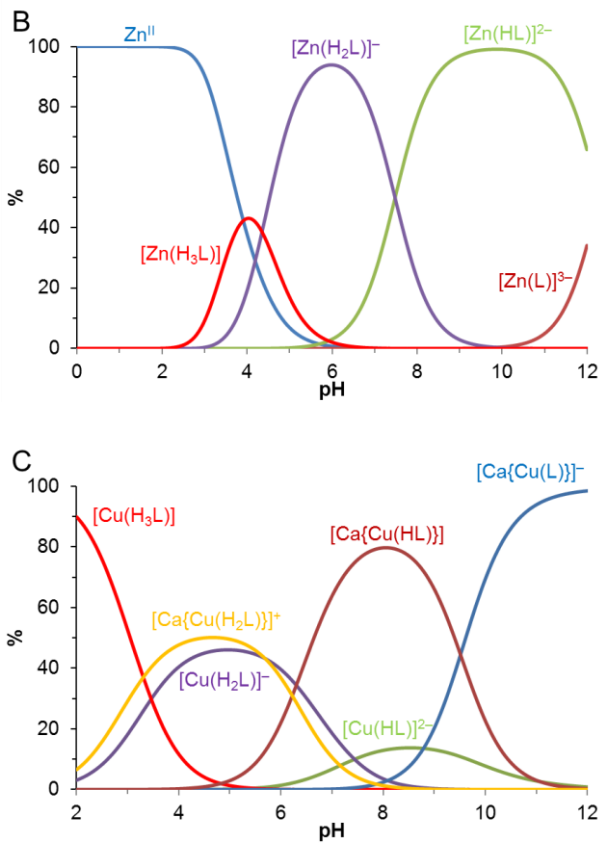

Figure 2. Distribution diagrams of Cu^{II}-te1P^{BP} (**A**, absorbance at 580 nm is shown as black dots) and Zn^{II}-te1P^{BP} (**B**) binary systems (c_M = c_L = 4 mM) and of the {Cu^{II}-te1P^{BP}}–Ca^{II} ternary system (**C**; c_{CuL} = c_{Ca} = 4 mM, only 1:1 species are shown for clarity); I = 0.1 M $(NMe_4)Cl$, 25 °C

Cu^{II} complex formation kinetics

Radioisotope activity decreases over time. For this reason, the complexation rate is one of the key parameters in developing metal-based radiopharmaceuticals. Cu^{II}-te1p^{BP} complexation kinetics was hence studied by UV-VIS spectroscopy.

Macrocyclic complexes with coordinating pendant arms are generally formed in two steps. An *out-of-cage* complex (indicated in the formulas below with superscript "oc") is immediately formed in the first equilibrium step. In this complex, donor atoms of the pendant arms are coordinated to the metal ion, two macrocyclic amines are protonated, and the protons

consequently block the macrocyclic cavity. In the next (rate-determining) step, nitrogen atoms of the macrocycle are deprotonated, and the metal ion is simultaneously transferred to the macrocyclic cavity, forming the final *in-cage* complex (indicated in the formulas below with superscript "ic").

Bis(phosphonate) is a strongly complexing pendant group. Concurrently, H_4te1P^{BP} behaves similarly to other ligands bearing bis(phosphonate) or to other strongly complexing side groups in the pendant arm(s). Recently, we have shown that these ligands form different types of the *out-of-cage* complexes under ligand *vs.* metal ion excesses.[17,34] Cu^{II} complexes with the bis(phosphonates) are quantitatively formed at pH > 3.5 in milimolar concentrations, even at equimolar amounts.[26] Accordingly, the 1:1 *out-of-cage* complex $[M(L)]^{oc}$ was quantitatively formed over the entire pH range (3.5–5.5), and the *in-cage* complex was formed in an isomerisation process with first-order kinetics (Figure S3).

In addition, bis(phosphonates) formed both dinuclear complexes $[M_2(L)]^{oc}$ and complexes with two coordinated ligands $[M(L)_2]^{oc}$ under a metal and ligand excess, respectively (see also Table 2).[26] The reaction rates under the metal ion excess significantly differed from the rates under a ligand excess (Figure 3), thus confirming the presence of *out-of-cage* species with different stoichiometries, as mentioned above. The overall system is described in Scheme 1, and the complexation rate can be expressed as a sum of contributions of all *out-of-cage* intermediates to the overall transformation into the *in-cage* complex (Equation 1, where different protonation states of the ligand in the *out-of-cage* complexes are not explicitly shown)

$$\frac{\mathrm{d}[\mathrm{ML}]^{\mathrm{ic}}}{\mathrm{d}t} = {}^{\mathrm{f}}k_2 \cdot [\mathrm{L}]_{\mathrm{tot}} \cdot [\mathrm{M}]_{\mathrm{tot}} = {}^{\mathrm{f}}k_{\mathrm{ML}} \cdot [\mathrm{M(L)}]^{\mathrm{oc}} + {}^{\mathrm{f}}k_{\mathrm{ML2}} \cdot [\mathrm{M(L)_2}]^{\mathrm{oc}} + {}^{\mathrm{f}}k_{\mathrm{M2L}} \cdot [\mathrm{M_2(L)}]^{\mathrm{oc}} \quad (1)$$

where ${}^{f}k_2$ is a second-order rate constant of the bimolecular reaction, $[L]_{tot}$ and $[M]_{tot}$ are the overall concentrations of the ligand and metal ion, respectively, and ${}^{f}k_{ML}$, ${}^{f}k_{ML2}$ and ${}^{f}k_{M2L}$ are the formation rates constants for the transformation of the corresponding *out-of-cage* complexes. Equation 1 was combined with equations for the conditional stability constants of the *out-of-cage* species, K_{M2L} and K_{ML2}, and with metal and ligand mass balance equations (Equations S1–S4). The data were treated to meet the minimization criterion for the overall fit (for a detailed description of the equations, see SI). The observed reaction rates as a function of metal and ligand concentrations were treated separately for each pH (Figure 3). The rate constants (${}^{f}k_{ML}$, ${}^{f}k_{ML2}$ and ${}^{f}k_{M2L}$) and stability constants (K_{ML2} and K_{M2L}) are outlined in Table S6.

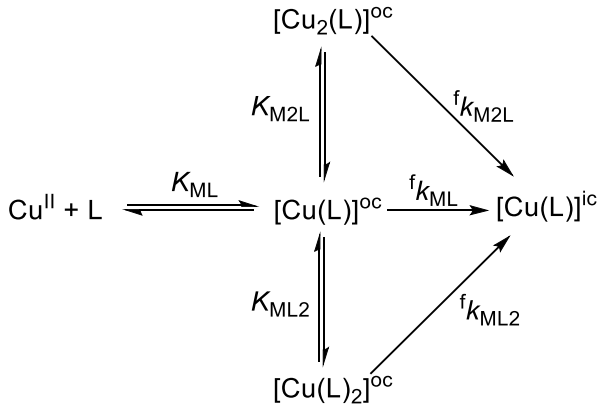

Scheme 1. Simplified mechanism of complexation in the Cu^{II}-H_5te1P^{BP} system, which does not explicitly show different protonation of ligands in the *out-of-cage* complexes; charges are omitted for simplicity. The overall complexation rate is described in Equation 1.

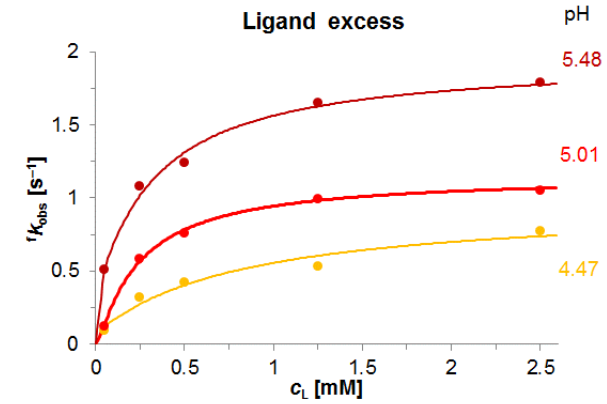
Ligand excess
pH
5.48
5.01
4.47
$^{f}k_{obs}$ [s^{-1}]
c_L [mM]

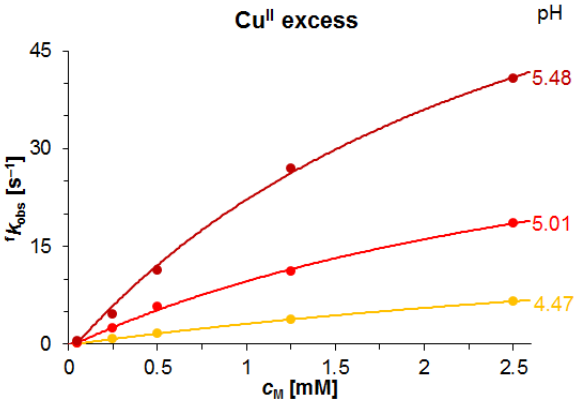
Cu^{II} excess
pH
5.48
5.01
4.47
$^{f}k_{obs}$ [s^{-1}]
c_M [mM]

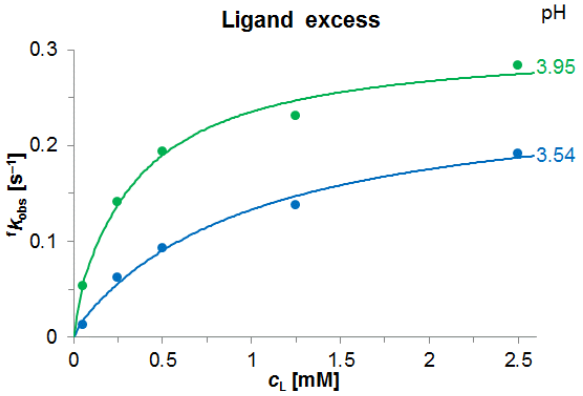
Ligand excess
pH
3.95
3.54
$^{f}k_{obs}$ [s^{-1}]
c_L [mM]

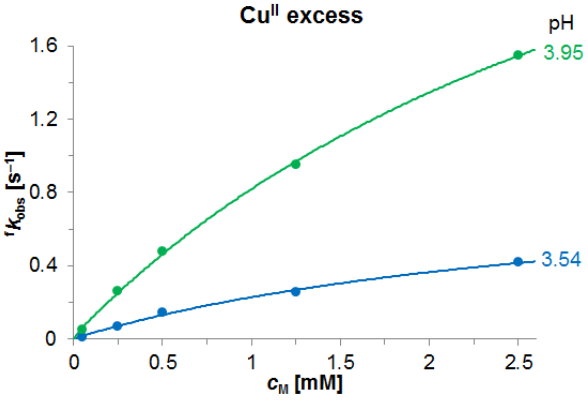
Cu^{II} excess
pH
3.95
3.54
$^{f}k_{obs}$ [s^{-1}]
c_M [mM]

Figure 3. Observed formation rate constants (I = 0.1 M KCl, 25 °C) as a function of ligand (left, c_M = 0.05 mM) or Cu^{II} (right, c_L = 0.05 mM) concentrations; the lines represent the best fits using Equations 1, S1 and S2 and the parameters given in Table S6.

The conditional stability constants K_{ML2} and K_{M2L} show negligible changes with the pH (see Table S6). The coordination of the second ligand molecule is stronger than that of the second metal ion, in line with the potentiometry results of Cu^{II} ion binding to the free bis(phosphonate) group of the pre-formed *in-cage* complex (see above, Table 2).

The rate-determining step in the complexation by macrocyclic ligands is deprotonation of the macrocyclic amines followed by metal ion transfer to the macrocyclic cavity. Therefore, formation rate constants usually show significant changes with pH. Such a phenomenon was also identified in the constants ${}^{f}k_{ML}$, ${}^{f}k_{ML2}$ and ${}^{f}k_{M2L}$ (Figure S4 and Table S6). Their non-linear shape as function of pH (Figure S4) is similar to the trend previously reported for the complexation of Eu^{III} ions with the analogous dota-like ligand H_8do3aP^{BP} (Chart 1), showing that each *out-of-cage* complex, [M(L)], [M_2(L)] and [M$(L)_2$], is present in two differently protonated forms. Thus, each constant, ${}^{f}k_{ML}$, ${}^{f}k_{ML2}$ and ${}^{f}k_{M2L}$, is expressed by Equation 2

$$ {}^{f}k_{M_xL_y} = \frac{({}^{OH}k_{M_xL_y} \cdot \frac{K_w}{[H^+]}) + ({}^{OH}k_{M_xHL_y} \cdot \frac{K_w}{{}^{H}K_{M_xL_y}})}{1 + \frac{[H^+]}{{}^{H}K_{M_xL_y}}} \qquad (2) $$

where ${}^{OH}k_{MxLy}$ and ${}^{OH}k_{MxHLy}$ are the rate constants of the specific OH^--dependent reaction pathways involving two differently protonated species, and ${}^{H}K_{MxLy}$ are the corresponding dissociation constants (for a detailed description of the equations, see SI). The suggested overall mechanism is described in Scheme 2.

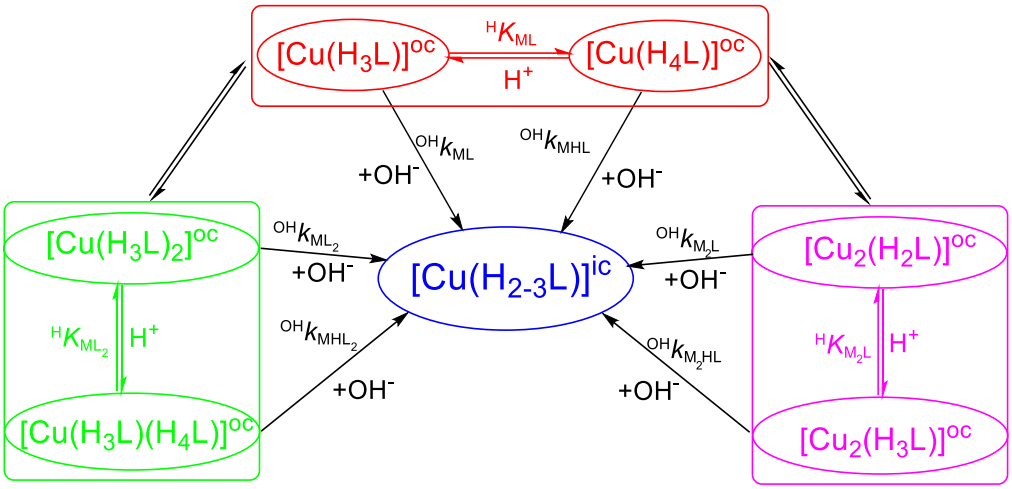

Scheme 2. Expected pathways of the *out-of-cage*-into-*in-cage* complex transformations in the Cu^{II}-H_5te1P^{BP} system; the overall complexation rate is described by Equation 2.

The results from fitting the constants $^{f}k_{ML}$, $^{f}k_{ML2}$ and $^{f}k_{M2L}$ to Equation 2 are summarized in Table 3 and Figure S4. Because the system is highly complicated and cannot be fully evaluated, we can only speculate about the mechanism. Two key factors nevertheless affect the overall *out-of-cage*-to-*in-cage* conversion rate – the strength of the Cu^{II}-bis(phosphonate) interaction and the efficiency of proton removal from the macrocyclic nitrogen atoms.

The dissociation constants pK_a of the *out-of-cage* complexes lie in the 3.5–4.5 range (Table 3), which is typical of the protonation of coordinated phosphonates in their complexes.[27] The comparison of the pK_a with protonation constants determined by potentiometry indicates that the constants likely correspond to the following equilibria (charges are omitted): $[Cu(H_3L)]\leftrightarrow[Cu(H_4L)]$, $[Cu(H_3L)_2]\leftrightarrow[Cu(H_3L)(H_4L)]$ and $[Cu_2(H_2L)]\leftrightarrow[Cu_2(H_3L)]$ (in the last equilibrium, the ligand protonation state is lower because the chelation of two metal ions efficiently repels proton(s) from the bis(phosphonate moiety)). In the species, each ligand molecule is diprotonated on the macrocyclic nitrogen atoms, and the remaining protons are bound to the bis(phosphonate) groups.

The $[ML]^{oc}$ intermediate shows the slowest conversion into the *in-cage* complex. Other two intermediates are more reactive. $[ML_2]^{oc}$ conversion is ~3–4-times faster than $[ML]^{oc}$

conversion because the neighboring second ligand molecule facilitates proton transfer from the macrocycle cage to the bulk solution. This acceleration is even stronger in $[M_2L]^{oc}$ intermediates, whose re-arrangement is two orders of magnitude faster than that of $[ML]^{oc}$, most likely due to the weaker binding of the second Cu^{II} ion in the intermediate. As a result, in this intermediate, the metal ion is more easily transferred from the bis(phosphonate) group to the macrocyclic cavity.

The rate constants of the more protonated forms of the intermediates, $^{OH}k_{MxHLy}$, are one order of magnitude higher than those of the deprotonated forms, $^{OH}k_{MxLy}$. This difference should also be related to the strength of Cu^{II} binding to the bis(phosphonate) group, which is weaker in the protonated intermediate and thus enables its transfer to the macrocycle cage. However, bis(phosphonates) are known to easily form coordination polymers both in the solid-state and in solution.[35,36] Therefore, the actual system is surely more complicated and our interpretation inherently entails simplification.

Table 3. Kinetic and thermodynamic parameters of Cu^{II}-H_5te1P^{BP} complex formation according to Scheme 2 and Equation 2

Second-order rate constant	$^{OH}k_{MxLy}$ [s^{-1} M^{-1}]	$^{OH}k_{MxHLy}$ [s^{-1}]	K_{MxLy} [M] (pK_a)
$^{f}k_{ML}$	$(1.2\pm0.2)\cdot10^{8}$	$(1\pm2)\cdot10^{9}$	$(2\pm5)\cdot10^{-4}$ (3.7)
$^{f}k_{M2L}$	$(1.8\pm0.4)\cdot10^{10}$	$(1.3\pm0.3)\cdot10^{11}$	$(3\pm1)\cdot10^{-5}$ (4.5)
$^{f}k_{ML2}$	$(3\pm1)\cdot10^{8}$	$(7.3\pm0.3)\cdot10^{9}$	$(7\pm4)\cdot10^{-5}$ (4.2)

Due to its complexity, the Cu^{II}-H_5te1P^{BP} system was directly compared with other ligands only in the terms of overall reaction times. Figure 4 and Table S7 show the times required for 99% complexation at a 10-fold metal ion excess for cyclam-based ligands with phosphonate and phosphinate pendant arms. Cu^{II} complexation with H_5te1P^{BP} under a metal ion excess is

the fastest among cyclam phosphonate/ phosphinate derivatives, presumably thanks to the appropriate stability of the *out-of-cage* reaction intermediate. This stability is sufficient to reach a quantitative formation of the *out-of-cage* species. Conversely, the stability of the *out-of-cage* species is not high enough to block the metal ion transfer from the bis(phosphonate) group to the macrocyclic cavity. Another reason for such a fast complexation could be the efficient proton transfer from the macrocycle nitrogen atoms to bulk water. This proton transfer may be assisted by the phosphinato-bis(phosphonate) pendant arm, which can easily form hydrogen bonds (the solid-state structure of the ligand zwitterion is shown above).

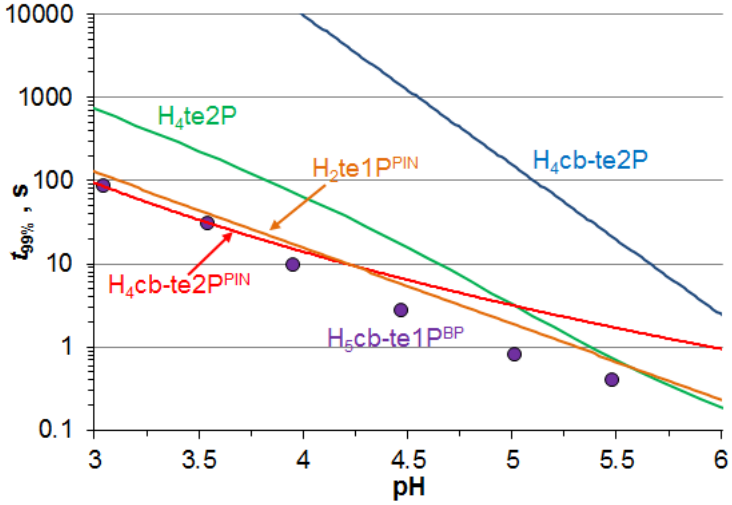

Figure 4. Comparison between the 99% complexation times (c_L = 0.05 mM, c_{Cu} = 0.5 mM, 25 °C) of H_5te1P^{BP} (violet dots), H_4cb-te2P (blue, ref. 37), H_4cb-te2P^{PIN} (red, ref. 37), H_2te1P^{PIN} (brown, ref. 31; corresponding to the initially formed *in-cage* complex) and H_4te2P (green, ref. 30).

Cu(II) complex dissociation kinetics

For radiomedicinal applications, complexes should have high kinetic inertness to avoid their dissociation and non-specific deposition of metal ions in tissues. As mentioned above, the pentacoordinated isomer of Cu^{II}-te1P^{BP} is formed during complexation under mild conditions. This isomer should also be the species formed during radiolabeling. For this reason, we studied

acid-assisted dissociation of the pentacoordinated Cu^{II}-te1P^{BP} isomer by UV-VIS in 1–5 M $HClO_4$.

The dissociation kinetics follows the first-order rate law, as shown by the reaction rate constants, ${}^{d}k_{obs}$, displayed in Figure 5. The saturation shapes of the curves indicate that the complex is present in two forms with different protonation states. $[Cu(H_3L)]^{+}$ is a thermodynamically stable species and, thus, protonation leads to $[Cu(H_4L)]^{2+}$. The data treatment showed that $[Cu(H_4L)]^{2+}$ is the only kinetically active species. Therefore, the observed dissociation rate constant is expressed by Equation 3

$$ {}^{d}k_{obs} = \frac{{}^{d}k \cdot K_H \cdot [H]}{1 + K_H \cdot [H]} \quad (3) $$

where ${}^{d}k$ is the dissociation rate constants of $[Cu(H_4L)]^{2+}$ species, and ${}^{d}K_H$ is the consecutive protonation constant of its formation (Scheme 3). After determining the ${}^{d}k$ and K_H values, outlined in Table 4, the analysis of temperature-dependent data provided the activation parameters (Table 5). The activation parameters and the dissociation half-lives are almost the same as those previously reported for related pentacoordinated Cu^{II} complexes with phosphinato-phosphonate pendant arms.[30] This similarity shows that the bis(phosphonate) group plays a minor role in the dissociation process. The dissociation half-lives of the Cu^{II}-te1P^{BP} are one order of magnitude longer than those reported for the cyclam *trans*-diphosphonate complex Cu^{II}-te2P.[31]

$$ [Cu(H_3L)] \underset{}{\overset{K_H}{\rightleftharpoons}} [Cu(H_4L)] \xrightarrow{{}^{d}k} Cu^{2+} + H_xL $$

thermodynamically stable species

Scheme 3. Dissociation mechanism of the Cu^{II}-te1P^{BP} complex

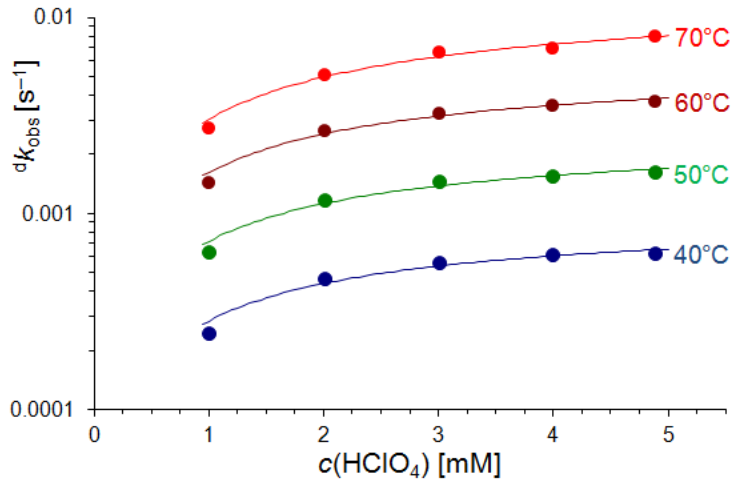

Figure 5. Dissociation rate constants $^{d}k_{obs}$ as function of acid concentration (c_{CuL} = 0.5 mM); the lines represent the best fits according to Equation 3

Table 4. Kinetic parameters of the acid-assisted decomplexation of Cu^{II}-te1P^{BP} complex

Parameter	40 °C	50 °C	60 °C	70 °C
^{d}k [s^{-1}]	$(1.0 \pm 0.1)\cdot10^{-3}$	$(2.6 \pm 0.2)\cdot10^{-3}$	$(5.9 \pm 0.6)\cdot10^{-3}$	$(1.4 \pm 0.2)\cdot10^{-2}$
K_H [M^{-1}]	0.4 ± 0.1	0.39 ± 0.09	0.37 ± 0.08	0.28 ± 0.7
$^{d}k_H$ [M$^{-1}\cdot$s^{-1}]	$0.4\cdot10^{-3}$	$1.01\cdot10^{-3}$	$2.18\cdot10^{-3}$	$3.92\cdot10^{-3}$

Table 5. Activation parameters of acid-assisted dissociation and dissociation half-lives of pentacoordinated isomers of the Cu^{II}-te1p^{BP} complex and related complexes

Parameter	Cu^{II}-te1P^{BP}	Cu^{II}-te1P^{PON}	Cu^{II}-te2P
	This work	Ref. 31	Ref. 30
E_A [kJ mol^{-1}][a]	79.1 ± 0.1	81	72; 85[d]
$\Delta H^{\#}$ [kJ mol^{-1}][b]	76.3 ± 0.8	78	70; 82[d]
$\Delta S^{\#}$ [J K^{-1} mol^{-1}][b]	–59 ± 3	–61	–71; –52[d]
ΔH [kJ mol^{-1}][c]	–9 ± 3	–13.6	–8.3
ΔS [J K^{-1} mol^{-1}][c]	–36 ± 12	–36	–23

$t_{1/2}$ (1 M $HClO_4$, 70 °C)	3.5 min	2.9 min	0.6 min
$t_{1/2}$ (1 M $HClO_4$, 25 °C)	2.7 h	3.3 h	0.3 h

[a]Arrhenius model: $\ln(^{d}k) = -(E_A/RT) + \ln A$. [b]Eyring model: $\ln(^{d}k/T) = -(\Delta H^{\#}/RT) + \Delta S^{\#}/R) + \ln(k_B/h)$. [c]$\ln K = -(\Delta H/RT) + \Delta S/R)$. [d]Data for two dissociation pathways

Sorption on hydroxyapatite

Hydroxyapatite is the major inorganic component of bone tissue and interacts with bis(phosphonates). Thus, sorption on hydroxyapatite is used as an *in-vitro* model. Our sorption experiments performed at pH = 7.4 showed that sorption is fast and efficient (Figures S6 and S7). When using 0.3 μmol of Cu^{II}-te1P^{BP}, the complex is quantitatively adsorbed on ~100 mg of hydroxyapatite, and equilibrium is reached in a few minutes. These values are comparable with data previously published for lanthanide(III) complexes of analogous bis(phosphonate)-bearing dota-like ligands.[6,38]

Radiolabeling

H_5te1P^{BP} radiolabeling with [^{64}Cu]$CuCl_2$ was performed in 0.1 M MES buffer (pH 5.5) at room temperature. Under these conditions, ligand labeling was fast and efficient, and quantitative labeling was reached at room temperature within 30 min, similarly to labelling with ligand H_2te1P^{PIN} bearing bis(phosphinate) pendant arms and its derivatives.[31,39] These excellent labeling properties are in line with the very fast complex formation described above. Moreover, the [^{64}Cu]Cu^{II}-te1P^{BP} tracer was obtained with a high specific activity of approximately 30 GBq/μmol of the ligand, which is a desirable property considering its potential applications.

Small animal PET imaging

After intravenously injecting [^{64}Cu]Cu^{II}-te1P^{BP} into healthy mice, small-animal PET showed bone-selective accumulation of the radiotracer, which plateaued 30−60 minutes later and

remained stable with a high target-to-background ratio for at least 24 h (Figure 6). The [^{64}Cu]Cu^{II}-te1P^{BP} tracer showed rapid blood clearance and elimination through the renal pathway within 30 min. This low extra-osseous accumulation and rapid elimination of the non-bound fraction of [^{64}Cu]Cu^{II}-te1P^{BP} through the kidneys is typical of bis(phosphonate) pharmaceuticals.[40,41]

[^{64}Cu]Cu^{II}-te1P^{BP} is unlikely to be metabolized and should be excreted unchanged based on our previous findings[39] although further research is required to confirm these assumptions. Nevertheless, [^{64}Cu]Cu^{II}-te1P^{BP} did not accumulate or, more specifically, show any activity in mouse liver. This observation indicates the high stability of [^{64}Cu]Cu^{II}-te1P^{BP} and its resistance to *in vivo* transchelation to liver proteins (such as superoxide dismutase) – a frequently observed metabolic fate of ^{64}Cu^{II}-labeled compounds, particularly in rodents, which is accompanied by ^{64}Cu trapping in the liver.[42-44]

The highest skeletal uptake of [^{64}Cu]Cu^{II}-te1P^{BP} in mice (Figure 6B) was detected in the distal ends of tubular bones (epiphyses), as well as in vertebral bodies, maxilla, and mandible (mean SUV 7.13). In the most proximal regions of the tubular bones, uptake was considerably lower (mean SUV 0.73), thus suggesting that [^{64}Cu]Cu^{II}-te1P^{BP} preferentially accumulates in skeletal regions with a high metabolic turnover, presumably at active sites of osteoblastic and/or osteoclastic bone remodeling. Similar bone region selectivity has also been reported for other radiolabeled bis(phosphonates), such as [^{99m}Tc]Tc-MDP and [^{99m}Tc]Tc-hydroxy-ethylidene-diphosphonate ([^{99m}Tc]Tc-HEDP), with evidence of [^{99m}Tc]Tc-MDP uptake in mature osteoblasts.[45,46]

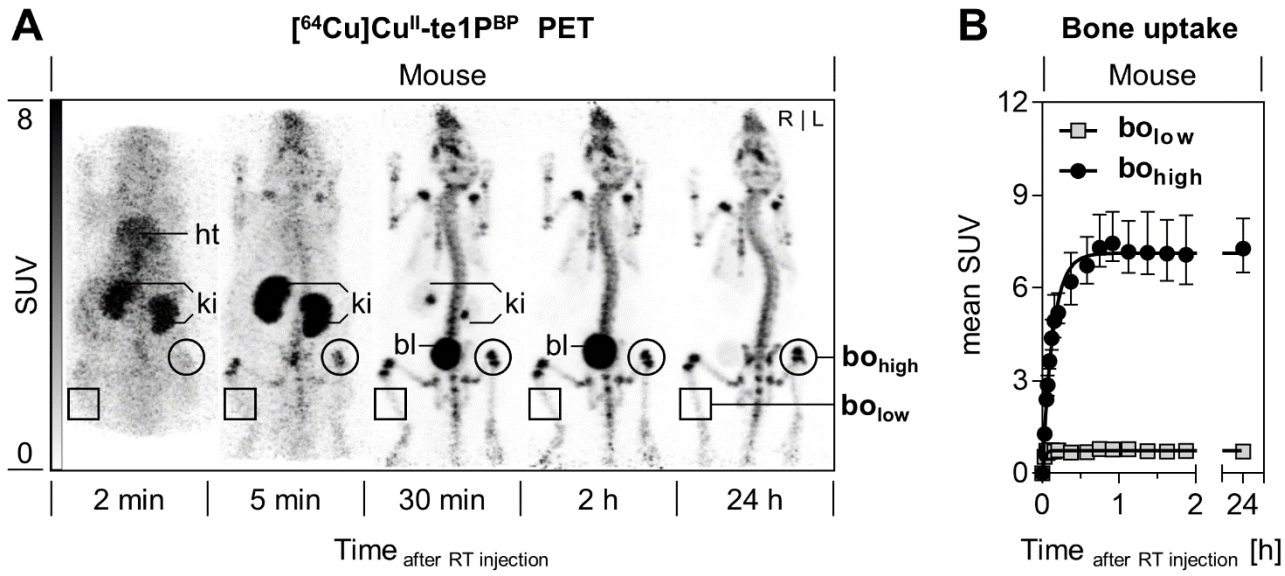

Figure 6. Dynamic PET imaging of [^{64}Cu]Cu^{II}-te1P^{BP} in mice: the tracer shows rapid renal excretion and efficient skeletal uptake (**A**), plateaus between 30 and 60 min after injection and remains stable for 24 h (**B**). Description: (bo$_{high}$) skeletal regions with the highest bone uptake; (bo$_{low}$) skeletal regions with the lowest bone uptake; (ht) heart; (ki) kidney; (bl) bladder; (SUV) standardized uptake value; (RT) radiotracer; (L) left; (R) right.

After intravenously injecting [^{64}Cu]Cu^{II}-te1P^{BP} in rats, we observed an uptake pattern similar to that identified in mice by small-animal PET (Figure 7). Concurrently, the muscle region selectivity of [^{64}Cu]Cu^{II}-te1P^{BP} in rats (Figure 7A) matched that of [^{18}F]fluoride, which was recorded three days earlier in the same animals (Figure 7B). Since [^{18}F]fluoride preferentially binds to bone minerals deposited by osteoblasts,[47,48] [^{64}Cu]Cu^{II}-te1P^{BP} selectivity for skeletal regions with high bone remodeling may underlie similar physiological mechanisms. Furthermore, both [^{64}Cu]Cu^{II}-te1P^{BP} and [^{18}F]fluoride uptake was higher in critical bone defect regions of the right femur (16 weeks after surgery) than in healthy reference regions of the left femur (Figure 7C). Bone defects supported with an absorbable hemostatic gelatin sponge and unsupported bone defects showed similar [^{64}Cu]Cu^{II}-te1P^{BP} uptake in this pilot experiment

(data not shown). Combined, these observations underscore the usefulness of [^{64}Cu]Cu^{II}-te1P^{BP} as a potential PET radiotracer for bone healing evaluation in preclinical and clinical settings with a diagnostic value equivalent to that of [^{18}F]fluoride.

Given that ^{64}Cu has a longer half-life (12.7 h) than ^{18}F (1.8 h), with virtually the same maximum positron energy (^{18}F, 0.634 MeV; ^{64}Cu, 0.653 MeV), [^{64}Cu]Cu^{II}-te1P^{BP} enables long observation times during longitudinal studies at the same resolution. In turn, differences in standard uptake values most likely reflect pharmacokinetic differences between [^{64}Cu]Cu^{II}-te1P^{BP} and [^{18}F]fluoride. Moreover, Cu^{II}-te1P^{BP} labeled with either ^{64}Cu or the beta-minus particle-emitting ^{67}Cu can be considered a 'matched pair'. Therefore, such a matched pair may be clinically applied in both bone tumor and metastasis imaging and treatment.

In the present experimental settings, the field of view allowed us to perform whole-animal scans in mice and pelvic scans in rats. When directly comparing the species, clear differences were found only in the lower urinary tract, with a high accumulation of [^{64}Cu]Cu^{II}-te1P^{BP} in rat ureters. Mineral deposits in the form of calcium phosphate in the lower urinary tract of aged rats may account for this finding. [49]

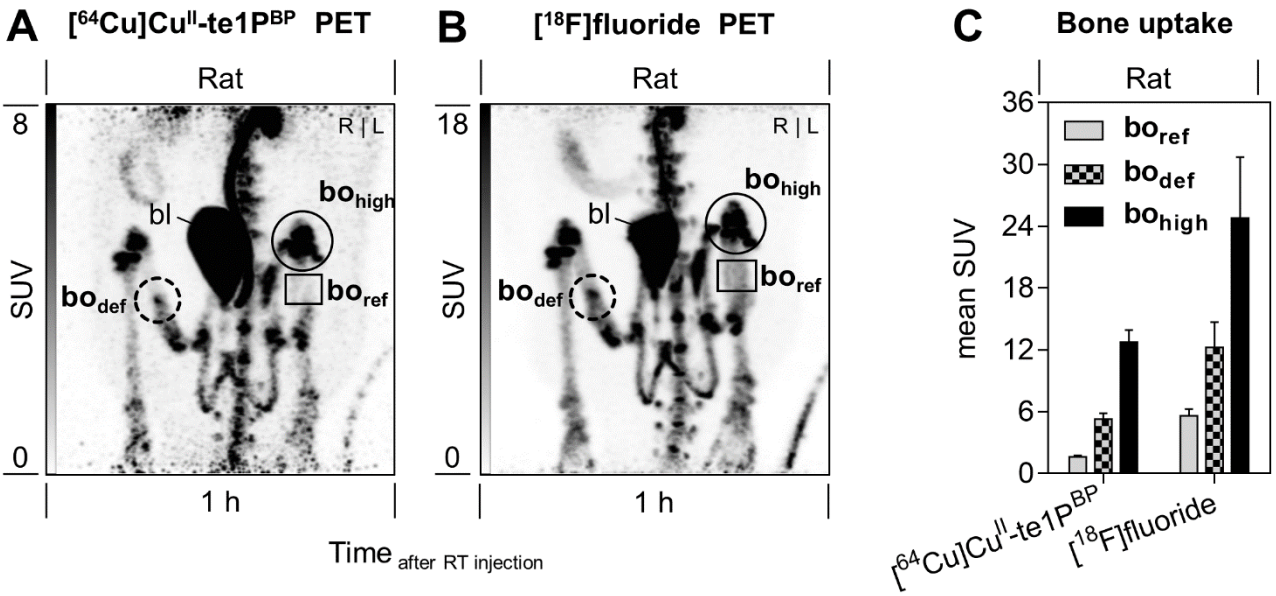

Figure 7. Comparison between [^{64}Cu]Cu^{II}-te1P^{BP} (**A**) and [^{18}F]fluoride (**B**) in the same rats; static PET imaging of a critical bone defect in rats 1 h after injection (**A**, **B**) and bone uptake (**C**); description: (bo_{def}) critical bone defect in the right femur; (bo_{ref}) healthy bone reference region in the left femur; (bo_{high}) skeletal regions with the highest bone uptake; (bl) bladder; (SUV) standardized uptake value; (RT) radiotracer; (L) left; (R) right

Conclusions

Our ligand, H_5te1P^{BP}, combining cyclam with a phosphinate-bis(phosphonate) pendant, shows high macrocycle basicity and thermodynamic selectivity for Cu^{II} over Ni^{II} and Zn^{II} ions. The Cu^{II}-te1P^{BP} complex is highly thermodynamically stable and highly kinetically inert. The complex forms almost immediately in a milimolar scale at pH > 5. The properties of the bis(phosphonate) group do not change near the macrocyclic moiety because the bis(phosphonate) group is not coordinated to the metal ion in the macrocyclic cavity. Thus, the Cu^{II}-te1P^{BP} complex binds to other metal ions in solution as do other bis(phosphonates), which is important for *in-cage* complex speciation in body fluids. Moreover, the bis(phosphonate) group is fully available for interaction with bone surfaces, and the Cu^{II}-te1P^{BP} complex is

efficiently adsorbed on both hydroxyapatite *in vitro* and bone tissue *in vivo*. H_5te1P^{BP} radiolabeling with [^{64}Cu]$CuCl_2$ is fast and efficient, with high specific activities. [^{64}Cu]Cu^{II}-te1P^{BP} shows excellent properties for imaging active bone compartments and a high uptake in critical bone defect regions, thus demonstrating its high potential as a longer living surrogate of [^{18}F]fluoride for bone healing evaluation in preclinical and clinical settings. This chelator also has a theranostics potential because therapeutic ^{67}Cu can be used for bone metastasis treatment. Overall, thanks to its combined properties, H_5te1P^{BP} is an excellent candidate for radiomedicinal applications.

Experimental

General

All commercially available starting materials were used without further purification. Tris(trifluoroacetyl)cyclam **1**[24] and bis(phosphonate)-phosphinate reagent **28**[8] were synthesized according to previously published procedures. Characterization ^{1}H (400 MHz), ^{13}C (100 MHz) and ^{31}P (161 MHz) NMR spectra were acquired at 25 °C on a Bruker 400 Avance spectrometer. Whenever required, NMR experiments were conducted at a higher temperature on a Varian S300 to measure ^{1}H (300 MHz) and ^{31}P (121 MHz) NMR spectra. All NMR measurements were performed in D_2O. For ^{1}H and ^{13}C NMR measurements, the methyl signal of *t*-BuOH was used as an internal standard (δ = 1.2 and 31.2 ppm for ^{1}H and ^{13}C NMR, respectively); ^{31}P NMR spectra were referenced to external 85% H_3PO_4 (δ = 0.0 ppm). All values of chemical shifts are given in ppm, and the coupling constants in Hz. ESI-MS spectra were recorded on a Bruker Esquire 3000 spectrometer with ion-trap detection in negative or positive modes. Merck aluminum foils with silica gel 60 F_{254} were used for TLC. ^{64}Cu was produced in a TR-FLEX cyclotron (Helmholtz-Zentrum Dresden-Rossendorf) by a ^{64}Ni(p,n)^{64}Cu nuclear reaction, giving specific activities of 500 GBq μM^{-1} Cu diluted in aqueous HCl (10 mM). Chelator radiolabeling was monitored by radio-TLC (ITLCSA-glass microfiber chromatography paper

impregnated with silicagel, Agilent Technologies, Lake Forest, CA, USA) and assessed on a radioactivity thin-layer analyzer (Rita Star, Raytest). Radioactivity was counted on an ISOMED 2010 (Nuklear-Medizintechnik Dresden GmbH).

Synthesis

Compound 3: $(CH_2O)_n$ (300 mg, 10.0 mmol, 2.5 equiv.) and pyridine hydrobromide (1.28 g, 8.0 mmol, 2.0 equiv.) were added to a solution of triprotected cyclam **1** (1.95 g, 4.0 mmol) and phosphinate-bis(phosphonate) reagent **2** (1.58 g, 4.0 mmol, 1.0 equiv.) in dry pyridine (30 mL). The mixture was heated to 40 °C and stirred under argon atmosphere, showing complete conversion in ^{31}P NMR after 18 h. The pyridine was evaporated in vacuum, and the residue was dissolved in chloroform (40 mL) and extracted with water (2 × 40 mL). The organic layer was dried over anhydrous Na_2SO_4, the suspension was filtered, and the filtrate was evaporated in vacuum. The crude reaction mixture was purified on a silica gel column (EtOAc/EtOH 12:1, R_f = 0.5), yielding compound **3** (2.82 g, 79 %).

^{1}H-NMR (300 MHz, DMSO-d_6, 90°C) δ 4.13–3.95 (10H, m, 5x CH_3CH_2O), 3.87–3.32 (15H, m), 3.07–2.58 (6H, m), 2.47–1.54 (4H, m), 1.29–1.15 (15H, m, 5xCH_3CH_2O); **^{31}P-NMR** (121 MHz, DMSO-d_6, 90°C) δ 49.7 (1P, bs, PO_2Et), 24.2 (1P, bs, PO_3Et_2), 23.4 (1P, bs, PO_3Et_2); **^{19}F-NMR** (282 MHz, DMSO-d_6, 90°C) δ –67.8 (3F, s, CF_3), –68.3 (6F, s, 2xCF_3); **MS** (+): 895.6 $[M+H]^+$; 917.5 $[M+Na]^+$.

H_5te1P^{BP}: The protected intermediate **3** (1.26 g, 1.4 mmol) was dissolved in aq. HCl (6 M, 40 mL). The reaction mixture was refluxed for 18 h. Volatiles were evaporated in vacuum. The crude reaction product was purified on a strong cation exchange resin (Dowex 50, 150 mL, H^+-form, water elution, followed by 5 % aq. ammonia). The ammonia fraction was evaporated to dryness. The yellow-orange product was dissolved in water (100 mL) and decolorized by a short reflux with active carbon. The solvent was removed, and the product was recrystallized by adding EtOH. The white crystalline material was filtered and dissolved in water (120 mL),

and the solution was lyophilized, yielding a white powder with the following composition: $H_5te1P^{BP}\cdot 5H_2O$ (480 mg, 74 % yield).

^{1}H-NMR (400 MHz, CsOD+D_2O, pD ≥ 12) δ 2.92–2.75 (m, 16H, 8x N–C*H*$_2$), 2.64–2.56 (m, 2H, N–C*H*$_2$–P), 2.16–1.91(m, 3H, P–C*H*–P, P–C*H*$_2$–CH), 1.89–1.82 (m, 2H, CH_2–C*H*$_2$–CH_2), 1.77–1.69 (m, 2H, CH_2–C*H*$_2$–CH_2); **^{13}C{^{1}H}-NMR** (100 MHz, D_2O + CsOD, pD ≥ 12) δ 54.9 (d, 1C, N–*C*H_2, $^3J_{CP}$ = 12 Hz), 54.5 (s, 1C), 53.5 (d, 1C, N–*C*H_2-P, $^1J_{CP}$ = 100 Hz), 50.0 (s, 1C), 49.7 (s, 1C), 46.28 (s, 1C), 46.26 (s, 1C), 46.1 (s, 1C), 44.8 (s, 1C), 36.0 (td, 1C, P–*C*H–P, $^1J_{CP}$ = 116 Hz, $^2J_{CP}$ = 6 Hz), 29.8 (dt, 1C, P–*C*H_2–CH, $^1J_{CP}$ = 88 Hz, $^2J_{CP}$ = 5 Hz), 26.5 (s, 1C, CH_2–*C*H_2–CH_2), 23.7 (s, 1C, CH_2–*C*H_2–CH_2); **^{31}P{^{1}H}-NMR** (121 MHz, D_2O+CsOD, pD ≥ 12) δ 41.1 (1P, t, $^3J_{PP}$ = 21 Hz, *P*O_2H), 19.43 (2P, d, $^3J_{PP}$ = 21 Hz, 2x*P*O_3H_2); **^{31}P-NMR** (121 MHz, D_2O+CsOD, pD ≥ 12) δ 41.7–40.6 (1P, m, *P*O_2H), 20.2-18.8 (2P, m, 2x*P*O_3H_2); **MS** (+): 467.05 $[M+H]^+$; **Elemental analysis**: found (calcd $C_{13}H_{33}N_4O_8P_3\cdot 5H_2O$): C 27.64 (28.06), H 7.29 (7.79), N 10.33 (10.07), P 16.71 (16.70).

Potentiometric titrations

Potentiometry was performed according to previously published procedures; for further details on the preparation of stock solutions and chemicals and on equipment, electrode system calibration, titration procedures and data treatment, see refs. 50,51. Extra HCl (~1 ekv.) was added to the ligand stock solution to fully dissolve the solid ligand zwitterionic form. Throughout the paper, pH means –log[H^+]. Protonation and stability constants were determined in 0.1 M (NMe_4)Cl at 25.0 °C with pK_w = 13.81. The stability constants of the Cu^{II}, Zn^{II} and Ni^{II} complexes were determined by simultaneous treatment of data from three or more parallel out-of-cell (pH range 1.6–5.0, ~20 points per titration) and in-cell (pH range 5.0–12.1, ~30 points per titration) titrations (c_L = c_M = 4 mM). For out-of-cell titrations (starting volume 1 ml), the batches were prepared under an argon stream in tubes with ground joints from the ligand, metal ion and HCl/(NMe_4)Cl stock solutions and water. Then, a known amount of the (NMe_4)OH

stock solution was added under Ar. The tubes were firmly closed with stoppers, and the solutions were equilibrated at room temperature for 1 week.

Solutions of the pre-formed Cu^{II}-te1P^{BP} complex were prepared by mixing stoichiometric amounts of the ligand and Cu^{II} stock solutions in a glass ampoule followed by a slow, portion-wise addition (2 h) of the stock $(NMe_4)OH$ solution (3 equiv.) under Ar. The ampoule was flame-sealed and left at 80 °C overnight to fully form the *in-cage* complex. The ampoule was opened under Ar, and aliquots of the *in-cage* complex solution were transferred into the titration vessel. Water, HCl and stock solutions of $(NMe_4)Cl$ and metal chlorides were added (to reach I = 0.1 M $(NMe_4)Cl$ in the final solution, with 5 mL starting volume, ~0.004 M *in-cage* complex concentration, and 2, 4 or 8 mM additional metal ion concentrations) before performing the in-cell titration (pH range 2.3–12.1, ~60 points per titration).[34]

The titration data were treated using the program OPIUM[52] and selecting the chemical model with the best fit and performance, according to the sum of squares of residuals, standard deviations, chemical meaning and reflecting abundance of species. Species with <10% abundance along the whole pH range were disregarded in all experiments. The full sets of determined constants (and their standard deviations given directly by the program) are shown in ESI (Tables S1 and S2).

UV-VIS titration

UV-VIS spectra of the Cu^{II}-H_5te1P^{BP} system were recorded on a Specord 50 Plus spectrophotometer (Analytik Jena AG) at $c_L = c_{Cu}$ = 4 mM in the pH range 0–1.3. The pH was calculated from the concentration of HCl added to the solutions. The solutions were equilibrated at room temperature for 1 week. The stability of the complex was determined from absorbance at the maximum of the absorption band at 580 nm by simultaneous treatment with potentiometric data using the program OPIUM.[52]

NMR titration

The ^{31}P NMR titration of H_5te1P was performed on a Bruker 400 Avance spectrometer. The samples were prepared in H_2O at a ligand concentration ~4 mmol dm^{-3} in the pH range 12.2–14.1. The pH of the samples was adjusted with aqueous NMe_4OH and calculated from the NMe_4OH concentration. Changes in ^{31}P NMR chemical shifts were evaluated by NMR titration. The data were treated with the program OPIUM.[52]

Formation and dissociation kinetics

Experiments were performed on a Bio Sequential SX-20 stopped-flow spectrophotometer (Applied Photophysics) equipped with a 150-W xenon lamp and with a diode-array accessory detector or on a Specord 50 Plus spectrophotometer (Analytik Jena AG). Formation kinetics were studied under an excess of metal ion (c_L = 0.05 mM, c_{Cu} = 0.05–2.5 mM) or ligand (c_{Cu} = 0.05 mM, c_L = 0.05–2.5 mM), at pH ~ 3.5–5.5, 25 ± 0.1 °C, I = 0.1 M KCl, and a fifty-fold molar excess of the appropriate buffers (chloroacetic acid, acetic acid or 2-(*N*-morpholino)ethanesulfonic acid (MES)). The pH of the solution remained unchanged after the measurement. Dissociation kinetics were analyzed using stock solutions of complexes prepared by mixing equimolar amounts of Cu^{II} and ligand solutions, subsequently adding a NaOH solution to reach pH ~ 5. The measurements were performed at c_{CuL} = 0.1 mM, I = 5.0 M (H,Na)ClO_4 and 40, 50, 60 and 70 ± 0.1 °C. The formation ($^fk_{obs}$) and dissociation ($^dk_{obs}$) rate constants were fitted from the absorbance at 273 nm as function of time using the Pro-KII software (Applied Photophysics) or the Scientist program, version 2.0 (Micromath), with the following general exponential function (Equation 4).

$$A_t = A_f + (A_0 - A_f) \cdot e^{-k_{obs} \cdot t} \quad (4)$$

X-ray diffraction study

Single crystals of $H_5te1P^{BP}\cdot 6H_2O$ were obtained by slow vapor diffusion of EtOH into an aqueous solution of the ligand. Diffraction data were collected at 120 K (Cryostream Cooler, Oxford Cryosystem) on a Bruker D8 VENTURE Kappa Duo PHOTON100 diffractometer with

an IμS micro-focus-sealed tube using Cu-Kα (λ = 1.54178 Å) radiation. Data were analyzed using the SAINT (Bruker AXS Inc.) software package and subsequently corrected for absorption effects using the numerical method (SADABS). The structure was solved using direct methods (SHELXT2014)[53] and refined with full-matrix least-squares techniques (SHELXL2014).[54] The structurally independent unit corresponds to the formula unit. One of phosphonate groups was disordered in two positions, sharing carbon and phosphorus atoms, with oxygen atoms turned in two positions with a relative occupancy of 78:22. Two hydration water molecules were disordered in two close positions, with relative occupancies of 66:34. All non-hydrogen atoms were refined anisotropically. All hydrogen atoms, except those belonging to disordered water molecules, were found in the difference density map. However, hydrogen atoms bound to carbon atoms were fixed in theoretical positions using $U_{eq}(H) = 1.2 \cdot U_{eq}(C)$ to keep the number of parameters low, and only hydrogen atoms bound to nitrogen and oxygen atoms were fully refined (except several hydrogen atoms belonging to some of water molecules, whose bond distances became unrealistically long when fully refined and were, thus, fixed in the original positions of the corresponding electronic maxima). Table S8 outlines selected crystallographic parameters. The complete structural data were deposited to the Cambridge Crystallographic Data Centre under CCDC reference number CCDC-2086453.

Sorption on hydroxyapatite

Hydroxyapatite was suspended in a TRIS-HCl buffer solution (pH = 7.5), and a stock solution of Cu^{II}-te1P^{BP} complex and water was added to reach a complex concentration of 1 mM, a buffer concentration of 0.1 M and a total solution volume of 3 ml. The resulting mixture was gently shaken at 25 °C for the appropriate time. The suspension was filtered through a Millipore syringe filters (0.22 μm), and the concentration of the remaining complex was determined by UV-VIS at 267 nm. Sorption kinetics: *m*(hydroxyapatite) = 50 mg, equilibration time *t* = 10, 30

min and 1, 3, 5, 7, 24, 48 h. Sorption efficiency: *m*(hydroxyapatite) = 10–110 mg, equilibration time *t* = 7 h.

^{64}Cu Radiolabeling

The pH of the non-carrier-added (NCA) [^{64}Cu]$CuCl_2$ solution (50 µL in 0.01 M HCl, 300 MBq) was adjusted to 5.5 by adding 150 µL of 0.1 M MES buffer to a final volume of 200 µL. After adding a solution of 0.5 µg H_5te1P^{BP} in water (50 µL), the reaction mixture was incubated in a thermomixer at 25 °C and 300 rpm. After 30 min of reaction time, the labeling yield was monitored by ITLC (ITLCSA-glass microfiber chromatography paper impregnated with silicagel, Agilent Technologies, Lake Forest, CA, USA; eluent 0.1 M Na_2EDTA). Yield: 100 % (33 GBq/µmol).

Animal experiment

Animal experiments were performed at HZDR according to guidelines of German Regulations for Animal Welfare and approved by the local Animal Ethics Committee for Animal Experiments (Landesdirektion, Dresden, Germany). Bone imaging in healthy rodents was performed using male athymic nude mice (Rj:NMRI-Foxn1$^{nu/nu}$, Janvier Labs, Le Genest-Saint-Isle, France), between 12 and 14 weeks of age, with body weights ranging from 35.9 to 37.4 grams (*n* = 3). Bone imaging in rodents with critical size bone defects was performed using 38-week-old male Wistar rats (RjHan:WI, Janvier), with body weights of 480 and 532 grams (*n* = 2). In a pilot experiment, a 5-mm critical size bone defect was surgically introduced in the right femur of two rats, as described elsewhere.[55] In one rat, the defect was left empty. In the other rat, an absorbable hemostatic gelatin sponge (spongostan) was press-fit inserted into the defect. Imaging was performed at 16 weeks after surgery. All animals were housed in a pathogen-free facility. Anesthesia was induced and maintained by inhalation of 10% desflurane (Baxter, Deerfield, IL, USA) in 30 vol% oxygen air, maintaining the body temperature of the animals at 37 °C.

PET imaging

Positron emission tomography (PET) and X-ray computed tomography (CT) were performed at HZDR using a small-animal nanoScan PET/CT scanner (Mediso, Budapest, Hungary). CT images were captured at 50 kVp and used for attenuation correction and anatomical referencing. PET data acquisition was started simultaneously with radiotracer intravenous infusion within 30 s through the tail vein in 0.2 mL of 0.154 M NaCl, respectively. The initially delivered dose of [^{64}Cu]Cu^{II}-te1P^{BP} was 227 MBq/kg (≈2.6 nmol/kg) in mice and 43.4 MBq/kg (≈0.53 nmol/kg) in rats, at a molar activity of ≈100 MBq/nmol. For [^{18}F]fluoride PET, a dose of 19.6 MBq/kg was administered in rats, at a minimum molar activity of 12.0 MBq/nmol.

Three-dimensional list mode data were binned using a 400–600-keV energy window and sorted into 36 time frames (15×10 s, 5×30 s, 5×60 s, 4×300 s, 3×600 s, 4×900 s). Time frames were reconstructed using the Tera-Tomo^{TM} 3D algorithm, applying a voxel size of 0.4 mm and corrections for decay, scatter, and attenuation. Images were post-processed and analyzed using Rover (ABX GmbH, Radeberg, Germany) and displayed as a maximum intensity projection (MIPs) at indicated time points and scaling.

In PET images, three-dimensional regions of interest were delineated by applying fixed thresholding at 30% of the measured maximum intensity. Standardized uptake values (SUV = [MBq detected activity/mL tissue] / [MBq injected activity/g body weight], mL/g) were determined in bone regions with the highest radiotracer uptake (bo_{high} averaging SUVs measured in knee and shoulder joints), in bone regions with the lowest radiotracer uptake (bo_{low} averaging SUVs measured in tibiae and ulnae), in critical bone defects of the right femur (bo_{def}), and in a healthy bone reference region within the left femur (bo_{ref}). SUVs were reported as means ± range. Time-activity curves of bone uptake were drawn and fitted to the one-phase association equation $y = y_0 + (\text{plateau} - y_0) \times (1 - e^{-kx})$ using Prism 8.0 (GraphPad Software, San Diego, CA, USA).

Supporting Information.

The following files are available free of charge: Overall protonation and stability constants, ^{31}P NMR and UV-VIS titrations, example UV-VIS data for complexation and dissociation kinetics, equations desribing Cu^{II} complex formation, formation rate constants and stability constants of *out-of-cage* complexes, comparison between calculated 99% complexation times, rate constants as function of pH, adsorption of complex on hydroxoapatite, experimental crystallographic data (SupportingInformation.pdf).

Corresponding Author

Vojtěch Kubíček: Department of Inorganic Chemistry, Faculty of Science, Charles University, Hlavova 8, 128 40 Prague 2, Czech Republic. Tel.: +420221951436; e-mail: kubicek@natur.cuni.cz

Author Contributions

The manuscript was written through contributions of all authors. All authors have given approval to the final version of the manuscript.

Funding Sources

Grant Agency of the Czech Republic (19-17380S), Ministry of Education of the Czech Republic (LTC20044), Masaryk University (MUNI/A/1192/2020), COST Action CA18202 (NECTAR), Deutsche Forschungsgemeinschaft (DFG) Collaborative Research Center Transregio 67 "Functional Biomaterials for Controlling Healing Processes in Bone und Skin - From Material Science to Clinical Application" (CRC/TRR 67/3); project B5 - In vivo and ex vivo investigation of the effects of artificial matrices on implant surfaces in long bones

Acknowledgement

We are grateful for the support from the Grant Agency of the Czech Republic (19-17380S), Ministry of Education of the Czech Republic (LTC20044) and from Masaryk University

(MUNI/A/1192/2020). This work was performed within the framework of COST Action CA18202 (NECTAR). We also thank the Deutsche Forschungsgemeinschaft (DFG) for supporting this work within the Collaborative Research Center Transregio 67 “Functional Biomaterials for Controlling Healing Processes in Bone und Skin - From Material Science to Clinical Application“ (CRC/TRR 67/3); project B5 - In vivo and ex vivo investigation of the effects of artificial matrices on implant surfaces in long bones (S.S., C.N., S.R., & J.P.). In addition, we thank Dr. I. Císařová (Charles University) for performing of X-ray diffraction measurements and Dr. Carlos V. Melo for editing the manuscript.

References

[1] Palma, E.; Correia, J. D. G.; Campello, M. P. C.; Santos, I. Bisphosphonates as radionuclide carriers for imaging or systemic therapy. *Mol. BioSyst.* **2011**, *7*, 2950–2966.

[2] Lange, R.; Heine, R.; Knapp, R.; de Klerk, J. M. H.; Bloemendal, H. J.; Hendrikse, N. H. Pharmaceutical and clinical development of phosphonate-based radiopharmaceuticals for the targeted treatment of bone metastases. *Bone* **2016**, *91*, 159–179.

[3] Zhang, S.; Gangal, G.; Uludag, H. Magic bullets for bone diseases: progress in rational design of bone-seeking medicinal agents. *Chem. Soc. Rev.* **2007**, *36*, 507–531.

[4] Kubíček, V.; Lukeš, I. Bone-seeking probes for optical and magnetic resonance imaging. Future Med. Chem. 2010, 2, 521–531.

[5] Barbosa, J. S.; Paz, F. A. A.; Braga, S. S. Bisphosphonates, old friends of bones and new trends in clinics. *J. Med. Chem.* **2021**, *64*, 1260–1282.

[6] Kubíček, V.; Rudovský, J.; Kotek, J.; Hermann, P.; Vander Elst, L.; Muller, R. N.; Kolar, Z. I.; Wolterbeek, H. T.; Peters, J. A.; Lukeš, I. A bisphosphonate mono-amide analogue of DOTA: a Potential agent for bone-targeting. J. Am. Chem. Soc. 2005, 127, 16477–16485.

[7] Vitha, T.; Kubíček, V.; Hermann, P.; Vander Elst, L.; Muller, R. N.; Kolar, Z. I.; Wolterbeek, H. T.; Breeman, W. A. P.; Lukeš, I.; Peters, J. A. Lanthanide(III) complexes of bis(phosphonate) monoamide analogues of DOTA: Bone-seeking agents for imaging and therapy. *J. Med. Chem.* **2008**, *51*, 677–683.

[8] Vitha, T.; Kubíček, V.; Kotek, J.; Hermann, P.; Vander Elst, L.; Muller, R. N.; Lukeš, I.; Peters, J. A. A Gd(III) Complex of a Monophosphinate-bis(phosphonate) DOTA Analogue with a High ^{1}H NMR Relaxivity; Lanthanide(III) Complexes for Imaging and Radiotherapy of Calcified Tissues. *Dalton Trans.* **2009**, 3204–3214.

[9] Fellner, M.; Biesalski, B.; Bausbacher, N.; Kubíček, V.; Hermann, P.; Rösch, F.; Thews, O. ^{68}Ga-BPAMD: PET-imaging of bone metastases with a generator based positron emitter. *Nucl. Med. Biol.* **2012**, *39*, 993–999.

[10] Holub, J.; Meckel, M.; Kubíček, V.; Rösch, F.; Hermann, P. Gallium(III) complexes of NOTA-bis(phosphonate) conjugates as PET radiotracers for bone imaging. *Contrast Media Mol. Imaging* **2015**, *10*, 122–134**.**

[11] Bergmann, R.; Meckel, M.; Kubíček, V.; Pietzsch, J.; Steinbach, J.; Hermann, P.; Rösch, F. ^{177}Lu-labelled macrocyclic bisphosphonates for targeting bone metastasis in cancer treatment. *EJNMMI Res.* **2016**, *6*, 5.

[12] Mishiro, K.; Hanaoka, H.; Yamaguchi, A.; Ogawa, K. Radiotheranostics with radiolanthanides: Design, development strategies, and medical applications. *Coord. Chem. Rev.* **2019**, *383*, 104–131.

[13] Pfannkuchen, N.; Meckel, M.; Bergmann, R.; Bachmann, M.; Bal, Ch.; Sathekge, M.; Mohnike, W.; Baum, R. P.; Rösch, F. Novel radiolabeled bisphosphonates for PET diagnosis and endoradiotherapy of bone metastases. *Pharmaceuticals* **2017**, *10*, 45.

[14] Fellner, M.; Baum, R. P.; Kubíček, V.; Hermann, P.; Lukeš, I.; Prasad, V.; Rösch, F. PET/CT imaging of osteoblastic bone metastases with ^{68}Ga-bisphosphonates: first human study. *Eur. J. Nucl. Med. Mol. Imaging* **2010**, *37*, 834.

[15] Passah, A.; Tripathi, M.; Ballal, S.; Yadav, M.P.; Kumar, R.; Roesch, F.; Meckel, M.; Sarathi Chakraborty, P.; Bal, C. Evaluation of bone-seeking novel radiotracer ^{68}Ga-NO2AP-bisphosphonate for the detection of skeletal metastases in carcinoma breast. *Eur. J. Nucl. Med. Mol. Imaging* **2017**, *44*, 41–49.

[16] Khawar, A.; Eppard, E.; Rösch, F.; Ahmadzadehfar, H.; Kürpig, S.; Meisenheimer, M.; Gaertner, F. C.; Essler, M.; Bundschuh, R. A. Biodistribution and post-therapy dosimetric analysis of [^{177}Lu]Lu-DOTAZOL in patients with osteoblastic metastases: first results. *EJNMMI Res.* **2019**, *9*, 102.

[17] Procházková, S.; Hraníček, J.; Kubíček, V.; Hermann, P. Formation kinetics of europium(III) complexes of DOTA and its bis(phosphonate) bearing analogues. *Polyhedron* **2016**, *111*, 143–149.

[18] Notni, J.; Plutnar, J.; Wester, H. J. Bone seeking TRAP conjugates: surprising observations and implications on development of gallium-68-labeled bisphosphonates. *EJNMMI Res.* **2012**, *2*, 13.

[19] Boros, E.; Packard, A. B. Radioactive transition metals for imaging and therapy. *Chem. Rev.* **2019**, *119*, 870–901.

[20] Ahmedova, A.; Todorov, B.; Burdzhiev, N.; Goze, C. Copper radiopharmaceuticals for theranostic applications. *Eur. J. Med. Chem.* **2018**, *157*, 1406–1425.

[21] Paterson, B. M.; Donnelly, P. S. Macrocyclic bifunctional chelators and conjugation strategies for copper-64 radiopharmaceuticals. *Adv. Inorg. Chem.* **2016**, *68*, 223–251.

[22] *Sun, X.; Wuest, M.; Kovács, Z.; Sherry, A. D.; Motekaitis, R.; Wang, Z.; Martell, A. E.; Welch, M.; Anderson, C. In vivo behavior of copper-64-labeled methanephosphonate tetraaza macrocyclic ligands. J. Biol. Inorg. Chem.* ***2003****, 8, 217–225.*

[23] Boschi, A.; Martini, P.; Janevik-Ivanovska, E.; Duatti, A. The emerging role of copper-64 radiopharmaceuticals as cancer theranostics. *Drug Discovery Today* **2018**, *23*, 1489–1501.

[24] Yang, W.; Giandomenico, Ch. M.; Sartori, M.; Moore, D. A. *Tetrahedron Lett.,* **2003**, *44,* 2481–2483.

[25] Lukeš, I.; Kotek, J.; Vojtíšek, P.; Hermann, P. Complexes of tetraazacycles with methylphosphinic/phosphonic acid pendant arms. A comparison with their acetic acid analogues. *Coord. Chem. Rev.* **2001**, *216-217*, 287–312.

[26] Kotek, J.; Vojtíšek, P.; Císařová, I.; Hermann, P.; Jurečka, P.; Rohovec, J.; Lukeš, I. Bis(methylphosphinic acid) derivatives of 1,4,8,11-tetraazacyclotetradecane (cyclam). Synthesis, crystal and molecular structures, and solution properties. *Collect. Czech. Chem. Commun*. **2000**, *65*, 1289–1316.

[27] Kubíček, V.; Kotek, J.; Hermann, P.; Lukeš, I. Aminoalkylbis(phosphonates): Their complexation properties in solution and in the solid state. *Eur. J. Inorg. Chem.* **2007**, 333–344.

[28] Meyer, M.; Dahaoui-Gindrey, V.; Lecomte, C.; Guilard, R. Conformations and coordination schemes of carboxylate and carbamoyl derivatives of the tetraazamacrocycles

cyclen and cyclam, and the relation to their protonation states. *Coord. Chem. Rev.* **1998**, *178–180*, 1313–1405.

[29] Bosnich, B.; Poon, C. K.; Tobe, M. Complexes of cobalt (III) with a cyclic tetradentate secondary amine. *Inorg. Chem.* **1965**, *4*, 1102–1108.

[30] Kotek, J.; Lubal, P.; Hermann, P.; Císařová, I.; Lukeš, I.; Godula, T.; Svobodová, I.; Táborský, P.; Havel, J. Unusually high thermodynamic stability and extraordinary kinetic inertness of copper(II) complexes with 1,4,8,11-tetraazacyclotetradecane-1,8-bis(methylphosphonic acid). Example of a rare isomerism between kinetically inert penta- and hexacoordinated copper(II) complexes. *Chem. Eur. J.* **2003**, *9*, 233–248.

[31] David, T.; Kubíček, V.; Gutten, O.; Lubal, P.; Kotek, J.; Pietzsch, H.-J.; Rulíšek, L.; Hermann P. Cyclam derivatives with a bis(phosphinate) or a phosphinato−phosphonate pendant arm: Ligands for fast and efficient copper(II) complexation for nuclear medical applications. *Inorg. Chem.* **2015**, *54*, 11751–11766**.**

[32] Füzerová, S.; Kotek, J.; Cíısařová, I.; Hermann, P.; Binnemans, K.; Lukeš, I. Cyclam (1,4,8,11-tetraazacyclotetradecane) with one methylphosphonate pendant Arm: A new ligand for selective copper(II) binding. *Dalton Trans.* **2005**, 2908–2915.

[33] Svobodová, I.; Lubal, P.; Plutnar, J.; Havlíčková, J.; Kotek, J.; Hermann, P.; Lukeš, I. Thermodynamic, kinetic and solid-state study of divalent metal complexes of 1,4,8,11-tetraazacyclotetradecane (cyclam) bearing two *trans* (1,8-)methylphosphonic acid pendant arms. *Dalton Trans.* **2006**, 5184–5197.

[34] Procházková, S.; Kubíček, V.; Böhmová, Z.; Holá, K.; Kotek, J.; Hermann, P. DOTA analogue with phosphinate-iminodiacetate pendant arm: modification of complex formation rate with a strongly chelating pendant. *Dalton Trans.,* **2017**, *46*, 10484–10497.

[35] Kubíček, V.; Vitha, T.; Kotek, J.; Hermann, P.; Vander Elst, L.; Muller, R. N.; Lukeš, I.; Peters, J. A. Towards MRI contrast agents responsive to Ca(II) and Mg(II) ions: metal-induced oligomerization of dota-bisphosphonate conjugates. *Contrast Media Mol. Imaging* **2010**, *5*, 294–296.

[36] Matczak-Jon, E.; Videnova-Arabinska, V. Supramolecular chemistry and complexation abilities of diphosphonic acids. *Coord. Chem. Rev.* **2005**, *249*, 2458–2488.

[37] Pazderová, L.; David, T.; Hlinová, V.; Plutnar, J.; Kotek, J.; Lubal, P.; Kubíček, V.; Hermann, P. Cross-Bridged cyclam with phosphonate and phosphinate pendant arms: Chelators for copper radioisotopes with fast complexation. *Inorg. Chem.* **2020**, *59*, 8432−8443.

[38] Vitha, T.; Kubíček, V.; Hermann, P.; Kolar, Z. I.; Wolterbeek, H. T.; Peters, J. A.; Lukeš, I. Complexes of DOTA-bisphosphonate conjugates: Probes for determination of adsorption capacity and affinity constants of hydroxyapatite. *Langmuir* **2008**, *24*, 1952–1958.

[39] David, T.; Hlinová, V.; Kubíček, V.; Bergmann, R.; Striese, F.; Berndt, N.; Szöllösi, D.; Kovács, T.; Máthé, D.; Bachmann, M.; Pietzsch, H.-J.; Hermann, P. Improved conjugation, 64-Cu radiolabeling, in vivo stability, and imaging using nonprotected bifunctional macrocyclic ligands: Bis(phosphinate) cyclam (BPC) chelators. *J. Med. Chem.* **2018**, *61*, 8774–8796.

[40] Fleisch, H. Bisphosphonates: mechanisms of action. *Endocrinol. Rev.* **1998**, *19*, 80–100.

[41] Rothe, R.; Hauser, S.; Neuber, C.; Laube, M.; Schulze, S.; Rammelt, S.; Pietzsch, J. Adjuvant drug-assisted bone healing: Advances and challenges in drug delivery approaches. *Pharmaceutics* **2020**, *12*, 428.

[42] Bass, L. A.; Wang, M.; Welch, M. J.; Anderson, C. J. In vivo transchelation of copper-64 from TETA-octreotide to superoxide dismutase in rat liver. *Bioconjugate Chem.* **2000,** *11*, 527–532.

[43] Gao, F.; Sihver, W.; Bergmann, R.; Walther, M.; Stephan, H.; Belter, B.; Neuber, Ch.; Haase-Kohn, C.; Bolzati, C.; Pietzsch, J.; Pietzsch, H.-J. Radiochemical and radiopharmacological characterization of a ^{64}Cu-labeled α-MSH analog conjugated with different chelators. *J. Labelled Compnd. Radiopharm.* **2019**, *62*, 495–509

[44] Ullrich, M.; Bergmann, R.; Pietzsch, M.; Zenker, E. F.; Cartellieri, M.; Bachmann, M.; Ehrhart-Bornstein, M.; Block, N. L.; Schally, A. W.; Eisenhofer, G.; Bornstein, S. R.; Pietzsch, J.; Ziegler, C. G. Multimodal somatostatin receptor theranostics using [^{64}Cu]Cu-/[^{177}Lu]Lu-DOTA-(Tyr^3)octreotate and AN-238 in a mouse pheochromocytoma model. *Theranostics* **2016**, *6*, 650–665.

[45] Zhong, Z. A.; Peck, A.; Li, S.; VanOss, J.; Snider, J.; Droscha, C. J.; Chang, T. A.; Williams, B. O. ^{99m}T$_C$-Methylene diphosphonate uptake at injury site correlates with osteoblast differentiation and mineralization during bone healing in mice. *Bone Res.* **2015**, *3*, 15013.

[46] Ventura, M.; Franssen, G. M.; Oosterwijk, E.; Boerman, O. C.; Jansen, J. A.; Walboomers, X. F. SPECT vs. PET monitoring of bone defect healing and biomaterial performance in vivo. *J. Tissue Eng. Regener. Med.* **2016**, *10*, 843–854.

[47] Toegel, S.; Hoffmann, O.; Wadsak, W.; Ettlinger, D.; Mien, L.-K.; Wiesner, K.; Nguemo, J.; Viernstein, H.; Kletter, K.; Dudczak, R.; Mitterhauser, M. Uptake of bone-seekers is solely associated with mineralisation! A study with ^{99m}Tc-MDP, ^{153}Sm-EDTMP and ^{18}F-fluoride on osteoblasts. *Eur. J. Nucl. Med. Mol. Imaging* **2006**, *33*, 491–494.

[48] Mathavan, N.; Koopman, J.; Raina, D. B.; Turkiewicz, A.; Tägil, M.; Isaksson, H. ^{18}F-fluoride as a prognostic indicator of bone regeneration. *Acta Biomater.* **2019**, *90*, 403–411.

[49] Frazier, K. S.; Seely, J. C.; Hard, G. C.; Betton, G.; Burnett, R.; Nakatsuji, S.; Nishikawa, A.; Durchfeld-Meyer, B.; Bube, A. Proliferative and nonproliferative lesions of the rat and mouse urinary system. *Toxicol. Pathol.* **2012**, *40*, 14S-86S.

[50] Kubíček, V.; Havlíčková, J.; Kotek, J.; Tircsó, G.; Hermann, P.; Tóth, É.; Lukeš, I. Gallium(III) complexes of DOTA and DOTA-monoamide: Kinetic and thermodynamic studies. *Inorg. Chem.* **2010**, *49*, 10960–10969.

[51] Försterová, M.; Svobodová, I.; Lubal, P.; Táborský, P.; Kotek, J.; Hermann, P.; Lukeš, I. Thermodynamic study of lanthanide(III) complexes with bifunctional monophosphinic acid analogues of H_4dota and comparative kinetic study of yttrium(III) complexes. Dalton Trans. **2007**, 535–549.

[52] a) Kývala, M.; Lukeš, I.. *International Conference Chemometrics '95*, Pardubice, Czech Republic, **1995**, p. 63; b) Kývala, M.; Lubal, P.; Lukeš, I. *IX. Italian–Spanish and Mediterranean Congress on Thermodynamics of Metal Complexes (ISMEC 98)*, Girona, Spain, **1998**. The full version of the OPIUM program is available (free of charge) on http://www.natur.cuni.cz/_kyvala/opium.html .

[53] Sheldrick, G. M. SHELXT-2014. Program for Crystal Structure Solution from Diffraction Data. University of Göttingen, Göttingen, **2014**.

[54] Sheldrick, G. M. SHELXL-2014. Program for Crystal Structure Refinement from Diffraction Data. University of Göttingen: Göttingen, **2014**.

[55] Neuber, C.; Schulze, S.; Förster, Y.; Hofheinz, F.; Wodke, J.; Möller, S.; Schnabelrauch, M.; Hintze, V.; Scharnweber, D.; Rammelt, S.; Pietzsch, J. Biomaterials in repairing rat femoral defects: In vivo insights from small animal positron emission tomography/computed tomography (PET/CT) studies. *Clin. Hemorheol. Microcirculat.* **2019**, *73*, 177–194.

Cyclam with a phosphinate-bis(phosphonate) pendant arm: a bone targeting carrier of copper radionuclides

Lucia Pazderová,[a] Martina Benešová,[a,b] Margareta Vojtíčková,[a] Jana Havlíčková,[a] Jan Kotek,[a] Přemysl Lubal,[c] Martin Ullrich,[d] Martin Walther,[d] Sabine Schulze,[e] Christin Neuber,[d] Stefan Rammelt,[f] Hans-Jürgen Pietzsch,[d,g] Jens Pietzsch,[d,g] Vojtěch Kubíček,[a*] Petr Hermann[a]

[a]Department of Inorganic Chemistry, Faculty of Science, Charles University, Hlavova 8, 128 40 Prague 2, Czech Republic. Tel.: +420221951436; fax: +420221951253; e-mail: kubicek@natur.cuni.cz

[b]Research Group Molecular Biology of Systemic Radiotherapy, German Cancer Research Center, Im Neuenheimer Feld 223, 69120 Heidelberg, Germany

[c]Department of Chemistry, Faculty of Science, Masaryk University, Kamenice 5, 625 00 Brno, Czech Republic

[d]Helmholtz-Zentrum Dresden-Rossendorf, Institute of Radiopharmaceutical Cancer Research, Bautzner Landstrasse 400, 01328 Dresden, Germany

[e]Technische Universität Dresden, Faculty of Medicine, Centre for Translational Bone, Joint and Soft Tissue Research, Fetscherstrasse 74, 01307 Dresden, Germany

[f]Technische Universität Dresden, University Hospital Carl Gustav Carus, University Center for Orthopaedics and Traumatology, Fetscherstrasse 74, 01307 Dresden, Germany

[g]Technische Universität Dresden, School of Science, Faculty of Chemistry and Food Chemistry, 01069 Dresden, Germany

Table of content

Table S1. Overall protonation constants $\log\beta_{hl}$ of H_5te1P^{BP} (I = 0.1 M NMe_4Cl, 25 °C)

Species	$\log\beta_{hl}$
H_2L	26.76(4) [a,b]
H_3L	38.59(1)
H_4L	45.91(1)
H_5L	49.20(2)
H_6L	51.27(2)

[a]Protonation over two steps

[b]Determined by NMR titration

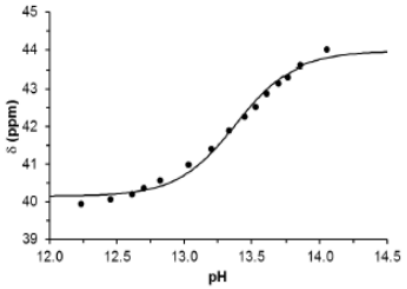

Figure S1. Chemical shift of the H_5te1P^{BP} phosphinate ^{31}P NMR signal in the strongly alkaline region; the line represents the best fit, giving the constant $\log\beta_2$ shown in Table S1 (c_L = 4 mM).

Table S2. Overall stability constants $\log\beta_{hlm}$ of *in-cage* complexes of H_5te1P^{BP} (I = 0.1 M NMe_4Cl, 25 °C)

Species	Cu^{II}	Zn^{II}	Ni^{II}
[M(L)]	29.11(4)	20.74(3)	25.92(5)
[M(HL)]	41.80(3)	33.03(3)	37.68(4)
[M(H_2L)]	49.24(2)	40.51(2)	44.54(4)
[M(H_3L)]	52.70(2)	44.86(4)	–

Table S3. Protonation constants $\log K_n$ of *in-cage* complexes of H_5te1P^{BP} (I = 0.1 M NMe_4Cl, 25 °C)

Species	Cu^{II}	Zn^{II}	Ni^{II}
$\log K_1$	12.69	12.29	11.76
$\log K_2$	7.44	7.48	6.86
$\log K_3$	3.46	4.35	–

Table S4. Overall stability constants $\log\beta_{hlmn}$ of the ternary complexes of H_5te1P^{BP} in which the Cu^{II} ion is bound in the macrocyclic cavity (I = 0.1 M NMe_4Cl, 25 °C)

Species	Cu^{II}	Zn^{II}	Ca^{II}	Mg^{II}
{M[Cu(L)]}	44.3(13)	42.67(4)	36.26(5)	37.00(4)
{M[Cu(HL)]}	50.35(9)	-	45.77(3)	45.97(2)
{M[Cu(H_2L)]}	54.38(8)	53.27(3)	51.99(2)	52.03(1)
{M(OH)[Cu(L)]}	-	32.75(5)	-	-
{M(OH)$_2$[Cu(L)]}	22.76(7)	20.68(4)	-	-
{M_2[Cu(L)]}	49.69(8)	47.65(3)	40.93(3)	41.04(3)
{M_2(OH)[Cu(L)]}	44.33(8)	40.57(3)	-	30.42(3)
{M_2(OH)$_2$[Cu(L)]}	35.21(8)	30.76(4)	-	17.98(3)
{M_2(OH)$_3$[Cu(L)]}	23.78(9)	20.64(3)	-	-
{M[Cu(L)]$_2$}	81.72(10)	79.21(10)	69.7(1)	-
{M[Cu(L)][Cu(HL)]}	-	-	82.30(8)	-
{M[Cu(HL)]$_2$}	98.63(11)	97.18(4)	90.91(5)	90.67(8)

Table S5. Protonation constants $\log K_h$ of the ternary complexes of H_5te1P^{BP} in which the Cu^{II} ion is bound in the macrocyclic cavity (I = 0.1 M NMe_4Cl, 25 °C)

Equilibrium	Cu^{II}	Zn^{II}	Ca^{II}	Mg^{II}
{M[Cu(L)]} + H → {M[Cu(HL)]}	6.05	2 × 5.30 [a]	9.51	8.97
{M[Cu(HL)]} + H → {M[Cu(H_2L)]}	4.03		6.22	6.06
{M(OH)[Cu(L)]} + H → {M[Cu(L)]}	2 × 10.77 [a]	9.92	-	-
{M(OH)$_2$[Cu(L)]} + H → {M(OH)[Cu(L)]}		12.07	-	-
{M_2(OH)[Cu(L)]} + H → {M_2[Cu(L)]}	5.36	7.08	-	10.62
{M_2(OH)$_2$[Cu(L)]} + H → {M_2(OH)[Cu(L)]}	9.12	9.81	-	12.44
{M_2(OH)$_3$[Cu(L)]} + H → {M_2(OH)$_2$[Cu(L)]}	11.43	10.12	-	-
{M[Cu(L)]$_2$} + H → {M[Cu(L)][Cu(HL)]}	2 × 8.46 [a]	2 × 8.99 [a]	12.6	-
{M[Cu(L)][Cu(HL)]} + H → {M[Cu(HL)]$_2$}			8.61	-

[a]Protonation over two steps

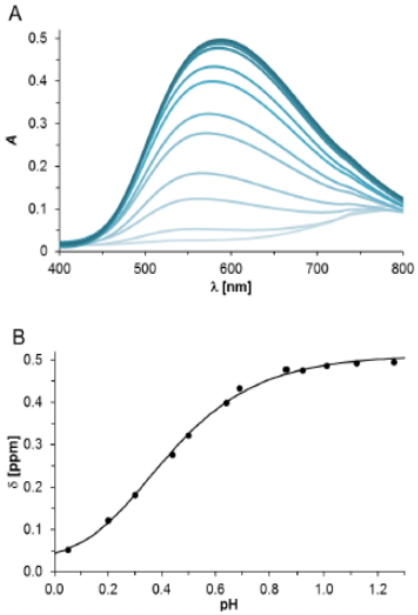

Figure S2. UV-VIS spectra of Cu^{II}-H_5te1P^{BP} system ($c_L = c_{Cu}$ = 4 mM) in the strongly acidic region (**A**) and absorbance at 580 nm as function of pH (**B**, the line represents the best fit, giving the constants outline in Table S2).

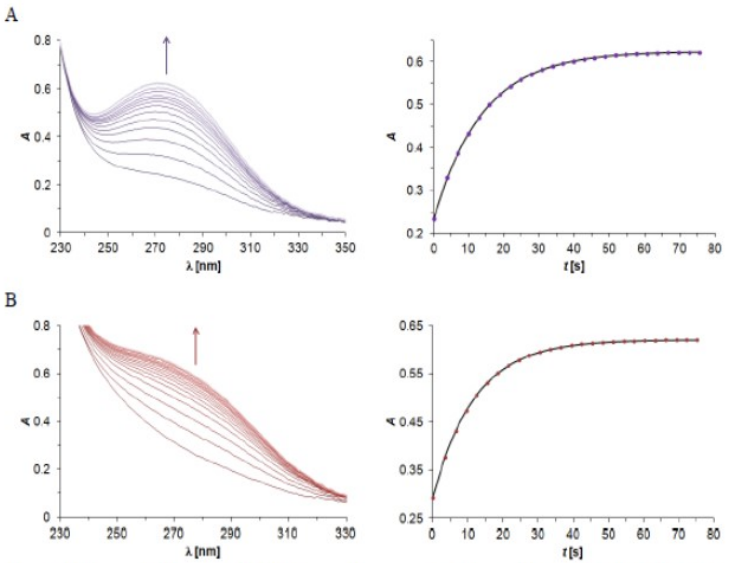

Figure S3. Spectra of the Cu^{II}-H$_5$te1P^{BP} system during complexation (pH = 3.54, I = 0.1 M KCl, 25 °C) and absorbance at 273 nm as function of time at a ligand excess (**A**, c_L = 0.25 mM, c_M = 0.05 mM) and at a Cu^{II} ion excess (**B**, c_L = 0.05 mM, c_M = 0.25 mM); the lines represent the best fit according to Equation 4.

Equations desribing Cu^{II} complex formation

Macrocyclic complexes with coordinating pendant arms are formed in two steps. An *out-of-cage* complex (indicated in the formulas below with superscript "oc") is immediately formed in the first equilibrium step. In the complex, donor atoms of the pendant arms are coordinated to the metal ion, two macrocyclic amines are protonated, and the protons block access to the macrocyclic cavity. In the next (rate-determining) step, nitrogen atoms of the macrocycle are deprotonated, and the metal ion is simultaneously transferred to the macrocyclic cavity, thus forming the *in-cage* complex (indicated in the formulas below with superscript "ic").

Because bis(phosphonate) is a strongly complexing pendant group, H$_4$te1P^{BP} forms different types of *out-of-cage* complexes under ligand vs. metal ion excesses. Cu^{II} complexes with bis(phosphonates) are quantitatively formed at pH > 3 even at equimolar amounts at milimolar concentrations. Hence, the 1:1 *out-of-cage* complex $[M(L)]^{oc}$ is quantitatively formed over the entire pH range. In addition, bis(phosphonates) form dinuclear complexes $[M_2(L)]^{oc}$ and complexes with two coordinated ligands $[M(L)_2]^{oc}$ under a metal and ligand excess, respectively (Scheme 1).

The rate of the overall complexation reaction forming the *in-cage* complex can be expressed as a sum of contributions of all expected *out-of-cage* intermediates to the overall transformation into the *in-cage* complex (Equation 1 , where different protonation states of the ligand in the *out-of-cage* complexes are not shown),

$$\frac{d[ML]^{ic}}{dt} = {}^{f}k_2 \cdot [L]_{tot} \cdot [M]_{tot} = {}^{f}k_{ML} \cdot [M(L)]^{oc} + {}^{f}k_{ML2} \cdot [M(L)_2]^{oc} + {}^{f}k_{M2L} \cdot [M_2(L)]^{oc} \quad (1)$$

where ${}^{f}k_2$ is a second-order rate constant of the bimolecular reaction. The relation between ${}^{f}k_2$ and the observed pseudo-first-order rate constant, k_{obs}, is ${}^{f}k_2 = {}^{f}k_{obs}/[M]_{tot}$ or ${}^{f}k_2 = {}^{f}k_{obs}/[L]_{tot}$ for a metal and ligand excess, respectively. In Equation 1, $[L]_{tot}$ and $[M]_{tot}$ are overall concentrations of the ligand and metal ion, respectively, and ${}^{f}k_{ML}$, ${}^{f}k_{ML2}$ and ${}^{f}k_{M2L}$ are formation rate constants for the transformation of the corresponding *out-of-cage* complexes into the *in-cage* complex. Quantitative formation of $[M(L)]^{oc}$ species is presumed to occur even at a 1:1 metal-to-ligand ratio, and the equilibrium concentrations of $[M(L)_2]^{oc}$ and $[M_2(L)]^{oc}$ species are expressed by Equations S1 and S2, respectively,

$$[M(L)_2]^{oc} = K_{ML2} \cdot [M(L)]^{oc} \cdot [L] \quad (S1)$$

$$[M_2(L)]^{oc} = K_{M2L} \cdot [M(L)]^{oc} \cdot [M] \quad (S2)$$

where K_{ML2} and K_{M2L} are the conditional stability constants of the *out-of-cage* intermediates (Scheme 1) and [L] and [M] are equilibrium concentrations of the free ligand and metal ion, respectively. Finally, the data were treated to Equations 1, S1 and S2 combined with metal and ligand mass balance equations (Equations S3 and S4) to meet the minimization criterion for the overall fit. For the experiments performed under a ligand excess, only $[M(L)]^{oc}$ and $[M(L)_2]^{oc}$ species were considered, calculating the constants ${}^{f}k_{ML}$, ${}^{f}k_{ML2}$ and K_{ML2} . For the experiments performed under a metal ion excess, only $[M(L)]^{oc}$ and $[M_2(L)]^{oc}$ species were considered, calculating the constants ${}^{f}k_{ML}$, ${}^{f}k_{M2L}$ and K_{M2L}. The constant ${}^{f}k_{ML}$ was determined from both experiments. Thus, two data sets are presented in Figure S4A, which match and therefore support our model.

$$[M]_{tot} = [M] + [M(L)]^{oc} + 2\times[M_2(L)]^{oc} + [M(L)_2]^{oc} \quad \text{(S3)}$$

$$[L]_{tot} = [L] + [M(L)]^{oc} + [M_2(L)]^{oc} + 2\times[M(L)_2]^{oc} \quad \text{(S4}$$

Rate constants of the complexation with macrocyclic ligands (such as ${}^{f}k_{ML}$, ${}^{f}k_{ML2}$ and ${}^{f}k_{M2L}$) typically show significant changes with pH. The key step of the complex formation is deprotonation of the macrocycle in the rate determining step. Thus, the rate constants are often linearly proportional to the hydroxide concentration $[OH^-]$. As such, the general constant ${}^{f}k$ can be expressed as in Equation S5,

$${}^{f}k = {}^{0}k + {}^{OH}k \cdot [OH^-] \quad \text{(S5)}$$

where ${}^{0}k$ and ${}^{OH}k$ are rate constants characterizing the OH^--independent and OH^--dependent transformation of the *out-of-cage* intermediate into the *in-cage* complex. In the Cu^{II}-H5te1P^{BP} system, all constants, ${}^{f}k_{ML}$, ${}^{f}k_{ML2}$ and ${}^{f}k_{M2L}$ show a linear change with pH at pH > 4 (Figure S4), whereas a non-linear trend is observed at lower pH. The non-linear trend indicates the presence of two differently protonated species. Each rate constant (${}^{f}k_{ML}$, ${}^{f}k_{ML2}$ and ${}^{f}k_{M2L}$) can be hence expressed as the sum of contributions from the two differently protonated species as in Equations S6, S7 and S8.

$${}^{f}k_{ML}\cdot[M(L)]_{tot} = ({}^{0}k_{ML} + {}^{OH}k_{ML}\cdot[OH^-])\cdot[M(H_nL)] + \\ +({}^{0}k_{MHL} + {}^{OH}k_{MHL}\cdot[OH^-])\cdot[M(H_{n+1}L)] \quad \text{(S6)}$$

$${}^{f}k_{M2L}\cdot[M_2(L)]_{tot} = ({}^{0}k_{M2L} + {}^{OH}k_{M2L}\cdot[OH^-])\cdot[M_2(H_nL)] +$$

$$+({}^{0}k_{M2HL} + {}^{OH}k_{M2HL}\cdot[OH^-])\cdot[M_2(H_{n+1}L)] \quad \text{(S7)}$$

$${}^{f}k_{ML2}\cdot[M(L)_2]_{tot} = ({}^{0}k_{ML2} + {}^{OH}k_{ML2}\cdot[OH^-])\cdot[M(H_nL_2)] + \\ +({}^{0}k_{MHL2} + {}^{OH}k_{MHL2}\cdot[OH^-])\cdot[M(H_{n+1}L_2)] \quad \text{(S8)}$$

In Equations S4–S6, $[X]_{tot}$ is the overall concentration of both forms of the corresponding *out-of-cage* species, and ${}^{0}k_{MxLy}$ and ${}^{OH}k_{MxLy}$ are the rate constants of the specific OH^--independent and OH^--dependent reaction pathways of the less protonated *out-of-cage* species, whereas ${}^{0}k_{MxHLy}$ and ${}^{OH}k_{MxHLy}$ are analogous constants of the more protonated species. Using the mass balance and the protonation equilibrium equations for the *out-of-cage* species, each rate constant (${}^{f}k_{ML}$, ${}^{f}k_{ML2}$ or ${}^{f}k_{M2L}$) as function of proton concentration is expressed by Equation S9.

$${}^{f}k_{M_xL_y} = \frac{({}^{0}k_{M_xL_y} + {}^{OH}k_{M_xL_y}\cdot\frac{K_w}{[H^+]}) + ({}^{0}k_{M_xHL_y} + {}^{OH}k_{M_xHL_y}\cdot\frac{K_w}{[H^+]})\cdot\frac{[H^+]}{{}^{H}K_{M_xL_y}}}{1 + \frac{[H^+]}{{}^{H}K_{M_xL_y}}} \quad \text{(S9)}$$

where ${}^{H}K_{MxLy}$ is the dissociation constant describing the equilibrium between the two differently protonated *out-of-cage* species. Data treatment showed that the contributions of the OH^--independent pathways (described by constants ${}^{0}k_{MxLy}$ and ${}^{0}k_{MxHLy}$) are negligible. Under these conditions, the mechanism can be described by Scheme 2, and the Equation S9 is then simplified to Equation 2.

$${}^{f}k_{M_xL_y} = \frac{({}^{OH}k_{M_xL_y}\cdot\frac{K_w}{[H^+]}) + ({}^{OH}k_{M_xHL_y}\cdot\frac{K_w}{{}^{H}K_{M_xL_y}})}{1 + \frac{[H^+]}{{}^{H}K_{M_xL_y}}} \quad \text{(2)}$$

Table S6. Formation rate constants and stability constants of *out-of-cage* complexes in the Cu^{II}-H_5te1P^{BP} system (I = 0.1 M KCl, 25 °C)

	pH	$^{f}k_{ML}$ [s^{-1}]	$^{f}k_{M2L}$ [s^{-1}]	K_{M2L} [M^{-1}]	log{K_{M2L}/M^{-1}}
Metal excess	3.54	$(1.8\pm1.3)\times10^{-2}$	$(9\pm2)\times10^{-2}$	$(3.3\pm1.3)\times10^{2}$	2.51 ± 0.17
	3.95	$(7\pm2)\times10^{-2}$	3.8±0.3	$(2.7\pm0.4)\times10^{2}$	2.43 ± 0.06
	4.47	$(7\pm3)\times10^{-2}$	23±2	$(1.7\pm0.2)\times10^{2}$	2.23 ± 0.05
	5.01	$(2\pm3)\times10^{-1}$	45±7	$(2.8\pm0.7)\times10^{2}$	2.45 ± 0.11
	5.48	$(4\pm2)\times10^{-1}$	88±15	$(3.5\pm1.1)\times10^{2}$	2.54 ± 0.14

	pH	$^{f}k_{ML}$ [s^{-1}]	$^{f}k_{ML2}$ [s^{-1}]	K_{ML2} [M^{-1}]	log{K_{ML2}/M^{-1}}
Ligand excess	3.54	$(1.7\pm0.9)\times10^{-2}$	$(2.6\pm0.3)\times10^{-1}$	$(1.0\pm0.3)\times10^{3}$	3.00 ± 0.13
	3.95	$(5.0\pm1.0)\times10^{-2}$	$(3.1\pm0.2)\times10^{-1}$	$(2.7\pm0.8)\times10^{3}$	3.43 ± 0.13
	4.47	$(1.2\pm0.7)\times10^{-1}$	0.9±0.2	$(1.2\pm0.8)\times10^{3}$	3.08 ± 0.29
	5.01	$(1.3\pm0.3)\times10^{-1}$	1.2±0.1	$(4.1\pm0.9)\times10^{3}$	3.61 ± 0.10
	5.48	$(5.2\pm10)\times10^{-1}$	2.0±0.3	$(2.9\pm1.6)\times10^{3}$	3.47 ± 0.24

Table S7. Comparison between calculated 99% complexation times (c_L = 0.05 mM, c_{Cu} = 0.5 mM, 25 °C) of H_5te1P^{BP} and related ligands

Ligand	Ref.	pH 4	pH 5	pH 6
H_5te1P^{BP}	this work	10 s	1 s	0.1 s [a]
H_4te2P	1	64 s	3 s	0.2 s
H_3te1P^{PIN}	2	16 s	2 s	0.2 s
H_4cb-te2P	3	3.6 h	3.4 min	3 s
H_4cb-te2P^{PIN}	3	14 s	3 s	1 s

[a] Extrapolated

[1] Kotek, J.; Lubal, P.; Hermann, P.; Císařová, I.; Lukeš, I.; Godula, T.; Svobodová, I.; Táborský, P.; Havel, J. Unusually High Thermodynamic Stability and Extraordinary Kinetic Inertness of Copper(II) Complexes with 1,4,8,11-Tetraazacyclotetradecane-1,8-bis(methylphosphonic Acid). Example of a Rare Isomerism Between Kinetically Inert Penta- and Hexacoordinated Copper(II) Complexes. *Chem. Eur. J.* **2003**, *9*, 233–248.

[2] David, T.; Kubíček, V.; Gutten, O.; Lubal, P.; Kotek, J.; Pietzsch, H.-J.; Rulíšek, L.; Hermann, P. Cyclam Derivatives with a Bis(phosphinate) or a Phosphinato-Phosphonate Pendant Arm. *Inorg. Chem.* **2015**, *54*, 11751–11766.

[3] Pazderova, L.; David, T.; Hlinová, V.; Plutnar, J.; Kotek, J.; Lubal, P.; Kubíček, V.; Hermann, P. Cross-Bridged Cyclam with Phosphonate and Phosphinate Pendant Arms: Chelators for Copper Radioisotopes with Fast Complexation. *Inorg. Chem.* **2020**, *59*, 8432–8443.

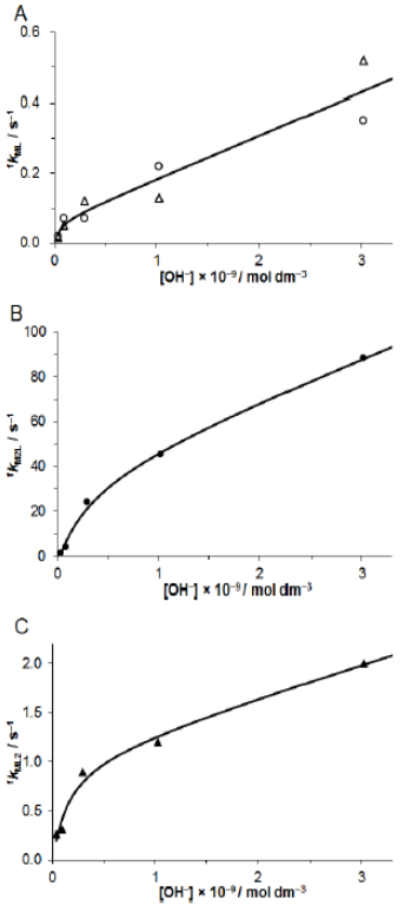

Figure S4. Rate constants $^{f}k_{ML}$ (**A**), $^{f}k_{M2L}$ (**B**) and $^{f}k_{ML2}$ (**C**) as function of pH (I = 0.1 M KCl, 25 °C); empty circles in **A** show values determined from experiments performed under a metal ion excess, and empty triangles in **A** show values determined from experiments performed under a ligand excess. Data points shown in **B** and **C** were calculated from experiments performed under a ligand and metal excess, respectively. The lines represent the best fits according to Equation 2 using parameters outlined in Table 3.

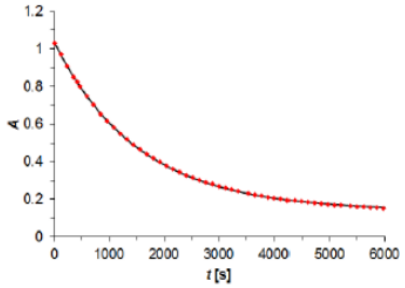

Figure S5. Absorbance at 580 nm as function of time during Cu^{II}-te1P^{BP} complex dissociation (c = 0.1 mM) in 1 M $HClO_4$ at 50 °C (I = 5 M H/$NaClO_4$); the line represents the best fit according to Equation 4.

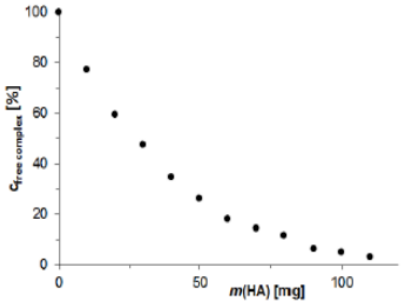

Figure S6. Adsorption of Cu^{II}-te1P^{BP} complex on hydroxoapatite (c_{tot} = 0.1 mM, V = 3 ml, pH = 7.5, 25 °C)

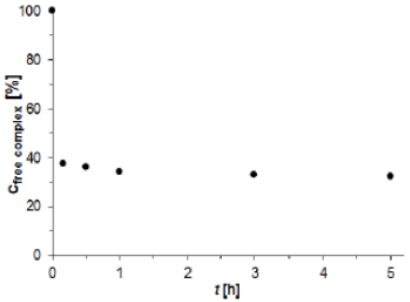

Figure S7. Adsorption of Cu^{II}-te1P^{BP} complex on hydroxoapatite (HA): concentration of Cu^{II}-te1P^{BP} complex in solution as function of time (c_{tot} = 0.1 mM, V = 3 ml, m(HA) = 40 mg, pH = 7.5, 25 °C)

Table S8. Experimental crystallographic data for the crystal structure of $H_5te1P^{BP}\cdot 6H_2O$

Parameter	$H_5te1P\cdot 6H_2O$
Formula	$C_{13}H_{45}N_4O_{14}P_3$
M_r	574.44
Habit	bar
Color	colorless
Crystal system	orthorhombic
Space group	P b c a
a, Å	13.2069(4)
b, Å	16.4828(6)
c, Å	22.8799(8)
α, °	90
β, °	90
γ, °	90
U, Å^3	4980.6(3)
Z	8
D_{calc}, g cm^{-3}	1.532
μ, mm^{-1}	2.857
Unique refl.	4397
Obsd. refl. ($I>2\sigma(I)$)	3772
$R(I>2\sigma(I))$	0.0533
R'(all)	0.0619
$wR(I>2\sigma(I))$	0.1403
wR'(all)	0.1463
CCDC number	2086453